In-cylinder experimental and modeling studies on producer gas fuelled operation of spark ignited gas engines

A Thesis

Submitted For the Degree of

Doctor of Philosophy

in the Faculty of Engineering

by

Anand M Shivapuji

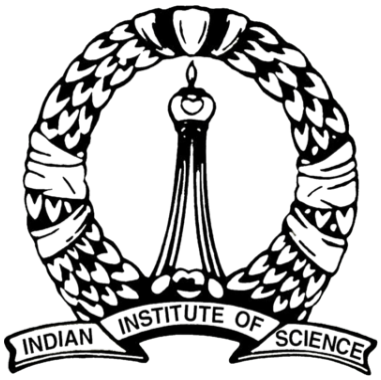

Center for Sustainable Technologies
Indian Institute of Science
BANGALORE – 560 012

AUGUST 2015

D E D I C A T E D

to my parents, teachers, my wife and son

Acknowledgements

No work is complete without acknowledging the efforts of all the people who made it possible either through direct or indirect contribution.

I would first like to extend my sincere thanks to Prof S Dasappa, my research supervisor and mentor. The way the work has shaped up would not have been possible without his active guidance and support. Particularly useful were the discussions over daily walks around the campus which enabled in-depth analysis of various concepts and possible directions. Special thanks are due to him for his role as a mentor in guiding me to take up what is right irrespective of how hard the path may be.

I would like to extend special thanks to our technician Mr Channakeshava, for the support extended throughout the engine testing phase. His competence with the engine and the in-cylinder instrumentation was particularly helpful. I also thank technicians for their support in various experimental activities. I would also like to thank Mr Srinivasan from AVL India for the support extended especially with the innumerable license extensions he has been arranging for the AVL Indicom. Special thanks are due to Arvind Iyer for providing in-depth inputs regarding fluid dynamics in general and turbulence in particular during our regular walks around Jubilee gardens. I thank Amit Kumar for his support towards domain modeling and discretization. I would also like to thank my other friends Sadhan Mahapatra, Sandeep Kumar, Varun, Snehesh, Abhishek, Gayathri and Aasha for the wonderful time I had at the institute.

I would like to extend special thanks to my parents for all the support extended. Lots of love and thanks to my wife and son for all the support extended, being patient and sacrificing quite a lot during the course of the work. Their support has been indispensable.

Thanks are due to all others who have supported in a variety of ways.

Publications from the current work

Journals

1. Shivapuji, A. M., & Dasappa, S. (2013). *Experiments and zero D modeling studies using specific Wiebe coefficients for producer gas as fuel in spark-ignited engines.* Proceedings of the Institution of Mechanical Engineers, Part C: Journal of Mechanical Engineering Science, 227(3), 504-519.

2. Shivapuji, A. M., & Dasappa, S. (2014). *Selection and thermodynamic analysis of a turbocharger for a producer gas-fuelled multi-cylinder engine.* Proceedings of the Institution of Mechanical Engineers, Part A: Journal of Power and Energy, 228(3), 340-356.

3. Shivapuji, A. M., & Dasappa, S. (2014). *In-cylinder investigations and analysis of a SI gas engine fuelled with H2 and CO rich syngas fuel: Sensitivity analysis of combustion descriptors for engine diagnostics and control.* International Journal of Hydrogen Energy, 39(28), 15786-15802.

4. Shivapuji, A. M., & Dasappa, S. (2015). *Influence of fuel hydrogen fraction on syngas fueled SI engine: Fuel thermo-physical property analysis and in-cylinder experimental investigations.* International Journal of Hydrogen Energy. doi:10.1016/j.ijhydene.2015.06.062

Conferences

1. Shivapuji, A. M., & Dasappa, S. (2011). *Experimental studies on multi-cylinder natural gas engine fueled with producer gas.* In Proceedings of 19th European biomass conference and exhibition - from research to industry and markets. 6-10 June 2011, Berlin, Germany.

2. Shivapuji, A. M., & Dasappa, S. (2013). *Knock and its prediction in producer gas fuelled SI engines.* In Proceedings of ICPS 2013 - International Conference on Poly-generation Strategies, 3-5 September 2013, Vienna, Austria.

3. Shivapuji, A. M., Kumar, A., & Dasappa, S. (2013) *Experiments and CFD simulation of producer gas fuelled SI engine: Towards addressing high exhaust enthalpy and cooling loads.* In Proceedings of NCICEC 2013 - 23rd National

Conference on I.C. Engine and Combustion, 13-16 Dec. 2013 Surat, Gujrat, India

4. Shivapuji, A. M., & Dasappa, S. (2013). *Sensitivity analysis of mixture quality on combustion phasing and its impact on 0D simulation of a producer gas fuelled multi-cylinder engine.* In Proceedings of ASPACC 2013 - 9th Asia-Pacific Conference on Combustion, 19-22 May 2013, Gyeongju, South Korea.

   The author has received the **YOUNG INVESTIGATOR AWARD FOR THE YEAR 2013** awarded by the **Combustion Institute - Korea Chapter** for this article.

5. Shivapuji, A. M., Kumar, A., & Dasappa, S. (2015). *Combustion characterization of compressed natural gas and syngas fuelled engine operation under steady and transient conditions.* In Proceedings of ASPACC 2015 - 10th Asia-Pacific Conference on Combustion, 19 - 22 July 2015, Beijing, China.

6. Shivapuji, A. M., & Dasappa, S. *Performance evaluation tool for simulating gas engine – a GUI package.* The International Bioenergy Conference and Exhibition 2015, Shanghai, China.

7. Shivapuji, A. M., & Dasappa, S. *Small capacity producer gas engine adaption from natural gas for decentralized power generation application.* The International Bioenergy Conference and Exhibition 2015, Shanghai, China.

Articles under preparation for journals

1. Shivapuji, A. M., & Dasappa, S. *Theoretical analysis of power estimation of an internal combustion engine for various fuels*

2. Shivapuji, A. M., & Dasappa, S. *Syngas fuelled operation of spark ignited engines: Steady state cyclic variations and transient analysis*

3. Shivapuji, A. M., & Dasappa, S. *Numerical investigation in zero and quasi dimensional space : Producer gas fuelled operational analysis*

4. Shivapuji, A. M., & Dasappa, S. *Knock rating analysis and Methane number estimation for gaseous fuels - a novel approach*

Contents

List of Figures

List of Tables

Nomenclature

α	Flame speed correlation pressure coefficient
β	Flame speed correlation temperature coefficient
δ_T	Laminar flame thickness (m)
η	Efficiency
η_f	Fuel conversion efficiency
η_v	Volumetric efficiency
γ	Ratio of specific heats
λ	Excess air ratio
μ	Viscosity $(Pa - s)$
σ	Sample standard deviation
τ_b	Characteristic burn time (s)
θ	Crank angle (deg)
ε	Emissivity
ξ	Connecting rod to crank length ratio
Da	Damkohler number
$EELB$	Eddy Entrainment and Laminar Burn-up
L_T	Characteristic turbulent length scale (m)

Le Levis number

MON Motor Octane Number

MW Molecular weight ($kg/kmol$)

N Engine speed (RPM)

NA Naturally Aspirated

Nu Nusselt number

Pr Prandtl number

Q Heat transfer (J)

Re Reynolds number

RON Research Octane Number

S_L Laminar flame speed (m/s)

TA Turbocharged After-cooled

U_T Characteristic turbulent velocity (m/s)

V_s Swept volume (m^3)

$\dot{m}$ Mass flow rate (kg/s)

μ Viscosity ($Pa - s$)

$\overline{T}$ Spatially averaged temperature (K)

ϕ Equivalence ratio

ρ Density (kg/m^3)

A_f Flame area (m^2)

B Cylinder bore diameter (m)

B Cylinder bore diameter

C_d Discharge coefficient

C_p Specific heat at constant pressure $(J/mol - k)$

C_v Specific heat at constant volume $(J/mol - k)$

CFR Cooperative Fuels Research

CR Compression ratio

CV Calorific value

E_a Activation energy (J/mol)

H Absolute enthalpy (J)

h Specific enthalpy (J/kg)

$h_{c,g}$ Gas side convective heat transfer coefficient $(W/m^2 - K)$

$HCCI$ Homogeneous Charge Compression Ignition

IC Internal Combustion

k Thermal conductivity $(W/m - K)$

k_t Constant

m Mass (kg)

NG Natural gas

P Pressure (Pa)

PG Producer gas

R Gas constant $(J/mol - K)$

T Temperature (K)

T_b Cylinder bulk gas temperature

U Absolute internal energy (J)

u Specific internal energy (J/kg)

V Volume (m^3)

W Work term (J)

X_i Specie mole fraction

Abstract

Fuelling an internal combustion engine with a fuel other than that for which it is designed entails various challenges, collectively culminating in (potentially) varied engine performance. The challenges primarily emanate from the differences in the thermo-physical properties of the alternative or non-regular fuels as compared to the reference fossil fuel. Change in the thermo-physical characteristics of the chemical energy carrier influences the in-cylinder fluid dynamics, degree of completeness of reaction, heat release pattern and heat transfer characteristics in the combustion chamber of the engine. These factors influence the engine thermo-kinematic response leading to potential degradation of the engine performance, quantified in terms of the supported load, specific energy consumption and emissions.

The current work, through experimental and numerical investigations, addresses the performance of commercially available multi-cylinder natural gas engine(s) with producer gas, a bio derived gaseous alternative. Producer gas has dry volumetric composition of 19 $\pm$ 1% carbon monoxide and hydrogen each, 2 $\pm$ 0.5% methane, 12 $\pm$ 1% carbon dioxide and 46 $\pm$ 1% nitrogen, as against excess of 98% combustibles (predominantly methane) in compressed natural gas. The difference in composition of the two gases extends to the thermo-physical properties and thermo-kinematic response. The changes in the air-to-fuel ratio, calorific value and the properties like laminar flame speed, coupled with the presence of hydrogen in the gas, pose various scientific and technological challenges.

Experimental investigations involved three multi-cylinder engine generator sets; a two cylinder engine (E2) and a four cylinder engine (E4) for naturally aspirated operation and a six cylinder engine (E6) for both naturally aspirated and turbocharged operation. Experimental work involved evaluating the general performance of the engines through energy balance and in-cylinder investigations at various operating

conditions. Combustion descriptors are used as reference indicators towards comparative assessment of producer gas and conventional fuel thermo-kinematic response. Numerical studies are addressed based on two mathematical models in the broad scope of thermodynamic simulation. The first is a zero dimensional model wherein the entire in-cylinder domain is considered as a lumped system and heat release is handled through a cumulative distribution type expression known as the Wiebe function, with producer gas specific coefficients. The second - a quasi dimensional model evolves the in-cylinder heat release based on the propagation of a hypothetical flame along the Eddy Entrainment Laminar Burn-up (EELB) concept. The hypothetical flame segregates the in-cylinder domain into a lumped burned and a lumped un-burned zone.

A peak load of 72.8 kWe (BMEP 9.47) is realized on engine E6 at maximum brake torque ignition angle of 22 deg before the top dead center and turbocharger compressor pressure ratio of 2.25. Realizing the peak load required turbocharged matching and optimization and is attributed to the variations in fuel thermo-physical properties. Specific biomass consumption of 1.00 $\pm$ 0.05 kg/kWh translating to biomass to electricity efficiency of 23.0 $\pm$ 1.1% is recorded. Engine energy balance established higher cooling load (in excess of 30%) compared to typical fossil fuel operation. Higher cooling load is attributed to the presence of nearly 20% hydrogen which enhances the convective cooling characteristics through the higher thermal conductivity. Modeling studies reveal the gas side convective heat flux to be different when pure specie transport properties are evaluated using kinetic theory correlations as compared to evaluation based on temperature specific correlations. The convective heat flux is observed to linearly respond to the mixture hydrogen fraction. This aspect is further investigated by parametric variation of hydrogen fraction on the two cylinder engine (E2) using four different syngas compositions with mixture hydrogen fraction varying from 7.1% to 14.2%. It is observed that the engine cooling load increases from 33.5% to 37.7% as the mixture hydrogen fraction increases from 7.1% to 14.2%,depicting the influence of hydrogen in enhancing the cooling load. Conventional fuel benchmarking, especially for the in-cylinder response, and subsequent comparison (for the same frame) is realized using the four cylinder engine (E4) which is operated with both natural gas and producer gas over a range of loads close

stoichiometry.

Fundamental difference between fossil fuel and producer gas operation has been established based on the in-cylinder response of the pressure crank angle, heat release and mass burn traces and their derivatives. Significant deviations in the heat release profile, particularly pronounced in the second half combustion duration (50% to 98%), are observed and are attributed to the presence of hydrogen in the mixture. In an extended investigation on the two cylinder engine (E2) involving hydrogen parametric variation, it has been observed that with an increase in mixture hydrogen fraction (from 7.1% to 14.2%), while the fast burn phase combustion duration reduces from 59.6% to 42.6%, the terminal stage duration increases from 25.5% to 48.9%. The enhanced cooling of the mixture (due to the presence of hydrogen), particularly in the vicinity of walls is argued to contribute towards the sluggish terminal phase combustion. The influence of the altered thermo-kinematic response for producer gas fuelled operation extends to zero dimensional simulations wherein the simulations fail when conventional fuel Wiebe coefficients are used, establishing the need for fuel specific coefficients. With fuel specific Wiebe coefficients, the present work has established the suitability of zero dimensional numerical analysis for varying operating conditions ranging from naturally aspirated to turbo charged engines, compression ratios and different engine geometries.

Acknowledging the limitation of zero dimensional model (deterministic nature), the thermodynamic analysis is extended to quasi dimensional model development and simulation. The laminar flame speed and turbulent parameters as required by the EELB module of the quasi dimensional model are estimated using pressure and temperature correlations and cold flow computation fluid dynamic analysis using ANSYS FLUENT solver. The flame speed ratio of 4.5 ± 0.5 for naturally aspirated operation with turbulent Reynods number of 2500 ± 250 and 9.0 ± 1.0 for turbocharged operation with turbulent Reynolds number of 5250 ± 250 are comparable with literature reported data, validate the choice of laminar flame speed and turbulent parameters. In-cylinder engine simulation results for engine E4 (for natural gas and producer gas fuelled naturally aspirated operation) and E6 (for naturally aspirated and turbocharged after cooled producer gas fuelled operation)are compared with experimental results. It has been shown that the deviations of simulation results

from experiments remain within the acceptable limits for mixture quality variations 1.0 ± 0.1 from stoichiometry. On the sensitivity to ignition angle, it is observed that flame kernel initialization angle cannot directly follow the physical ignition angle change from maximum brake torque timings and the start of combustion needs to be fixed based on experimental mass burn fraction analysis. The quasi dimensional analysis is extended to simulation of end gas auto-ignition in the un-burned mixture region. The model is validated by using the experimental manifold conditions for turbocharged operation of engine E6 for which knock has been observed. Extending the model to a Waukesha cooperative fuels research engine, motor octane number between 105 and 110 is reported for standard composition producer gas. The reported number is midway between AVL methane number of 90 and experimentally reported methane number of 125.

Both the experimental and the numerical studies presented in the current work establish that the influence of thermo-physical properties of the fuel on the engine thermo-kinematic response and general performance is significant

Chapter 1

Introduction and literature review

1.1 Overview

The past century has relied, rather overwhelmingly, on fossilized energy resources to meet the ever increasing energy demand (Heinberg 2010) (Lamarque, Bond, Eyring, Granier, Heil, Klimont, Lee, Liousse, Mieville, Owen, et al. 2010). The extraction and combustion of fossilized resources formed over millions of years of natural processing within a short span of about a century and a half has brought to the fore two significant challenges. The first pertains to increasing demand-supply mismatch due to rapidly dwindling fossilized resources against robust growth in demand, leading to straining of economies around the world (Hoel and Kverndokk 1996) (Höök and Tang 2013). The second pertains to overall deterioration of global environmental health attributed to increased carbon-dioxide emissions due to combustion of fossilized fuels (Stocker, Qin, Plattner, Tignor, Allen, Boschung, Nauels, Xia, Bex, and Midgley 2014) (Meinshausen, Meinshausen, Hare, Raper, Frieler, Knutti, Frame, and Allen 2009) (Allen, Frame, Huntingford, Jones, Lowe, Meinshausen, and Meinshausen 2009). The described challenges demand critical intervention, of emergency nature, to prevent or atleast slow down further deterioration of the environmental health and economic condition which otherwise could prove catastrophic for the entire mankind.

One of the potential mitigation option corresponds to the use of bio-derived non-regular fuels in existing energy conversion infrastructure, enabling partial / complete

displacement of fossilized resources (Demirbas 2008) (Demirbas 2009b) (Demirbas 2009a). Among the various energy conversion systems prevalent that use fossilized resources as input, internal combustion (IC) engines are one of the key technologies, particularly in the oil and gas space. The transport sector (especially the land and sea based) and the power generation sector (especially the sub Mega Watt per unit scale) almost exclusively depend on the IC engines route for chemical to mechanical energy conversion. Considering that IC engines constitute a major chemical to mechanical energy conversion technologies, intervention towards displacing fossilized fuel resources using bio-derived alternatives can contribute significantly towards realizing the broader goal of mitigation of economic and environmental challenges. The current investigations broadly addresses the use of producer gas (PG), a bio-derived gaseous alternative fuel in conventional natural gas (NG) engines, enabling complete displacement of conventional fossilized fuels with bio a derived alternative fuel.

Internal combustion engines potentially represent the most successful of chemical to mechanical energy conversion devices, their success largely attributed to the simple but robust nature of the underlying kinematics, versatility of the chemical compounds that can be used as fuel sources and the range of power requirement they can cater to. The conversion process is through phased heat release in the combustion chamber and represents a thermo-kinematic response. One of the key features of the thermo-kinematic response (and hence the generic engine performance) pertains to the sensitivity to the fuel-air mixture thermo-physical properties. In replacing NG with PG, a hydrocarbon fuel (predominantly methane) is replaced by a mixture of carbon monoxide, hydrogen and methane with inerts in excess of 50%, having thermo-physical properties significantly different from NG (refer table 1.1).

Such a change in the very basic nature of the energy carrier influences various segments of the thermodynamic cycle, potentially introducing substantial differences in the engine thermo-kinematic and hence generic response as compared to the base fuel response. Considering that fuelling of an NG engine with PG represents displacement of a high calorific value baseline hydrocarbon fuel with a low calorific value non-regular fuel, the response alteration could potentially be adverse. As such, detailed investigation of a PG fuelled operation of an NG engine is critical towards identification and quantification of various factors that influence the engine

Table 1.1: Thermo-physical properties of natural gas compared with producer gas

Property	Natural gas	Producer gas
Combustible components	$CH_4 - 96.5\%$	$CO - 20\%$
	$C_2H_6 - 1.8\%$	$H_2 - 20\%$
		$CH_4 - 2\%$
Fuel lower calorific value (MJ/kg)	46.04	5.0
Stoichiometric mixture calorific value (MJ/kg)	2.64	2.13

NOTE: Gas compositions are based on actual measurements

thermo-kinematic and generic full cycle response. The current work addresses the influence of fuel thermo-physical property variations on the engine thermo-kinematic and generic performance through investigations on stationary multi-cylinder generator application engines, operated under naturally aspirated and turbocharged after cooled mode. It is important to note that very limited work is reported in this sector, particularly in the scientific and technological sphere even though PG has been used as a fuel for IC engines since the second world war.

Having arrived at the need for investigating PG fuelled NG engines, the key areas requiring attention are to be identified. Towards the same, the available literature is reviewed and the scope of the study established.

1.2 Review of literature

Use of PG as a fuel for engines has been reported for both automotive and stationary power generating applications. The pre 1980 era is mostly replete with PG usage for automotive applications (Fernald 1909) (Heywood 1943) (Hurley and Fitton 1949) while post 1980, power generation has taken complete precedence. With stationary power generation using PG being of interest for the current investigation, the literature published in the past three decades is reviewed. It is important to note that over three decades, the literature addressing PG fuelled operation is meager as compared to the literature on engine operation with conventional fuels. The current section presents a brief overview of the available literature addressing both experimental

and numerical investigation of PG fuelled engine operation. In line with the broad theme of the current investigation, the review of literature is limited to stationary spark ignited (SI) engines for power generating applications. The key findings are summarized and are expected to serve as broad guidelines for defining the problem statement for the current work. The review of literature is presented in three broad sections covering PG as a fuel for engines, experimental investigations and numerical investigations.

1.2.1 Producer gas characterization

Reviewing the available literature pertaining to characterization of PG as a fuel for IC engines indicates limited availability. The available literature primarily deals with numerical and experimental characterization of PG in terms of the adiabatic flame temperature, flammability limits and laminar flame speed. A recent effort also explores estimating knock rating for producer gas in terms of methane number.

The first systematic work towards experimentally quantifying the critical properties of PG has been reported by Kanitkar et al (Kanitkar, Chakravarty, Paul, and Mukunda 1993). Kanitkar et al have reported on the laminar flame speeds, temperature and limits of flammability for producer gas combustion using a flame tube under atmospheric conditions. The peak flame speed has been reported to be 50 ± 5 cm/s in the vicinity of stoichiometry while the flammability limits are reported to be 0.47 ± 0.01 (lean) and 1.6 ± 0.05 (rich) with the corresponding flame speed being 10.3 cm/s and 13 cm/s respectively. On a parallel note, Chakravarthy et al (Chakravarthy, Mishra, Paul, and Mukunda 1993), based on numerical investigation, have reported on the speed of one dimensional planar laminar flame by considering variable transport properties and heat loss by radiation and have compared the results with the experimental results of Kanitkar et al (Kanitkar, Chakravarty, Paul, and Mukunda 1993). Chakravarthy et al have reported a peak flame speed of 52 cm/s at stoichiometry while the flammability limits are reported to be 0.42 and 1.93 respectively with the corresponding flame speeds of 5.82 cm/s and 6.2 cm/s. The wider flammability limits are attributed to the absence of convective effects in the simulation. Extending the work of Chakravarthy et al (Chakravarthy, Mishra, Paul, and Mukunda 1993), Mishra et al (Mishra, Paul, and Mukunda 1994), based on computational studies

have reported on laminar flame speed and structure for a slightly more energetic PG composition (hydrogen and carbon monoxide composition of 22.0% and 23.0% respectively). Mishra has reported a peak flame speed of 61 cm/s at ϕ of 1.2, consistent with the higher hydrogen and carbon monoxide levels and richer than stoichiometric peaking of laminar flame speeds (Lipatnikov 2012) (Turns) (Kuo and Acharya 2012). In increasing the pressure from 1 to 10 and 40 bars, the flame speed is seen to reduce to 4.8 and 2.8 cm/s respectively. Mishra has also attempted to correlate the behavior of PG with the major individual combustible components i.e, hydrogen and carbon monoxide by individually replacing the combustible components once with hydrogen and once with carbon monoxide respectively. The hydrogen dominated flame speed has been reported at 98 cm/s while the carbon monoxide dominated flame speed is at 9.8 cm/s. The heat release profiles for PG and hydrogen/carbon monoxide dominated gas are also significantly different. Mishra has concluded that since the behavior of hydrogen/carbon monoxide dominated gas combustion is substantially different from PG behavior, no concrete influence of either hydrogen or carbon monoxide can be brought out. Further, towards addressing the significance of detailed chemistry for evolving the PG laminar flame characteristics, based on an analysis involving estimation of the activation parameter $\left(\frac{E}{RT_{ad}}\right)$, Mishra et al conclude that a single step reaction or a reduced mechanism involving 2 steps may not be able to address the combustion of PG.

Hernandez et al (Hernandez, Lapuerta, Serrano, and Melgar 2005) have reported on the estimation of PG laminar flame speed at various equivalence ratios using the PREMIX module of CHEMKIN (Kee, Rupley, Miller, Coltrin, Grcar, Meeks, Moffat, Lutz, Dixon-Lewis, Smooke, et al. 2006). The simulation results have been compared with centrally ignited constant volume bomb results. For typical PG composition, peak laminar flame speed is reported at an equivalence ratio of around 1.4 with experimental and simulation flame speeds being 65 cm/s and 55 cm/s respectively. Hernandez attributes the lower simulation flame speed to the absence of stretch effects considering that CHEMKIN evaluates the speed of a planar flame. It is further suggested that the chemical auto-catalysis on the rich side of stoichiometry renders the mixtures highly reactive as against stoichiometric mixtures, leading to the flame speed peaking for rich mixture quality. Extending the analysis of Hernandez et al

Ouimette et al (Ouimette and Seers 2009) have compared the numerically estimated laminar flame speeds using CHEMKIN with experimental results. The experimental flame speeds are arrived at based on photographic measurements of conical flame area of a Bunsen burner for a known volumetric mixture flow rate. At 300 K and 1 bar pressure, experimental results indicate the peak flame speed to be around 23 cm/s, occurring at equivalence ratio of 0.97. The extremely low laminar flame speed is attributed to the rather poor quality gas used (hydrogen and carbon monoxide composition of 10.0% and 14.0% respectively). Numerical simulations however report the peak flame speed to be much lower at around 20 cm/s at equivalence ratio of around 1.1. The adiabatic flame temperature is reported to be around 1750 K.

Tinaut et al (Tinaut, Melgar, Giménez, and Reyes 2010) have reported on characterization of PG towards analyzing the maximum rate of heat release through OH chemiluminescence in a constant volume bomb. Tinaut et al have established a linear relation between the maximum rate of heat release and the time of maximum OH chemiluminescence. The influence of operating equivalence ratio on the propagation rate of the spherical flame front has also been analyzed. Based on the constant volume experiments and the results reported by Mishra et al (Mishra, Paul, and Mukunda 1994), Tinaut et al in an extended work (Tinaut, Melgar, Horrillo, and De La Rosa 2006) have reported on the PG specific coefficients ($\alpha = 2.0, \beta = -0.4$) for the standard laminar flame speed correlation as a function of pressure and temperature ratio (Metghalchi and Keck 1980) (Metghalchi and Keck 1982). The flame speed correlation and the use of coefficients α and β is described in detail in a subsequent section.

Serrano et al (Serrano, Hernandez, Mandilas, Sheppard, and Woolley 2008) have reported on the characterization of PG through experimental investigations involving Schlieren photography analysis of flame propagation in a constant volume bomb. The analysis is extended to numerical investigations involving estimation of planar one dimensional flame using the PREMIX module of CHEMKIN and GRIMech 3.00 reaction mechanism. Serrano et al have reported a close match of the peak laminar flame speed between simulations (65 cm/s) and experimental data (67 cm/s) under ambient conditions but indicate significant deviations at elevated pressures. Serrano et al has attributed the deviation to the early inception of flame cellularity and

associated increase in the laminar flame speed under practical conditions and the absence of any such physics in the PREMIX module.

Sridhar et al (Sridhar, Paul, and Mukunda 2005) have reported on the numerical analysis of PG laminar flame speed under engine like conditions (peak pressure of 50 bar, temperature of 1082 K and 10% recycled gas fraction). Laminar flame speed estimation has been based on one dimensional analysis of a propagating adiabatic laminar flame in the double infinity domain. A correlation for the laminar flame speed in terms of the mixture pressure and quality (equivalence ratio and recycled gas fraction) has been proposed which is subsequently extended to include the composition of the principle PG combustibles of carbon monoxide and hydrogen. The proposed correlation is unique in the sense that the laminar flame speed is not a function of the mixture temperature.

Summarizing the producer gas characterization results, based on experimental results, it is established that the laminar flame speed for PG is around 50 cm/s with adiabatic flame temperature of about 1800 K. Higher flame speed is attributed to the presence of hydrogen while lower adiabatic flame temperature is primarily attributed to the presence of close to 50% diluents in the fuel

1.2.2 Experimental investigations

Operational experiences, covering both lab and field installations pertaining to the use of PG in SI engines is reviewed in the current section.

The use of PG for fuelling SI engines dates back to the early 19th century. The pre 1980 era, covering a period close to two centuries, is replete with rather sporadic use of PG for fuelling automotive engines, mostly limited to situations when the availability of liquid hydrocarbons got disrupted. As such, systematic analysis of PG fuelled operation is very sparse prior to 1980. On the other hand, in last few decades, as the need for alternative fuels intensified, more systematic investigations involving PG fuelled operation has been reported. The current section presents the outcome of operational experience from 1990s till date. The discussion is segregated into three decades of 1990 to 1999, 2000 to 2009 and 2010 till present.

Period 1990 to 1999

The early literature pertaining to PG fuelled engine operation deals as much with

the conversion methodology of diesel engines as with the performance aspects. Prior to the discussion on operational experience, a work by Dasappa (Dasappa 2001) addressing the (analytical) estimation of power from a diesel engine converted for gas operation is discussed. The work by Dasappa primarily deals with identification and quantification of the key parameters that influence the power developed by such converted engines. The interpretations have been drawn primarily from available engine specifications and operational experience. It is expected that the arguments forwarded by Dasappa would help to appreciate the subsequent operational performance (reported by other authors) better. Based on a detailed theoretical analysis Dasappa suggests the compression ratio (CR), calorific value (CV), change in the number of moles post combustion and turbocharger pressure ratio as the key factors that influence converted engine power rating. Adaption of diesel engine to gas mode requires the reduction of CR (Heywood 1988) considering the knock limitations. Per unit reduction in the CR is reported to reduce the power rating between 1% to 3% of the peak load rating with a commensurate effect on the engine efficiency. The effect of CR on efficiency is verified by the CR parametric analysis in the Otto cycle efficiency also (Heywood 1988). Comparing the influence of mixture CV (fuel CV has been consciously avoided) for diesel with NG and PG, the higher mixture energy density of NG (by about 6%) is seen to be counteracted by the influence of reduced CR and efficiency, leading to a net power drop of about 8% from the base rating for CR change from typical diesel values of 17 to SI upper limits of 12. The influence with PG as the fuel is reported to be much severe considering that 15% lower mixture CV as compared to diesel gets compounded to the influence of reduction in CR and efficiency. The reduction in the number of moles of gases in the engine cylinder post combustion and the lower adiabatic flame temperature have been (qualitatively) reported to adversely affect the peak thermodynamic conditions and hence the fuel conversion efficiency. Addressing the turbocharged engine operation, Dasappa argues that the change in the in-cylinder thermodynamic conditions have a cascading influence on the turbocharger turbine inlet conditions with reduced enthalpy availability across the turbine. This in turn leads to lower pressure ratio across the compressor and hence lower engine power output. Towards qualifying the positioned arguments, Dasappa has reported on two test cases wherein estimated

peak power for diesel converted gas engines (based on the above arguments) is compared with experimentally realized loads. A three cylinder kirloskar diesel engine (RB33) rated at 28 kWe on converting to PG fuelled operation is reported to deliver 16.8 kWe with PG while the estimated load based on the presented analysis is 17.4 kWe. Similarly, a 6 cylinder Liebherr engine rated at 96 kWe on NG is reported to deliver 58 kWe on PG as against the estimated load of 56 kWe. As is evident, the estimated load for both the cases remains very close the realized load, validating the positioned arguments. In the current investigation, the reported information as presented in the foregone discussion is used as a broad guideline and the analysis is further strengthened and presented in terms of extended quantifiable parameters.

As for operational experience, Shashikantha et al (Shashikantha and Parikh 1992) (Shashikantha and Parikh 1993) have reported on the adoption of a diesel engine for PG fuelled operation in neat gas mode . In adapting the engine, the combustion chamber is modified to reduce the CR from 17 to 11.5. Knock free peak supported load of 12 kWe against baseline diesel rating of 17 kWe diesel is reported with highest thermal efficiency of 32 %. The pressure crank angle trace for different operating conditions is also reported. In an extended work (Shashikantha and Parikh 1999), the performance of the engine on PG and NG is compared and it is reported that the maximum brake torque timing for PG is at 35 deg while for natural gas it is 22 deg before the top dead center. Similarly Ramachandra (Ramachandra 1993) has also reported on PG fuelled operation of a diesel engine converted for gas mode operation. A de-rating of about 40% as compared to diesel mode is reported with a drop in the overall efficiency from 24% to 19%. The specific biomass consumption is reported at 1.13 kg/kWh at peak load.

Period 2000 to 2009

Munoz et al (Munoz, Moreno, Morea-Roy, Ruiz, and Arauzo 2000), in comparing the performance of a gasoline and PG fuelled operation report power de-rating of around 52% on PG fuelled operation while Tewari et al (Tewari, Subrahmanyam, and Babu 2001) report a de-rating of 20% and 40% from diesel rating for a diesel converted SI engine operating on gasoline and PG respectively. The corresponding peak load brake thermal efficiency is reported at 28% and 22% respectively.

Sridhar et al have reported on the adaptation and operation of small and medium

power level engines with PG (Sridhar, Paul, and Mukunda 2001) (Sridhar, Sridhar, Dasappa, Paul, Rajan, and Mukunda 2005). Detailed in-cylinder investigations are reported with focus on identifying maximum brake torque timing and the knock limited compression ratio. Considering the relevance of the work by Sridhar et al to the current investigation, a detailed review is presented as below.

Sridhar et al have converted a three cylinder naturally aspirated diesel engine rated at 24 kW for PG operation. The engine is operated at CR between 11.5 and 17.0, the upper limit being attributed to the reported drop in efficiency beyond CR of 17 (Caris and Nelson 1959). The maximum power output of 20 kW has been reported at CR of 17 with phi of around 1.1 as against 24 kW for corresponding diesel operation, representing a de-rating of about 17%. The maximum brake torque timing has been reported to be 6 deg and 16 deg before the top dead center for CR of 17 and 11.5 respectively. The other important aspect highlighted is the fact that no abnormal combustion has been reported at high CR of 17 even at ignition angle of 33 deg before the top dead center. This is interesting considering that the maximum brake torque timing has been set at 6 deg before the top dead center for 17 CR and the engine is operated 27 deg advanced from maximum brake torque timings. The knock resistance is attributed to the presence of hydrogen in the gas. Sridhar et al have also reported an increase in the exhaust gas temperatures by about 75 deg apart from higher cooling load (based on engine energy balance). Producer gas fuelled operation is subsequently extended to a medium power 12 cylinder turbocharged NG engine derived from diesel frame rated at 260 kW on NG at CR of 12. It is reported that this particular engine could be operated only at slightly leaner conditions of ϕ around 0.95 due to some limitations on the gasifier side. The maximum brake power is reported to be 182 kW at an efficiency of 28.3% when the ignition timing was set between 12 and 14. The corresponding load with NG is 270 kW at an efficiency of 34% indicating a power de-rating of about 28% for PG operation. The maximum brake torque timing for the medium power engine is around 3 deg retarded as compared to the small power engine which is attributed to turbocharging and higher mean piston speed. Higher cooling have also been observed for the medium power engine. On the emissions, NO emissions at around 0.05 g/MJ especially for CR typical of SI engines are reported to be well below various national and international standards and the

reason attributed for the same is the lower adiabatic flame temperature and close to top dead center ignition timing. On the other hand the CO emissions have been observed to be between 5 and 10 g/MJ, above the established norms and hence a cause of concern.

Ando et al (Ando, Yoshikawa, Beck, and Endo 2005) report on the performance of the single cylinder gasoline engine fuelled with PG. In adaption of the engine for PG operation, the CR was changed from 8.47 to 9.4 to potentially take advantage of the higher flame speeds of PG. A power de-rating of about 33% is reported at around 2000 rpm which subsequently increases to about 50% at higher engine speeds under wide open throttle conditions. The brake thermal efficiency for NG and PG operation is similar at about 23% for low speeds which reduces marginally for NG while dropping by 3% points for PG fuelled operation. The effect of excess air ratio has also been addressed. It is reported that while the stable lambda limit for gasoline is less than 1.5, the same for PG is around 2.0. The reason attributed is the wide flammability limit of hydrogen. The PG fuelled operation reports the exhaust gas temperature higher by about 100 K. While cumulative heat release profiles have been drawn up for various operating conditions, results are unclear considering that the line types for representing the graphs are very poorly chosen making it practically impossible to identify the fuel and operating condition for a given graph.

Henriksen et al (Henriksen, Ahrenfeldt, Jensen, Gøbel, Bentzen, Hindsgaul, and Sørensen 2006) in a work on uninterrupted operation of a gasifier engine system have reported a 20% power de-rating for PG fuelled operation of a NG engine with gas to mechanical efficiency of 28%. Papagiannakis et al (Papagiannakis, Rakopoulos, Hountalas, and Giakoumis 2007) have compared the performance of a 20 cylinder turbocharged gas engine fuelled with NG and PG. The maximum brake torque timing is reported at 25 deg before the top dead center with a corresponding peak load of 790 kWe at brake mean effective pressure of 13 bar and brake specific fuel (gas) consumption of around 700 g/kWh and 35% efficiency. The CO and NO emissions are reported at 94 g/kWh and 8.54 g/kWh respectively.

Period 2010 till present

Shah et al (Shah, Srinivasan, To, and Columbus 2010), on operating a gasoline fuelled portable generator with PG report power de-rating of about 43% as compared

to gasoline operation. The fuel to electricity efficiency is reported to be same at around 19% for both the fuels while CO / NOx emissions have been reported to be higher for PG fuelled operation. In a more recent work, Son et al (Son, Yoon, Kim, and Lee 2011) in comparing the performance of liquefied petroleum gas with PG in a three cylinder engine, reported the exhaust gas temperatures to be higher by around 100 deg for PG fuelled operation as compared to liquefied petroleum gas.

Dasappa has adopted a systematic approach towards addressing the fuelling of SI engines with PG for power generation by first addressing the unmodified adoption of small capacity naturally aspirated NG engines for PG operation (Dasappa, Sridhar, and Paul 2011). Subsequently, turbocharged operation of engines of two difference volumetric capacities is reported (Dasappa, Sridhar, and Indrajit 2011). Considering the relevance of the work by Dasappa et al to the current investigation, a detailed review is presented as below.

The preliminary work reported by Dasappa et al involving the adoption of a NG engine for PG operation is on a six cylinder NG engine with reported rating of 55 kWe on NG. The adaptation process involves fuel line modification (reportedly to accommodate higher PG flow rates) while no geometric modifications to the engine cylinder are made. Spark sweep tests based maximum brake torque timing is reported at 20 deg before the top dead center as against 28 deg for NG operation, the 8 deg retard is attributed to higher flame speeds for PG. Peak load of 27.2 kWe is reported with specific biomass consumption of 1.45 $\pm$ 0.05 kg/kWh and gas and biomass to electricity efficiency of 21$\pm$1.5% and 16$\pm$1% respectively. The peak supported load represents a de-rating of 50%. The gas to electricity efficiency of 21$\pm$1.5% for PG represents a drop of 8% (absolute) over NG gas to electricity of 29%. Based on engine diagnosis and tuning, the specific biomass consumption is reduced to the 1.15$\pm$0.05 kg/kWh range with a gas to electricity of 27%. The emissions under steady load and engine transient response are reported to be within the respective acceptable limits. It is also reported that lubricating oil analysis based on long duration test (500 hours) indicate various critical parameters like the viscosity, total base number etc to be within acceptable limits. While the tests qualify the unmodified operation of the engine with PG, the rather high de-rating prompted the adoption of a turbocharger towards power recovery. Preliminary results indicate a peak load of 36 kWe, a jump

of around 32% from naturally aspirated peak load. Extending the turbocharged operational experience, on field performance of two turbocharged engines, a twin bank 12 cylinder engine with CR 10 rated at 355 kWe on NG and a 6 cylinder engine with CR 8.5 rated at 168 kWe on NG is reported. Peak load of 230 kWe for the 12 cylinder engine and 110 kWe for the 6 cylinder engine is reported with gas to electricity efficiency of 28%. In both the cases, the power de-rating is around 35% from the respective NG rating, consistent with the de-rating on the small capacity engine. A detailed thermodynamic analysis of the turbocharger is also reported with compressor isentropic efficiency of around $73 \pm 3\%$. Dasappa et al have also reported on the long duration (1000 hours) operational experience of a 100 kWe gasifier-engine system grid connected system (Dasappa, Subbukrishna, Suresh, Paul, and Prabhu 2011). A 120 kWe turbocharged engine develops an average load of 85 kWe with peak loads of 100 kWe. The specific biomass consumption has been reported to be 1.36 kg/kWh with gas to electricity efficiency of 25% and biomass to electricity of efficiency of 18%.

Summarizing the results of experimental investigations, in general engine power de-rating in the range of 45 ± 5 % is reported on fuelling an NG engine with PG with the conversion efficiencies being in the range of 20 ± 2 %. An overall skewed energy balance is also reported with higher cooling loads and exhaust enthalpy. The increase in cooling and exhaust loads comes at the cost of the useful mechanical output. On the exhaust enthalpy, the contribution is reported from both thermal components (close to 100 K higher exhaust gas temperature as compared to conventional fuels) and chemical component (higher exhaust CO content). It is also interesting to note that, for comparable operating conditions and engine geometry, a wide range of maximum brake torque ignition timings from 15 deg before the top dead center to 35 deg before the top dead center have been reported. While most of the reported work pertains to naturally aspirated operation, some preliminary initiatives towards turbocharged operation suggest a mismatch for engine and turbocharger (conventional fuel optimized).

It is important to note that no concrete scientific reasons have been assigned to some of the observations made like skewed energy balance, power de-rating, higher exhaust gas temperature etc and they remain as such. Data pertaining to in-cylinder

investigation is also critically missing. Thus, while PG as a fuel for SI engines is broadly established, critical gaps pertaining to optimization efforts and scientific analysis of the thermo-kinematic response persist.

1.2.3 Numerical Simulations

Review of literature pertaining to numerical investigation of spark ignited internal combustion engines indicates exhaustive work in the area of fossil fuels. However, in the case of non-regular fuels in general and PG in particular, literature is extremely limited. The available literature corresponding to numerical simulations is presented in two broad segments. The first segment reviews the general philosophy adopted for modeling and simulation of spark ignited engines primarily towards understanding the broad classification of the models, the governing physics and model formulation strategy. The second segment reviews the available literature related to numerical investigation of PG fuelled operation of spark ignited engines and some of the key points reported are highlighted.

Modeling and simulation of SI engines – General methodology

Numerical simulations of spark ignited internal combustion engines indicates two broad categories of models; thermodynamic and fluid dynamic (Heywood 1988) (Stone 2012), with further sub-classification of the thermodynamic model as zero and quasi dimensional models. The thermodynamic models are basically phenomenological models based on the first law of thermodynamics and adopt a lumped approach. The complete engine response is expressed in terms of key identifiable and quantifiable processes which are generally modeled along the empirical approach, commensurate with experimentally observed results (Blumberg, Lavoie, and Tabaczynski 1979) (Heywood 1988) (Hrovat and Sun 1997) (Chiodi and Bargende 2001). The fluid dynamic models are characterized by the solution of the governing conservation equations in one, two or three dimensions (Blumberg, Lavoie, and Tabaczynski 1979) and are as such exhaustive. The described models represent two extreme ends of the spectrum. While the thermodynamic models emphasizing on evolution of spatially averaged properties (Heywood 1988) (Stone 2012) based primarily on the principle of conservation of energy, the fluid dynamic models emphasizing on the

spatial and temporal evolution of thermodynamic properties based primarily on the principle of conservation of energy as well as momentum (Versteeg and Malalasekera 2007)(Chung 2010).

The thermodynamic model is primarily based on the first law of thermodynamics (Heywood 1988) (Stone 2012) with the cylinder pressure rise being a function of the volume change and the heat transfer across the system boundary (during the closed phase of the cycle). The temperature change can be estimated based on the equation of state. The thermodynamic model in its simplest form is shown in the pair of ordinary differential equations as below and integrating the pair with appropriate initial and boundary conditions leads to the evolution of the spatially averaged thermodynamic properties of the engine.

$$\frac{dP}{d\theta} = \pm\frac{dV}{d\theta} \pm \frac{\delta Q}{\delta\theta} \qquad \frac{1}{T}\frac{dT}{d\theta} = \frac{1}{V}\frac{dV}{d\theta} + \frac{1}{P}\frac{dP}{d\theta}$$

With the temperature and pressure change within the engine cylinder being a function of the volume change rate and heat transfer rate and with the volume change rate being a kinematic parameter (dictated by engine geometric parameters only), thermodynamic modeling of the engine boils down to the estimation of the heat transfer across the system boundary. The engine heat transfer term is constituted of the convective heat transfer and heat release within the engine. Convective heat transfer is modeled along the Newton's cooling law (Bergman, Incropera, and Lavine 2011) (Yan and Guo 2012) using emperical correlations for the estimation of the convective heat transfer coefficient (Annand et al. 1963) (Borman and Nishiwaki 1987) (Finol and Robinson 2006). The thermodynamic modeling of an engine finally narrows down to mathematically capturing the heat release process within the engine which is in turn estimated from the mass burn profile. Thus, numerical simulation of SI engines primarily involves evolving the in-cylinder mass burn profile. The two models (zero and quasi dimensional) primarily differ in the mechanism adopted for heat release and the subsequent mathematical formulation. The approach adopted for modeling in-cylinder heat release through the mass burn in the zero and quasi dimensional model, as reported in the literature is briefly described below.

The zero dimensional model is the simpler of the two thermodynamic models and treats the in-cylinder heat release as a pure boundary phenomena with no in-cylinder dynamics considered (Ghojel 2010) (Heywood 1988). Heat release is modeled using pure empirical correlations of the cumulative distribution of a continuous variable type (Ghojel 2010) (Heywood 1988), the most widely used being the Wiebe function. The Wiebe function was proposed by the Russian scientist Ivan Ivanovitch Wiebe (hence the function name) in the 1950s for simulating the heat release in an engine. The heat release is modeled through three empirical parameters of combustion duration (considered curve fit range spanning from 2 % to 98 % for wide band consideration to 10% to 90% for narrow band consideration), the efficiency factor (representative of fuel conversion efficiency) and the shape factor, a generic tunable parameter. Literature reports the considered shape and efficiency factors of 2 and 5 (considering fuel conversion efficiency of 99.32%) respectively for conventional fuels (Ghojel 2010) (Heywood 1988) (Alla 2002) (Soylu 2002) (Soylu and Van Gerpen 2004). One of the critical observations made in the review of literature pertains to the use of efficiency factor as a randomly tunable parameter rather than parameters dictated by the exhaust analysis. Instances of choice of efficiency factors as high as 6.9 (Borg and Alkidas 2009) and 10 (Shiao and Moskwa 1995) in an effort to match the Wiebe heat release profile with the experimentally profiles are observed. Choice of efficiency factor as high as 10 is rather surprising considering that the fuel conversion efficiency achieves a value of 99.32 % at a=5 and changes to 99.99 % for a=10. The fuel conversion efficiency in a typical SI engine seldom crosses 98 % even under lean conditions (Heywood 1988). Tuning of a to match the heat release profile thereby seems unrealistic and is thermodynamically untenable. While the choice of the efficiency factor beyond a certain value is thermodynamically untenable, the fact that in absolute magnitude terms, the difference in the fuel conversion efficiency for any values beyond 4 remains negligible and also the fact that in-cylinder dynamics is consciously sought to be avoided, is seen to be the motivating factor for researchers to consider the efficiency factor as a general tunable parameter. Beyond the challenge associated with the choice of the coefficients, review of literature suggests that the thermodynamic model provides unmatched accuracy with experimental results over a range of operation conditions, quantified in terms of the magnitude and position of

peak pressure and the gross indicated mean effective pressure (Ramos 1986) (Stone and Green-Armytage 1987) (Gallo and Milanez 1992) (Caton 2000) (Rakopoulos, Michos, and Giakoumis 2008).

Reviewing the work on quasi dimensional models, heat release within the engine is modeled along the framework of propagation of a hypothetical flame front consuming the unburned mixture and releasing heat within the engine cylinder (Heywood 1988). The model is designated so considering the fact that the in-cylinder heat release is dictated by a propagating flame front (a geometric entity) within the ambit of lumped approach. Considering that the heat release is dictated by the propagation of a hypothetical flame front, the crux of quasi dimensional modeling rests in appropriately capturing the physics of the flame propagation. Towards modeling the flame propagation within the engine, the regimes of turbulent combustion as relevant for engine like conditions are reviewed (Abraham, Williams, and Bracco 1985) (Poinsot, Veynante, and Candel 1991) (Peters 2000) (Veynante and Vervisch 2002). With the smallest turbulent scale being larger than (or comparable in size) laminar flame thickness, turbulent combustion within the engine is reported to be in the Wrinkled laminar flame regime (Abraham, Williams, and Bracco 1985) (Poinsot, Veynante, and Candel 1991) (Peters 2000) (Veynante and Vervisch 2002) with the sole effect of turbulence on the flame front being to convolute / wrinkle it while the flame structure (temperature and concentration profile) remaining largely unaffected. Turbulent burn rates in the engine are realized by an increase in the flame propagation area due to convolution of the front. Review of experimental evidences based on schlieren and laser techniques support the argument of wrinkled laminar flame regime (Keck 1982) (Gatowski, Heywood, and Deleplace 1984) (Keck, Heywood, and Noske 1987). Along the identified regime of turbulent combustion, the turbulent burn rate has been modeled based on the conservation of mass principle as the product of the un-burned mixture density, flame area and flame propagation velocity. The most widely used model reported in literature towards realizing the turbulent burn rates within an engine cylinder corresponds to the Eddy Entrainment and Laminar Burn-up model proposed by Keck et al and others (Blizard and Keck 1974) (Tabaczynski 1976) (Tabaczynski, Ferguson, and Radhakrishnan 1977) (Keck 1982) (Beretta, Rashidi, and Keck 1983). In the model, the convoluted tur-

bulent flame is considered to be a regular sphere intersecting with the containing surfaces and propagating at local laminar flame speed. Turbulent burn rate is realized by considering convection of unburned turbulent eddies across the flame front from the unburned side to the burned side. The eddies that are convected (termed entrainment) to the burned side of the flame front side considered to instantly ignite and burn peripherally inwards at local laminar flame speed. The adopted approach completely eliminates the need for modeling the complicated convolution process (Gouldin 1987) (Chen, Lumley, and Gouldin 1988) but elegantly captures the turbulent burning rate. The eddies are considered to be of the size of turbulent length scale while the convection of the eddies across the flame front is dictated by the prevailing local turbulent intensity. Literature reports the use of a variety of correlations towards estimating the turbulent parameters, primarily the turbulent intensity in terms of the un-burned density and the mean intake flow velocity [Keck, J. C. (1982)]. The laminar flame speed under engine like conditions is estimated using a best fit correlation with the reference laminar flame speed (ambient conditions), and in-cylinder pressure and temperature as the parameters (Metghalchi and Keck 1980) (Gülder 1984) (Stone, Clarke, and Beckwith 1998). The quasi dimensional model following the eddy entrainment and laminar burn up concept is used exhaustively for thermodynamic engine simulation and is found suitable for a variety of operating conditions and fuels (Shen, Hinze, and Heywood 1996) (Grill, Billinger, and Bargende 2006) (Verhelst and Sierens 2007) (Verhelst and Sheppard 2009).

On the full scale computational fluid dynamics approach for numerical simulation, while there are established solvers like ANSYS-CFX, ANSYS-FLUENT, STAR CD, CONVERGE etc, the fundamental question that needs to be addressed pertains to the suitability of such models for the task at hand which primarily involves characterizing the engine response for non regular fuelled operation. Blumberg et al (Blumberg, Lavoie, and Tabaczynski 1979) in comparing the fluid and thermodynamic models as applicable for a variety of engines and simulation situations recommend the use of detailed fluid dynamics based models for evolving sophisticated phenomenological models (zero and quasi dimensional models discussed) which themselves can subsequently be used for extensive parametric investigation. In essence, (Blumberg, Lavoie, and Tabaczynski 1979) suggest the use of full three dimensional

fluid dynamics models primarily to refine the different phenomenological, empirical correlations that form a part of the thermodynamic models thereby improving their degree of accuracy and level of confidence in them. The thermodynamic models so developed, based on evolved phenomenological correlations, are to be subsequently used for extensive parametric investigations. The suggestion is made primarily in light of the temporal challenge and hence the limited utility of computational fluid dynamics models for rapid parametric investigation (Gosman 1999). Richard et al (Richard, Bougrine, Font, Lafossas, and Le Berr 2009) report on the use of full three dimensional computational fluid dynamics with extended coherent flame model towards refining the turbulent surface evolution, knock and pollutant formation modules for subsequent use in a zero dimensional model. It is reported that the refined 0D model provides a very good agreement with the experimental results. Some work along similar lines has also been reported by Babajimopoulos et al (Babajimopoulos, Assanis, Flowers, Aceves, and Hessel 2005) wherein certain critical inputs are drawn from full computational fluid dynamic simulations towards parametric investigation of a premixed charge compression engine.

Modeling and simulation of SI engines – Producer gas fuelled operation

Shashikantha et al have reported on the development of first law based zero dimensional model (Klose, Parikh, et al. 1994) where the turbulent flame speed is a product of laminar flame speed and a tuned flame factor. Turbulent combustion within an engine is thus realized based on random tuning to establish a close match for the position and magnitude peak pressure. Centeno et al (Centeno, Mahkamov, Lora, and Andrade 2012) have reported on the zero dimensional numerical investigation of a downdraft gasification system combined with a spark ignited engine system. Heat release in the engine is modeled along an empirical cosine burning law. The model is principally use to estimate the extent of engine power de-rating when gasoline is replaced with PG and power de-rating of up to 40% is estimated for a range of engine speeds. No in-cylinder data, either experimental or numerical is reported.

Sridhar (Rao 2003) has reported on the development of a quasi dimensional model towards numerically investigating PG fuelled operation of an engine. The reported quasi dimensional model adopts a lumped approach following the eddy entrainment

and laminar burn concept. Sridhar (Rao 2003) has used the quasi dimensional model to simulate a range of operating conditions, primarily covering different compression ratios (11.5 to 17.0) and ignition timings. The reported simulations correspond to a 28 kW (diesel rating) three cylinder engine with a hemi-spherical bowl in piston and central ignition and a 310 kWe (diesel rating) 12 cylinder engine with a cylindrical bowl in piston and offset ignition. Sridhar (Rao 2003) reports a close match for the simulation results with the experimental results (in terms of the position of the magnitude and position of peak pressure) for advanced ignition (indicated mean effective pressure deviation less than 10 %) while substantial deviations are reported for retarded ignition. The deviations are attributed to reverse squish effects and are accounted by a *Reverse Squish Flame* hypothesis. While some improvements are reported on adoption of reverse squish flame hypothesis, significant differences still persist. Based on the analysis, Sridhar concludes that thermodynamic models are too simplistic in nature to accommodate complex fluid dynamic effects towards accurately predicting the engine operation.

1.2.4 Summary

Summarizing the literature reviewed in the scope of experimental investigations, almost all the reported work primarily deals with generic engine performance, restricted primarily to peak load analysis and emissions. The range of operating conditions explored is also limited with the investigation infrastructure restricted to lab scale test setup. Overall, it is observed that a critical and exhaustive analysis addressing the influence of variations in fuel thermo-physical properties (as a result of fuelling a natural gas engine with a non regular fuel like PG) on the complete cycle generic performance and the in-cylinder thermo-kinematic analysis is missing and needs exploration. No attempt to address the influence of fuel thermo-physical properties and variation in thermo-kinematic response on elements upstream and downstream of the engine cylinder is evident.

In the scope of numerical investigations, while a range of models, from zero dimensional to full three dimensional are reported in literature. However, applications specific to PG fuelled operation and subsequent analysis is limited. Further, in many instances, empirical/general coefficients tuned for conventional fuels are summarily

extended for simulation of non regular fuels, which could potentially be thermodynamically untenable. Another key aspect pertains to the enabling of end gas auto-ignition feature in the simulation models for normal combustion. It is observed that while models with higher dimensionality (computational fluid dynamics models) overwhelmingly adopt empirically tuned induction time based correlation, enabling reaction kinetics based knock prediction ability is generally limited to zero and quasi dimensional models primarily using reduced reaction kinetics mechanism. Knock prediction through numerical investigation for PG fuelled operation is virtually non-existent.

1.3 Approach of the current thesis

Addressing the engine response towards quantifying the influence of variations in fuel thermo-physical properties on the process and cycle response on fuelling an NG engine with PG based on experimental investigations and numerical studies is the primary objective of the current work.

Experimental investigations are carried out on three multi-cylinder stationary power generation application NG engines derived from baseline diesel frames with different ratings. One of the engine is turbocharged after cooled while the other two are naturally aspirated. The generic cycle average performance (emissions and energy balance) is quantified through the analysis of energy distribution involving the quantification of peak supported load, the cooling load and the exhaust thermal and chemical enthalpy (also covers emissions). The thermo-kinematic response is quantified through the acquisition and analysis of in-cylinder pressure traces, subsequently used for deriving the heat release / mass burn trace. The in-cylinder pressure traces are acquired as a function of crank angle using a spark plug adapted pressure sensor. Parametric investigations involve ignition angle (spark sweep test), load and mixture quality. Being production engines, parametric variation of CR is not realized. The analysis is primarily restricted to stationary power generation engine considering that PG as a fuel is consumed in-situ. The overview of experimental investigations proposed in the current work is presented in figure 1.1.

Numerical investigations involve the characterization of PG of standard compo-

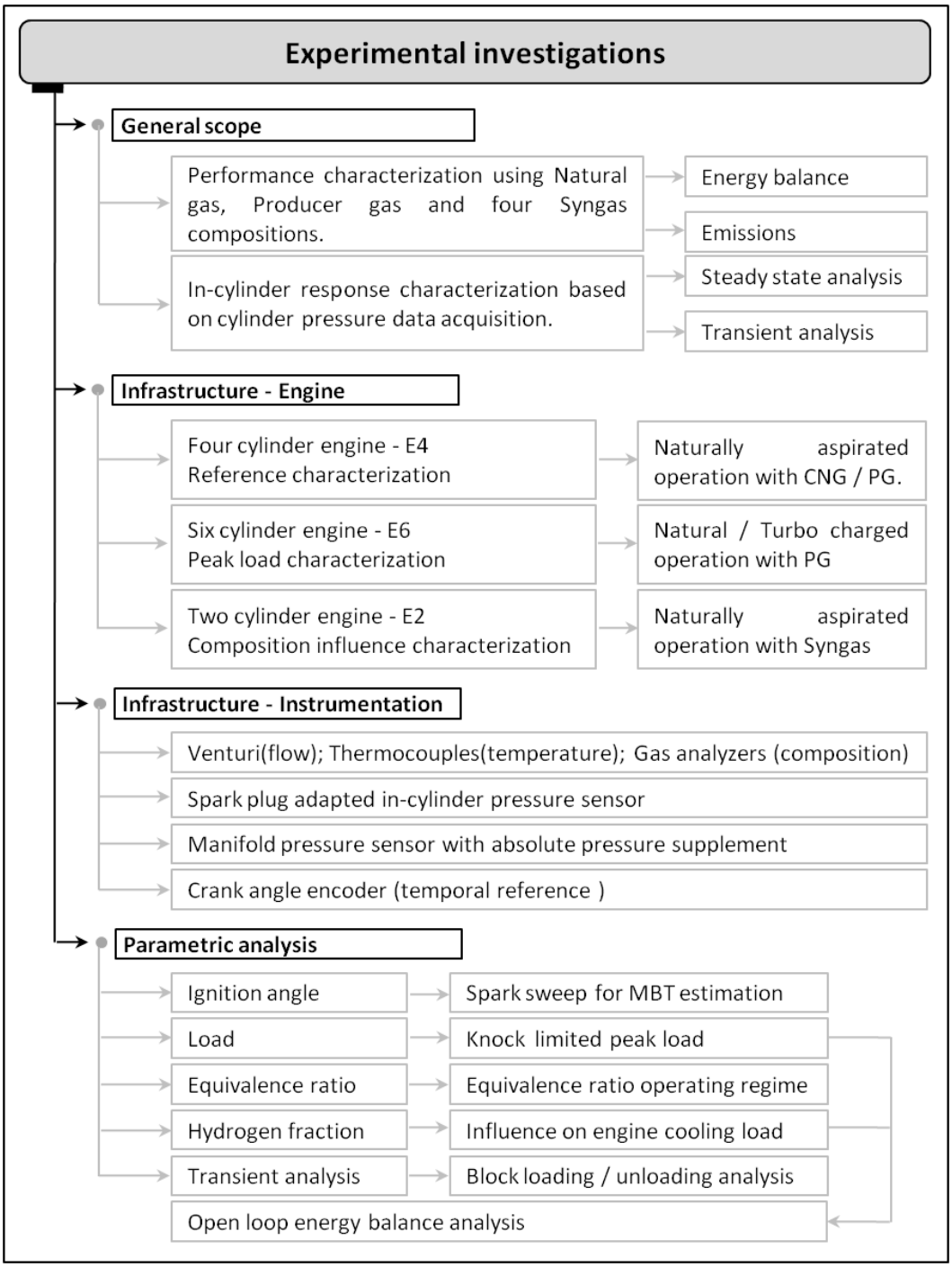

Figure 1.1: Overview of experimental investigations proposed in the current work

sitions in terms of parameters like adiabatic flame temperature, laminar flame speed and structure etc., and simulation of engine operation adopting two models within the broad framework of thermodynamic models. The two models developed in the

current investigation correspond to a pure zero dimensional model and a quasi dimensional (pseudo one dimensional model). The zero dimensional model adopts a full domain lumped approach and handles the in-cylinder heat release as a pure boundary phenomena through an empirically tuned cumulative distribution function. The quasi dimensional model handles the in-cylinder heat release through the propagation of a turbulent flame which segregates the in-cylinder domain into lumped burned zone and lumped un-burned zone. The quasi dimensional model is extended to enable knock prediction, primarily the occurrence and crank angle, by releasing the frozen chemistry constraint and introducing reaction kinetics. The overview of numerical investigations proposed in the current work is presented in figure 1.2.

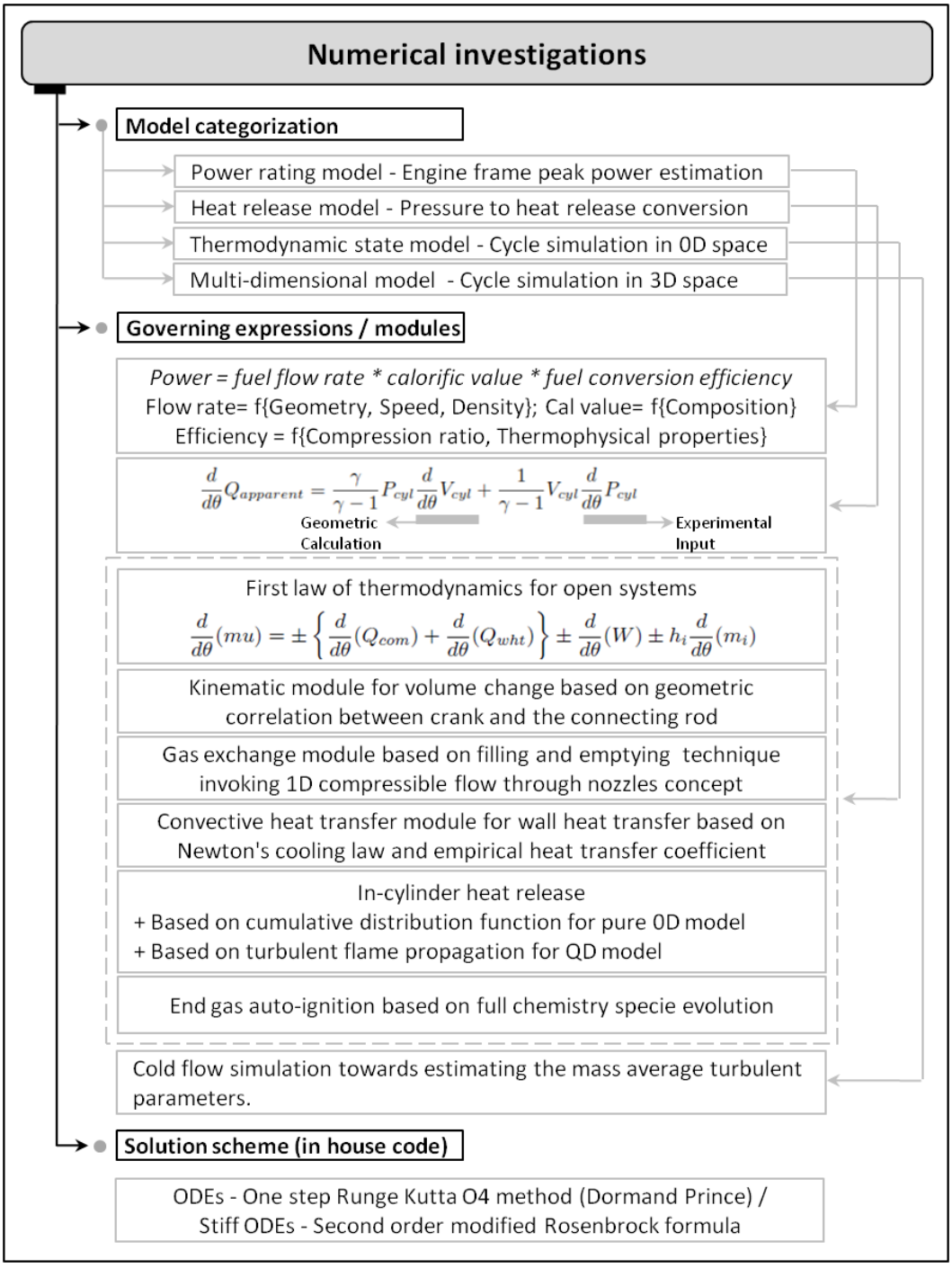

Figure 1.2: Overview of numerical simulations proposed in the current work

1.4 Road map

The complete work is organized into eight different chapters. The first chapter (Introduction and literature review)introduces the need for and concept of fuelling conventional engines with non regular fuels. The available literature is reviewed in detail to get a complete overview in respect of fuelling conventional fuel engines with non regular fuels and the scope of the current work is broadly defined. The second chapter (Generation and thermo-physical properties of syngas) addresses the basic principles of producer gas / syngas generation, the rector configuration used for generating producer gas/syngas, and the key thermo-physical properties of producer gasas relevant for engine operation.In discussing the thermo-physical properties, the emphasis is on the key thermo-physical properties of producer gas that differ substantially from conventional fuels, primarily natural gas. The third chapter (Experimental investigations: Apparatus and procedure) described the engine and instrumentation infrastructure, the scope of investigations and the methodology adopted. The experimental procedure adapted in the present study and the methodology used for analyzing the data is highlighted. The fourth chapter (Theoretical analysis for peak load estimation for an engine frame), based on the first principles, arrives at an expression for estimating the peak power rating of an engine frame in terms of key governing parameters and estimates the power rating for the engine frames considered in the current investigation for diesel, natural gas and producer gas/syngas.The analysis reported in this chapter account for all possible factors that influence the engine power rating as a result of displacing the conventional fuel with the non regular fuel.The estimates arrived in this chapter form the theoretical benchmarks for producer gas fuelled operation and provide a direction for diagnostic intervention in the event of critical differences in estimated and realized performance.The fifth chapter (Experimental investigations and results) describes the experimental investigations of the different engine frames with natural gas and producer gas/syngas and the key results covering both generic performance and in-cylinder investigation are reported.Some of the key response deviations observed are analyzed and correlated with the fuel thermo-physical properties. The sixth chapter (Numerical simulation - Model formulation) describes the governing philosophy and mathematical formula-

tion of two thermodynamic models considered for numerical simulation in the current investigation while the seventh chapter (Numerical simulation - Results) presents the results of the numerical simulation and compares them with the experimental results. The eighth and final chapter (Conclusions and future Work) consolidates the overall outcome of the investigation and describes the scope of future work.

Chapter 2

Generation and thermo-physical properties of syngas

The generation and thermo-physical properties of producer gas and syngas, the two bio-derived fuels used in the current investigation are discussed in this chapter. The chapter first briefly introduces the basic principles of biomass gasification towards generation of producer gas and syngas. Subsequently the downdraft gasifier is described in open top mode for air gasification as required for producer gas generation and closed top mode for oxy-steam gasification as required for syngas generation. Finally the key thermo-physical properties of producer gas and syngas (of considered composition) that have an influence on the overall engine performance are discussed in detail in comparative reference to typical conventional fuels like natural gas and gasoline.

2.1 Biomass gasification basics

Gasification is a sub-stoichiometric (overall excess air ratio of 0.25) thermo-chemical biomass conversion process involving a combination of oxidative pyrolysis and hot char reduction reaction. Gasification yields a predominantly gaseous combustible mixture with components like carbon monoxide, hydrogen, small fraction of methane, carbon dioxide and nitrogen. While the overall excess air ratio is maintained at 0.25, within the reactor, the excess air ratio may vary from close to zero to well above unity

at various local zones or pockets. As such, in a gasifier, a biomass particle undergoes thermo-chemical processes of drying, pyrolysis, combustion and reduction involving both homogeneous and heterogeneous reactions as it passes through various zones of the gasifier. Gasification of biomass with air as the gasifying agent yields what is commonly known as producer gas while replacing air with oxygen and/or steam yields hydrogen rich combustible gas known as syngas.

Using air as the gasifying agent and excess air ratio (λ) of around 0.25, biomass gasification yields a combustible gas known as producer gas with typical composition of 19 $\pm$ 1 % carbon monoxide and hydrogen, 2 $\pm$ 0.5 % methane with balance 45 $\pm$ 1 % in-combustibles (carbon dioxide and nitrogen) and lower calorific value of 4.9 $\pm$ 0.1 MJ/kg. Replacing air as the gasifying agent with super-heated steam and oxygen leads to generation of hydrogen rich gas. The variation of hydrogen to carbon monoxide molar ratio and lower calorific value with steam to biomass ratio is shown in figure 2.1. The reader is directed to Sandeep and Dasappa (Sandeep and Dasappa 2014b) for further details pertaining to oxy-steam gasification.

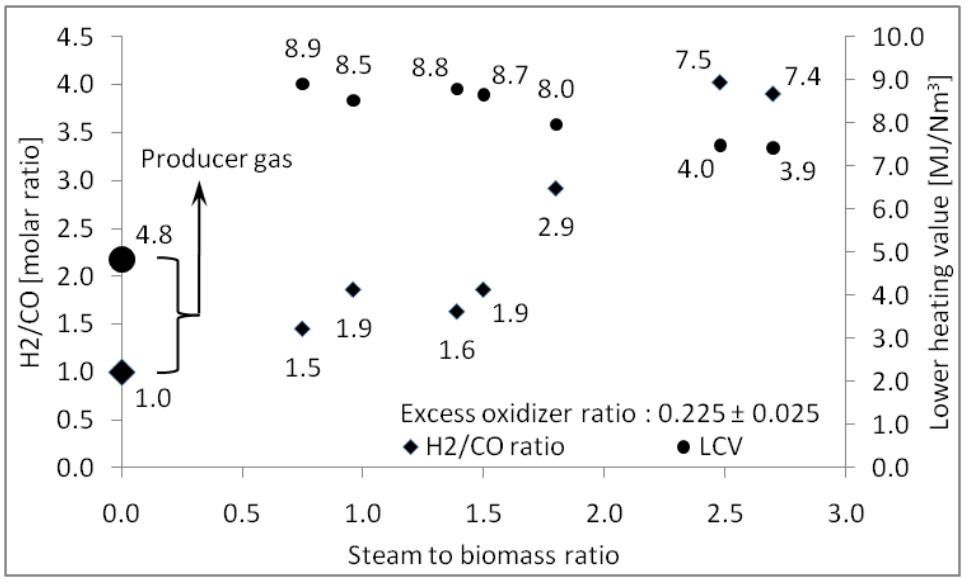

Figure 2.1: Influence of steam to biomass ratio on syngas H2/CO ratio and lower calorific value

Thus, biomass can be converted into producer gas / syngas of desired combustibles composition by the judicious choice of the gasifying agent (air / oxy-steam) and maintaining excess air ratio in the 0.225 $\pm$ 0.025 regime.

2.2 Down-draft gasification system

Figure 2.2 presents the configuration an open top downdraft gasification system developed at and patented by Combustion Gasification Propulsion Laboratory at the Indian Institute of Science (Dasappa, Paul, Mukunda, Rajan, Sridhar, and Sridhar 2004). The two principle segments of the gasification system are (a) the reactor and (b) the downstream gas cooling and cleaning train and are discussed individually as below.

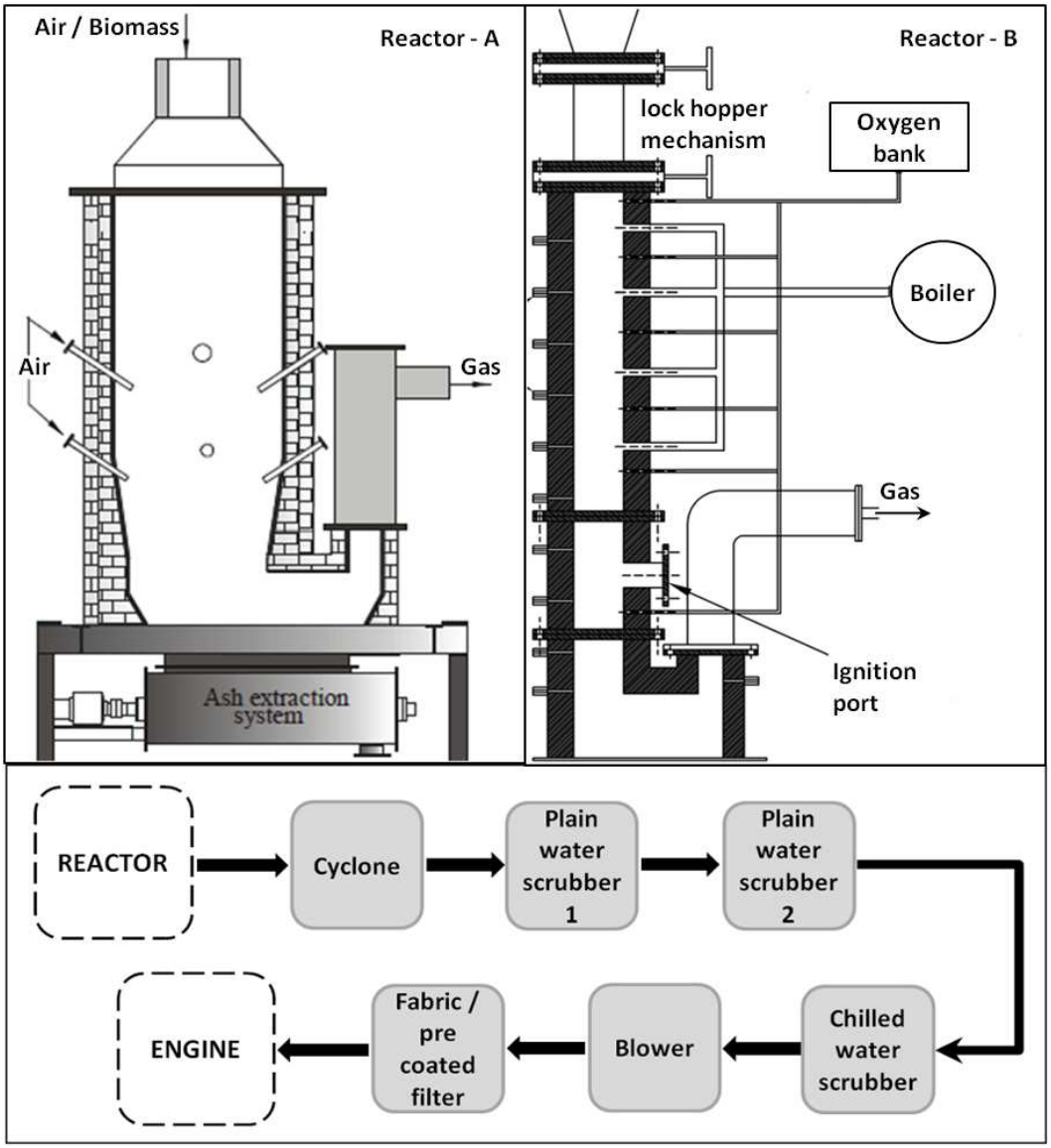

Figure 2.2: Downdraft gasification system. Reactor(s) and process flow diagram

2.2.1 The reactor

The reactor is the principle component of the gasification system where the thermo-chemical conversion of biomass to gaseous fuel takes place. In figure 2.2, two reactor conigurations, Reactor-A and Reactor-B are shown. On both the configurations, the reactor is predominantly a cylindrical chamber lined with ceramics on the inside and connected to a screw conveyor type ash/char extraction unit at the bottom. The screw conveyor based ash extraction system permits positive ash and char extraction, permitting the use of a variety of biomass with different ash content. The gas is drawn from the reactor base being connected to the suction side of the blower.

Reactor-A represents an open top re-burn downdraft configuration, developed at and patented by Indian Institute of Science, for air gasification. The reactor has a twin air entry configuration drawing air from the top as well as side air nozzles. Nearly 70 % of the air is drawn from the top and balance from the side air nozzles. With the top being open, biomass can be fed continuously / periodically into the reactor without any disruption in the operation. With air as the gasifying media, under steady state operation, the reactor generates combustible gas with composition typical of producer gas. Reactor-B is a slightly modified version of Reactor-A and is used for oxy-steam gasification. The principle difference is that the reactor is now isolated from the atmosphere and oxygen and steam are supplied through separate arrangements. Lock hopper mechanism is made available for both biomass feeding and ash/char extraction so as to ensure uninterrupted operation of the gasifier. The complete description of construction and performance of oxy-steam gasification system has been reported by Sandeep and Dasappa (Sandeep and Dasappa 2014b) (Sandeep and Dasappa 2014a).

2.2.2 Gas cleaning and cooling system

The gas issuing out of the reactor is hot and contains tar (condensables higher hydrocarbons) and ash, conditions not favorable for engine operation. While the high gas temperature adversely affects the engine volumetric efficiency, presence of tar leads to sticky operation of moving parts and presence of particulate potentially damages the cylinder liner and the valve seats (Reed 1981). The tar and ash content of pro-

ducer gas at the exit of the reactor is consolidated in table 2.1 (refer (Dasappa, Paul, Mukunda, Rajan, Sridhar, and Sridhar 2004) (Mukunda 2011)) while the prescribed gas quality requirement for smooth operation of engine/turbine application is consolidated in table 2.2 (refer (Milne, Abatzoglou, and Evans 1998) (Stassen 1993) (Hasler and Nussbaumer 1999)). The significant gap between the required gas quality and what is available at the exit of the reactor, necessitates a train of gas cleaning and cooling systems downstream of the reactor.

Table 2.1: Producer gas quality at the exit of the reactor

Parameter	Units	Magnitude
Temperature	$^{\circ}C$	500 ± 50
Tar	mg/Nm^3	< 200
Particles	mg/Nm^3	< 1000
Particle size	μm	< 200

Table 2.2: Gas quality requirements for power generation application

Parameter	Units	IC engines	Gas turbines
Particles	mg/Nm^3	< 50	< 30
Particle size	μm	< 10	< 05
Tar	mg/Nm^3	< 100	–
Alkali metals	mg/Nm^3	–	0.24

The gas issuing out of the reactor is first passed through a cyclone with particulate cleaning efficiency of 85 ± 5 %. The gas exiting the cyclone has particulate content of under 200 mg/Nm^3 and with a temperature drop of about 250 K, cooling to gas to about 300 $^{\circ}C$. Subsequent to the cycle is a system of water scrubbers wherein the gas is sprayed directly with high pressure atomized water. The gas existing the cyclone is first passed through a couple of ambient temperature water scrubbers and lastly through a chilled water scrubber wherein externally chilled water at temperature of about 6 $^{\circ}C$ is used. Scrubbing of the gas with ambient and chilled water leads to

separation of water soluble tar and fine sized particles (through agglomeration) that escape separation in the cyclone. The gas exiting the scrubber system would be at a temperature of close to 10 $^{\circ}C$ and tar and particulate content of under 2 mg/Nm^3 (Dasappa, Paul, Mukunda, Rajan, Sridhar, and Sridhar 2004) (Mukunda 2011)), well within the prescribed gas quality for engine and turbine (relevant for turbocharger compressor from engine perspective) operation (refer table 2.1 and 2.2). The gas is finally passed through a filtration system which traps all particulates at and above the size of 5 microns, as dictated by the need for turbine operation. The engine quality gas coming out of the filtration system is supplied to the internal combustion engine. It is important to note that in passing through the train of cooling and cleaning systems, the gas experiences significant pressure drop and to overcome the same, an appropriately sized blower is used which delivers the gas to the engine at close to ambient pressure.

It may be noted that, the gasification technology of open top downdraft configuration used in the current investigation has been exhaustively used for power generation ranging from 5 kWe to 1000 kWe (Dasappa, Subbukrishna, Suresh, Paul, and Prabhu 2011) (Dasappa, Sridhar, and Paul 2012) (Dasappa, Sridhar, and Indrajit 2011) . The gas composition and quality has been exhaustively evaluated and found to be acceptable for engine operation. The typical arrangement of an opentop downdraft gasification system with the downstream cooling and cleaning elements is as indicated in figure 2.3

2.3 Thermo-physical properties of gaseous fuels

Chemical to mechanical energy conversion in an SI engine, through phased heat release in the combustion chamber, is significantly influenced by the thermo-physical properties of the fuel air mixture. The key thermo-physical properties of producer gas/syngas considered in the current research are evaluated and compared with the properties of typical conventional fuels.

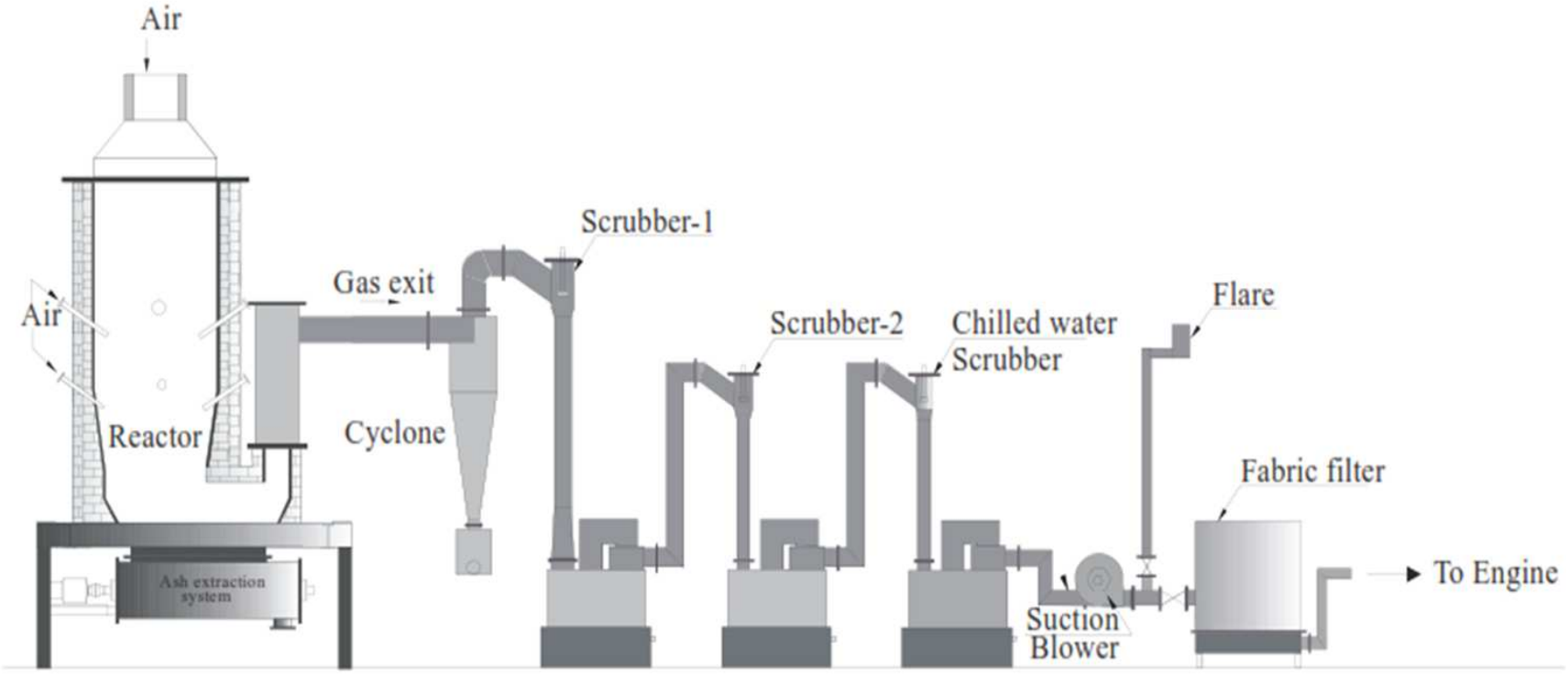

Figure 2.3: Open top downdraft gasification system configuration

2.3.1 Gas and mixture composition

In the current work, five different gas compositions have been considered, catering to specific requirements. One of the compositions is typical of standard producer gas while the other four pertain to varying combustible composition, primarily hydrogen. Producer gas is designated as PG while the four syngas compositions are designated from SG-1 to SG-4. The gas composition and corresponding stoichiometric mixture composition in volume fraction are consolidated in table 2.3. Of the four syngas compositions, SG-1 and SG-2 are direct products of oxy-steam gasification (Sandeep and Dasappa 2014b) while SG-3 and SG-4 are obtained by appropriate mixing of syngas of typical composition 45 ± 2 % H_2 , 24 ± 1 % CO, 26 ± 2 % CO_2 and 5 ± 1 % CH_4 with standard producer gas, each generated in a separate system.

Table 2.3: Producer gas / Syngas and stoichiometric mixture composition (volume %)

Designation	CO	H_2	CH_4	CO_2	N_2	O_2
	Fuel gas (%)					
PG	19.0	18.0	01.8	12.0	49.2	00.0
SG-1	11.5	12.8	02.3	10.8	62.6	00.0
SG-2	13.0	19.4	02.8	11.3	53.5	00.0
SG-3	14.4	25.9	02.9	19.0	37.8	00.0
SG-4	16.4	37.2	03.6	24.7	18.1	00.0
	Stoichiometric mixture (%)					
PG	09.3	08.8	00.9	05.8	64.5	10.8
SG-1	06.4	07.1	01.3	06.0	69.9	09.3
SG-2	06.4	09.5	01.4	05.5	66.5	10.7
SG-3	06.4	11.6	01.3	08.5	60.6	11.6
SG-4	06.3	14.2	01.4	09.4	55.7	13.0

From table 2.3 it can be observed that, for the four gas-air mixture compositions, only the H_2 fraction varies (from 7.1 % for SG-1 to 14.2 % for SG-4) while the other combustibles CO and CH_4 remain broadly invariant in the fuel air mixture. The

variation in composition is to address the (isolated) influence of hydrogen on the engine performance.

2.3.2 Fuel and stoichiometric mixture thermo-physical properties

The thermo-physical properties like calorific value, specific heat, thermal conductivity and diffusivity for producer gas/syngas, H_2, CH_4 and gasoline along with their corresponding stoichiometric mixture are estimated and consolidated in this section. The thermo-physical properties are estimated based on correlations as presented in appendix A and are consolidated in Table 2.4.

It is important to note that one of the key parameters of the fuel i.e., the lower calorific value is significantly lower for syngas, close to a tenth of the conventional fuels (refer table 2.4). Due to the low air to fuel ratio, the stoichiometric mixture calorific value for syngas (the parameter of significance for practical combustion systems) is lower by about 20 ± 5 % compared to conventional fuels. The direct influence of the lower mixture calorific value is on the engine energy input and the corresponding energy output for a given engine capacity. Thus, an engine operating under stoichiometric conditions fuelled with methane air mixture is expected to experience a de-rating (atleast) commensurate with the difference in mixture calorific value between the two fuels.

The other key properties are the mixture thermal conductivity and diffusivity. It is evident from table 2.4 that for producer gas air mixture, the thermal conductivity is close to three times that of conventional fuels like methane and gasoline. The higher thermal conductivity coupled with low density for producer gas air mixture also ensures higher thermal diffusivity as compared to methane-air and gasoline-air mixtures. The direct consequence of enhanced thermal conductivity and diffusivity is on the engine cooling load. Invoking the physics of turbulent convective heat transfer for flow through pipes / between flat plates (for an engine, the former is relevant when the ratio of instantaneous cylinder head - piston distance to bore diameter is large and the later is relevant when the ratio is small), the convective heat flux is estimated

using Newton's cooling law as in equation 2.1.

$$\dot{Q}''_{wht} = h_{c,g}[\overline{T}_g - \overline{T}_w] \tag{2.1}$$

As evident from equation 2.1, for a given temperature difference, the heat flux is a function of the convective heat transfer coefficient $h_{c,g}$. For the considered configuration, $h_{c,g}$ is evaluated based on the correlation relating the Nusselt number (Nu) with the Reynolds (Re) and Prandtl (Pr) number (Incropera 2011) as in equation 2.2. From equations 2.1 and 2.2, it can be observed that the heat flux is linearly dependent on the thermal conductivity.

$$Nu = \varrho Re^{\alpha} Pr^{\beta} = \Phi Re^{\alpha} \quad ; \quad h_{c,g} = \Phi \frac{k}{B} Re^{\alpha} = \Phi \frac{k}{B} \left[\frac{\rho V B}{\mu}\right]^{\alpha} \tag{2.2}$$

It is evident from the above analysis that higher thermal conductivity of producer gas - air mixture influences the convective heat flux and adversely affects the engine energy balance, potentially leading to engine power de-rating.

2.3.3 Flame properties

The laminar flame characteristics; temperature, speed and structure are determined using the chemical kinetics package CHEMKIN (Kee, Rupley, Meeks, Miller, and Chemkin-III 1996) which uses a freely propagating one dimensional laminar flame in double infinity domain by solving for the relevant conservation equations. The GRI-Mech 3.0 reaction mechanism (Smith, Golden, Frenklach, Moriarty, Eiteneer, Goldenberg, Bowman, Hanson, Song, Gardiner Jr, et al. 1999) involving 325 reactions (with 3 duplicates) and 53 species is used for the reaction kinetics.

Three flame related properties are evaluated and compared with that of methane which is the reference fuel. The comparison is reported for both ambient and engine like conditions; the former provides the reference information while the latter is relevant for engine application.

Adiabatic flame temperature

The adiabatic flame temperature at considered mixture quality and prevailing conditions basically dictates the peak cylinder temperature and fuel conversion efficiency.

In case of turbocharged engines, the influence of adiabatic flame temperature is experienced in terms of the exhaust gas enthalpy, a key parameter influencing the performance of the turbocharger. The adiabatic flame temperature for the considered fuels under ambient and engine like conditions are consolidated in figure 2.4.

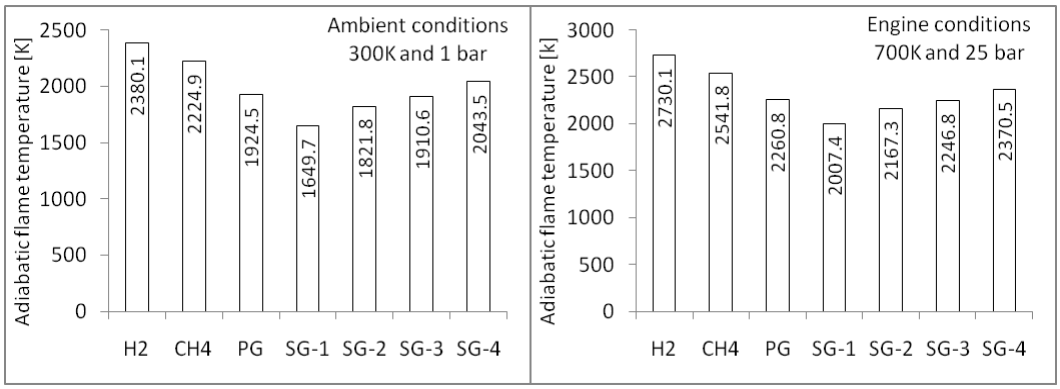

Figure 2.4: Adiabatic flame temperature of different fuels at ambient and engine like conditions

It can be observed that the adiabatic flame temperature for producer gas and the four syngas compositions remains lower than H_2 and CH_4 temperatures. The reduction is primarily attributed to the presence of diluents CO_2 and N_2, influencing the gas calorific value (refer table 2.4) leading to lower adiabatic flame temperature. From ambient to engine like conditions (700 K and 25 bar corresponding to end of compression thermodynamic state) the increase in the adiabatic flame temperature is in the range of 325 ± 10 K. The increase is primarily attributed to the increase in unburned gas temperature with pressure having very nominal effect; restricted only to suppression of dissociation of the gaseous species (Turns).

Laminar flame speed

The laminar flame speed data for the relevant fuels under both ambient and engine like conditions is consolidated in figure 2.5. It can be observed that for both ambient and engine like conditions,the laminar flame speed increases with increasing hydrogen fraction which is consistent with general understanding. A review of literature (Rao 2003) (Sridhar, Sridhar, Dasappa, Paul, Rajan, and Mukunda 2005) indicates the laminar flame speed for producer gas to be higher by about 25 % as compared

to methane, attributed to the presence of hydrogen in the mixture. Further, all the literature corresponding to producer gas fuelled operation of SI engines, reports ignition angle retard as compared to baseline natural gas operation towards realizing knock free maximum brake torque (Sridhar, Sridhar, Dasappa, Paul, Rajan, and Mukunda 2005) (Dasappa, Sridhar, and Paul 2011). It is however, important to note that the consolidated results in figure 2.5 suggest producer gas laminar flame speed to be lower by about 16 % as compared to natural gas.

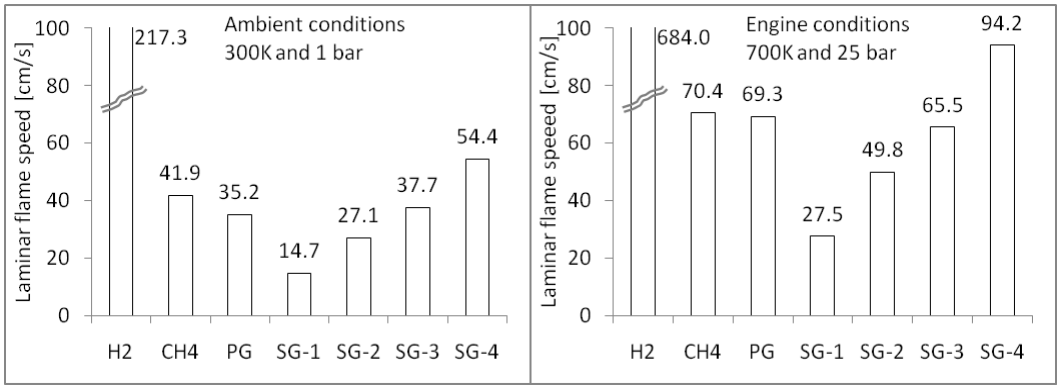

Figure 2.5: Estimated laminar flame speed for various fuels under under ambient and engine like conditions at stoichiometry

Towards addressing this discrepancy, a number of experimentally reported values for producer gas laminar flame speed are compared with simulation results in table 2.5. The $\pm$ band about the mean accounts for all possible errors associated with the measurement of the laminar flame speed. It is interesting to note that CHEMKIN with GRIMech 3.0 reaction mechanism consistently underestimates the laminar flame speed for producer gas. While the typical reported experimental laminar flame speed is 50 $\pm$ 2 cm/s, the estimated laminar flame speed is around 35 cm/s. This behavior is seen to be typical for hydrogen-carbon monoxide-methane-carbon dioxide mixture flames (Natarajan, Nandula, Lieuwen, and Seitzman 2005) not generally observed for methane flames (Halter, Chauveau, Djebaili-Chaumeix, and Gökalp 2005) (Gu, Haq, Lawes, and Woolley 2000).

Towards addressing the differences between the numerical and experimental flame speeds, it is important to note that in CHEMKIN, the laminar flame speed corresponds to a steady, un-stretched one dimensional flame in the double infinity domain.

Experimental flames however experience stretch due to curvature and aerodynamic strain, potentially leading to flame acceleration (Law 1989). Further, literature suggests that the presence of hydrogen in the combustible mixture leads to the domination of H based radicals, resulting in a lower than unity Lewis number and reduced laminar flame thickness. The direct consequence of the above two factors is the appearance and subsequent increase of flame surface instabilities resulting in flame *cellularity* (Kwon, Rozenchan, and Law 2002) (Li, Li, Sun, Zhai, and Zhou 2014) (Moccia and D'Alessio 2013). Cellularity is basically the wrinkling of the flame leading to an increase in the effective flame surface area (Mandilas, Ormsby, Sheppard, and Woolley 2007) (Tang, Huang, Wang, and Zheng 2009). The weaker influence of curvature and increased intensity of baroclinic torque (due to reduced flame thickness) and competing effects of thermal and mass diffusion ($Le < 1$) (Kwon, Rozenchan, and Law 2002) induce instability and cellularity in the flame causing a transition from smooth to cellular structure. The increase in the flame surface area due to cellularity leads to an increase in the flame propagation rate (Bradley, Sheppart, Woolley, Greenhalgh, and Lockett 2000) (Jomaas, Law, and Bechtold 2007) (Tang, Huang, Wang, and Zheng 2009) (Vu, Park, Kwon, and Kim 2009); similar to turbulent eddies increasing the flame propagation rate.

In the absence of the necessary physics governing the above described effects, especially the flame cellularity, CHEMKIN is bound to under predict the laminar flame speed. Further, considering that the flame instability is a combined thermo and fluid dynamic effect, capturing the governing principles in a one dimensional code is neither feasible nor practical. Such an exercise would require full three dimensional analysis and would become prohibitively expensive.

A review of literature corresponding to the estimation of the laminar flame speed using CHEMKIN for hydrogen-carbon monoxide-methane-carbon dioxide mixture system indicates the possibility of addressing this under prediction by changing the reaction mechanism considered. Yan et al (Yan, Wu, Liu, Yu, Li, Li, Chen, Bai, Aldén, and Konnov 2011) compared the experimental laminar flame speed using a flat flame burner with the results from CHEMKIN for four different syngas compositions. They have noted that while CHEMKIN under predicts the results with GRIMech 3.0 (upto 10 cm/s near stoichiometry), the results are comparable when the

reaction mechanism is changed to GRMech 2.11. Similar results have been reported by Huang et al (Huang, Sung, and Eng 2004) in the laminar flame speed analysis of reformer gas (with composition 28% hydrogen, 25 % carbon monoxide and 47 % nitrogen) wherein GRIMech 3.0 consistently under predicts the laminar flame speed by 10 cm/s in the mixture quality regime of $0.7 \leq \phi \leq 1.4$ while GRIMech 2.11 provides a very close match with experimental results. Som et al replace GRIMech 3.0 with the Davis mechanism (Davis, Joshi, Wang, and Egolfopoulos 2005) for precisely the same reason in assessing the flame characteristics of hydrogen - carbon monoxide flame (Som, Ramirez, Hagerdorn, Saveliev, and Aggarwal 2008). Considering that literature supports the use of alternative mechanism to realize matching predictions with experimental data, in the current work, the GRIMech 3.0 reaction mechanism is replaced with GRIMech 2.11 reaction mechanism considering its suitability in predicting the laminar flame speed. The GRIMech 2.11 reaction mechanism involves 277 elementary reactions involving 49 species and represent a reduction of 48 reactions and 4 species as compared to GRI Mech 3.0.

The laminar flame speed of producer gas / syngas under both ambient and engine like conditions, estimated with CHEMKIN using GRIMech 2.11 reaction mechanism is consolidated in figure 2.6. The estimated laminar flame speed is now comparable and well within the error band of the reported experimental laminar flame speed.

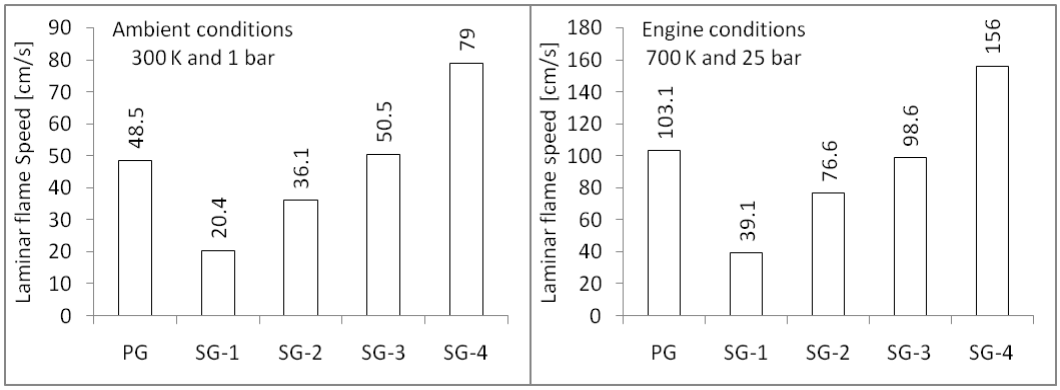

Figure 2.6: Estimated laminar flame speed for producer gas / syngas with CHEMKIN using GRIMech 2.11 reaction mechanism

2.4 Summary

The foregone discussions presented in this chapter clearly establishes the difference in properties for producer gas as compared to conventional fuels. The property estimation formulations (refer appendix A) and the consolidated data clearly establish the influence of hydrogen on the thermo-physical properties. The possible influence of the variations in the thermo-physical properties on the engine performance has been qualitatively stated.

Table 2.4: Thermo-physical properties of producer gas/syngas and corresponding stoichiometric mixtures

Property	Units	PG	SG-1	SG-2	SG-3	SG-4	CO	H_2	CH_4	Gasoline
Fuel properties										
Molecular weight	$(kg/kMole)$	25.02	26.12	24.43	23.96	21.85	28.00	2.00	16.00	102.50
Density (NTP#)	(kg/m^3)	1.023	1.068	0.999	0.979	0.893	1.14	0.08	0.65	5.11
Calorific value	(MJ/kg)	4.47	3.14	4.34	5.28	7.55	10.20	120.00	46.70	44.8
	(MJ/Nm^3)	4.57	3.35	4.34	5.17	6.74	11.63	09.84	30.45	228.90
Thermal conductivity	$(mW/m-K)$	40.1	35.9	41.8	46.7	56.3	22.80	182.00	34.30	11.20
Thermal diffusivity	(cm^2/s)	0.326	0.292	0.339	0.371	0.441	0.192	1.530	0.235	0.013
Stoichiometric air-fuel ratio	(kg/kg)	1.21	0.88	1.12	1.49	2.14	2.45	34.5	17.2	14.7
Fuel-air mixture properties corresponding to $\phi = 1.00$										
Molecular weight	$(kg/kMole)$	26.98	27.33	26.68	26.66	26.17	28.59	20.99	27.62	30.22
Density (NTP#)	(kg/m^3)	1.103	1.117	1.090	1.090	1.070	1.17	0.868	1.13	1.24
Calorific value	(MJ/kg)	2.02	1.67	1.95	2.12	2.41	2.96	3.38	2.57	2.85
	(MJ/Nm^3)	2.23	1.86	2.13	2.57	2.23	3.46	2.90	2.90	3.53
Thermal conductivity	$(mW/m-K)$	32.45	31.33	33.15	34.36	35.67	11.8	35.1	12.5	11.9
Thermal diffusivity	(cm^2/s)	0.268	0.259	0.274	0.282	0.293	0.100	0.296	0.103	0.090

Temperature 298.15 K and Pressure 1.01325 bar

Table 2.5: Literature reported laminar flame speed reported for producer gas under ambient conditions and $\phi = 1.0$

Reference	Combustibles			Experimental results		Simulation results	
	CO	H_2	CH_4	Set-up	S_L	Code	S_L
	% Volume				cm/s		cm/s
Kanitkar et al [a]	19.5	20.0	2.0	FT	50 ± 5	Not Reported	
Chakravarthy et al [b]	19.5	20.0	2.0	Referred [a]		In-House	52.0
Serrano et al [c]	24.0	21.0	0.0	CVB	49.0 ± 3	CHEMKIN [#]	42.5
Yan et al [d]	19.0	12.0	5.8	FFB	29.0 ± 2	CHEMKIN [#]	23.0
Hernandez et al [e]	24	20	2.0	CVB	54.0 ± 3	CHEMKIN [#]	41.0

[a] : (Kanitkar, Chakravarty, Paul, and Mukunda 1993)

[b] : (Chakravarthy, Mishra, Paul, and Mukunda 1993)

[c] : (Serrano, Hernandez, Mandilas, Sheppard, and Woolley 2008)

[d] : (Yan, Wu, Liu, Yu, Li, Li, Chen, Bai, Aldén, and Konnov 2011)

[e] : (Hernandez, Lapuerta, Serrano, and Melgar 2005)

FT - Flame tube; FFB - Flat face burner; CVB - Constant volume bomb; [#] Using GRIMech 3.0

Chapter 3

Experimental investigations : Apparatus and procedure

This chapter presents the specifications of the engines, the instruments used in the current investigation and the procedure adopted for performance evaluation. Since baseline NG engines are being used for PG fuelled operation, the basic engine adaptation procedure is also described. In the discussion on the engine instrumentation, special emphasis is on in-cylinder instrumentation considering that the in-cylinder response forms a critical component of the analysis. A detailed discussion regarding the uncertainty associated with the measurements and the cascading influence on calculated parameters is also presented.

3.1 Engine specifications

Towards analyzing the engine thermo-kinematic response, three multi-cylinder engines, with different volumetric capacities and in-cylinder geometry, have been investigated. The engines having two, four and six cylinders are designated as $E2$, $E4$ and $E6$ respectively. All the three engines are derived from baseline diesel framework and are available as natural gas fuelled SI generator sets. The engine $E4$ is equipped with a natural gas supply kit and is used for performance evaluation using natural gas as a fuel. It is important to note that since the engines are derived from baseline diesel frame, natural gas performance specifications are either not available or are

limited. The key geometric specifications along with baseline diesel power rating of the engines are consolidated in table 3.1.

Table 3.1: Engine geometric specifications

Geometric specifications				
	Units	$E2$	$E4$	$E6$
Number of cylinders	–	2	4	6
Bore	mm	91.4	97.0	102.0
Stroke	mm	127.0	100.0	120.0
Displaced volume	L	1.7	2.9	5.9
Connecting rod	mm	234.0	182.0	192.0
Piston bowl type	–	Conical	Conical	Cylindrical
Bowl depth	mm	20.0	16.0	19.0
Bowl top diameter	mm	70.0	67.0	72.0
Bowl base diameter	mm	63.0	57.3	72.0
Diesel power rating				
Engine speed	RPM	1500	1500	1500
Compression ratio	–	18.5:1	17.5:1	16.5:1
Electrical output	kWe	15.0	25.0	100.0
BMEP	bar	7.2	6.8	13.6
Spark ignited mode specifications				
Engine speed	RPM	1500	1500	1500
Compression ratio	–	11.0	11.20	10.5

Considering that the current work also forms a part of engine adaptation for non regular fuel, certain details like the engine model and some other specifications (especially pertaining to turbochargers) are not mentioned as per the non disclosure agreements.

3.2 Adaptation for producer gas operation

Operation of a natural gas engine on producer gas/syngas requires the modification of the intake section upstream of the throttle body. The substantially different fuel calorific value and the stoichiometric air-fuel ratio along with the different supply conditions for syngas demand modification of the standard gas engine fuel metering line/system. A simple analysis quantifying the fuel, air and mixture flow rates for unit MW energy input (refer table 3.2) based on the fuel thermo-physical properties (refer table 2.4) provides an insight into the modifications required upstream of the throttle body.

Table 3.2: Flow parameters ($\phi = 1$) upstream of throttle body per MW energy input

	Units	NG	PG	C1	C2	C3	C4
Fuel flow rate	kg/h	72.0	800	1146.5	863.3	681.4	476.8
Air flow rate	kg/h	1224.0	1080.0	1008.9	966.9	1015.9	1020.4
Mixture flow rate	kg/h	1296.0	1880.0	2155.4	1830.2	1697.7	1497.2

For similar energy input, the syngas flow rates are about ten times (composition dependent) that of natural gas, requiring re-sizing of the fuel line. Beyond duct re-sizing, the fact that syngas generated from biomass gasification route is close to ambient pressure, renders the natural gas pressure regulator, used for reducing the supply pressure from as high as 200 bar to close to ambient conditions, redundant and is accordingly eliminated. The fuel air mixer for natural gas (plunger needle type), designed for high air-fuel ratio, is replaced by a 'Y' shaped area ratio based mixer (refer figure 3.1 b) where the fuel and air are brought in along the individual arms and mixed at the throat. The relative proportions of gas and air entering mixing junction at the throat are controlled by a flap plate that controls the gas/air exit area. The area ratio based control of gas and air flow and hence the mixture quality requires the gas and air line pressures to be equal just upstream of the throat. To ensure the same, a zero pressure regulator (refer figure 3.1 a) is introduced in the gas line which reduces the gas pressure to the air line pressure. The zero pressure regulator is named so since it eliminates the pressure difference between the air and

gas line. The operational details and load response characteristics of the mixer-zero pressure regulator assembly (ability to supply set mixture quality over the entire load range) has been discussed in detail by Sridhar et al., (Rao 2003) (Sridhar, Sridhar, Dasappa, Paul, Rajan, and Mukunda 2005) and Dasappa et al. (Dasappa, Sridhar, and Paul 2012). Figure 3.2 shows the engine $E4$ before and after adaptation for producer gas fuelled operation with the key modified components highlighted.

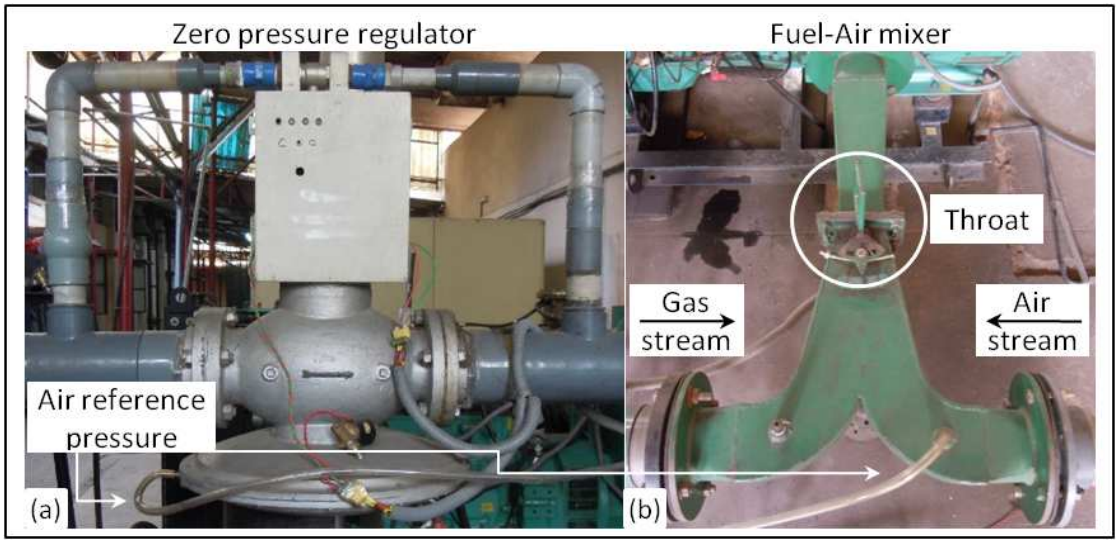

Figure 3.1: The zero pressure regulator and fuel-air mixer for producer gas fuelled operation

3.3 Instrumentation

As identified in the scope of work, the current investigation involves both general performance characterization and in-cylinder analysis. The instrumentation used in the investigation are described as below.

3.3.1 For general performance characterization

General performance characterization essentially involves arriving at the energy balance and quantifying the emissions. Drawing the energy balance primarily requires the measurement and quantification of parameters such as the gas composition, flow rate and temperature at various locations. The details pertaining to (stream wise)

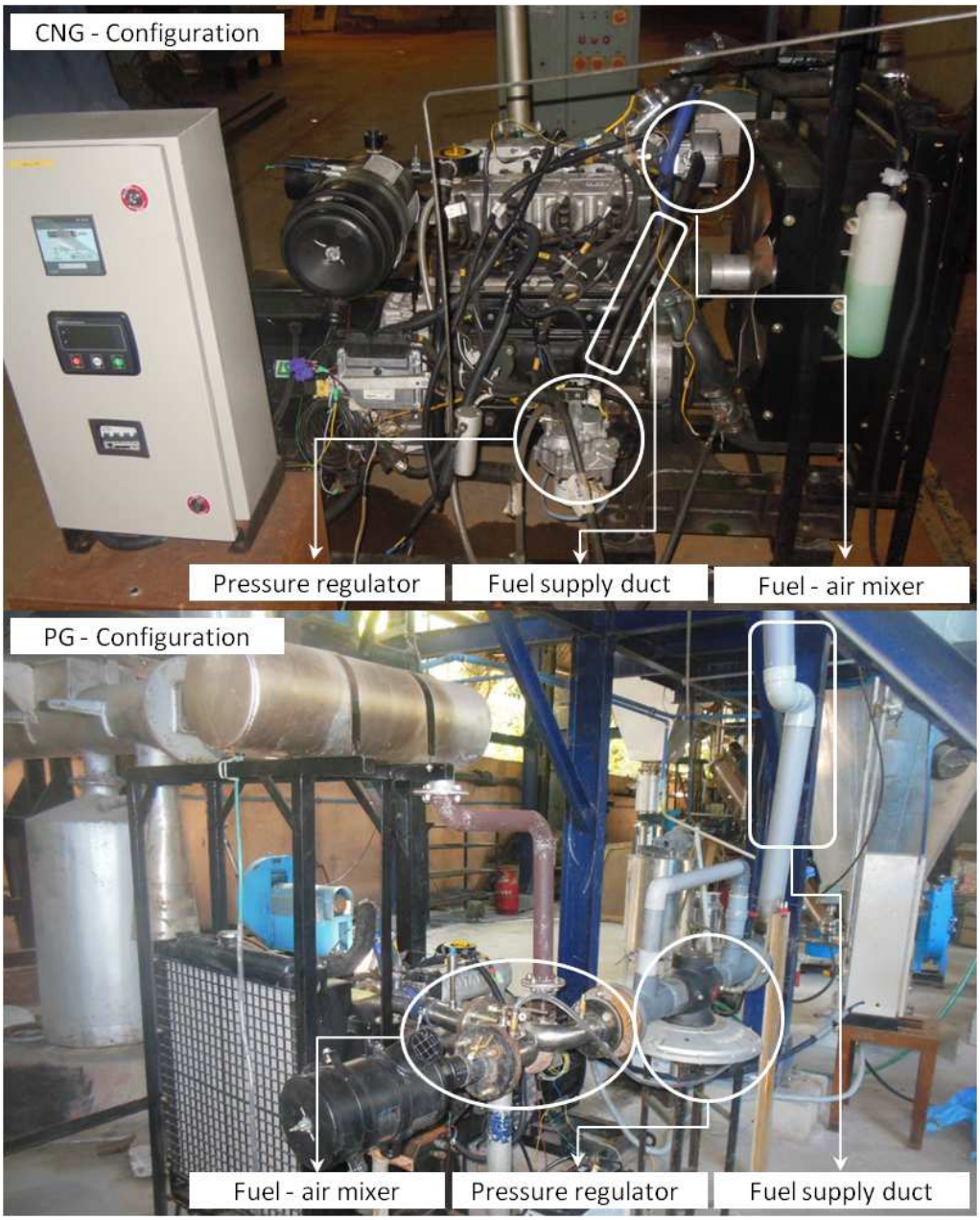

Figure 3.2: The four cylinder engine $E4$ in (a) natural gas mode and (b) producer gas mode

quantification of various parameters required for arriving at the energy balance are as discussed below.

1. **Energy input** : The energy input to the engine is quantified by measuring the gas composition using the SICK MAIHAK gas analyzer and the flow rate using a calibrated venturi with a manometer. The product of the lower calorific

value, estimated based on the gas composition and the mass flow rate from the venturi gives the energy input to the system as described in equation 3.1.

$$P_{in} = LCV_{ga} * \dot{m}_{ga} = \left[\sum_{1}^{n} X_{i,fu} * LCV_i\right] * \dot{m}_{ga} \tag{3.1}$$

2. **Brake load** : The brake load delivered by the engine is indicated by a Watt meter connected to the loading panel. The phase average voltage, current and the phase lag information is also indicated which permits explicitly verifying the indicated Wattage using the following equation;

$$P_{el} = \sqrt{3} * V_{av} * I_{av} * \cos(\phi) \tag{3.2}$$

3. **Cooling load** : The engines used in the current investigation are water cooled systems having a closed cooling water jacket circuit with a radiator. In the closed loop configuration the flow rate measurement is not possible and towards enabling the same, the radiator is replaced by a cooling tower allowing access to the coolant through a flow switch valve. Under steady state conditions the coolant flow rate is measured using fixed volume method wherein the time required for the accumulation of a fixed volume of coolant is measured using a stopwatch. The coolant flow rate along with the temperature at the inlet and exit permits quantifying the cooling load using equation 3.3.

$$\dot{Q}_{co} = \dot{m}_{co} * C_{p,co} * (T_{co,e} - T_{co,i}) \tag{3.3}$$

4. **Exhaust load** : The exhaust load refers to the enthalpy of the products of combustion exiting from the exhaust valve and comprises of the thermal and chemical enthalpy. The thermal enthalpy is quantified based on the exhaust mass flow rate and the difference in temperature between the exhaust gas (closest to the exhaust valve) and the ambient as described in equation 3.4.

$$\begin{aligned} \dot{Q}_{ex,th} &= \dot{m}_{ex} * C_{p,ex} * (T_{ex,e} - T_{am}) \\ &= (\dot{m}_{ga} + \dot{m}_{ai}) * \left[\sum_{i=1}^{i=n} \frac{X_{i,ex} * C_{pi,ex}}{MW_{ex}}\right] * (T_{ex,e} - T_{am}) \end{aligned} \tag{3.4}$$

The exhaust mass flow rate is the sum of fuel and air flow rate both of which are measured using a venturi with a manometer while the temperature is measured using K type thermo-couples. The chemical enthalpy refers to the chemical energy content of the fuel components that are present in the engine exhaust. The estimation of chemical enthalpy is described in equation 3.5. In equation 3.5, the standard state enthalpy is used (h_i^o) considering that the thermal component is already taken care of in equation 3.4.

$$\dot{Q}_{ex,ch} = \sum_{i=1}^{i=n} \dot{m}_i * h_i^o = \sum_{i=1}^{i=n} \left[X_{i,fu} * \frac{MW_{i,ex}}{MW_{ex}} * \dot{m}_{ex} \right] * h_i^o \tag{3.5}$$

The engine emissions are measured and quantified using KANE QUINTOX portable gas analyzer and emissions monitor. A stream of hot products of combustion is continuously extracted from the engine exhaust and passed through a condenser - calcium carbonate candle arrangement to cool and dry the same before supplying to the analyzer. The gas analyzers indicate the compositions in % or PPM of volume on dry basis. The technical specifications of the fuel and flue gas analyzer and other instruments are listed in table 3.3.

Table 3.3: Specifications of the instruments used in the experimental investigations

Parameter	Instrument	Range	Accuracy
Fuel gas	SICK MAIHAK		
CO		$0-100\%$	$\pm 0.05\%$
H_2		$0-100\%$	$\pm 0.05\%$
CH_4		$0-100\%$	$\pm 0.05\%$
$CO2$		$0-100\%$	$\pm 0.05\%$
O_2		$0-025\%$	$\pm 0.005\%$
Flue gas	KANE QUINTOX		
Air/gas flow	Venturi (C_d)		$\pm 1.0\%$ (full scale)
	Manometer		± 1.00 mm
Temperature	Thermocouple (K type)	$-200\text{to}1250^0C$	$>$ of $2.2^0C/0.75\%$
Power	Watt-meter	$0-100$ kW	$\pm 1.0\%$

3.3.2 For in-cylinder investigation

In-cylinder investigation is carried out by acquiring and analyzing the in-cylinder pressure trace(s) as a function of crank angle. The indicating system used in conjunction with data acquisition module for real time / post processing of the data is also described. The complete engine in-cylinder combustion diagnostic instrumentation is acquired from AVL LIST GmbH, Graz, Austria.

Pressure and crank angle measurement

In-cylinder pressure measurement requires access to the combustion chamber and in the current investigation, the same is achieved using a spark plug adapted pressure sensor, eliminating the need for any modification to the engine cylinder head. The sensor used in the current investigation is an un-cooled Gallium Orthophosphate ($GaPO_4$) differential pressure transducer mounted flush with the spark plug electrode end as shown in figure 3.3. The cylinder pressure is acquired in reference to the crank angle for which an optical encoder is used. The optical function is based on a slot mark disk and adopts the reflection light principle. The pressure crank angle data is acquired through a high speed data acquisition unit with built-in plausibility check for safe operation. The technical specifications of the in-cylinder pressure sensor, crank angle encoder and the data acquisition module are consolidated in table 3.4 below.

Zero level correction for differential to absolute conversion

The functional philosophy of piezo-electric pressure transducers permits them to pick up only the dynamic component of pressure $P_{dif}(\theta)$ and as such they can transmit only the differential pressure. The differential pressure has to be converted to absolute pressure by adjusting (essentially adding) against a reference pressure as in equation 3.6.

$$P_{abs}(\theta) = P_{dif}(\theta) + P_{ref}(\theta) \tag{3.6}$$

The intake manifold pressure close to the cylinder inlet for the crank angle range from the maximum valve lift to the bottom dead center is considered as the reference

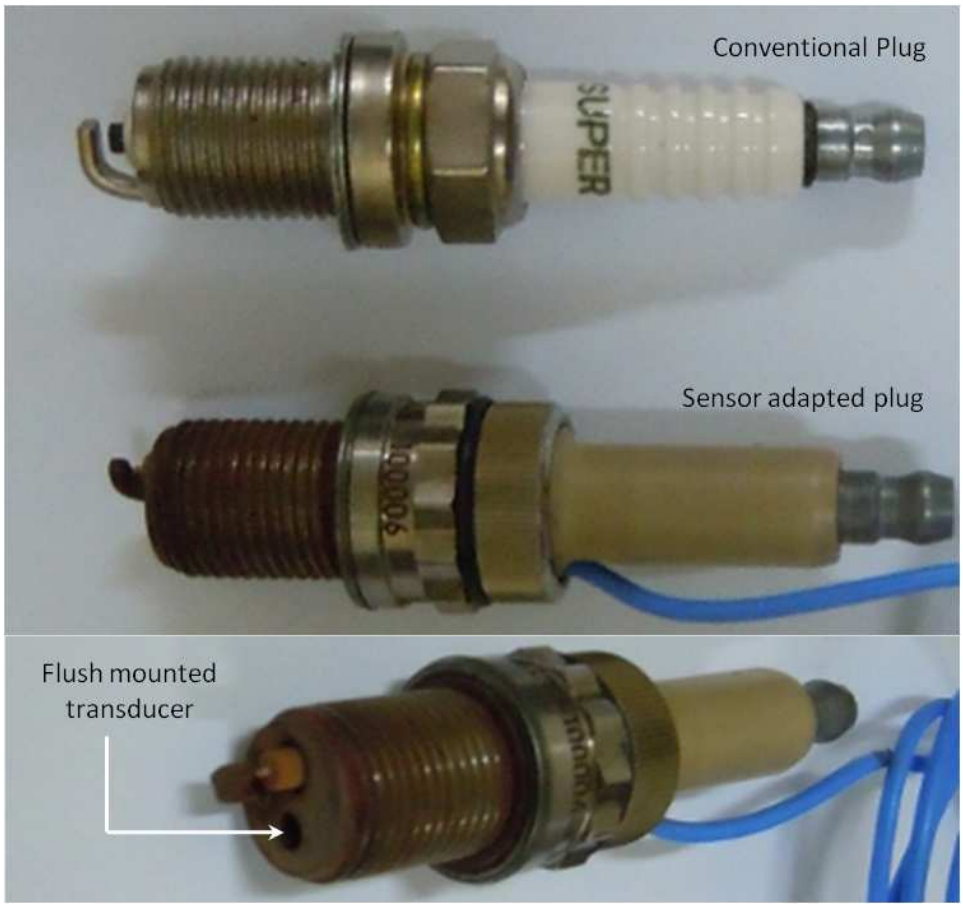

Figure 3.3: Spark plug adapted in-cylinder pressure sensor

pressure $P_{ref}(\theta)$. Literature suggests this approach to be an accurate method for establishing the reference pressure (Lancaster, Krieger, and Lienesch 1975) (Hayes, Savage, and Sorenson 1986) and is one of the recommended methods by AVL for differential to absolute pressure correction.

Determination and assignment of top dead center

Accurate phasing of the acquired pressure trace with respect to the top dead center is extremely critical for any engine analysis based on the in-cylinder pressure traces. The top dead center determination methodology adopted is briefly described as below.

Theoretically, the crank angle encoder should be mounted on the engine shaft such that when the reference cylinder piston is at the top dead center, the encoder

Table 3.4: Specifications of the in-cylinder diagnostic system

Parameter	Specifications
In-cylinder pressure sensor	
Model	GH13Z-24
Measuring range	0 to 250 bar
Lifetime	10^6 load cycles
Crank angle encoder	
Model	365C
Maximum speed	20,000 RPM
Pulse per revolution	Maximum 3600 (0.1 deg crank angle)
Data acquisition module	
Model	IndiModul GigaBit
Analog channels	8
Sampling rate	14 Bit/800 kHz per channel
Resolution	0.1 deg crank angle
On board memory	64 Mega bytes
Plausibility	Yes, with bit/message error output

should also be at the reference zero position. While this provides an accurate location of the top dead center, this is not very practical for frequent handling of the sensor. The current work adopts the dynamic top dead center determination method based on the motored pressure trace and requires the knowledge of thermodynamic loss angle. In this method, the crank angle encoder and the pressure sensor are mounted independently without any restriction of the piston being at the top dead center or the crank angle being at the reference zero. The reference cylinder is motored for a number of cycles and the absolute pressure value is acquired. For each of the cycles, the crank angle corresponding to the peak pressure is determined. It is important to note that, due to pressure sampling resolution limitations and rather flat nature of the pressure trace near the top dead center, a bisection algorithm is used rather than the position of peak pressure for establishing the inflection point of the symmetric pressure trace. The bisection algorithm is based on acquiring the

absolute pressure at some crank angle in the rising section of the motoring pressure trace and subsequently acquiring the crank angle in the falling section of the motoring curve when the pressure becomes equal to the pressure acquired in the rising section. Bisection of the acquired crank angle range or the average of the two crank angles (in absolute terms) provides the crank angle corresponding to the inflection point of the motored pressure trace. The process is repeated over a number of points for a given cycle and over many consecutive cycles to ultimately arrive at the crank angle corresponding to the motoring cycle top dead center. The AVL Indicom internally uses the peak pressure crank angle and the reference angle marking on the crank angle encoder to position the pressure trace such that the point of inflection is at the top dead center. A second level position correction is introduced by accounting for the thermodynamic loss angle which needs to be explicitly provided by the user. In the current case, the thermodynamic loss angle has been determined by using a capacitance based dedicated top dead center sensor. The top dead center sensor also operates using the bisection algorithm as discussed earlier with the input signal being the mixture capacitance against the absolute pressure signal as in case of pressure trace based method. The top dead center estimation for a specific case is shown in figure 3.4. In the inset, the dotted trace indicates the pressure trace with preliminary correction while the continuous trace is the final pressure trace corrected for the thermodynamic loss angle.

Knock detection

End gas auto-ignition leading to abnormal combustion in SI engines is a key limiting phenomena of the engine operating regime. Knock primarily limits the spark advance and hence the maximum torque that can be realized and is one of the key limiting factors on the peak achievable load on the engine. The issue becomes critical especially under turbocharged conditions and while operating under fuel rich conditions. Continued operation under conditions of abnormal combustion leads to substantial power loss along with increased emissions at the least and catastrophic engine failure at the worst. Thus, detection of knock in the incipient stage and subsequent corrective action becomes critical.

Engine knock is essentially an auto-accelerating thermo-kinetic process in which

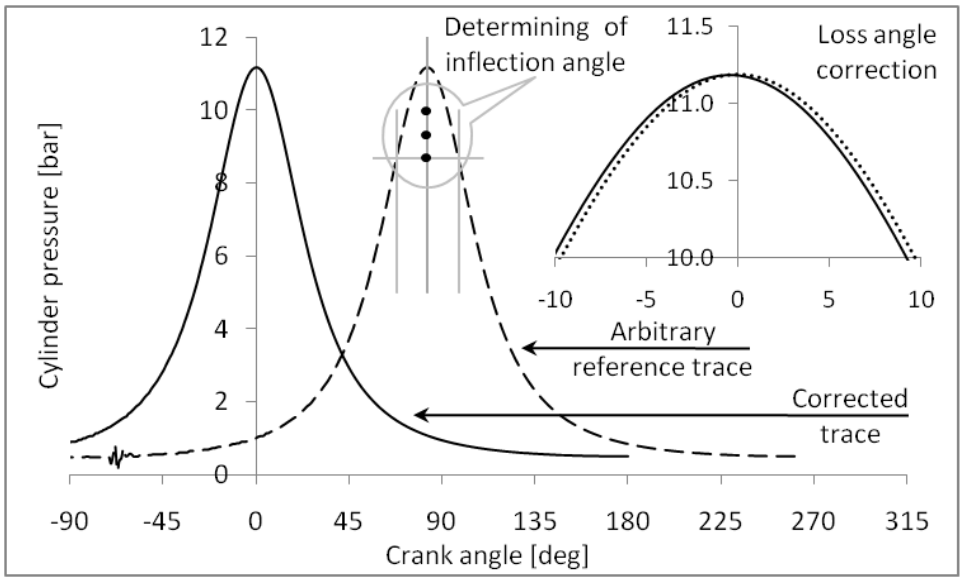

Figure 3.4: Top dead center estimation using the motored pressure trace

rapid spatial and temporal changes to the heat release rate is observed (Heywood 1988) (By, Kempinski, and Rife 1981). The in-cylinder pressure and temperature being strongly coupled to the heat release rate (refer equation 3.7), spatial and temporal variations of heat release rate act as excitation source for the resonant oscillation modes of the in-cylinder gases. The excitation triggers a combination of longitudinal, radial and tangential pressure oscillations within the engine cylinder (C 1997). For typical automotive sized engines the frequencies of the pressure oscillations triggered by end gas auto-ignition are reported to be generally in the 5 to 25 kHz range (Heywood 1988) (Szwaja, Bhandary, and Naber 2007). The fundamental frequency excited is typically in the 5 kHz to 7 kHz range and depends primarily on the cylinder bore diameter and bulk gas temperature (refer equation 3.8) (Brunt, Pond, and Biundo 1998). The higher frequencies are basically some multiples of the fundamental frequency and are characteristic of the acoustic vibration modes corresponding to the combustion chamber geometry (Brunt, Pond, and Biundo 1998). The knock free operation baseline pressure trace has sub 4 kHz frequencies with the dominant frequency being in the 2.5 to 3.0 kHz regime (Fathi, Holland, Ansari, and Weber 2011). From the foregone discussions it is evident that, while a normal combustion pressure trace contains characteristic frequencies only in the sub 4 kHz

regime, presence of frequencies above 5 kHz is an indication of end gas auto-ignition.

$$\frac{1}{C^2}\frac{\delta^2 P}{\delta T^2} - \nabla^2 P = \frac{\gamma - 1}{C^2}\frac{\dot{Q}'''}{\delta t} \quad \text{Refer Morse et al., (Morse and Ingard 1968)} \tag{3.7}$$

$$fn = \frac{k_t}{B}\sqrt{T_b} \tag{3.8}$$

The current investigation adopts the in-cylinder pressure trace spectral analysis method to detect frequencies at and above 4 kHz to establish the occurrence of auto-ignition. Among the various knock detection methods (Schmillen and Rechs 1991) (Millo and Ferraro 1998) (Zhen, Wang, Xu, Zhu, Tao, Xu, and Song 2012), the in-cylinder pressure trace spectral analysis method is potentially the most accurate considering that the in-cylinder pressure trace contains the fundamental information characteristic of end gas auto-ignition and hence permits the detection of extremely low intensity incipient knock. Apart from detection, the spectral analysis method also permits quantification of the knock intensity. The spectral analysis procedure for knock detection is described as below;

1. In-cylinder pressure traces are acquired in continuous mode. If the cycle has the end mixture auto-igniting the base pressure will contain high frequency components in the vicinity of the top dead center which may or may not be explicitly visible depending on the intensity of knock. Figure 3.5 (a) presents a typical knocking (heavy) pressure trace where the high frequency fluctuations are explicitly evident.

2. The pressure signal is filtered using a high pass filter with frequency set at 4 kHz. The high pass filter permits only frequency components above 4 kHz to pass through and everything below 4 kHz is suppressed. Figure 3.5 (b) presents a 4 kHz low pass filtered signal (for representation purpose only) where the cleaning up of the high frequency component is evident while figure 3.5 (c) presents the high frequency component which is subsequently useful.

3. The high pass filtered signal is subject to Fast Fourier Transformation to identify the frequencies excited by the auto-ignition event. Figure 3.5 (d) presents the frequency spectrum of the high pass filtered pressure trace. The presence of spike(s) in the 5 kHz to 7 kHz range is indicative of end gas auto-ignition.

Real time analysis of each operating cycle to test for end gas auto-ignition is made possible by the use of AVL IndiCom indicating software

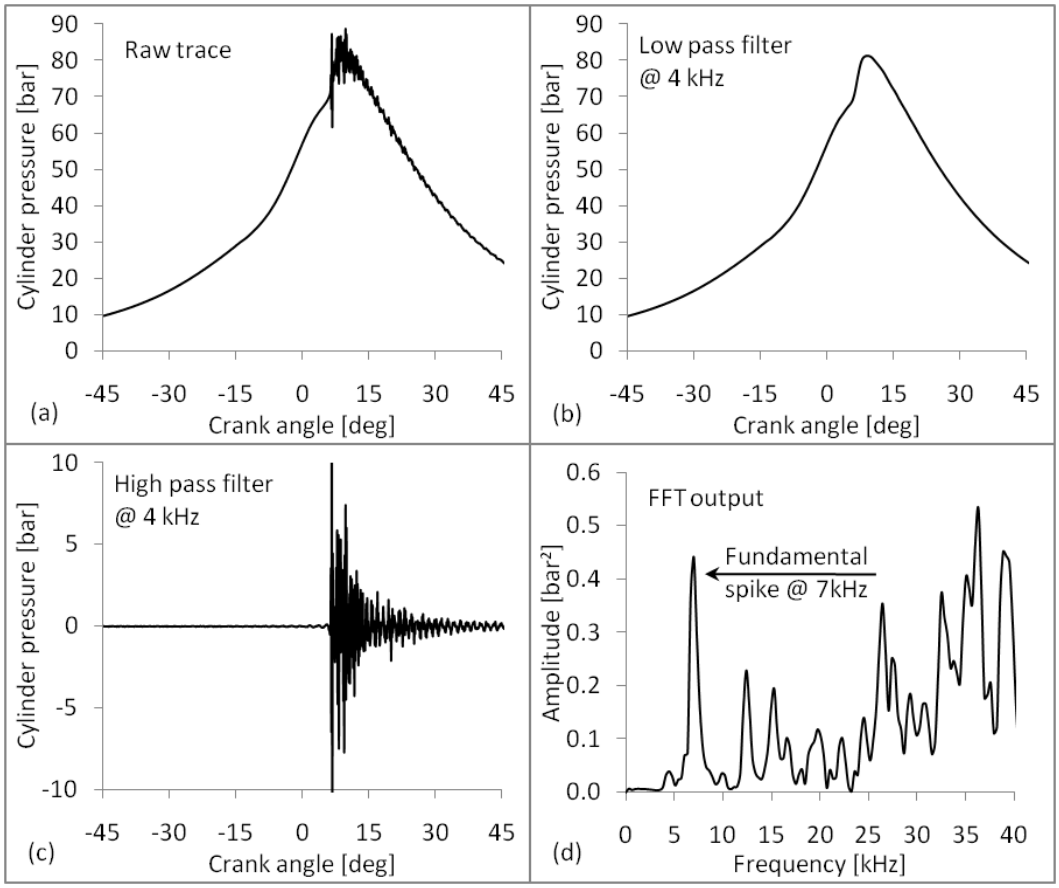

Figure 3.5: Spectral analysis of knocking in-cylinder pressure trace

Indicating system

Indicating, in reference to engine in-cylinder combustion diagnostics, at the minimum refers to the real time display of the acquired in-cylinder pressure as a function of the crank angle. However, superior data acquisition and transfer capabilities of the underlying hardware along with sufficient computational power permits achieving lot more than that. The AVL combustion diagnostics package includes AVL INDICOM, an advanced combustion analysis and indicating software package with data acquisition control, graphical presentation and data evaluation features. The combustion diagnosis using the described hardware is realized through AVL INDICOM using the following key features;

1. IndiPar - IndiPar is the parameter editor that offers a graphical representation of the current installed hardware and lists the supported signals. The channel connection sequence for required parameters and user defined inputs like the units, resolution of acquisition etc along with instrument specifications like calibration factor, sensor sensitivity etc are set using the IndiPar. The engine specifications like bore, stroke, connection rod length, compression ratio, firing order etc and measurement control parameters like measurement mode, data type (crank angle / time based) buffer cycles etc also specified in the IndiPar. The entire data acquisition is controlled through IndiPar.

2. CalGraph - CalGraph is the graphical formula editor with a large library of predefined thermodynamic, statistical and data processing function and with provision for creating user specific formulas for processing the acquired data. In the current investigation, CalGraph is used exhaustively for plausibility check and for processing the acquired in-cylinder data for such key activities like ensemble averaging, estimation of mean effective pressure, signal filtering and Fourier transformation, extraction of heat release and mass burn fraction traces from the pressure trace, estimation of average in-cylinder temperature etc.

3. IndiView - IndiView is the data representation module of Indicom and offers data visualizations in the forms of diagrams, tables, reports etc in both predefined and user defined format. IndiView also provides for exporting the data in ASCII, HTML and graphical format depending on the requirement.

In all, the AVL-INDCOM software package enables complete real-time automated control of data acquisition along with processing, visualization and storage.

3.4 Uncertainty analysis

Imperfections are inherent in all real world measurements irrespective of the care exercised in the selection of instruments, performing experiments and acquisition of data. The direct consequence of such imperfections is that the results obtained from experimental investigations will have an element of uncertainty and when such results are used in the estimation of other dependent parameters, the uncertainties

associated with all the dependent parameters propagate to the estimated parameters. Thus, in the reporting of experimental data and the parameters estimated thereof, the extent of uncertainty needs to be reported. Qualitative inferences drawn from results that do not indicate the degree of uncertainty (especially in cases involving comparative assessment) are questionable. Thus, specifying the uncertainty associated with measured and estimated parameters, commonly christened as uncertainty analysis, is critical. Considering the criticality of uncertainty analysis, the general methodology adopted for estimating the uncertainties associated with measured parameters and their subsequent propagation when used for estimating dependent parameters is consolidated in the current section. The discussion pertaining to uncertainty is broadly based on references (Taylor 1997), (de Rocquigny, Devictor, and Tarantola 2008) and (Coleman and Steele 2009).

3.4.1 Uncertainty in measurements

Uncertainties or errors in measurement could arise due to various factors, both systematic and random, and when multiple sources are present, the total or consolidated uncertainty for the measured parameter must be evaluated. Systematic uncertainties or errors arise in a measurement primarily due to factors like calibration error, instrument drift/instability, resolution of the instrument, reference attribute bias, operator bias etc. The systematic uncertainties affect the accuracy i.e., the closeness to the correct value, of the measurement. Unknown changes in the environmental conditions or the measuring instrument itself cause the measurable values to be inconsistent when measurements are repeated for the same attribute or quantity. Such errors are known as random errors and influence the precision i.e., the repeatability of the instrument. Essentially, if systematic errors can be properly quantified, considering that the precision is (generally) high, correction can be introduced to improve the accuracy. Random errors on the other hand are generally beyond control and invariably contribute to the total uncertainty. In uncertainty analysis literature, generally, the uncertainties evaluated from statistical analysis i.e., the random errors are designated as *Type-A* uncertainties while the systematic uncertainties are generally designated as *Type-B* uncertainties. Measurements, however sophisticated they are, generally experience both systematic and random errors and both need

to be accommodated in the assessment of total or consolidated uncertainty. In the consolidation of various contributing uncertainties, one of the critical requirements is to express all of them at the same confidence level by converting them to *standard uncertainties*, corresponding to a margin of ± one standard deviation. The approach adopted towards expressing type A and type B uncertainties in terms of standard uncertainty and subsequent use of the individual standard uncertainties to arrive at consolidated uncertainty for measured parameters is as described below.

Type A uncertainties are quantified by statistical analysis of the results of repeated measurement of the considered parameters. The mean and standard deviation are the parameters of interest in the assessment of uncertainty. In the assessment of mean and standard deviation, while the entire population is considered and one standard deviation on either side of mean can be taken as the associated uncertainty, the fact that the considered population set (comprising of the outcome of finite number of repeated experiments) does not represent the complete set of *all possible* samples (which is theoretically infinity), the sample standard deviation is evaluated (against the population standard deviation; $\sigma_{sample} > \sigma_{population}$) and the standard uncertainty is estimated as the ratio of the sample standard deviation to the square root of the number of samples. This standard uncertainty represents the approximation to true standard deviation if all the possible cases were considered. The expression for sample standard deviation (σ) and the uncertainty due to random errors (u_r) is as shown in equation below;

$$\sigma = \sqrt{\frac{1}{(n-1)} \sum_{i=1}^{i=n} (x_i - \overline{x})^2} \qquad\qquad u_r = \frac{\sigma}{\sqrt{n}} \tag{3.9}$$

Based on the above calculations, the final result including the uncertainty in the measured parameter due to random errors is represented as $\overline{x} \pm u_r$.

In type B or the systematic uncertainty, the errors involved are generally determined and quantified heuristically i.e., primarily based on a detailed knowledge of the measurement process and on the experience of the person involved in the measurements. Along the lines of random error, the identified systematic errors are also to be expressed in terms of the standard uncertainty, which is possible with the knowledge of the individual probability distribution of the involved uncertainties. For half

width of the uncertainty 'a' (uncertainty is ± a) the standard uncertainty for different probability distribution functions (non exhaustive) of the involved uncertainties can be estimated from the correlations as below.

$$\begin{aligned} u_s &= \frac{a}{\sqrt{3}} \quad \text{for rectangular distribution} \\ &= \frac{a}{\sqrt{2}} \quad \text{for U shaped distribution} \\ &= \frac{a}{\sqrt{6}} \quad \text{for triangular distribution} \\ &= a \quad \text{for normal distribution} \end{aligned}$$

Having identified and quantified the systematic and random uncertainties associated with a particular measurement, the combined standard uncertainty for the measurement (u_m) is estimated based on the method of *summation in quadrature* which is essentially the square root of sum of squares of all the standard uncertainty components (half width). The combined standard uncertainty is expressed as in equation 3.10.

$$u_m = \sqrt{\sum_{i=1}^{i=n} u_i^2} \qquad u_i \text{ represents individual uncertainty} \tag{3.10}$$

The final result of measurement M is represented as $M \pm u_m$.

3.4.2 Propagation of uncertainty

While the results of individual measurements can be used independently for evaluating the parameter itself, more often than not, the measured results are used in some mathematical expression to arrive at a different parameter. Equation 3.11 being a typical case in point where E representing the estimated parameter with M_i and O_i representing the measured and other parameters respectively.

$$E = f(M_i \pm u_i, O_j \pm u_j); i = 1...n, j = 1...m \tag{3.11}$$

When parameters with uncertainties are combined in some mathematical operations to arrive at a different parameter of interest, the uncertainties associated with

the individual parameters propagate to the final estimated result. While the worst case scenario of propagation of uncertainty pertains to direct addition of the individual parameter uncertainties, in which case the calculated parameter uncertainty will be substantially higher, in practice, the probability of all the uncertainties being at the limiting condition and on the same side of mean are extremely remote. This particular scenario is again dealt with by adopting the summation in quadrature method. The uncertainty for the calculated parameter is estimated based on equation 3.12, when the parameters are in addition / subtraction and equation 3.13, when the parameters are in subtraction / division. It is important to note that in case of multiplication / division, the uncertainties are to be converted to relative numbers and the outcome also will be in relative term with respect to the mean. The relative uncertainty should be converted back to absolute uncertainty prior to reporting the final result.

$$u_e = \sqrt{\sum_{i=1}^{i=n} u_{m_i}^2 + \sum_{j=1}^{j=m} u_{m_j}^2} \tag{3.12}$$

$$\frac{u_e}{E} = \sqrt{\sum_{i=1}^{i=n} \left[\frac{u_{m_i}}{M_i}\right]^2 + \sum_{j=1}^{j=m} \left[\frac{u_{m_j}}{M_j}\right]^2} \tag{3.13}$$

3.5 Methodology

While the broad philosophy of the investigation is to address and analyze the engine thermo-kinematic response for Syngas fuelled operation, based on the capability and operational flexibility of the available engines, different scenario and mandate are envisioned and defined for each of the three engines. The key mandates for the three engine are briefly described as below;

1. **Engine** $E4$: The engine $E4$ is basically a naturally aspirated compressed natural gas automotive engine adapted for generator application and comes with the compressed natural gas kit. The engine is used for characterizing the performance on natural gas to establish the baseline characteristics / reference standard to be used as benchmark. As such, the engine is first fuelled with natural gas and subsequently with producer gas under naturally aspirated mode of operation.

2. **Engine** $E6$: The engine $E6$ is a natural gas engine adopted from a diesel frame and is used for evaluating the producer gas fuelled performance under naturally aspirated and turbocharged after-cooled mode of operation. The investigation is directed at optimizing the engine on both naturally aspirated and turbocharged after-cooled mode considering that the thermodynamic and fluid dynamic properties for producer gas fuelled operation are expected to be significantly different as compared to natural gas fuelled operation. The difference arising primarily due to the fuel thermo-physical properties and mass flow rate (especially in turbocharged mode). Towards the same the engine is first operated with producer gas under naturally aspirated mode which establishes the baseline characteristics and is used as the reference for turbocharger selection and optimization. Subsequently, the engine is characterized under turbocharged mode of operation.

3. **Engine** $E2$: The small capacity engine $E2$ is a naturally aspirated engine and is used to address the influence of syngas composition, especially mixture H_2 fraction on the engine performance.

While different objectives are set out for the three engines, a select few or all of the following parameters have been addressed on each of the three engines depending on the relevance and feasibility.

1. Maximum brake torque ignition timing

2. Peak supported load limited by engine stable operation (end gas auto-ignition / cyclic variation)

3. Equivalence ratio for optimal engine operation

4. Stable operation equivalence ratio regime

5. Knock characterization and

6. Transient operation involving block loading and unloading of the engine.

3.6 Summary

The chapter summarizes the equipment, instruments and methodology used in the present study. Details regarding the specification of the engine hardware used is also highlighted. Further, as a part of experimental methodology, the need of data acquisition and analysis is also established.

Chapter 4

Theoretical analysis for peak load estimation for an engine frame

One of the fundamental features of bio derived fuels having low energy content pertains to lower power output per unit engine swept volume as compared to typical conventional fuels. Along similar lines, engines fuelled with syngas, a non regular low calorific value fuel, are also expected to experience power de-rating of various degrees, depending primarily on the thermo-physical properties of syngas. The current chapter addresses the theoretical estimation of peak load potential for a given engine size. A generic expression, applicable for any engine size - fuel combination, is developed based on the first principles in terms of various governing parameters. The key parameters that influence the engine power rating are quantified for different engines and for designed fuel(s) and syngas. The quantified parameters and estimated power rating form an indicative benchmark for the experimental investigations and also provide a well defined direction for diagnosis in case of significant deviation in engine performance.

4.1 Estimation of peak supported load

Fuelling an engine with non-regular or alternative fuel generally entails certain performance variability, attributed primarily to the differences in the fuel thermo-physical properties like calorific value, air-fuel ratio, density etc (Heywood 1988) (Dasappa

2001). The most prominent performance variability is the engine power rating. Considering that the power developed by an engine is a function of the fuel thermophysical properties and the engine geometric and kinematic parameters, an expression, in terms of the relevant governing parameters is developed for the estimation of peak power. The expression governing the conversion of chemical to mechanical/electrical energy through the internal combustion engine route can be expressed as in equation 4.1.

$$\text{Power (P)} = \text{Energy input} * \text{Conversion efficiency} \tag{4.1}$$

The power equation (equation 4.1) is expressed in terms of formally quantifiable parameters like the engine swept volume and speed, fuel and air flow rate, fuel lower calorific value, thermodynamic efficiency etc to evolve independent expressions for naturally aspirated and turbocharged after cooled mode of operation as in equations 4.2 and 4.3.

Naturally aspirated operation

$$P = \underbrace{\left[\eta_v * V_s * \frac{N}{60n}\right]}_{\text{Engine parameters}} * \underbrace{\left[\rho_{mix-a} * \frac{Q_{fuel-lcv}}{\frac{m_a}{m_f}+1} * \eta_f\right]}_{\text{Thermophysical properties}} \tag{4.2}$$

Turbocharged aftercooled operation

$$P = \underbrace{\left[\xi * \frac{P_{mix-co}}{P_{mix-a}} * V_s * \frac{N}{60n}\right]}_{\text{Engine parameters}} * \underbrace{\left[\rho_{mix-a} * \frac{Q_{fuel-lcv}}{\frac{m_a}{m_f}+1} * \eta_f\right]}_{\text{Thermophysical properties}} \tag{4.3}$$

While the power equations are mostly self explanatory, under turbocharged mode, a correction factor ξ with an upper limit of unity, a function of pressure loss and increase in temperature occurring downstream of the compressor is used.

Having arrived at the power rating expressions, diesel ratings for the three engine capacities/frames under consideration are estimated and compared with the specifications for a qualitative assessment of the derived equations. For the three engine frames, the governing parameters as required for peak load estimation are available

either directly as specifications or through personal communications. The engine power rating, relevant parameters and the estimated power based on equation 4.2 and 4.3 for the three engines are consolidated in table 4.1. As evident from table 4.1, equations 4.2 and 4.3 estimate the peak supported load with significant accuracy, the maximum deviation being 8 %. Considering the uncertainty associated with some of the governing parameters, the difference in the specified and estimated power rating is well within acceptable limits and as such the feasibility of using equation 4.2 and 4.3 for estimation of the power using appropriate parameters is established.

Table 4.1: Estimation of diesel power rating for the engines $E2$, $E4$ and $E6$

Parameter ↓ Engine →	Units	$E2$	$E4$	$E6$
Peak power @ unity PF [s1]	kWe	16	27	106
Prime power @ unity PF [s1]	kWe	15	25	100
Aspiration	–	Natural	Natural	Charged
Engine speed [s1]	rpm	1500	1500	1500
Power stroke coefficient	–	2	2	2
Total swept volume	m^3	0.00167	0.00296	0.00589
Volumetric efficiency [d,l]	kg/kg	0.90		NA
Ambient density [c1]	kg/m^3	1.16	1.16	1.16
Fuel used [s1]	–	High Speed Diesel		
Fuel lower calorific value [l]	MJ/kg	43.26		
Peak load air to fuel ratio [s1]	kg/kg	21.0		
Fuel conversion efficiency [s1]	kW/kW	0.41	0.40	0.39
Compressor pressure ratio [s1]	bar/bar	NA		2.25
Pressure correction factor [s1,d]	bar/bar	NA		0.80
Estimated peak load	kWe	16.5	28.5	114.7
Difference from specification	%	3.1	5.5	8.2

[s1] Specification references same as that for peak power ; [l] Literature

[d] Personal communication

[c1] at 1 bar and 298.15 K (as per specifications)

4.1.1 Assessment of NG and PG power rating

The procedure adopted for estimating the diesel power rating is extended for estimating the peak load potential for the three engine frames on natural gas and syngas. The power rating for the three engine frames under natural gas and syngas fuelled operation forms the benchmark for conventional and non-regular fuel(s) respectively.

One of key challenges in the use of equations 4.2 and 4.3 for estimation of spark ignited peak supported load arises from the limited availability of SI engine frames with complete standard specification data sheets. Considering that information from specifications and literature is not available for the exact replica of the three engines frames, a tolerance of $\pm 5\%$ for compression ratio, total displacement and peak load air to fuel ratio is accommodated and average value based on multiple data points for each parameter is arrived at. Accordingly, the estimated power is expressed within a $\pm$ band which is realized by adopting the *fractional uncertainties add in quadrature* principle (Cohen 1998). The fractional variation in power based on the principle of sum of quadrature (neglecting the variation in swept volume, speed and power stroke coefficient) is estimated for the naturally aspirated and turbocharged mode of operation from expressions 4.4 and 4.5 respectively.

$$\left[\frac{\delta P}{P}\right]_{NA} = \sqrt{A+B} \tag{4.4}$$

$$A = \left(\frac{\delta \eta_v}{\eta_v}\right)^2 + \left(\frac{\delta \rho}{\rho}\right)^2 + \left(\frac{\delta Q}{Q}\right)^2 \; ; B = \left(\frac{\delta [m_a/m_f]}{[m_a/m_f]}\right)^2 + \left(\frac{\delta \eta_t}{\eta_t}\right)^2$$

$$\left[\frac{\delta P}{P}\right]_{TA} = \sqrt{A+B} \tag{4.5}$$

$$A = \left(\frac{\delta \xi}{\xi}\right)^2 + \left(\frac{\delta P_r}{P_r}\right)^2 + \left(\frac{\delta \rho}{\rho}\right)^2 \; ; B = \left(\frac{\delta Q}{Q}\right)^2 + \left(\frac{\delta [m_a/m_f]}{[m_a/m_f]}\right)^2 + \left(\frac{\delta \eta_t}{\eta_t}\right)^2$$

Variations in governing parameters and their influence on engine power rating

Considering that baseline diesel engines are adopted for SI operation with NG and syngas, the engine operating and thermodynamic conditions are expected to be significantly different, potentially influencing the power developed by the engine. Prior

to the estimation of peak load power rating of the three engine frames with natural gas and syngas, the variations in some of the key governing parameters and their potential influence on the peak load rating is briefly discussed.

1. **Mixture calorific value** : The energy input to an engine is basically governed by the overall quality of the fuel-air mixture in the engine cylinder. Keeping all other parameters same, the power rating of an engine is directly proportional to the mixture calorific value (at stoichiometry and lean operating conditions) as evident from equations 4.2 and 4.3. Assessing the influence of calorific value on power rating, if (hypothetically) all other parameters are maintained same for all the fuels under consideration, natural gas with a mixture calorific value of 2.64 MJ/kg (fuel calorific value of 46.07 MJ/kg and stoichiometric air to fuel ratio of 16.44; Refer table 4.2) returns the highest power followed by producer gas with a mixture calorific value of 2.11 MJ/kg (fuel calorific value of 4.95 MJ/kg and peak load operating air to fuel ratio of 1.35; Refer table 4.4) and diesel with a mixture calorific value of 1.97 MJ/kg (fuel calorific value of 43.26 MJ/kg and peak load operating air to fuel ratio of 21.00; Refer table 4.1). As is evident, producer gas fuelled engine operation experiences a minimum power de-rating of 20% over the corresponding natural gas fuelled engine operation.

2. **Fuel conversion efficiency**: In the adoption of a diesel engine for gas operation, reduction of compression ratio is mandatory to prevent engine knock (Heywood 1988). A simple air standard cycle based thermodynamic analysis indicates that a reduction in the compression ratio leads to corresponding reduction in the fuel conversion efficiency. While the change in the Otto cycle efficiency is under 1% per unit change of compression ratio for higher compression ratio values (compression ratio > 14), it is in close to 2% for lower compression ratio values (compression ratio < 9) leading to a commensurate reduction in the engine power rating. This has been verified by Dasappa (Dasappa 2001) in comparing the performance of various gas engines derived from diesel frame, wherein it is established that a unit change in compression ratio can change the engine peak power rating between 1% and 3% from the nominal output.

While SI engine operation experiences reduced fuel conversion efficiency over diesel mode due to reduction in the compression ratio, a simple analysis suggests potential differences in fuel conversion efficiency amongst SI engines operating at the same compression ratio but on different fuels. The differences are attributed to variations in fuel thermo-physical properties, particularly the adiabatic flame temperature. The influence of adiabatic flame temperature on the thermal efficiency can be captured through the ratio of Carnot efficiency for any two fuels for the same reference sink temperature as captured in equation 4.6. In equation 4.6 $\eta_{c,a}$, $\eta_{c,b}$ and η_r represent the efficiency for fuel 'a' and 'b' and the efficiency ratio while T_{aft} and T_l refer to the adiabatic flame temperature and common reference sink temperature respectively.

$$\eta_r = \frac{\eta_{c,a}}{\eta_{c,b}} = \frac{\frac{(T_{aft,a} - T_{l,a})}{T_{aft,a}}}{\frac{(T_{aft,b} - T_{l,b})}{T_{aft,b}}} = \frac{(T_{aft,a} - T_{l,a})}{(T_{aft,b} - T_{l,b})} * \frac{T_{aft,b}}{T_{aft,a}}$$

$$\eta_{bth,a} = \eta_r * \eta_{bth,b} \tag{4.6}$$

Thus, the knowledge of fuel conversion efficiency for a particular fuel permits estimating the fuel conversion efficiency for a different fuel based on the adiabatic flame temperature.

3. **Density and volumetric efficiency**: The quantity governed nature of SI engines generally renders them volumetrically less efficient as compared to a typical diesel engines by the virtue of reduced manifold pressure and hence density (Heywood 1988) (Cho and He 2007) (Korakianitis, Namasivayam, and Crookes 2011). Apart from the presence of a physical restriction (throttle body), the absence of evaporative cooling effects and lower density for natural gas - air and syngas - air mixtures for the same pressure and temperature (due to lower molecular weight) leads to reduction in the volumetric efficiency and energy input to the engine, culminating in lower power output.

4. **Compressor pressure ratio and correction factor**: The compressor pres-

sure ratio and pressure correction factor of diesel fuelled operation are carried forward to SI operation for both the fuels. This consideration is made under the assumption that the engine frame has an independently matching turbocharger corresponding to natural gas and syngas fuelled operation.

Natural gas power rating

The natural gas power rating for the three engine frames, based on equations 4.2 and 4.3, is consolidated in table 4.2.

Table 4.2: Estimation of natural gas power rating for the engines $E2$, $E4$ and $E6$

Parameter ↓ Engine →	Units	$E2$	$E4$	$E6$	
Aspiration	–	Natural	Natural	Natural	Charged
Fuel used	–	CNG - Grade 2.5			
Fuel lower calorific value	MJ/kg	46.07			
Peak load air to fuel ratio	kg/kg	16.44			
Mix calorific value ($\phi = 1$)	MJ/kg	2.64			
Ambient density	kg/m^3	1.12			
Volumetric efficiency	kg/kg		0.82		NA
Compression ratio (CI)	–	18.5	17.5	16.5	16.5
Compression ratio (SI)	–	11.0	12.5	10.5	10.5
Fuel conversion efficiency	kW/kW	0.31	0.32	0.32	0.31
Compressor pressure ratio	bar/bar		NA		2.25
Pressure correction factor	–		NA		0.80
Estimated peak load	kWe	16.0	29.2	58.4	119.3
Variation in peak load	$\pm kWe$	1.1	2.1	4.1	10.3
Diesel rating deviation	%	0.0	8.2	–	12.6

It is evident from table 4.2 that for natural gas fuelled operation, while engines E4 and E6 experience power increase in the range of 10 ± 2 %, the baseline (specification) diesel rating is realized by engine E2. Analyzing the 10 ± 2 % power increase, referring to table 4.2, the 34.5% higher mixture calorific value is the primary contributing factor. The relatively low increase realized as compared to the

contribution from the mixture calorific value is primarily attributed to the reduction in volumetric and fuel conversion efficiency. The natural gas volumetric efficiency at 82 ±4% (Das and Watson 1997) (Korakianitis, Namasivayam, and Crookes 2011) (De Nicolao, Scattolini, and Siviero 1996) and fuel conversion efficiency of 30±1.5% represents a drop of about 10 % (in absolute points for fuel conversion efficiency) from baseline diesel scenario. The factors contributing to the de-rating of the two parameters have already been discussed in the previous section.

Syngas power rating

The current investigation involves engine operation with producer gas and four different syngas compositions. The gas and stoichiometric mixture compositions considered are reproduced in table 4.3. The power rating and governing parameters for the three engines corresponding to the syngas composition used are consolidated in table 4.4. Since the two cylinder engine ($E2$) is operated with four different syngas compositions, the engine is rated for each of the four compositions. With natural gas rating as the (SI operation) benchmark for syngas operation, the % change in each parameter corresponding to respective natural gas values is consolidated in table 4.5.

The key feature of syngas fuelled operation, as evident from the data consolidated in table 4.4, is the rather substantial power de-rating experienced as compared to corresponding natural gas fuelled operation for all the three engines considered in the current study. The minimum de-rating is as high as 39 % (for E2 with syngas SG-4) while the maximum de-rating approaches 67 % (for E2 with syngas SG-1). Even under turbocharged mode the de-rating is as high as 42 %. Reviewing the influencing parameters and comparing with typical natural gas fuelled operation, the mixture calorific value emerges as potentially the most significant factor contributing to the power de-rating. The stoichiometric mixture calorific value for producer gas is lower by 23.4 % while it varies from 39.4 % to 12.6 % for various syngas compositions (refer table 4.5). While the mixture calorific value contributes significantly to engine power de-rating, the de-rating is not completely accounted for by the lower calorific value alone. The other key factor contributing to the engine power de-rating corresponds to lower in-cylinder pressure, typical of syngas fuelled operation. The factors contributing to lower in-cylinder pressure(s) and the subsequent influence on

Table 4.3: Syngas and stoichiometric mixture composition in % volume

Designation	CO	H_2	CH_4	CO_2	N_2	O_2
	Gas composition					
SG-1	11.5	12.8	02.3	10.8	62.6	00.0
SG-2	18.0	18.0	01.2	11.3	51.5	00.0
SG-3	14.4	25.9	02.9	19.0	37.8	00.0
SG-4	16.4	37.2	03.6	24.7	18.1	00.0
PG	20.0	20.0	02.0	12.0	44.0	00.0
	Stoichiometric mixture composition					
SG-1	06.4	07.1	01.3	06.0	69.9	09.3
SG-2	09.1	09.1	00.6	05.7	65.1	10.3
SG-3	06.4	11.6	01.3	08.5	60.6	11.6
SG-4	06.3	14.2	01.4	09.4	55.7	13.0
PG	09.4	09.4	00.9	05.6	63.6	11.2

engine power rating is discussed as below.

A simple thermodynamic analysis of an air standard Otto cycle suggests the cycle work to be proportional to the in-cylinder peak pressure, as indicated in equation 4.8.

$$W_{cycle} = W_{exp} - W_{com} \tag{4.7}$$

$$= \int_{exp} PdV - \int_{com} PdV = \frac{\eta_{otto}}{\gamma - 1} * V_{cl} * \left\{ \frac{P_h}{P_l} + 1 \right\} \tag{4.8}$$

An engine fuelled with syngas experiences peak cylinder pressures significantly lower than that corresponding to natural gas fuelled operation. Apart from the lower mixture calorific value and adiabatic flame temperature, an important factor that causes lowering of in-cylinder pressure for syngas fuelled operation is the reduction in the total number of moles post combustion. One of the typical features of CO and H_2 (stoichiometric) combustion is that the total moles of products are lower by about 15 % as compared to the number of reactant moles. Such a reduction in the number

of product moles contributes significantly to the lowering of the in-cylinder pressure. The influence of reduction in the peak cylinder pressure on the engine power rating is accounted for by estimating the ratio of peak post combustion to pre-combustion pressure using the equation of state (refer equation 4.9) for both natural gas and syngas.

$$\frac{P_P}{P_R} = P_{pr} = \frac{n_P}{n_R} * \frac{R_P}{R_R} * \frac{T_P}{T_R} = \frac{n_P}{n_R} * \frac{MW_R}{MW_P} * \frac{T_P}{T_R} \tag{4.9}$$

The extent of reduction of syngas pressure ratio over the natural gas pressure ratio is representative of the potential de-rating experienced by syngas fuelled engines. Referring to table 4.5, the extent of de-rating due to the pressure effects contributes to the tune of 35 $\pm$ 6 %, depending on the fuel composition and associated thermophysical properties. It is evident that the influence of pressure effects is much severe as compared to the mixture calorific value and together these two components account for the bulk of the engine power de-rating. Another 6 % to 10 % de-rating is accounted for by the reduction in the mixture density (primarily due to the presence of hydrogen) and the reduction in fuel conversion efficiency due to lower adiabatic flame temperature for stoichiometric syngas - air mixtures (refer foregone discussion).

4.2 Summary

The chapter has provided a mathematical tool towards estimating the peak power for an engine frame operating with a particular fuel. The estimation is based on thermodynamic properties of the fuel that influence the in-cylinder thermodynamic conditions and the engine geometric parameters.

Table 4.4: Estimation of Syngas power rating

Parameter ↓ Engine →	Units	$E2$				$E4$	$E6$	
Aspiration	–	NA	NA	NA	NA	NA	NA	TA
Fuel used	–	SG-1	SG-2	SG-3	SG-4	PG	PG	PG
Fuel lower calorific value	MJ/kg	3.14	4.17	5.28	7.55	4.95	4.95	4.95
Peak load air to fuel ratio	kg/kg	0.88	1.12	1.49	2.14	1.35	1.35	1.35
Mixture calorific value	MJ/kg	1.67	1.97	2.12	2.41	2.11	2.11	2.11
Ambient density	kg/m^3	1.10	1.08	1.08	1.06	1.08	1.08	1.08
Volumetric efficiency	kg/kg	0.82	0.82	0.82	0.82	0.82	0.82	NA
Compressor pressure ratio	bar/bar	–	–	–	–	–	–	2.25
Pressure correction factor	–	–	–	–	–	–	–	0.85
Carnot temperature factor	–	0.926	0.968	0.974	0.986	0.976	0.976	0.976
Fuel conversion efficiency	kW/kW	0.287	0.300	0.302	0.306	0.312	0.298	0.298
Pressure ratio factor	bar/bar	0.588	0.683	0.710	0.739	0.710	0.710	0.710
Estimated peak load	kWe	5.31	7.47	8.37	9.82	15.33	29.17	69.43
Variation in peak load	$\pm kWe$	0.4	0.5	0.6	0.7	1.1	2.1	6.0
De-rating from NG rating	%	66.8	53.3	47.7	38.6	47.5	50.1	41.8

Table 4.5: Parameter and power de-rating contribution chart

% reduction in parameter magnitude with respect to natural gas						
Fuel	–	SG-1	SG-2	SG-3	SG-4	PG
Mixture calorific value	%	39.4	28.6	22.9	12.6	23.4
Reference density	%	1.6	3.2	4.0	5.7	3.5
Fuel conversion efficiency /						
Adiabatic flame temperature	%	7.4	3.2	2.6	1.4	2.4
In-cylinder pressure effects	%	41.2	31.7	29.0	26.1	29.0

Chapter 5

Experimental investigations and results

The focus of the current chapter is to capture, at various degrees of details, the engine performance at different operating conditions; peak load operation being of primary interest. Accordingly, experiments are carried out on the three different engine frames and the results consolidated into three sections. The first section describes the characterization of engine E4 for natural gas fuelled operation. The general performance and in-cylinder investigation data from natural gas fuelled operation forms the benchmark against which syngas fuelled operational performance can be compared. The second section covers the engine performance with producer gas fuelled operation of the engines E4 and E6 while the third section covers the operation of engine E2 with different syngas compositions. While the broader theme of the investigation pertains to characterizing the wide open throttle thermo-kinematic response of the engine on fuelling with syngas in general and producer gas in particular, key interventions towards achieving optimal engine performance are also discussed.

5.1 Reference performance

In the chapter *Theoretical analysis for peak load estimation for an engine frame*, the peak load potential of the three engine designs has been established. Based on a detailed literature review the engine efficiency/specific fuel consumption data for

gasoline, natural gas and producer gas are consolidated in table 5.1 and the energy balance data for the considered fuels is consolidated in figure 5.1. While the data for natural gas and gasoline (fossil fuels) forms the reference for higher calorific value fuel based engine performance, the producer gas data forms the reference for the current investigation.

It may also be noted that the performance data consolidated in table 5.1 and figure 5.1 corresponds to maximum brake torque ignition, peak load, stoichiometric operation of multi-cylinder engines under natural and turbocharged aspiration at a speed of 1500 RPM. The reported energy balance corresponds to Yuksel et al., (Yüksel and Ceviz 2003) for gasoline, Ghareghani et al., (Gharehghani, Koochak, Mirsalim, and Yusaf 2013) for natural gas, Imdat et al., (Taymaz 2006) for diesel and Sridhar et al., (Rao 2003) for producer gas. Except for producer gas, the energy balance data reported for the other fuels from the references correspond to the average of five values for each fuel based on literature/specifications and personal communications.

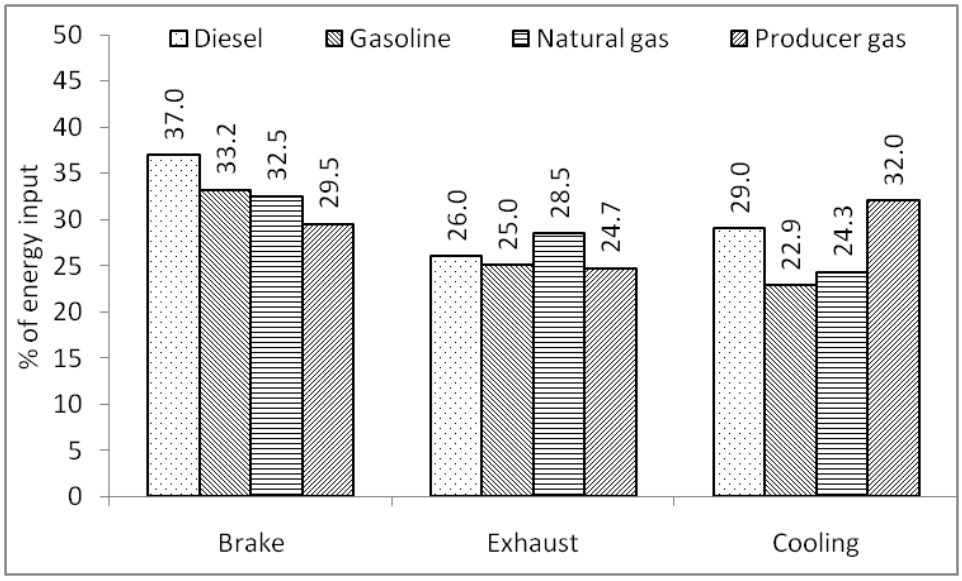

Figure 5.1: Literature reported energy balance data for various fuels

General performance of the engines with respect to efficiency/specific fuel consumption and energy balance are consolidated from the literature. The engine exhaust emissions are to be compared with the prescribed standards for fossil fuels.

Table 5.1: Literature reported specific fuel consumption / efficiency and BMEP

Operating conditions	SFC (g/kWh); Eff (%) and BMEP (bar)
Gasoline fuelled operation	
Naturally aspirated[a]	295; 27.7 and 8.4 @ CR 8.6:1
	300; 27.3 and 8.4 @ CR 8.1:1
Turbocharged[b]	298; 27.5 and 8.0 @ CR 10.3:1
Natural gas fuelled operation	
Naturally aspirated[c]	230; 31.0 and – @ CR 8.3:1
	290; 28.2 and 10.3 @ CR 10.0:1
Turbocharged[d]	209; 34.5 and 14.5 @ CR 9.8:1
Producer gas fuelled operation	
Naturally aspirated[e]	2881.3; 25.5 and 4.1 @ CR 11.5:1
Turbocharged[e]	2681.4; 27.4 and 7.8 @ CR 12.0:1

[a] : Ali et al. (Pourkhesalian, Shamekhi, and Salimi 2010)

[a] : Fikret et al., (Yüksel and Yüksel 2004)

[b] : Lecointe et al., (Lecointe and Monnier 2003)

[c] : Das et al.,(Das, Gulati, and Gupta 2000)

[c] : Kalam et al.,(Kalam and Masjuki 2011)

[d] : Gharehghani et al.,(Gharehghani, Koochak, Mirsalim, and Yusaf 2013)

[e] : Sridhar (Rao 2003)

Further, it is important to note that, depending on the application and capacity rating, various norms have been established and an engine has to satisfy these norms to qualify for continuous operation. The emission norms currently prescribed for stationary power generation application through SI engines are established only for gasoline and are referred to in the current study. The emission norms prescribed by Central Pollution Control Board (CPCB), India and Environmental Protection Agency (EPA), USA for gasoline fuelled SI engine for stationary power generation application are consolidated in table 5.2 as below.

In India, the sub 20 kWe sector is dominated by gasoline / kerosene generators

Table 5.2: Exhaust emission standards for spark ignited engines

Displacement	CO $g/kW-hr$	$HC+NO_x$ $g/kW-hr$
CPCB India - Gasoline/Kerosene generators upto 19 kWe (of Environment 2015)		
Up to 99 cc (0.099 L)	≤ 250	≤ 12
Between 99 cc (0.099 L) and 225 cc (0.225 L)	≤ 250	≤ 10
Greater than 225 cc (0.225 L)	≤ 250	≤ 08
EPA USA - Non road SI engines upto 19 kWe		(Agency 2015b)
Up to 225 cc (0.225 L)	≤ 610	≤ 10
Greater than, including 225 cc (0.225 L)	≤ 610	≤ 08
EPA USA - Non road large SI engines		(Agency 2015a)
–	$\leq 4.4^a$	≤ 2.7
–	$\leq 130^b$	≤ 2.7

(for household and commercial lighting applications) while for power rating at and above 20 kWe diesel generators are prominently used. Thus, while the diesel norms are available for the whole spectrum of power ranges (upto 800 kWe) the gasoline / kerosene generator specifications are restricted to 19 kWe. For higher power ratings, the norms by EPA are referred to in the present work.

5.2 Performance of natural gas fuelled operation

The four cylinder engine E4 is operated with natural gas under naturally aspirated mode of operation and provides the benchmark data, both generic performance and in-cylinder, for evaluating the performance of syngas fuelled operation. The peak load performance data including energy balance is consolidated in table 5.3.

The engine E4 realizes a peak load of 25.1 kWe at maximum brake torque timing of 28 deg before the top dead center (Thurnheer, Soltic, and Eggenschwiler 2009) (Huang, Liu, Zeng, Huang, Jiang, Wang, and Miao 2007). Comparing with the theoretical estimation (refer table 4.2) the experimentally realized load suggests a drop of 14 % over the average and 7.4 % over the lower estimated limit. However,

Table 5.3: Natural gas fuelled operation of engine E4 - performance and energy balance

General engine performance		
Peak supported load	kWe	25.1
MBT Ignition timing (set)	deg bTDC	28
BSFC	g/kWh	254.1
BSEC	MJ/kWh	12.0
η_{bth}	%	30.1
Emissions		
CO	g/kWh	1.48
$HC + NO_x$	g/kWh	19.85
Energy balance		
Input energy	kW (%)	83.4 (100.0)
Electrical output	kW (%)	25.1 (30.1)
Cooling load	kW (%)	24.9 (29.8)
Exhaust enthalpy	kW (%)	21.6 (25.9)

the brake thermal efficiency of 30.1 % is comparable to the literature reported values (refer table 5.1). Addressing the 14 % de-rating, a simple analysis of the various measured parameters reveals that the volumetric efficiency realized is 73.1 % as against 82 % considered for the estimation of the peak power (refer table 5.1). The drop in volumetric efficiency almost completely accounts for the experienced power de-rating. On the engine energy balance, while the brake and exhaust components are comparable with the literature, the recorded cooling load is higher by about 5.5 % and approaches the lower limit of typical diesel engines. Considering that the engines used in the current analysis are adopted from diesel frames, the enhanced cooling load could be attributed to higher in-cylinder turbulence. On the emissions, while CO is well within the prescribed emission limits, $HC + NO_x$ remain higher than the prescribed limits (refer table 5.2).

5.3 Performance of producer gas fuelled engine operation

Two engines, E4 and E6 are operated with producer gas as the fuel. The engine E4 is operated under naturally aspirated mode and the engine E6 is operated under both naturally aspirated and turbocharged after-cooled mode. The primary focus is to;

1. establish the wide open throttle optimal operating condition, with particular focus on peak load and
2. analyze the general engine performance and thermo-kinematic response at the optimal operating condition

The emphasis is towards establishing the optimal operating condition so as to minimize the potential power de-rating as indicated in literature (Sridhar, Paul, and Mukunda 2001) (Dasappa, Sridhar, and Paul 2011) (Dasappa, Sridhar, and Indrajit 2011) and the power equation (refer equations 4.2 and 4.3; table 4.4). In the current investigation, considering that the engines being tested are all production engine coupled to an alternative current generator for electricity production, optimization is primarily restricted to maximum brake torque ignition timing under stoichiometric operation at respective frame compression ratio and engine speed of 1500 rpm (corresponding to power frequency of 50 Hz). The ignition time optimization process adopted for normal combustion peak load is described in the following section.

5.3.1 Maximum brake torque ignition timing and peak supported load

Chemical to mechanical energy conversion through the internal combustion engine route represents a thermo-kinetic response. The finite rate heat release and subsequent pressure rise in the engine cylinder constitutes the *thermo-dynamic* response while the motion of piston leading to piston pressure conversion to torque at the crank shaft constitutes the *kinetic* response. Finite rate in-cylinder heat release renders the thermodynamic and kinetic effects strongly coupled, requiring the heat release to be phased optimally for maximizing the chemical to rotary mechanical

energy conversion. The displacement of heat release rate phasing, henceforth designated as *combustion phasing*, from the optimal position leads to a reduction in the shaft power. Advanced combustion phasing (reference to optimal) entails additional energy expenditure against compressing gases, increasing the negative torque component at the crank shaft. Similarly, retarded combustion phasing (reference to optimal) lowers the in-cylinder pressures (due to higher in-cylinder volume) leading to reduction in the positive torque at the shaft. The phasing of combustion relative to the crank angle can be controlled by means of the ignition timing. The ignition timing corresponding to optimal combustion phasing and maximum brake torque at the shaft with normal in-cylinder combustion is known as the maximum brake torque ignition timing.

The maximum brake torque ignition timing is established by means of *spark sweep test* involving the operation of engines over a range of ignition timings. In the current investigation, the spark sweep is realized by turning the distributor cap of the mechanical ignition system. The system provides a resolution of 1 deg crank angle and hence all recorded ignition timings are within an uncertainty of $\pm$ 0.5 degrees.

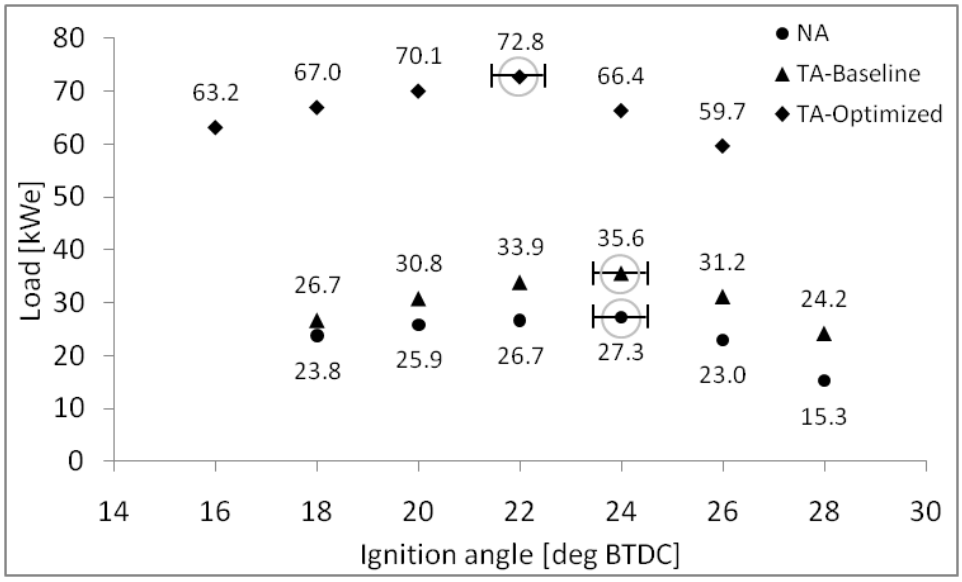

Figure 5.2: Spark sweep test on engine E6 for MBT determination under NA and TA mode

The peak supported load at each ignition angle for the spark sweep test on engine E6 is consolidated in figure 5.2 for three different operating condition. One of the

operating conditions pertains to naturally aspirated mode and the other two correspond to turbocharged after-cooled modes, designated as *baseline* and *optimized*. The specifics pertaining to the latter two are presented after the discussion on maximum brake torque ignition timing. The key features of the spark sweep test are consolidated as below;

- The mentioned load at each ignition angle is the peak supported load under knock free engine operation with crank shaft speed variation being within the permissible engine speed (alternator frequency) fluctuation band of 1485 rpm (49.5 Hz) and 1506 rpm (50.2) Hz (Indian standards) as specified in the Indian Electricity Grid Code (Commission et al. 2010).

- The maximum brake torque ignition timing for producer gas fuelled operation is at 24 and 22 deg before the top dead center for naturally aspirated and turbocharged after-cooled mode of operation. This corresponds to ignition retard of 4 and 6 degree crank angle respectively as compared to typical natural gas ignition setting (28 deg before the top dead center).

- The maximum brake torque ignition timing is dictated by the in-cylinder turbulent flame propagation velocity (U_t) which is itself a function of laminar flame speed and the turbulence intensity (refer equation 5.1 ; (Lipatnikov 2012)). Higher the turbulent flame speed, greater will be ignition regard required and vice-versa.

$$U_t = S_L + Cu' \tag{5.1}$$

  The ignition retard from natural gas ignition settings is attributed to higher laminar flame speed for producer gas as compared to natural gas (refer table 2.4) while further retard of 2 deg crank angle for turbocharged operation is attributed to the higher turbulence levels under turbocharged mode as compared to naturally aspirated mode (Heywood 1988) (Bozza, Fontana, Galloni, and Torella 2007) (Bozza, Gimelli, Strazzullo, Torella, and Cascone 2007).

While the spark sweep test establishes the maximum brake torque ignition timing, the other concurrent outcome is the magnitude of the peak supported load

for a particular engine design. The peak load supported by the engine (E6) under turbocharged mode with baseline diesel turbocharger at 35.6 kWe is a key concern considering that it represents a drop of 33.8 kWe amounting to 48.7 % de-rating compared to the predicted power rating of 69.4 kWe (refer table 4.4). The rather severe power de-rating (in reference to the estimated power) calls for a diagnostic intervention towards root cause analysis and initiation of action towards power recovery. The diagnostic intervention towards addressing the reduced power output is described in the following sections.

5.3.2 Engine diagnostics

Towards identification of the factors contributing to the engine power de-rating, the relevant governing parameters of the power rating expression for turbocharged operation (equation 4.3) are evaluated for the actual engine operation with the baseline diesel turbocharger and compared with values considered in the estimation of the peak power. Critical deviations, if any, would immediately be evident in such a comparison and interventions to minimize the deviations could be initiated. The aforementioned consolidation is presented in table 5.4.

Table 5.4: Consolidation of actual and considered parameters for baseline turbocharged operation of E6

Parameter	Units	Considered	Achieved	Difference (%)
Fuel lower calorific value	MJ/kg	4.95	4.47 [a]	0.48 (9.7) ↓
Air to fuel ratio	kg/kg	1.35	1.30	0.05 (3.7) ↓
Mixture density	kg/m^3	1.08	1.09 [a,b]	0.01 (0.9) ↑
Compressor pressure ratio	bar/bar	2.25	1.18	1.07 (47.6)↓
Pressure correction factor	bar/bar	0.85	0.87	0.02 (2.4) ↑
Brake thermal efficiency	kW/kW	0.298	0.279	0.02 (6.4) ↓

[a] Gas composition ; CO 19.0%, H_2 18.0%, CH_4 1.8%, CO_2 12.0%, balance N_2

[b] Ambient condition ; Pressure - 96kPa, Temperature - 297.15 K

A review of the data consolidated in table 5.4 suggests that some of the governing parameters realized during the engine operation differ significantly in magnitude as

compared to the values used in estimating the engine power rating. The realized values for most of the parameters are on the lower side with fuel calorific value (along with air-fuel ratio), compressor pressure ratio and brake thermal efficiency being critical considering the extent of reduction. Having arrived at the factors that adversely influence the peak load, the factors are reviewed which permits establishing the potential for intervention to realize power recovery.

- **Fuel calorific value** : The fuel calorific value experiences a reduction of close to 10% while the mixture calorific value reduces by close to 8%. It is important to note that the fuel calorific value is gas composition and hence gasifier performance dependent which is influenced by various parametric perturbations (Reed 1981). In the event of some perturbations in the gas composition, engine power de-rating is inevitable since the energy input to the engine itself is reduced. Isolating any control on the gasifier operation, no intervention to alter the fuel calorific value is possible. It may however be noted that, at large capacity systems, the assumed calorific value (4.95 MJ/kg) is generally realized (Dasappa, Krishna, Bose, and Tauri 2015).

- **Brake thermal efficiency** : On the brake thermal efficiency, the close to 6% reduction is primarily attributed to the fact that the achieved load, even though the peak for the particular operating condition, represents part load operation for the particular engine frame and part load operation always experiences higher losses. One of the important features of brake thermal efficiency is that no explicit control can be exercised on the same. Any change will have to be realized by tuning other primary parameters like the compression ratio, ignition timing, operating load corresponding to the supported engine frame etc. Considering that there is no provision to change the compression ratio and spark sweep test accounts for the ignition timing, any attempt to increase the brake thermal efficiency has to be through an increase in the load. Thus, no independent intervention from the brake thermal efficiency is possible.

- **Compressor pressure ratio** : The compressor pressure ratio represents the density boost to the fuel-air mixture and directly influences the mass of mixture and hence the energy input to the engine. The pressure ratio achieved with the

baseline (diesel) turbocharger at 1.18 represents a drop of close to 50 % from the typical engine pressure ratio values of about 2.25 for brake mean effective pressure values of 10 to 12 bar (Ltd 2015), the baseline rating of the engine. With compressor pressure ratio of 1.18 and pressure correction factor of 0.87, the effective pressure ratio translates to a meager 1.03, virtually indicating no pressure boost. It is evident from the above analysis that load recovery is possible by realizing the required pressure boost and intervention if any has to be directed towards the same.

With the preliminary engine diagnostics indicating the load limitation to be arising from the turbocharger, the performance data of the baseline turbocharger is analyzed towards identifying potential causes of compressor under-performance so that subsequent intervention towards realizing the required pressure ratio can be initiated. The baseline turbocharger performance analysis and diagnostic intervention discussed in the following sections.

5.3.3 Turbocharger diagnostics

The most ideal but exhaustive means of analyzing the performance of a turbocharger is through the mapping of the operational data onto the turbocharger compressor / turbine map, depending on the component to be analyzed. The peak load operating point for the baseline turbocharger on the corresponding compressor map is identified in figure 5.3.

One of the key features of baseline turbocharger performance is that the turbine fails to support the compressor in achieving even the threshold speed. It is evident that for the used turbine and compressor set, the available thermodynamic parameters at the turbine inlet are well below the minimum threshold limit required for supporting the compressor to achieve the threshold speed. It is important to note that the same turbocharger that supported a peak load of 100 kWe (@ unity power factor) with diesel fails to even spool up the compressor to the threshold speed. A simple analysis suggests that the conversion of the engine from throttle less quality governed system to a throttled quantity governed system is potentially the biggest contributing factor towards the failure of the turbocharger to support the desired

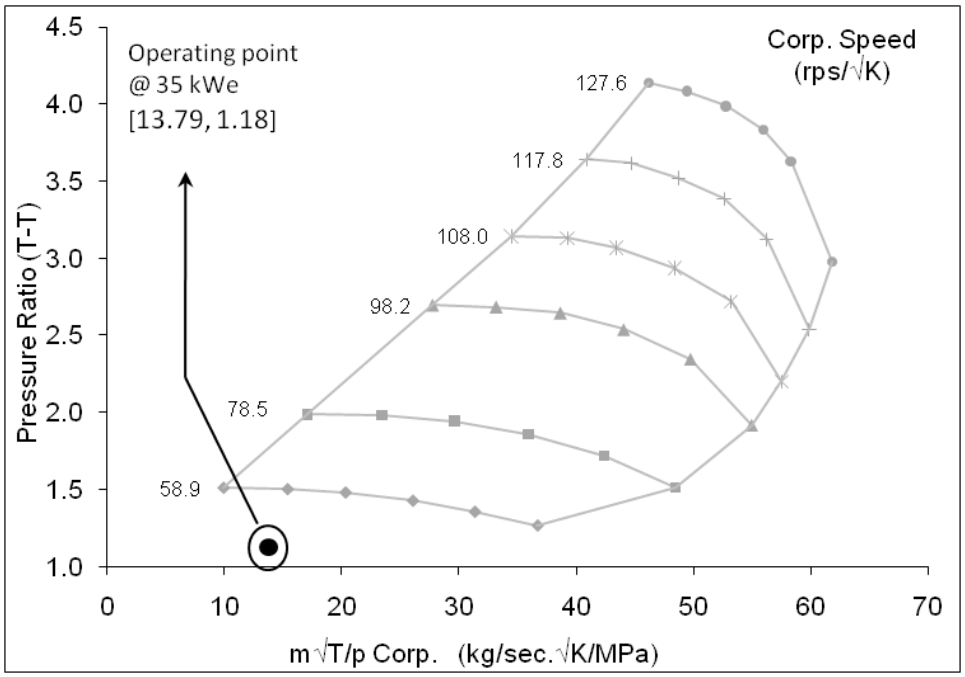

Figure 5.3: Baseline diesel turbocharger compressor map

load. The other key factor pertains to the thermo-physical properties, especially the lower mixture calorific value, lower adiabatic flame temperature and lower than unity product to reactant mole ratio. The above two factors, over the entire load range, collectively prevent the turbine from spooling the compressor to the minimum threshold speed. It is important to note that since the air flow through a centrifugal compressor increases as the square of the impeller speed (Lüdtke 2004) (Hartman 2007), if in the early stages of the engine load, the turbo compressor can attain the threshold speed, subsequently, achieving the boost should not be difficult. Any subsequent challenge would the be from the surge / choke / efficiency limits. From the above analysis, it is evident that the current turbocharger frame is a mismatch for the engine in the selected mode of operation for the desired power rating. As such, realizing the desired boost and hence the power output requires turbocharger matching corresponding to the desired power rating for the fuel used. While the general procedure for turbocharger matching is rather well established, couple of points from the foregone discussion, as indicated below, provide preliminary guidelines towards the turbocharger selection.

- The turbine throat / housing cross sectional area should preferably be smaller than that of the baseline turbocharger. This ensures damming of exhaust gases upstream of the turbine resulting in higher pressure ratio across the turbine. This is expected to improve the turbine performance, especially in terms of speed it can deliver to the compressor.

- If choice of a smaller turbine is possible, considering that the discharge varies as the square of the impeller speed, to prevent potential choking, a smaller compressor wheel diameter may be required.

The general methodology adopted for matching a turbocharger for a particular engine frame is discussed in Appendix C. The broad guidelines consolidated in appendix C are implemented towards identifying a suitable turbocharger for the engine frame E6. Towards turbocharger matching, a peak load target of 75 kWe was set for the engine frame (upper limit of the peak load supported by the engine frame for producer gas fuelled operation; refer table 4.4). Corresponding to the set target, the mass flow rate required to be handled by the compressor and the corresponding pseudo mass flow rate along with the pressure ratio across the compressor are evaluated for the 50% to 100% load range as indicated in table 5.5 towards mapping onto the compressor map for the preliminary selection / elimination.

Table 5.5: Estimated mass flow and pressure ratio for the 50% to 100 % flow range

Load		Mass flow rate	Pseudo mass flow rate *	Pressure ratio
%	kWe	(kg/s)	$(kg/s).\frac{\sqrt{K}}{MPa}$	bar/bar
100	75.0	0.118	21.05	2.22
90	67.5	0.111	19.73	2.12
80	60.0	0.103	18.30	2.00
70	52.5	0.094	16.74	1.87
60	45.0	0.085	15.04	1.74
50	37.5	0.074	13.16	1.59

* Corresponds to 303.15 temperature and 95 kPa pressure

Based on the mapping of the mass flow rate and pressure ratio data, three turbochargers from a family of compressors and turbines are selected. The key geometric specifications of the three selected turbochargers along with the baseline diesel turbocharger are consolidated in table 5.6. The turbochargers are designated as TC-1 (Diesel-base), TC-2, TC-3 and TC-4 respectively. It may be noted that the choice reflects the recommendations of smaller frames for both compressor and turbine as in section 5.3.3.

Table 5.6: Turbocharger specifications

Designation		TC-1	TC-2	TC-3	TC-4
Discharge	L	5.0 to 6.5 at PR 3		upto 5 at PR 3	
Peak flow rate	kg/s	0.46		0.35	
Power range	kW	75 - 208		67 - 179	
Turbine housing c/s	cm^2	10	8	6	8
Compressor wheel dia	mm	82	77	68	

As indicated in the turbocharger matching and selection discussion, the final choice of turbocharger is based on experimental investigations wherein each of the turbochargers is mounted on the engine individually and tested for the peak supported load. The key features of the experimental investigation for turbocharger selection are consolidated as below. The complete technical details pertaining to the turbocharger selection can be accessed from Shivapuji and Dasappa (Shivapuji and Dasappa 2014) where the turbocharger selection philosophy is discussed exhaustively.

1. Investigation on TC-2: The turbocharger TC-2 failed to even approach the estimated peak load, supporting only 40 kWe as against 35.6 kWe of the baseline diesel turbocharger with producer gas as the fuel, an improvement of less than 5 kWe as compared to TC-1. A simple analysis indicated that while the estimated operating regime had a minimum margin of 20% from the surge limit (one of the key considerations in the selection of the compressor), for the mass flow rates typical of sub 50% part load operation, the turbine is unable to spool up the compressor to deliver a pressure ratio of about 1.4 required for the compressor operating point to be positioned within the response regime (i.e,

inside the map). It is evident that the current compressor - turbine frame remains over sized and is unable to support the initial spool up.

2. Investigation on TC-3: In the operation of the engine with turbocharger TC-3, it was observed that the turbine inlet temperature approached 700 deg Centigrade at 25 kWe. The rise in temperature to limiting conditions at close to a third of the lower limit support load indicated suggest the turbine cross section to be too small leading to excessive damming of the exhaust gases at the inlet.

3. Investigation on TC-4: Considering that the constraint came from the turbine side, the next combination tested as TC-4 with same compressor frame as TC-3 but 30% larger turbine housing cross sectional area. The compressor - turbine frame corresponding to TC-4 could deliver the estimated power while maintaining the critical parameters within safe operation limit.

Based on the experimental investigations, the turbocharger TC-4 is found to be suitable for the operation of engine frame E6 with producer gas and the generic performance of the engine and turbocharger is presented in the next section.

5.3.4 Energy balance and emissions

The producer gas fuelled performance of engine E6 under naturally aspirated and turbocharged mode (optimized turbocharger; TC-4) is addressed in the current section. The general performance and energy balance for the engine under naturally aspirated and turbocharged after cooled mode of operation is consolidated in table 5.7.

Addressing the load, with turbocharger matching, a peak load of 72.8 kWe is realized which is very close to estimated peak load of 69 kWe (refer table 4.4). The peak load is realized at a gas to electricity and biomass to electricity conversion efficiency of 29 % and 23 % respectively. In comparing the efficiencies realized on engine E6 with the numbers reported by Sridhar (Rao 2003) (refer table 5.1), it is observed that under turbocharged mode, the realized efficiency on engine E6 is higher by about 2 % points at 1.5 units lower compression ratio. Under naturally aspirated mode, of operation, the realized efficiency is lower by about 3 % points at 1 unit

Table 5.7: Producer gas fuelled operation of engine E6 - performance and energy balance

Aspiration		Natural	Turbocharged
Estimated peak load potential based on equation 4.2			
Upper limit	kWe	31.3	75.4
Lower limit	kWe	27.1	63.4
General engine performance			
Peak supported load	kWe	27.3	72.8
MBT Ignition timing	deg bTDC	24.0	22.0
BSFC (Biomass)	kg/kWeh	1.30 ± 0.05	1.00 ± 0.05
BSFC (Gas)[a]	kg/kWeh	3.30 ± 0.13	2.50 ± 0.13
BSEC [b]	MJ/kWeh	16.3 ± 0.6	12.4 ± 0.6
η_{bth} (gas to electricity)	%	22.1 ± 0.8	29.0 ± 1.4
η_{bth} (biomass to electricity) [c]	%	17.7 ± 0.6	23.0 ± 1.1
Energy balance			
Input energy	kW	123.5	250.8
	(%)	100.0	100.0
Electrical output	kWe	27.3	72.8
	(%)	22.1	29.0
Cooling load	kW	39.4	88.5
	(%)	31.9	35.3
Exhaust enthalpy [d]	kW	32.4	79.8
	(%)	26.2	31.8

[a] Biomass to gas conversion ratio - 2.5 (Dasappa, Paul, Mukunda, Rajan, Sridhar, and Sridhar 2004)

[b] Gas lower calorific value - 4.95 MJ/kg

[c] Gasifier efficiency (cold gas) - 80 % (Dasappa, Paul, Mukunda, Rajan, Sridhar, and Sridhar 2004)

[d] Includes both thermal and chemical enthalpy

lower compression ratio. A comparative analysis suggests that under turbocharged mode, while the engine E6 achieves a power 72.8 % of the frame peak load (diesel

rating), Sridhar has managed to realize only 53.9 % of the corresponding frame rating. As for the lower efficiency under naturally aspirated mode of operation, one of the key factors is the lower operating compression ratio. In comparison with literature reported natural gas fuelled operation, engine E6 experiences efficiency drop of around 7 % and 5 % respectively for the naturally aspirated and turbocharged mode of operation respectively. Some of the factors contributing to efficiency drop for syngas fuelled operation have already been discussed in detail in section 4.1.1.

Analyzing the engine energy balance, especially the cooling load, it can be observed that the cooling load observed for producer gas fuelled operation of the engine under both naturally aspirated (31 %) and turbocharged mode (33 %) for the engine E6 is similar to that recorded by Sridhar et al (32 $\pm$ 3 %) for producer gas fuelled operation of an engine with different in-cylinder geometry over a range of operating conditions. A review of literature pertaining to engine energy balance reveals the typical cooling loads for SI engines to be much lower than what is observed in the current investigation. In representing the cooling load as a fraction of the developed brake power, Heywood (Heywood 1988), Howarth (Howarth 1966) report a range of 0.8 $\pm$ 0.1 for the fraction for typical SI engines fuelled with gasoline (amounting to 22 $\pm$ 3 % of the energy input)and 1.2 $\pm$ 0.2 for typical compression ignition engines fuelled with diesel (amounting to about 35 $\pm$ 3 % of the energy input) for engine operating conditions similar to the current investigation. Similar results have been reported by Ferguson et al (Ferguson and Kirkpatrick 2001). Some of the more recent works also report similar cooling load fractions for compression ignition (Ajav, Singh, and Bhattacharya 2000) and spark ignition engines (Reitz 2013). As such, it is apparent that, the observed cooling load in excess of 30 % for producer gas fuelled operation is significantly higher than typical gasoline fuelled operation and is more inline with the lower limit of diesel fuelled operation (also refer section 5.1). It may be noted that the increase in engine cooling load potentially amplifies the influence of lower adiabatic flame temperature and in-cylinder pressure accounting for the efficiency loss, as observed in the current investigation as well as that reported by Sridhar (Rao 2003).

Preliminary analysis addressing the enhanced heat loss with producer gas fuelled operation suggests to the enhanced thermal diffusivity of the mixture due to the

presence of hydrogen in the fuel (refer table 2.4). Towards verifying the assessment, the investigation is extended to a twin cylinder engine fuelled with four different syngas compositions with varying hydrogen fraction in the fuel - air mixture. The results of the investigation are presented in a subsequent section and the discussion on the argument of hydrogen enhancing the cooling load is deferred till such time.

On the emissions, the data for engine E6 for CO and $NO_x + HC$ is consolidated in table 5.8 for 5% and 15% oxygen dilution levels. Comparing the emissions with the reference data as consolidated in table 5.2, it can be observed that both CO and the total of NO_x and HC are well within the reference standards.

Table 5.8: Emissions from 6B5.9 under NA and TA mode of operation

Mode	O_2%	Units	CO	NO_x + HC
NA	05	mg/nm^3	2994.52	139.37
		g/kWh	11.66	0.55
	15	mg/nm^3	1156.26	53.78
		g/kWh	4.50	0.21
TA	05	mg/nm^3	2403.01	640.12
		g/kWh	8.74	2.33
	15	mg/nm^3	931.45	248.11
		g/kWh	3.39	0.90

Having addressed the generic engine performance, the turbocharger performance is analyzed in details considering that it has been the key component that has enabled the engine to reach the thermodynamic limit in terms of the peak supported load.

5.3.5 Turbocharger analysis

Performance of the turbocharger is primarily analyzed by quantifying the pressure, temperature and density ratio across the compressor and the isentropic efficiency for the compressor and turbine. Quantifying the compressor and turbine work as required for the estimation of respective efficiency permits quantifying the turbocharger mechanical efficiency.

Figure 5.4 presents the compressor map for the optimized turbocharger (TC-4) compressor with the estimated and realized mass flow pressure ratio data mapped. It is important to note that, the estimated and realized data follow each other closely. At the peak load, while the mass flow rates are similar (refer inset data), the realized pseudo mass flow and pressure ratio are higher by about 15.4% and 3.6% respectively. The higher values are attributed to a close to 8 % reduction in the compressor inlet pressure. At the peak mass flow, the map suggests the compressor efficiency to be 74 %. It is also important to note that with an increase in the load, the compressor operating point gets positioned towards the center of the map leaving sufficient margin for choke and surge limit. Another feature of interest is that the peak load operating point achieved with the baseline diesel turbocharger just about crosses the minimum threshold speed limit and enters into the compressor operating regime.

It is important to note that while the compressor analysis is rather straight forward based on the measured pressure and temperature, the same is not true for the turbine. The fact that the turbocharger turbine operation is clearly diabatic as against the near adiabatic operation of the compressor render the analysis of the turbine more involved as compared to the analysis of the compressor (Heywood 1988). While the measured pressure and temperature across the compressor can be used directly to estimate the compressor work and efficiency, for the turbine, exit temperature corrections will have to be accommodated to account for various heat losses. The nature of heat loss from the turbine including the segregation into constituent components and general methodology of quantifying the total heat transfer is discussed next followed by the performance analysis of the compressor and turbine.

One of the key challenges pertaining to the analysis of a turbocharger turbine is that the turbine looses significant amount of heat to the ambient (predominantly through radiation from casing surface) and the mechanical shaft rendering the turbine flow process strongly diabatic (Rautenberg, Malobabic, and Mobarak 1984). The direct consequence of such diabetic operation of the turbine is on the estimation of the turbine efficiency (Baines, Wygant, and Dris 2010) (Serrano, Olmeda, Paez, and Vidal 2010). Due to the heat transfer (loss), the actual turbine exit temperature (T_{ex-ac}) will not be larger than the isentropic turbine exit temperature (T_{ex-is}) esti-

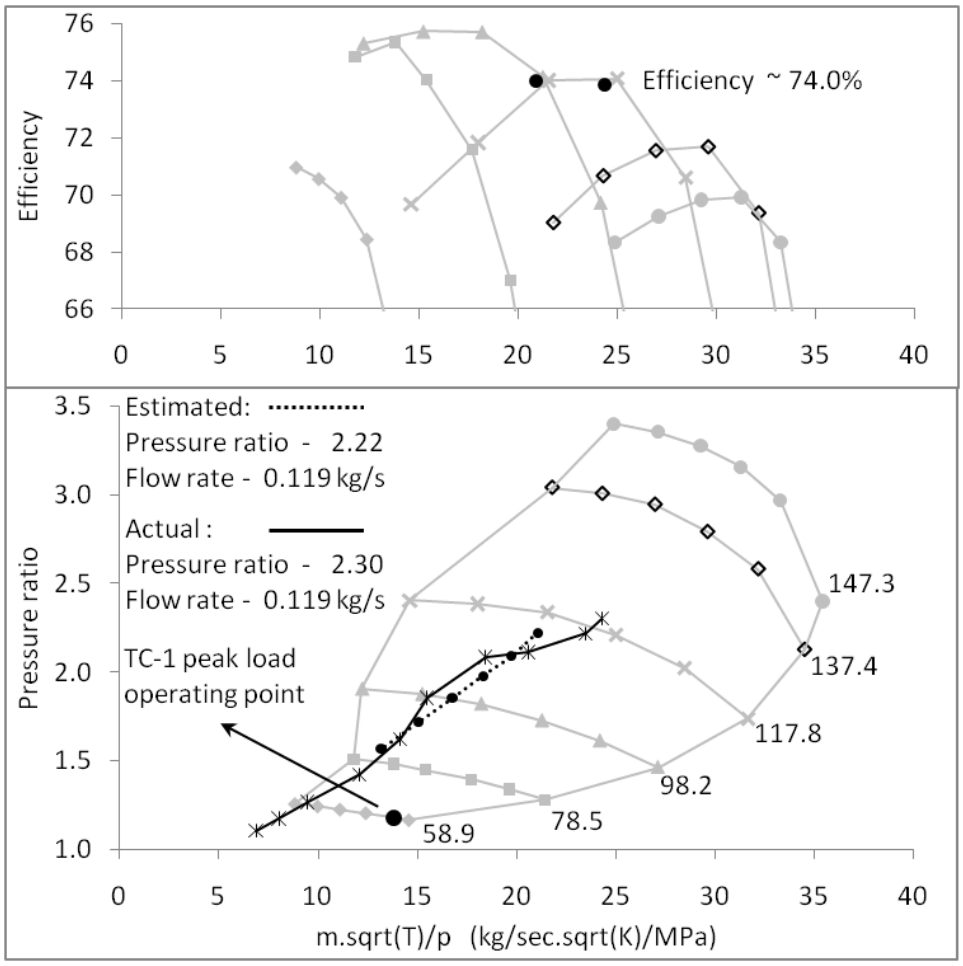

Figure 5.4: Estimated and realized mass flow and pressure data mapping on compressor map

mated based on the realized pressure ratio across the turbine, leading to the turbine diabatic efficiency being significantly higher than the adiabatic efficiency. Towards rectifying this anomaly, the heat transfer from the turbine will have to be quantified and accounted for, in the estimation of the turbine efficiency. The heat transfer from the turbine is segregated into external and internal heat transfer with the radiative and (generally) free convective losses loss from the turbine external surface and conductive losses through the connections and mountings being accounted for as external losses and the (predominantly) conductive heat loss through the connecting shaft with the bearing oil as the sink accounting for the internal losses. It is important to note that quantifying external losses is rather straight forward considering that the sections of turbine through which the heat loss occurs are easily accessible

and parametric measurements can be easily made using some standard instruments. Evaluation of internal heat transfer is however very challenging considering that it involves dealing with sections of turbine that are not directly exposed and involve high temperature corrosive gases with components rotating at extremely high speeds.

Considering the complexity of accurate measurement of turbine internal losses, the current work adopts the philosophy of explicitly quantifying the external losses based on standard measurements and the internal losses are quantified as a fraction the external losses, permitting the quantification of all the losses from the turbocharger turbine. A detailed literature review suggests the external and internal losses to constitute approximately 70 % and 30 % respectively (Baines, Wygant, and Dris 2010) (Shaaban 2004) (Shaaban and Seume 2006) (Westin, Rosenqvist, and Ångström 2004) (Cormerais, Chesse, and Hetet 2009). It may be noted that while there is some scatter pertaining fraction of internal and external losses, 70 % and 30% seem to be broadly accepted external and internal heat loss distribution for typical turbocharger turbines on SI engines. The methodology for the estimation of external heat loss on the turbine is as described below.

The external heat loss (Q_{T-ext}) from the turbine is broadly constituted of radiative (Q_{T-rd}) and free convective (Q_{T-cv}) heat loss from the external surface and conductive (Q_{T-cd}) heat loss through the connecting shaft. The external heat transfer expressed as the sum of the constituent components in terms of individual governing equations is presented as in equation 5.2.

$$Q_{T-ext} = Q_{T-rd} + Q_{T-cv} + Q_{T-cd}$$

$$Q_{T-ext} = \epsilon\sigma A_s \left[T_s^4 - T_a^4\right] + h_c A_s \left[T_s - T_a\right] + k_m A_{mc} \frac{\left[T_s - T_m\right]}{X} \tag{5.2}$$

In the estimation of external heat transfer, some of the assumptions made and material property and coefficients considered are discussed below.

1. All the components that the turbine external surface *views* and the ambient air are at ambient temperature (301.15 K) and the atmosphere is quiescent.

Thus, the ambient temperature acts as the sink temperature for the convective and radiative terms. This is a reasonable assumption as reported by Baines et al (Baines, Wygant, and Dris 2010).

2. The convective heat transfer coefficient (h_c) is estimated based on the dimensionless correlation for free convective heat transfer (Incropera 2011) as described in equation 5.3.

$$Nu = aGr^b Pr^c$$

$$\frac{h_c L}{k} = a \ * \ \left[\frac{\beta g \rho^2 L^3 [T_s - T_a]}{\mu^2}\right]^b \ * \ \left[\frac{C_p \mu}{k}\right]^c \tag{5.3}$$

3. The values used for the thermo-physical properties and dimensionless correlation coefficient are as consolidated in table below.

Having estimated the total heat transfer (loss) from the turbocharger turbine, the same is used to estimate the adiabatic turbine exit temperature and then on the turbine isentropic efficiency. It may be noted that the accuracy of the turbine isentropic efficiency is limited by the accuracy of turbine heat loss estimation.

The performance map for the compressor and turbine is consolidated in figure 5.5 (a) and (b) respectively.

The maximum isentropic efficiency for the compressor is 74.5 % which is similar to the efficiency identified from the compressor map (refer figure 5.4) and is in line with literature reported values of around 75 % (Heywood 1988) (Dasappa, Sridhar, and Indrajit 2011). Dasappa et al (Dasappa, Sridhar, and Indrajit 2011) have reported an isentropic efficiency of around 77 % for a different engine turbocharger at a load of 110 kWe operating on producer gas. The peak load compressor work evaluates to 14.2 kWe amounting to 20 % of the peak load delivered by the engine. Analysis of the turbine performance indicates that for loads greater than 70% of the peak load, the under 10 K difference prevailing between the isentropic and actual exit temperatures increases to about 50 K on applying the heat loss correction as

Table 5.9: Thermo-physical and material properties and other coefficients used in the estimation of turbine heat loss

Parameter	Units	Magnitude
Turbine material property		
Casing emissivity (ϵ) (Sinha 2003)	–	0.75
Casing base conductivity (k_m)(Sinha 2003)	$W/m-K$	53.3
Constant coefficients		
Stefan–Boltzmann constant (Incropera 2011)	W/m^2K^4	5.67 x 10^{-8}
Dimensionless correlation a (Baines, Wygant, and Dris 2010)		0.20
Dimensionless correlation b (Baines, Wygant, and Dris 2010)		0.25
Dimensionless correlation c (Baines, Wygant, and Dris 2010)		0.25
Acceleration due to gravity	m/s^2	9.81
Thermo-physical properties * (representative data for peak load)		
Thermal conductivity (k) x 10^3	$W/m-K$	40.8
Density (ρ)	kg/m^3	0.6921
Dynamic viscosity (μ) x 10^7	Ns/m^2	280.3
Specific heat at constant pressure (C_p)	$kJ/kg-K$	1.032
Volumetric thermal expansion coefficient (β)	$1/K$	0.0019

Corresponding to temperature of 515 K (peak load surface - ambient average)

discussed above. The isentropic turbine efficiency estimated based on the corrected temperature approaches 73 % at the peak load and remains between 60 % and 65 % at the other loads. It is important to note that, the turbine efficiency remains rather flat at around 63 % till about 50 kWe and then increases with load. The turbine work at peak load is estimated at 16.4 kW amounts to about 5 % of the input energy and 23 % of the engine output.

Quantification of the turbine and compressor work permits estimating the turbocharger mechanical efficiency. The mechanical efficiency varies from 60 % at no load conditions to reach a maximum of about 88 % at peak load operation.

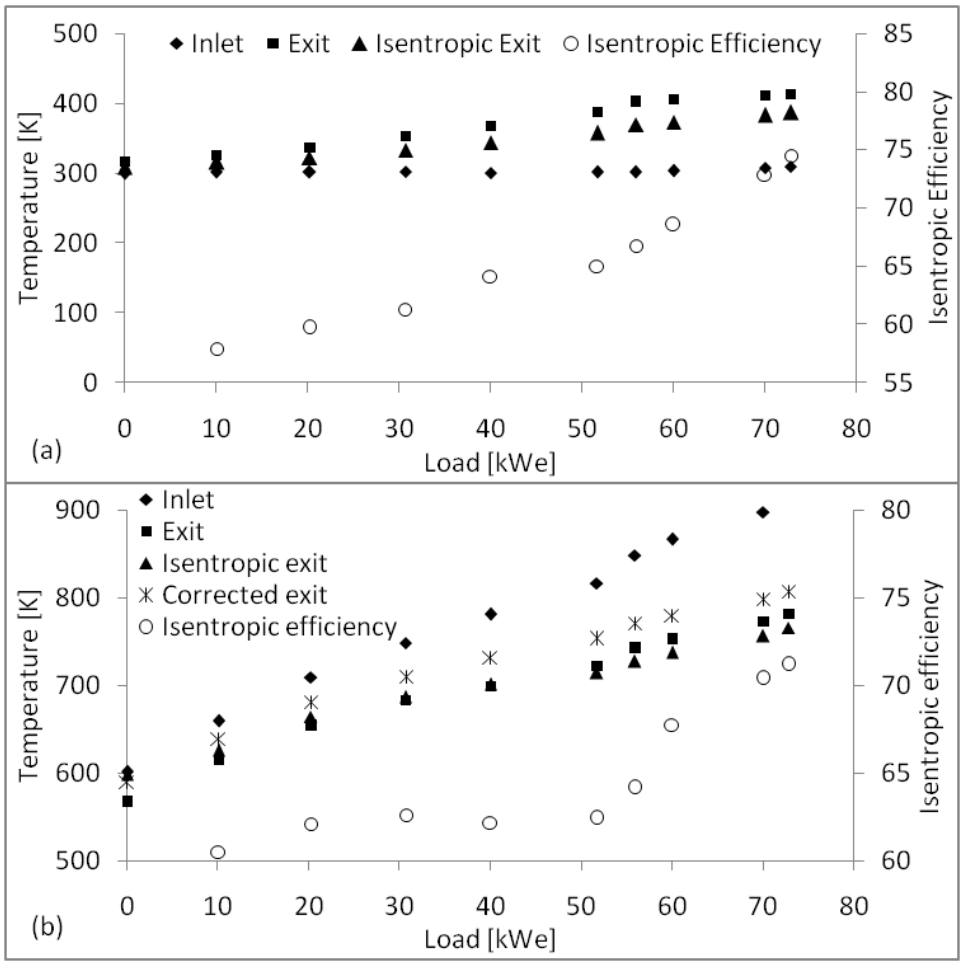

Figure 5.5: Thermodynamic analysis of the turbocharger turbine and compressor

5.4 Studies on hydrogen rich syngas fuelled operation

Towards verifying the preliminary assessment based argument that hydrogen in producer gas alters the mixture thermo-physical properties, leading to enhanced engine cooling load, a two cylinder engine is operated with four different syngas compositions and the engine peak load performance data is acquired. Towards isolating the influence of syngas hydrogen fraction on the engine performance in general and cooling load in particular, the four syngas compositions selected are such that, at the same equivalence ratio, the mixture hydrogen fraction increases while keeping the concentration of other combustibles like carbon monoxide and methane constant

(refer table 4.3). The peak load realized, corresponding conversion efficiency and the engine energy balance for the four syngas compositions operating at respective maximum brake torque ignition timings are consolidated in table 5.10.

Table 5.10: Syngas fuelled operation of engine E2 - performance and energy balance

		SG-1	SG-2	SG-3	SG-4
General engine performance					
Estimated peak load	kWe	05.3	07.5	08.4	09.8
Experimental peak load	kWe	05.4	06.0	06.4	07.1
MBT Ignition timing	deg bTDC	25	23	20	18
BSFC	g/kWh	6235	4285	2887	2050
BSEC	MJ/kWh	19.6	17.9	15.2	15.5
η_{bth}	%	18.4	20.1	23.6	23.3
Energy balance					
Input energy	kW	29.4	29.8	27.1	30.5
	(%)	100	100	100	100
Electrical output	kW	05.4	06.0	06.4	07.1
	(%)	18.4	20.1	23.6	23.3
Cooling load	kW	09.9	10.4	10.0	12.0
	(%)	33.5	34.8	36.7	37.7
Exhaust thermal enthalpy	kW	09.5	08.7	07.3	07.8
	(%)	32.4	29.3	27.0	25.4

Some of the key features of syngas fuelled operation of engine E2 are as consolidated below;

1. Comparing the peak load realized with the estimated peak load (refer table 4.4) it can be observed that the delivered load falls short of the estimated load for all the compositions except for SG-1. What is rather interesting is, the shortfall increases with increasing mixture hydrogen fraction and calorific value (deficiency of 16% for SG-2 with 9.5 % mixture hydrogen fraction increases to 28% for SG-4 with 14% mixture hydrogen fraction).

2. The brake thermal efficiency increases with increasing mixture calorific value and hydrogen fraction. The efficiency is in general lower than the typical values for conventional fuels (about 30%; refer table 5.1).

3. The engine cooling load, the parameter of interest for the current investigation, is significantly higher (by over 10 %), as compared to typical values for gasoline operation and approaches / surpass the general upper limit for typical diesel operation (refer figure 5.1). Towards addressing the overall higher cooling load for syngas fuelled operation as compared to typical spark ignition engine operation, it is important to note that the current engine, similar to most natural gas engines, is adapted from a baseline diesel engine (Johansson and Olsson 1995). In the adaptation process, while the combustion chamber is modified to reduce the compression ratio, the original inlet port of the engine (designed for generating highly swirling gas motion as required for efficient droplet evaporation and subsequent combustion (Heywood 1988) (Lyn 1963)) and the cylinder head generally remains unaltered considering the adaptation challenges involved. The piston is modified to (generally) render a cylindrical or narrow angle frustum of cone bowl in piston geometry (Lyn 1963) as in the current investigation. The considered in-cylinder geometry (ies) along with the unmodified inlet port (that gives high swirl) and the squish ensures significantly higher levels of in-cylinder turbulence as compared to inlet port combustion chamber geometry tuned for SI operation. This has been explicitly established by Johansson et al (Johansson and Olsson 1995) based on laser doppler velocimetry based in-cylinder turbulence measurement. High in-cylinder turbulence leads to enhanced convective losses from the containing surfaces (Borman and Nishiwaki 1987) (Alkidas 1980) (Han and Reitz 1997). The increase in convective cooling losses with a commensurate increase in the level of turbulence has been explicitly established by Poulos and Heywood (Poulos and Heywood 1983). In an engine simulation work based on a thermodynamic model proposed by Keck (Keck 1982) and Beretta (Beretta, Rashidi, and Keck 1983), Poulos and Heywood have reported that on doubling the turbulence intensity, the engine cooling load increased by around 15%. It is explicit from the foregone discussion that SI engines adopted from baseline diesel frames without corresponding

tuning of the intake port (as in the current investigation) experience significantly higher cooling loads. Thus, one of the factors contributing to the higher cooling loads is the significantly higher in-cylinder turbulence.

4. The engine cooling load increases with mixture hydrogen fraction, indicating sensitivity to mixture hydrogen fraction. The near doubling of mixture hydrogen fraction from 7% to 14 % leads to an increase in the cooling load by about 4% points.

One of the key outcome of the above discussion in respect of SI engines adopted from diesel frames and fuelled with hydrogen containing gaseous mixtures is the evidence towards the influence of fluid dynamic and thermodynamic effects on the convective heat losses. The current work focuses explicitly on addressing the influence of mixture hydrogen fraction on the thermo-physical properties and subsequent influence on the cooling load. Quantifying and addressing the influence of in-cylinder fluid dynamics is not in the scope of the current investigation. A discussion on the potential factors contributing to enhanced engine cooling load for producer gas fuelled operation is deferred till section 5.5 where in-cylinder pressure trace and apparent heat release profiles are discussed. Increased engine cooling load is expected to influence the in-cylinder pressure profile in general and peak pressure in particular, altering the apparent heat release profile. A more concrete argument can be made in reference to the apparent heat release profile representing the full combustion process as compared to the energy balance which is representative of a complete cycle.

5.5 In-cylinder response

The current section addresses the in-cylinder response of the three engine frames, $E2$, $E4$ and $E6$ through the analysis of in-cylinder pressure and heat release traces. The primary focus is on the comparison of producer gas fuelled response with that of natural gas towards formally quantifying the differences between bio-derived low calorific value fuel and a conventional high calorific value fuel. The comparison is expected to assist in addressing the influence of fuel-air mixture thermo-physical properties on various segments of the engine cycle. The significance of pressure

trace based analysis rests in the fact that, the pressure crank angle trace essentially represents the thermo-kinematic response of an engine i.e., the finite rate heat release and subsequent pressure change in a dynamic kinematic environment involving non linear variation of containing volume.

5.5.1 Pressure evolution comparison

The general evolution of in-cylinder pressure with crank angle is presented in figure 5.6. Figure 5.6 (a) presents the profiles for the spark sweep test on the six cylinder engine ($E6$) under naturally aspirated mode of operation. It is important to note that, while the extent of spark advance is generally limited by end gas auto-ignition (Chun and Heywood 1989) (Yates, Swarts, and Viljoen 2005), at least for the conventional fuels, no such behavior was observed for producer gas fuelled operation under naturally aspirated mode. This is evident from the smooth evolution of the profile at 28 deg before the top dead center. Even at ignition 30 deg before the top dead center, no high frequency components were observed on the pressure trace. The limiting condition was set at 28 deg before the top dead center because of the unstable engine operation, in terms of engine speed fluctuation, at 30 deg before the top dead center. It is apparent from the observed behavior that, irrespective of the degree of spark advance, the thermodynamic conditions within the engine cylinder do not evolve to the extent of triggering rapid build up of radicals to trigger auto-ignition in the mixture. One of the primary factors contributing to the observed behavior pertains to the enhanced cooling of the mixture, especially in the vicinity of the cylinder chamber walls, as observed in the engine energy balance analysis. As for the turbocharged mode of operation is concerned, the ignition advance was largely limited by cyclic variations. However, in one odd over advanced cycles (due to cyclic variations) faint traces of knock were evident.

Having reviewed the evolution of the pressure traces for the spark sweep under naturally aspirated mode, the full load range pressure crank angle traces for the turbocharged mode of operation at maximum brake torque ignition timing are consolidated in figure 5.6 (b). The peak load pressure crank angle traces for producer gas fuelled operation under both naturally aspirated and turbocharged after-cooled mode of operation are compared with corresponding traces for gasoline and natural

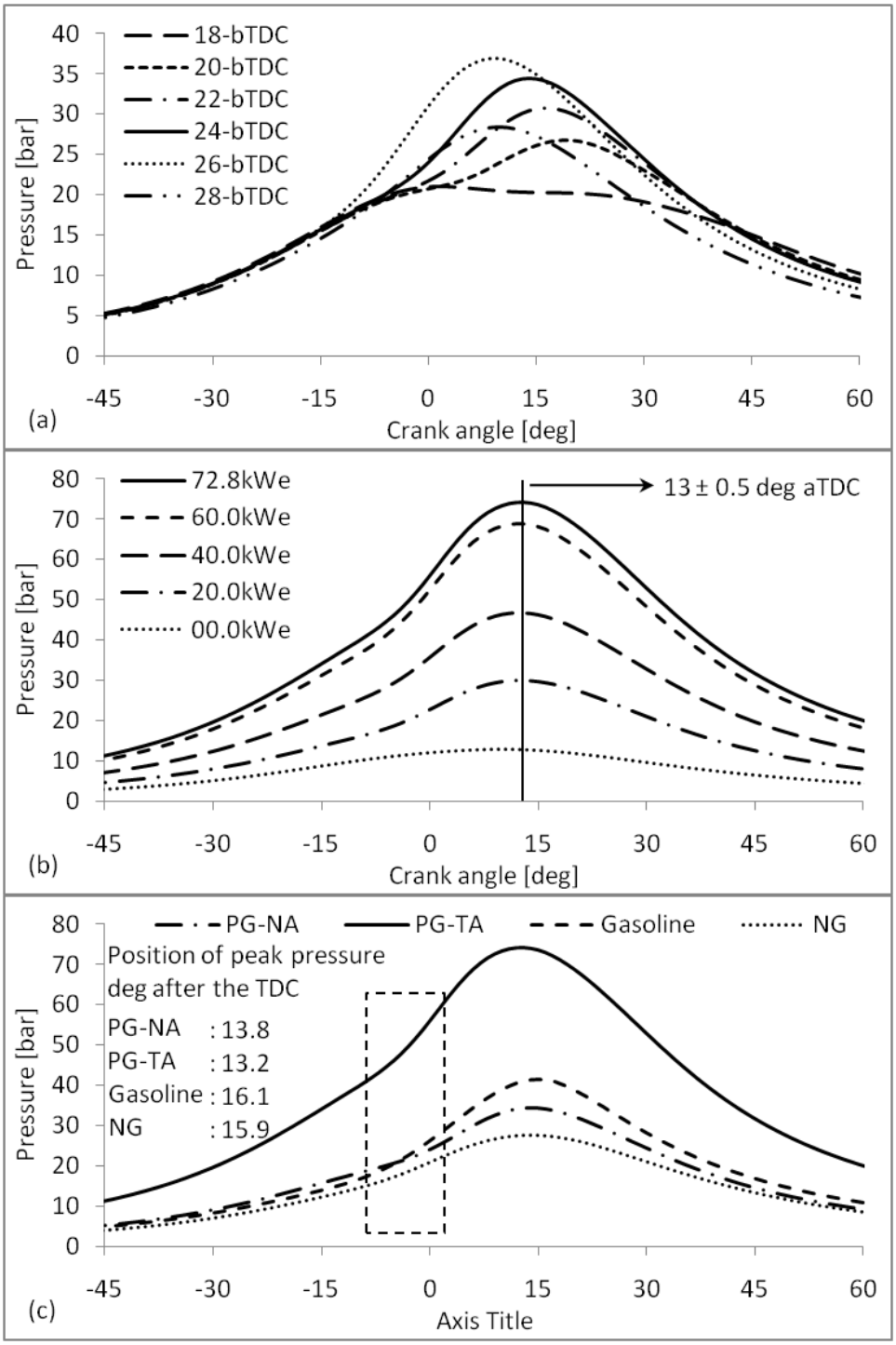

Figure 5.6: Pressure crank angle traces for producer gas, natural gas and gasoline (a) Engine $E6$ - naturally aspirated spark sweep test (b) Engine $E6$ - turbocharged maximum brake torque load range test and (c) Maximum brake torque ignition pressure trace comparison for producer gas, natural gas and gasoline

gas in figure 5.6 (c). The gasoline trace is from a four cylinder engine sample data pre-loaded with the AVL indicating system.

The nature of pressure profile evolution between conventional fuels and producer gas is non trivially different. The difference is pronounced in the compression region in the vicinity of the top dead center [boxed region in figure 5.6 (c)] and the position of peak pressure. This behavior in the compression region can be clearly analyzed by plotting the pressure rise rate as a function of crank angle as in figure 5.7 where, a bi-modal profile is clearly evident for producer gas fuelled operation as against smooth and continuous evolution for natural gas and gasoline. For producer gas fuelled operation, the pressure rise due to heat release overcomes the kinematics dictated reduction in pressure rise only late into the cycle due to the ignition retard as compared to natural gas / gasoline, hence the behavior. The advantage of such a well defined transition is in the identification of start of combustion crank angle, crucial in numerical simulation studies. This aspect is discussed in details in modeling and simulation chapter.

The other point relates to the position of peak pressure. As indicated, the position of peak pressure in case of producer gas fuelled operation is advanced towards the top dead center by about 3 deg crank angle as compared to conventional fuels. It is interesting to note that the the position of peak pressure advance occurs over coming the ignition retard towards maximum brake torque ignition, indicating an overall reduction in the combustion duration. The response can be attributed to the higher laminar flame speed for producer gas as compared to typical conventional fuels.

The deviation(s) in producer gas fuelled incylinder pressure profile from characteristics conventional fuel profiles manifest as deviation in the heat release profile. The deviation(s) in heat release profile and subsequent consequences on engine operation, especially diagnostics and control, are discussed in the next section dealing with the heat release profiles.

5.5.2 Cumulative heat release profiles

Comparing the heat release pattern for producer gas fuelled operation with that of natural gas and gasoline permits quantifying the differences and assessing the influ-

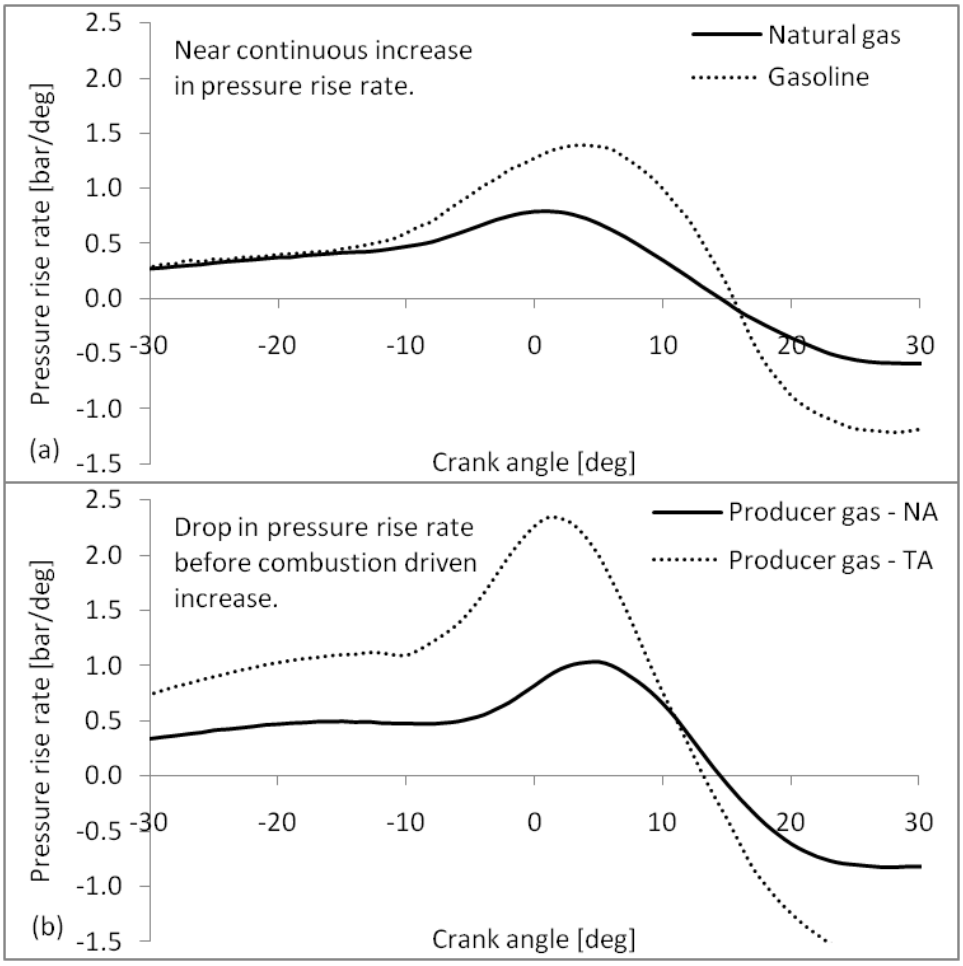

Figure 5.7: Pressure rise rate against crank angle for (a) conventional fuels and (b) producer gas

ence of fuel thermo-physical properties on various stages of the combustion process. Figure 5.8 (a) compares the maximum brake torque ignition peak load cumulative (apparent) heat release profiles for producer gas (both naturally aspirated and turbocharged) with the profiles for gasoline and natural gas. The duration of various stages of combustion / heat release is quantified in terms of corresponding crank angle degrees as in figure 5.8 (d). The key features of the heat release profile are as below;

1. The overall nature of heat release profile for producer gas and conventional fuels is significantly different with producer gas and conventional fuel profiles banding out separately. While the conventional fuels heat release profile present

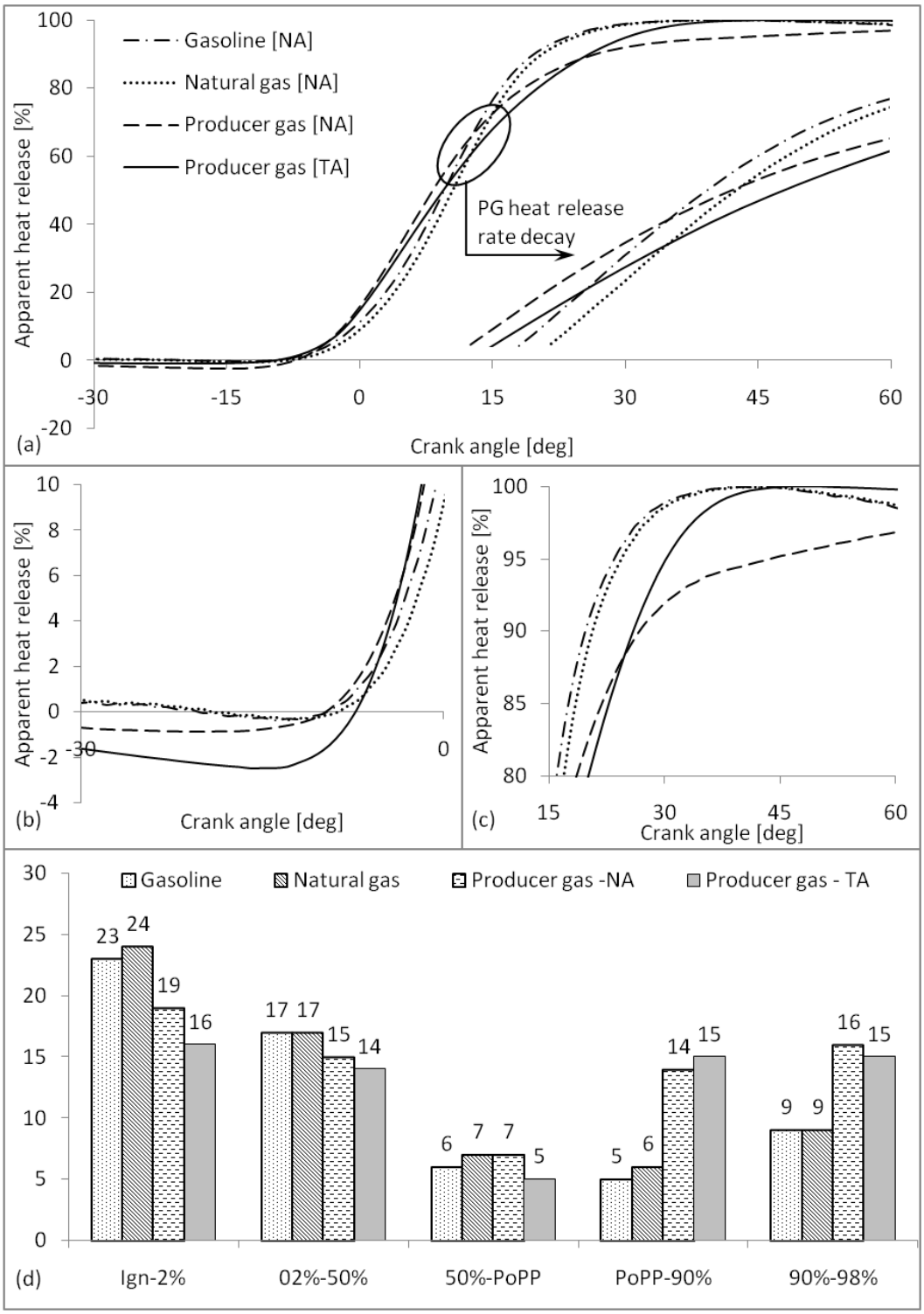

Figure 5.8: Heat release profiles and combustion duration for producer gas and conventional fuels

a rather well defined **S** shaped profile, the profile for producer gas is a well defined concave as seen from the top left corner.

2. Reviewing the initial heat release stage (refer figure 5.8 b), two interesting features become apparent. The first feature pertains to the significantly negative apparent heat release for producer gas. From a pure thermodynamic view point, negative apparent heat release indicates a lower in-cylinder pressure than the commensurate adiabatic pressure corresponding to the compression process. Larger the negative apparent heat release, lower will be the in-cylinder pressure. For a typical closed system compression process, as in the case of internal combustion engines, the only major source of pressure reduction is through the heat loss from the walls. It is important to note that the significantly larger negative heat release trend is commensurate with the higher engine cooling loads recorded. The second feature corresponds to the slope of the pressure trace as the heat release enters into the positive territory (pressure in the cylinder is greater than that due to compression alone). It can be observed that for producer gas fuelled in-cylinder heat release rate; in both naturally aspirated and turbocharged modes of operation, is substantially higher than corresponding gasoline and natural gas heat release rate. In an engine, higher heat release rates essentially correspond to faster burning of the mixture, attributed to the higher laminar flame speed for producer gas as compared to gasoline and natural gas. The initial heat release stage, considered from the time of ignition to 10% of cumulative heat release, is faster by 17% and 21% for producer gas fuelled naturally aspirated operation over gasoline and natural gas respectively while it is 30% and 35% for turbocharged operation.

3. Reviewing the fast burn phase, it can be observed that producer gas fuelled combustion is significantly superior in terms of duration as compared to natural gas and gasoline, suggesting to the possibility of significantly faster burning of the mixture.

4. Reviewing the terminal phase of combustion (refer figure 5.8 (c)), it is interesting to note that producer gas combustion is rendered sluggish beyond the 90 % heat release pattern. Sluggishness of heat release suggests potential de-

speeding of the engine flame, attributed to the enhanced cooling of the mixture upstream of the flame due to higher thermal diffusivity (refer section 2.3.2). In the assessment of terminal stage combustion, of particular importance is the duration from the position of peak pressure to 98 % heat release. The terminal phase culmination is set at 98% considering the uncertainty involved in exact determination of completion of combustion angle (Shayler, Wiseman, and Ma 1990) (Brunt and Emtage 1997) (Brunt, Rai, and Emtage 1998) (Baratta, dAmbrosio, Spessa, and Vassallo 2006). The time taken for position of peak pressure to 98% heat release segment for producer gas fuelled operation under both naturally aspirated and turbocharged mode, is double the time taken by gasoline and natural gas.

Some of the key differences between producer gas and gasoline / natural gas pressure and heat release profiles have been attributed to the presence of hydrogen in producer gas. While the analysis of producer gas thermo-physical properties (refer section 2.3.2) supports the arguments forwarded, investigating an engine with different syngas compositions permits further analysis. Such an investigation also allows for analyzing the isolated influence of mixture hydrogen fraction alone considering that other influencing parameters like geometry of intake port and combustion chamber (with influence on turbulence) and compression ratio (influence on engine thermodynamic conditions and turbulence through squish) all remain fixed.

The influence of syngas mixture hydrogen fraction on the heat release pattern and the duration of combustion is consolidated in figure 5.9. With increasing H_2 fraction in syngas, the first half heat release rate is significantly higher and the second half, especially the post position of peak pressure regime tends to become sluggish. This is consistent with the observation on PG fuelled operation (refer figure 5.8). The heat release regime is segregated into the initial flame development phase (10% of heat release), the rapid burn phase (10% to 90% of heat release) and the terminal phase (from 90% to 98%) (Heywood 1988). The duration of the three stages of combustion in absolute degrees and fraction of full cycle (%) for the four compositions are consolidated in figure 5.9 (c) and (d) respectively. The following discussion, pertaining to the three stages of combustion, brings out the physics governing the observed pattern.

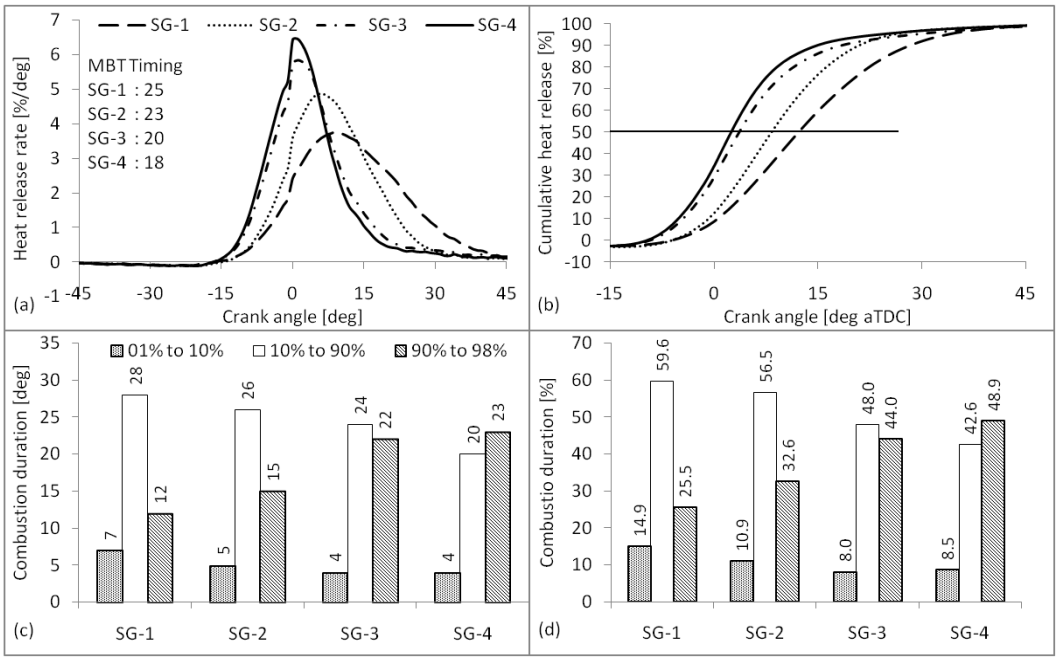

Figure 5.9: Influence of syngas hydrogen fraction on heat release profile

1. **Initial development phase:** With an increase in the mixture H_2 fraction, the initial flame development period reduces. This response can be addressed by analyzing the key factors that influence the flame development period in the operational scenario like the mixture thermo-physical properties and the flame kernel energy balance (Pischinger and Heywood 1991) (Shen, Hinze, and Heywood 1994) (Eisazadeh-Far, Parsinejad, Metghalchi, and Keck 2010). The reduction is primarily attributed to higher mixture reactivity and hence flame speed and the reduction of minimum ignition energy required with increasing H_2 fraction (in mJ ; $E_{min} : SG-1 \propto 0.00337$, $E_{min} : SG-2 \propto 0.00058$, $E_{min} : SG-3 \propto 0.00031$ and $E_{min} : SG-4 \propto 0.00011$; estimates based on equation 5.4, refer (Kurdyumov, Blasco, Sánchez, and Linan 2004)).

$$E_{min} \propto \rho C_p T \left(\frac{\alpha}{S_L}\right)^3 \tag{5.4}$$

With increasing H_2 fraction, while the minimum ignition energy required reduces, the spark energy remains constant for all the four compositions (except for the change accompanying charge capacitance variation) and the fraction of energy in excess of the minimum required increases. The increase in the

electrical energy leads to the establishment of a larger flame kernel with higher mean temperature that transits faster into a turbulent chemical flame (Maly 1984) (Eisazadeh-Far, Parsinejad, Metghalchi, and Keck 2010) leading to a reduction in the initial flame development period. The same argument holds for the reduction in the initial burn period for producer gas as compared to gasoline and natural gas.

2. **Fast burn phase :** Response of the fast burn phase of combustion is along expected lines with the combustion duration decreasing with an increasing in mixture H_2 fraction. Analysis of the nature of premixed turbulent combustion prevalent in typical engine like environments is useful to describe the observed trend. Photographic evidence based on schlieren/shadowgraphy techniques (Gatowski, Heywood, and Deleplace 1984), laser scattering techniques (Keck 1982) (Mounaïm-Rousselle, Landry, Halter, and Foucher 2013) and comparison of laminar flame thickness - Kolmogorov scale as in Borghi - Peters diagrams (Peters 1989) (Peters 1999) indicates the combustion in SI internal combustion engines to be mostly being in the flamelet (wrinkled laminar flame) regime and some times extending to flamelet in eddies regime (Stephen 2000) (Abraham, Williams, and Bracco 1985) depending on the operating condition. In the flamelet regime, while the eddies wrinkle the thin flame front, the combustion itself is at the characteristic laminar flame speed. Wrinkling of the flame front leads to the formation of islands or peninsular regions of unburned mixture (Keck 1982) (Heywood 1988) (Borghi 1985) (Pope 1987) (Peters 2000) increasing the flame area and the unburned mixture consumption rate. As such the the influence of turbulence is reduced to wrinkling the flame front with the actual burning still governed by the mixture thermo-physical properties. The essence of the flamelet regime has been captured by various researchers as below.

$$S_t = S_L + V_{rms} \qquad \text{(Damkohler model (Stephen 2000))} \tag{5.5}$$

$$S_t = S_L + S_L V_{rms}^2 \qquad \text{(Clavin and Williams model (Stephen 2000))} \tag{5.6}$$

$$S_t = 3.5 S_L^{0.3} V_{rms}^{0.7} \qquad \text{(Klimov model (Stephen 2000))} \tag{5.7}$$

As evident from the above argument, for similar turbulence conditions in the engine cylinder, the burning rate directly depends on the laminar flame speed. Thus, the reduction in fast burning duration from SG-1 to SG-4 is primarily attributed to the increase in the mixture H_2 fraction.

3. **Terminal phase :** In the terminal phase, doubling of mixture H_2 fraction (from C1 to C4) leads to doubling of the combustion duration, both in absolute degrees and fraction of full cycle terms. Towards addressing this response, some aspects pertaining to the thermal boundary layers and flame position in the vicinity of the position of peak pressure are reviewed.

   Under typical SI engine like conditions, the boundary layer thickness is reported to be of the order of about a millimeter in the immediate vicinity of top dead center for typical hydrocarbon fuels (Lyford-Pike and Heywood 1984). The boundary layer grows as per the equation 5.8.

$$\delta_T = 0.6(\alpha t)^{\frac{1}{2}} Re^{\frac{1}{5}} \tag{5.8}$$

   It is evident from equation 5.8 that the boundary layer thickness grows as the square root of thermal diffusivity. Thus, with increasing H_2 fraction, the boundary layer thickness also increases and an increasing portion of mixture is present in the boundary layer. Considering the fact that higher H_2 fraction also entails enhanced convective losses (as discussed in section 5.3.4) a greater fraction of mixture runs increasingly cooler as the mixture H_2 fraction increases. On the flame position in the vicinity of the position of peak pressure, simultaneous analysis of flame development (photographic) and in-cylinder pressure evolution suggests that the turbulent flame touches the wall farthest from the spark plug just after the position of peak pressure (Beretta, Rashidi, and Keck 1983) (Keck 1982) (Heywood 1988) and at this stage, another 20 to 25 % of the mixture is yet to burn. The combustion of this 20 to 25 % of the mixture constitutes the terminal phase. With increasing mixture H_2 content, increasing fraction of relatively cooler mixture is burned in the terminal phase of combustion leading to an increase in the corresponding combustion duration. Based on the observations, the laminar flame propagation retard caused by the

temperature drop is significant enough to overcome the laminar flame speed increase associated with higher mixture H_2 fractions (from SG-1 to SG-4). This is verified from the comparison of laminar flame speed data for the four gas compositions as consolidated in Table 5.11.

Table 5.11: Laminar flame speed variation with temperature at stoichiometry

	SG-1	SG-2	SG-3	SG-4
	Laminar flame speed (cm/s)			
400 K	27	52	63	93
450 K	37	68	83	120
500 K	48	88	106	152
550 K	64	113	135	191
600 K	83	144	172	236
650 K	108	185	215	292
700 K	140	230	268	359

It can be observed from Table 5.11 that for stoichiometric mixtures of gases SG-1 and SG-2, within a temperature difference of 100 K, the laminar flame speeds almost become equal while for SG-3 and SG-4, the laminar flame speed of SG-3 surpasses that of SG-4. This behavior is more pronounced at higher temperature as compared to lower temperatures.

The comparative assessment of heat release pattern for producer gas fuelled operation with that of natural gas and gasoline and the subsequent analysis of syngas hydrogen fraction on the heat release pattern unequivocally establishes the differential influence of hydrogen on the heat release pattern and hence the pressure profile.

The modification of heat release pattern and the pressure profile, while influencing the chemical to mechanical energy conversion process, also has a profound influence on the engine diagnostics and control. This aspect is as described in the next section.

5.5.3 Combustion descriptors

Having the engine to respond to dynamically varying parameters to position the ignition to deliver maximum (or knock limited) brake torque is one of the most critical requirements of an engine electronic control unit. Modern control systems adopt stochastic closed loop systems that (predominantly) use in-cylinder pressure trace derived information as a control parameter (Kawamura, Shinshi, Sato, Takahashi, and Iriyama 1989) (Mueller, Hart, Truscott, Noble, Kroetz, Eickhoff, and Cavalloni 2000). A review of the literature indicates that, under maximum brake torque ignition settings, pressure-crank angle profiles and their derivatives (like heat release and mass burn fraction traces) attain inflection characteristics at fixed crank angles and deviation from these angles suggest **OFF** maximum brake torque operation. The pressure and heat release trace derived inflection parameters are known as combustion descriptors (Pipitone 2008) as they quantify phasing of the combustion process in relation to crank angle. Stochastic control systems use the deviations in combustion descriptors from maximum brake torque reference values to tune the ignition timing to re-position the engine operation at maximum brake torque. Literature reports the use of a number of combustion descriptors towards engine control for maximum brake torque operation (Pipitone 2008). Some of the prominent combustion descriptors used are the position of peak pressure (reported by Hubbard et al., (Hubbard, Dobson, and Powell 1976)), the position of peak pressure rise rate (reported by Cook et al. (Cook, Heinicke, and Haynie 1947)), position of maximum heat release rate (reported by Pipitone (Pipitone 2008) and Beccari (Beccari and Pipitone 2004)), position of 50% mass burn fraction (proposed by Bargende (Bargende 1995) and Leonhardt (Leonhardt, Muller, and Isermann 1999)) and pressure ratio 10 degrees after the top dead center. It is important to note that almost the whole of literature available deals with and quantifies combustion descriptors for conventional fuels and none for alternative fuels like producer gas.

The discussion on combustion descriptors for producer gas fuelled operation is critical considering that the differences between the pressure and heat release profiles of producer gas and natural gas / gasoline are bound to influence the combustion descriptors in terms of magnitude at maximum brake torque timing and parametric variations. In such a scenario, a naive adaptation of control logic based on charac-

teristics for conventional fuels is expected to have detrimental effect on the overall engine performance.

Considering the significance of analysis of combustion descriptors for producer gas fuelled operation, the maximum brake torque operation descriptors magnitude for naturally aspirated and turbocharged operation of engine E6 with producer gas are consolidated and compared with the standard literature reported values for conventional fuels (gasoline) in table 5.12.

Table 5.12: Comparison of producer gas descriptors with literature reported values at maximum brake torque ignition timing

	PoPP (degrees)	PoMBF50 (degrees)	PoMHR (degrees)	PRM10
Producer gas - NA	13.8	10.0	10.1	0.45
Producer gas - TA	13.2	9.90	9.50	0.46
Gasoline / Natural gas	16.0	10.1	10.1	0.52
Standard	14-16[a]	~ 9[b]	~ 9[c]	0.55[d]

[a] : (Heywood 1988)(Hubbard, Dobson, and Powell 1976)
(Kawamura, Shinshi, Sato, Takahashi, and Iriyama 1989)

[b] : (Bargende 1995)(Leonhardt, Muller, and Isermann 1999)
(Beccari, Beccari, and Pipitone 2010)

[c] : (Pipitone 2008)(Beccari and Pipitone 2004)

[d] : (Matekunas 1986)

An interesting feature evident from the above consolidation is that, while the position of maximum heat release and the 50% mass burn fraction show a close match with conventional fuels, the position of peak pressure and the pressure ratio factor are significantly different. If the conventional logic is adopted, the engine control unit would identify the maximum brake torque operation as over advanced and would retard the ignition timing. As such, the need for redrawing the reference data map is explicitly evident. Beyond the reference data map, it is also important to note that, the sensitivity of the descriptors to ignition angle, a factor critical for the control logic could be significantly different from producer gas fuelled operation as

compared to engine operation with conventional fuels. The sensitivity of key combustion descriptors to ignition angle for producer gas fuelled operation is consolidated in figure 5.10. Null hypothesis based goodness of fit (R^2) (Ross 2009) for the linear correlation is presented as inset data. Legends around the data points correspond to maximum brake torque ignition timing descriptor magnitude for respective fuel / mode of operation.

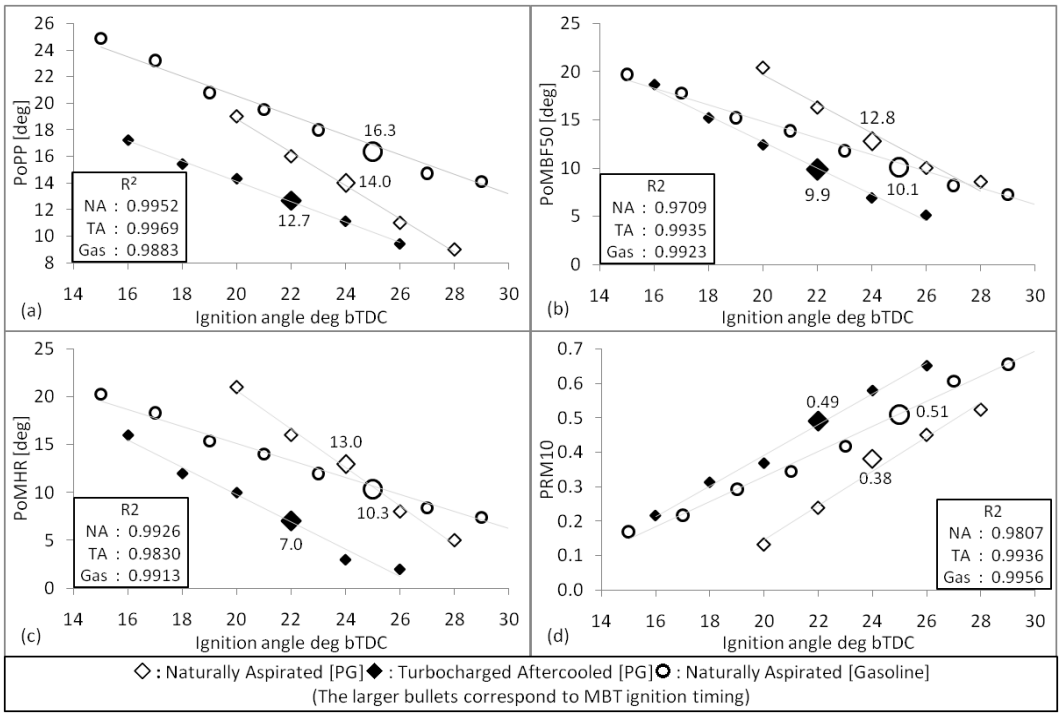

Figure 5.10: Ignition angle sensitivity analysis

It is evident from figure 5.10 that all descriptors vary linearly with respect to ignition angle. Further, least square curve fit indicates a goodness of fit greater than 0.97, consistent with gasoline operation (Pipitone 2008). Slopes (sensitivity coefficient) of linear least square curve fit for producer gas fuelled naturally aspirated and turbocharged mode of operation along with gasoline/natural gas operation are consolidated in table 5.13. A comparison of the sensitivity is also presented.

It is evident from the data presented in figure 5.10 and table 5.13 that the sensitivity to ignition angle is significantly different for producer gas fuelled operation, being much severe, as compared to conventional fuels.

The foregone discussion unequivocally establishes the need for complete re-calibration

Table 5.13: Sensitivity of descriptors for producer gas and Gasoline operation

Descriptor	NA	TA	Gas/NG
PoPP	-1.250	-0.764	-0.738
PoMBF50	-1.505	-1.359	-0.859
PoMHR	-2.000	-1.429	-0.887
PRM10	+0.050	+0.044	+0.037

of the engine control logic when adopting for producer gas fuelled operation. A direct consequence of the differences in the fuel thermo-physical properties.

5.5.4 Steady and transient analysis

Internal combustion engines, even under steady state operating conditions, experience cycle to cycle variation in the heat release and hence pressure evolution, primarily due to cyclic variations in the thermo-physical and fluid dynamic characteristics. The variations are attributed to property fluctuations especially in the immediate vicinity of the spark plug during the flame kernel growth phase (Keck, Heywood, and Noske 1987) (Ozdor, Dulger, and Sher 1994) (Johansson 1996). Cyclic variations, through their influence on the pressure profile and phasing, significantly influence the individual cycle indicated mean effective pressure and as such statistical analysis of indicated mean effective pressure is suggested as ideal and comprehensive method of quantifying cyclic variations. A review of literature indicates the upper threshold of 10% for the coefficient of variation beyond which the vehicle driveability seems to deteriorate significantly (Heywood 1988). Hydrogen is generally used as an additive in Methane / Gasoline fuelled engines towards reducing engine cyclic variability. While a general reduction in cyclic variability is observed with increasing hydrogen fraction (Hu, Huang, He, Jin, and Zheng 2009) (Ji and Wang 2009) (Arroyo, Moreno, Muñoz, Monné, and Bernal 2014), the influence seems to be significant in the lean operating regime, where the combustion characteristics of the fuel-air mixture are rather poor. On approaching stoichiometry, the influence of hydrogen on the cyclic variability seems to diminish significantly (D'Andrea, Henshaw, and Ting 2004) (Ma, Wang,

Liu, Li, Wang, and Zhao 2007) (Ma and Wang 2008). Considering that producer gas contains close to 20 % hydrogen, the engine performance should theoretically be superior as compared to conventional fuels. Statistical analysis of the producer gas fuelled operation indicated mean effective pressure data for 250 consecutive cycles on the engine E6 indicates the coefficient of variation of under 2% for both naturally aspirated and turbocharged mode of operation. This, significantly superior response for producer gas fuelled operation is primarily attributed to the rather robust initial flame kernel development period as discussed in the previous section.

While the engine operation is significantly superior in terms of steady state cyclic variations, being well within the threshold conditions, another key feature relevant for power generating engines is the block loading/unloading response time. In the current investigation, all the engines used adopted Class – 1 governing system which is required to provide a maximum frequency recovery time of 10 seconds for no load to 64 % of peak block loading as per ISO 8528. The block load response of the engine E6 on fuelling with producer gas under turbocharged mode and engine E4 on fuelling with both natural gas and producer gas under naturally aspirated mode of operation is presented in figure 5.11.

On the response of the engine E6 for block loading, it is important to note that for block loading of upto 50 %, the response time was well within the specified limitations, being 5.2 seconds for unloading and 6.3 seconds for loading. However for block loading of 65 %, the design criterion for qualifying the governing system, the engine transited into hunting mode. The recovery on unloading (from unstable operating condition) was however very swift with the operation becoming stable within 7.4 seconds of unloading. Extending the analysis to the four cylinder engine which is tested with both natural gas and producer gas, the engine response in terms of speed recovery time and indicated mean effective pressure variation is presented in figure 5.11 (e) and (f) respectively for no load to 10 kWe block loading. It may be noted that, for the sake of visual clarity, the cycle average speed for the two fuels has been shown on two different vertical axes with 50 RPM offset while maintaining the range of 400 RPM (for visual consistency). Figure 5.11 (e) presents an interesting trend for producer gas and natural gas block load operation. On 10 kWe block loading, while the peak drop in engine speed is about 150 RPM for NG with first

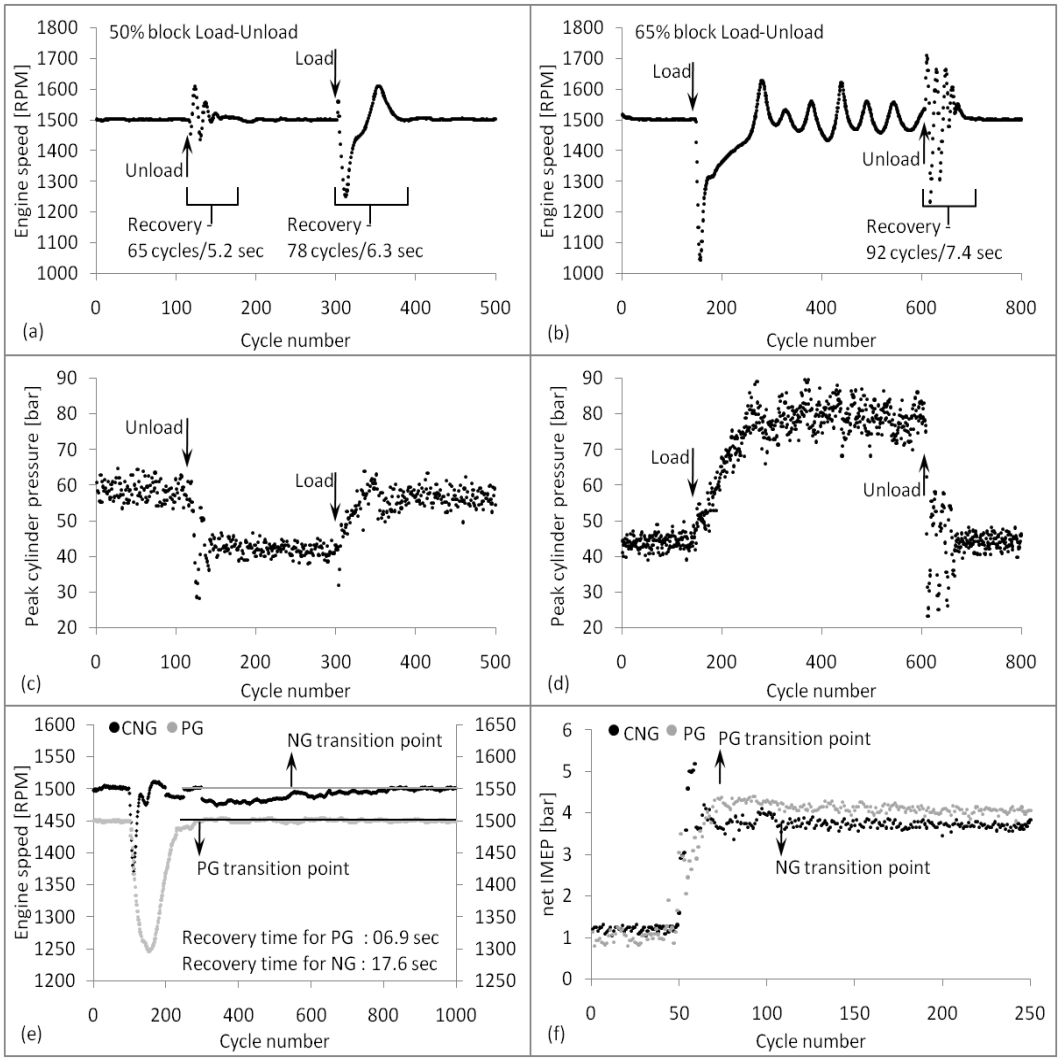

Figure 5.11: Engine transient response. Analysis as per ISO 8528

recovery (speed touching back 1500 RPM) in about 50 cycles, it is about 250 RPM for PG requiring about 150 cycles for the first recovery. It may be noted that the maximum drop in engine speed for Class – 1 governors as per ISO 8528 is (with 64 % block loading) is 375 RPM and with a drop of 250 RPM, the governor response for producer gas fuelled operation is well within specified limits. While the first recovery for natural gas is significantly superior, stable operation (50 consecutive cycles with speed of 1500 $\pm$ 15) is achieved by the producer gas engine within 171 cycles (6.84 sec) while natural gas operation requires 439 cycles (17.56 sec) from the instance of block loading. This is also evident from the variation of indicated mean effective pressure as in figure 5.11 (f).

The transient response of both the engines for producer gas fuelled operation need to be appreciated in light of the fact that, apart from fuel combustion characteristics, the response of upstream elements from intake manifold all the way to the fuel source influences the transient response. This is especially relevant for producer gas fuelled operation wherein the in-situ fuel generation involves thermo-chemical reactions with response time in minutes.

5.5.5 End gas auto-ignition

End gas auto-ignition in an internal combustion engine basically represents the surpassing of the threshold thermodynamic limit for normal engine operation and calls for diluting the manifold conditions, either in terms of the mixture quality or the thermo-physical state to revert back to normal operation. The primitive approach of detecting end gas auto-ignition is based on identifying the peculiar ringing sound made by the engine when knock sets in. While it is the least expensive approach, the fundamental drawback of the approach pertains to the need for trained personnel with ability to detect the initiation of auto-ignition in the incipient stages. This is a challenge in itself because, the engine starts emitting the peculiar pinging sound only when knock surpasses a certain threshold considering that the source energy (effectively an impulse input in the engine cylinder) must be sufficient enough to move though the various connecting mechanical elements and appear as a distinct sound. As described in section 3.3.2 the most effective approach of detecting end gas auto ignition in an engine is based on the analysis of the in-cylinder pressure trace considering that with the rapid, uncontrolled release of energy the in-cylinder pressure is the parameter most critically affected. The nature and extent of distortion of the pressure trace on end gas auto-ignition is discussed in the current section with reference producer gas fuelled operation of engine $E6$.

In the analysis of engine $E6$ under turbocharged mode, the peak supported load is limited by end gas auto-ignition. As the engine is loaded beyond the peak load of 72.8 kWe, it is observed that incipient knock (auto-ignition occurring near the fag end of the cycle when the fraction of un-burned mixture available is very small) sets in with few intermittent cycles indicating minor disturbances in the pressure profile. For incipient knock the disturbances are not explicitly evident on the pressure trace but

when the heat release trace is derived, the disturbances on the differential heat release profile become explicitly evident. It is important to note that, the onset of incipient knock does not significantly affect the peak supported load, though stability of the engine operation starts to deteriorate. Any further increase in the applied load leads to heavy knock wherein the fraction of the un-burned gas auto-igniting is significant enough to substantially distort the pressure trace. The distortion of the pressure trace is significant enough for knock to be detected based on visual examination of the pressure trace. The pressure and differential heat release traces as a function of crank angle for producer gas fuelled turbocharged after cooled operation of engine $E6$ for normal combustion (72.8 kWe), incipient knock (73.2 kWe) and heavy knock (74.5 kWe) are indicated in figure 5.12.

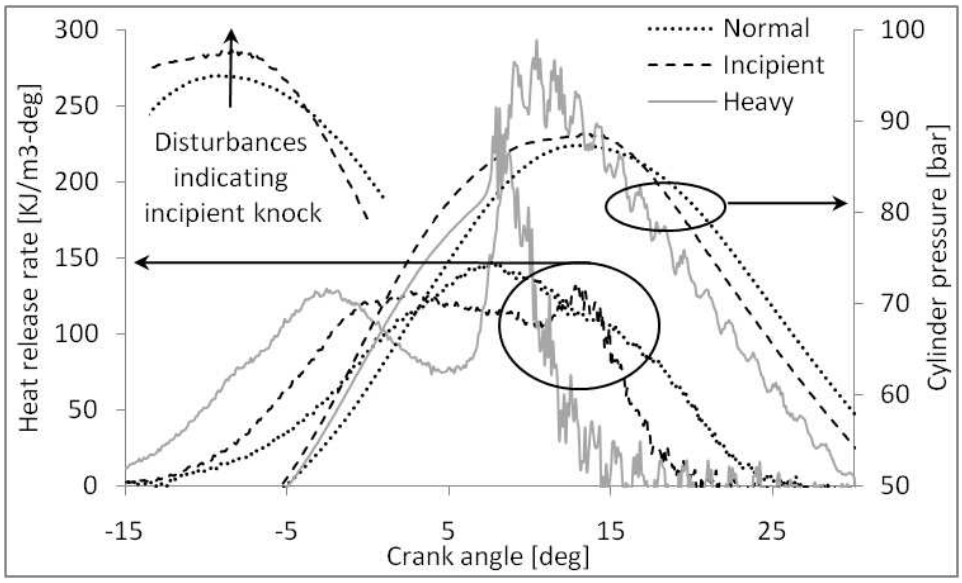

Figure 5.12: Pressure and differential heat release trace for turbocharged operation of engine $E6$

The complete analysis of two in-cylinder pressure traces representing incipient and heavy knock is presented as below. The raw pressure trace, filtered pressure trace and spectral analysis of the filtered trace is presented in figure 5.13.

With combustion descriptors being used for monitoring optimal operating condition of normal combustion cycles, the possibilities of extending the same for detecting end gas auto-ignition would be interesting and useful considering that the existing infrastructure would be able to detect knock. With end gas auto-ignition

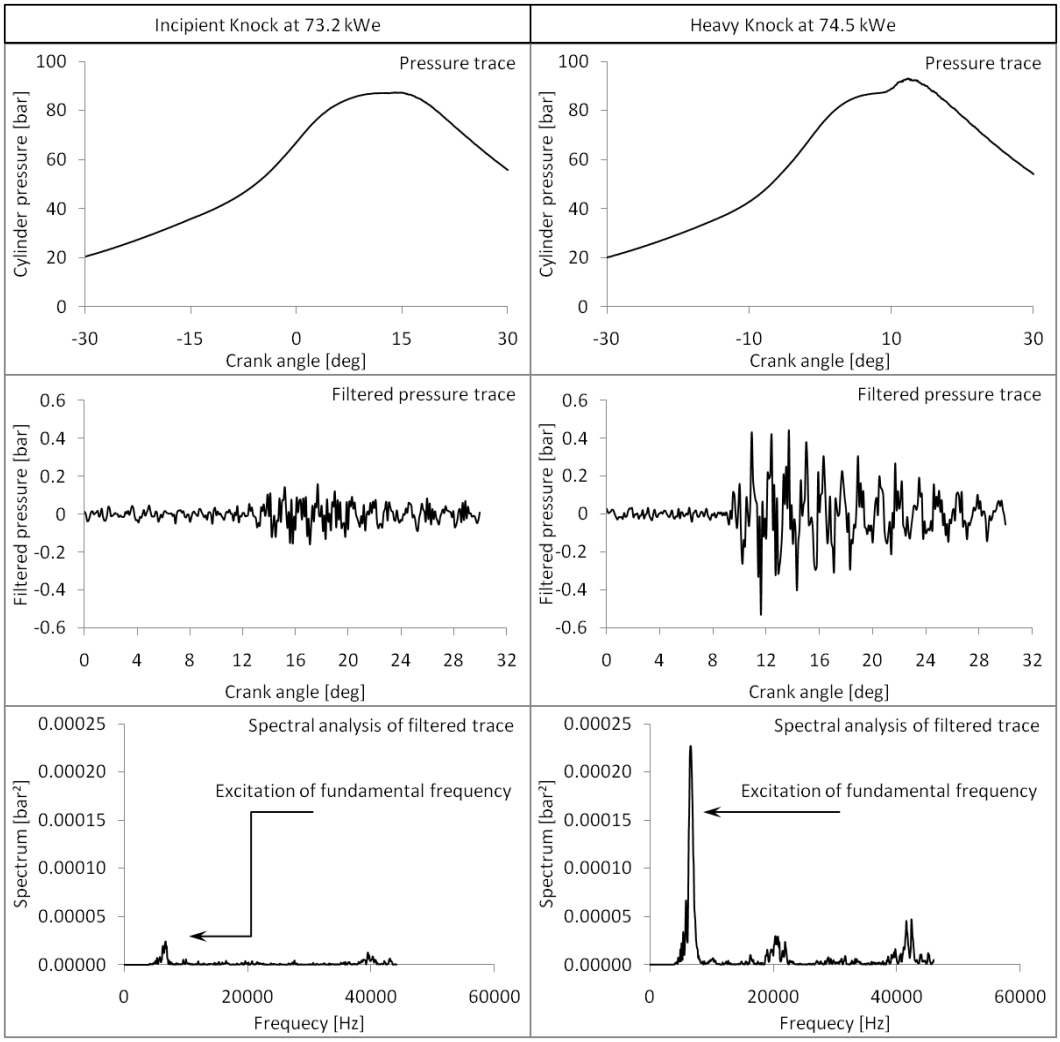

Figure 5.13: Incipient and heavy knock on engine $E6$ - pressure traces and spectral analysis

distorting the pressure profiles to varying degrees depending on the knock intensity, such a possibility exists. The current section addresses the sensitivity of various descriptors to pressure profile distortion and their ability to detect knock. Three end gas auto-ignition conditions representing incipient, established and heavy knock are considered for deriving the descriptors. The descriptors derived from four random knocking cycles are compared with normal operation descriptors as in table 5.14.

Analysing the data in table 5.14, no conclusive inference on knocking tendency can be drawn from PoPP. On the other hand, considerable differences in PoPPR and PoMHR can be observed for different knocking regimes. On the PoMBF50, when

Table 5.14: Descriptors for knocking cycles

	PoPP	PoPPR	PoMHR	PoMBF-50	PRM-10
Normal	**12.6**	**1.5**	**06.4**	**10.0**	**0.49**
Incipient Knock	15.3	-1.5	14.0	5.0	0.65
	15.8	0.5	14.0	5.3	0.64
	15.4	1.5	05.0	7.0	0.61
	15.8	2.5	14.0	6.1	0.64
Established Knock	12.5	8.5	10.0	5.1	0.74
	12.1	9.5	10.0	6.0	0.75
	12.7	8.5	10.0	6.0	0.72
	12.3	10.5	10.0	6.2	0.71
Heavy Knock	10.2	8.5	08.0	4.0	0.95
	10.8	7.5	08.0	4.0	0.91
	10.4	8.5	08.0	4.6	0.89
	09.4	7.5	07.0	3.9	0.88

the end gas auto-ignites, heat release is near instantaneous and leads to a reduction in the overall burn duration. Accordingly, there is an overall shift in the mass burn fraction position(s). Re-visiting PoPPR, PoMHR and PoMB-50, it can be observed that, with end gas auto-ignition the descriptors experience deviation from normal combustion values, but do not indicate any particular sensitivity to the intensity of knock. On the other hand, PRM-10 indicates an increasing trend with knock intensity allowing to approximately identify the knock regime. Increase in PRM-10 with knock intensity is attributed to an increase in intensity of the pressure spikes at 10 degrees aTDC (refer figure 5.12) leading to larger values of PRM-10. Thus, PoMHR and PoMBF-50 along with PoPPR can be used for knock detection. PRM10 can be used to detect knock, as well as the knock regime.

Chapter 6

Numerical simulation - Model formulation

This chapter addresses the the governing principle and mathematical formulation of the zero and quasi dimensional models under the scope of thermodynamic engine simulation. Prior to the discussion on the thermodynamic models, the key quantifiable deliverables from numerical simulation are identified and are used as guidelines for model (dimensionality) selection. Having addressed the mathematical formulation of the models, the solution strategy adopted for evolving the full cycle simulation is also addressed.

6.1 Deliverable(s) and model selection

A mathematical model of an internal combustion engine is a numerical tool that captures the science of the energy conversion process to the desired level of details and complexity. Well defined and validated mathematical models add technical and economic value to engine development and/or fuel exploration process (Benson, Annand, and Baruah 1975). The economic value emanates from rapid preliminary testing and analysis curtailing the need for costly and time intensive experiments and thereby reducing the time and development effort (Heywood 1988). Technical value addition is through their diagnostic nature providing intricate information beyond what is generally possible or exorbitantly expensive to acquire from experimental investiga-

tions, and by enhancing the understanding of the underlying science (Hiroyasu and Kadota 1975). From a scientific perspective, satisfactory performance of developed model(s) (in terms of the ability to reproduce experimental performance) reinforces the faith in understanding of the physics and the reliability of empirical correlations that go into the model. This is perhaps a significant take away considering that validated segments form the stepping stone for subsequent evolution of the simulation tools.

Internal combustion engines can be modeled to capture varying degree of details depending on the requirement. At one end of spectrum are the models with bare minimum level of sophistication, capturing the behavior of the engine purely in terms of spatially averaged thermodynamic properties. At the other end are the models that include detailed reaction kinetics with thermodynamic and fluid dynamic effects. While current computational facilities generally permit accommodating the full fluid dynamic models, the choice of the model has to based on one golden rule (Merker, Schwarz, Stiesch, and Otto 2005);

Every model, irrespective of how exhaustive or complex it is, represents an approximation to reality and perfect confirmation is impossible, at least in the realm of time and resource availability. Hence, a model should be made as simple as possible and only as complex as necessary.

Towards choosing the type of the model(s) following the broad guideline of *as simple as possible and as complex as necessary*, the first and foremost task would be to identify the key requirements as described below;

1. Generic requirements

    - Generic fast response model : The proposed model should basically be a fast response model to permit rapid parametric investigation with ability to predict both normal and abnormal combustion. The primary requirement would be the in-cylinder pressure and temperature data as a function of crank angle which would permit stage based comparison with experimental data. In case of abnormal combustion, the model should be able to predict the occurrence of knock and the angle at which the end gas

auto-ignites.

- Composition sensitive knock module : Most of the engine simulation tools model knock or end gas auto-ignition based on empirical correlations involving induction time correlation of the Arrhenius form (refer Livengood and Wu (Livengood and Wu 1955)). These correlations having functional parameters like fuel octane number, in-cylinder pressure, temperature, engine speed, operating equivalence ratio etc, each with respective power coefficients (Douaud and Eyzat 1978) (tuned based on experimental data), are fuel specific. The proposed model should incorporate necessary **generic** mechanism(s) to predict end gas auto-ignition without using any empirical coefficients.

2. Specific requirements

   - Empirical correlations validation and coefficients tuning : Various submodules of the prevalent engine simulation models, both thermo dynamic and fluid dynamic, make use of empirical correlations and coefficients derived from operational experience with conventional high calorific value hydrocarbon based fuels. With the thermo-physical properties of PG being substantially different, the validity of such correlations and coefficients needs to be verified and new correlations and coefficients are to be adopted if required.
   - Analysis of convective heat loss from the engine : Experimental investigations have indicated sensitivity of engine cooling load to mixture hydrogen fraction. The sensitivity has been attributed to the enhanced thermal conductivity and diffusivity of the mixture with increasing hydrogen content. The proposed model should permit quantifying the influence of mixture thermo-physical properties on the engine cooling load.

In the realm of modeling and simulation of internal combustion engines, there are generally two distinct categories of models as described below;

1. Thermodynamic models : Thermodynamic models correspond to the mathematical framework involving conservation of mass and energy with the complete

in-cylinder domain (the region occupied by the working fluid) considered as a lumped system. The domain average state properties vary only with time. The thermodynamic models represent the simplest frame work of engine models and are mathematically represented by a system of ordinary differential equations with time as the independent parameter. The thermodynamic models are also known as zero dimensional models considering the lumped approach of the analysis.

2. Fluid dynamic models : The fluid dynamic models correspond to mathematical framework involving the conservation of mass, momentum and energy, wherein the in-cylinder domain is discritized to evolve the state properties both spatially and temporally. The fluid dynamic models are mathematically represented by a system of partial differential equations involving both time and space(three independent dimensions) as the independent variable. Commercial solvers like ANSYS FLUENT, AVL-FIRE, STAR-CD etc are generally used to model and simulate internal combustion engines in the fluid dynamic space.

Based on the review of the identified generic and specific requirements against the capabilities of the thermodynamic and fluid dynamic models, the current analysis adopts the thermodynamic model to numerically investigate the PG fuelled operation of an SI engine. The choice of thermodynamic model is based on the fact that most of the specific requirements, particularly the thermo-kinematic response and convective heat transfer analysis can be accurately analyzed by the cylinder averaged properties and do not draw any significant additional benefit from spatial discretization. On the contrary, the lumped analysis permits rapid parametric analysis of thermo-physical and other properties to attribute behavioral variations. Further, on the other key requirement of composition sensitive end gas auto-ignition model, it is important to note that the fluid dynamic models adopt an Arrhenius type empirical correlation tuned for a particular fuel or a substantially reduced reaction mechanism against the full reaction mechanism, rendering them fuel specific. The exclusion of full reaction mechanism in favor of a reduced mechanism is necessitated by the order of magnitude increase in the computation time if full chemistry is coupled with the analysis of turbulent flow. The thermodynamic models being devoid of spatial

discretization can easily handle full reaction mechanisms making them truly generic, limited only by the accuracy of the reaction mechanism. While the fluid dynamic models claim superiority over thermodynamic models in terms of the availability of inherent mechanism for handling specie convection, considering that the chemical and physical time scales differ by orders of magnitude, it can be argued that any model accommodating full chemistry is substantially superior in respect of prediction of end gas auto-ignition over fluid dynamics models.

Having decided on the use of thermodynamic model for numerical analysis of PG fuelled engine operation, the model is sought to be constructed in house. The strategy and methodology adopted towards the development of thermodynamic model is described in detail in the following section.

6.2 Thermodynamic model

The governing principle, corresponding mathematical formulation and the solution scheme to realize a completely functional thermodynamic model with features addressing the identified requirements are described in the current section.

6.2.1 Governing principle and equation

An internal combustion engine at the very fundamental level can be represented as a thermodynamic system which remains *open* during part of the cycle (exchanging both energy and mass with the surroundings) and remains *closed* during the rest of the cycle (exchanging only energy with the surrounding). Considering the nature of the cycle, an internal combustion engine can be elegantly represented by the first law of thermodynamics involving the conservation of energy for the change of state of an open system. The principle conservation equation based on the mass and energy transfers (refer figure 6.1), establishing the mathematical framework for the thermodynamic model is of the form as in equation 6.1. Equation 6.1 can be extended to the rate form as a function of crank angle θ as in equation 6.2.

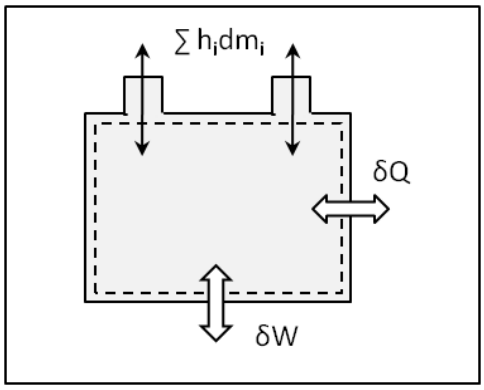

Figure 6.1: Energy and mass transfer for an open system

$$dU = \delta Q + \delta W + \sum h_i dm_i \tag{6.1}$$

$$\frac{dU}{d\theta} = \frac{\delta Q}{d\theta} + \frac{\delta W}{d\theta} + \sum h_i \frac{dm_i}{d\theta} \tag{6.2}$$

dU Change in the absolute internal energy of the system (J)

δQ Heat transfer across the system boundary (J)

δW Work transfer across the system boundary (J)

dm_i Mass of the element crossing the system boundary (kg)

h_i Specific enthalpy of mass element m_i (J/kg)

In an internal combustion engine, work transfer is only due to the deformation of the system boundary (and hence the change in volume) and can be represented as $\delta W = PdV$. On the heat transfer, while one of the components pertains to heat transfer between the working fluid and cylinder wall (due to temperature gradient), the heat release in the engine due to combustion of the fuel air mixture is also represented as a boundary phenomena (even through theoretically it is not) to confirm with the consideration of first law. Further, on the mass flow, the current analysis

considers mass transfer across the system boundary through the inlet and exit valves only and no blow-by across the piston rings is considered. Accounting for the displacement work, the two heat transfer terms and the mass flow across the intake and exhaust valves, equation 6.2 takes the form as in equation 6.3. Equation 6.3 representing the internal energy change rate can be extended to represent temperature change rate, as in equation 6.4 by some mathematical rearrangement. The equation for system pressure change rate is evaluated from the equation of state as in equation 6.5. The volume change rate as required by equations 6.4 and 6.5 is estimated based on geometric analysis involving the crank and connecting rod length and the compression ratio as in equation 6.6.

$$\frac{dU}{d\theta} = \frac{\delta Q_{wht}}{d\theta} + \frac{\delta Q_{chr}}{d\theta} + P\frac{dV}{d\theta} + h_{iv}\frac{dm_{iv}}{d\theta} + h_{ev}\frac{dm_{ev}}{d\theta} \tag{6.3}$$

$$\begin{aligned}\frac{\delta T}{d\theta} = \frac{1}{mC_v}\left[\frac{\delta Q_{wht}}{d\theta} + \frac{\delta Q_{chr}}{d\theta} + P\frac{dV}{d\theta}\right] \\ + \frac{1}{mC_v}\left[(h_{iv} - C_vT)\frac{dm_{iv}}{d\theta} + (h_{ev} - C_vT)\frac{dm_{ev}}{d\theta}\right]\end{aligned} \tag{6.4}$$

$$\frac{dP}{d\theta} = \frac{P}{T}\frac{dT}{d\theta} + \frac{P}{m}\frac{dm}{d\theta} + \frac{P}{R}\frac{dR}{d\theta} - \frac{P}{V}\frac{dV}{d\theta} \tag{6.5}$$

$$\frac{dV}{d\theta} = \frac{V_c}{2}(CR - 1)\left[\sin\theta + \frac{\sin\theta\cos\theta}{\sqrt{\xi^2 - \sin^2\theta}}\right] \tag{6.6}$$

While the set of equations 6.4, 6.5 and 6.6 broadly represent the change of state of an internal combustion engine, modifications are required, especially for equation 6.4 when the heat release due to combustion regime comes into scope. This is because of the fact that in a typical SI internal combustion engine, the turbulent flame front essentially segregates the in-cylinder domain into a well defined burned region and an un-burned region and thermodynamic conditions will have to be evolved separately for the two regions. Towards the same, the principle of conservation of energy and

the equation of state are applied individually to the burned and un-burned zones leading to the formulation of equations as in equation 6.7 through 6.10. The un-burned and burned state properties are distinguished based on the subscripts u and b respectively.

$$\frac{dU_u}{d\theta} = \frac{d}{d\theta}(m_u u_u) = m_u \frac{du_u}{d\theta} + u_u \frac{dm_u}{d\theta} = \frac{\delta Q_u}{d\theta} + P\frac{dV_u}{d\theta} + h_u \frac{dm_u}{d\theta}$$

$$m_u \frac{\delta u_u}{\delta T_u}\frac{dT_u}{d\theta} + u_u \frac{dm_u}{d\theta} = m_u C_{v,u}\frac{dT_u}{d\theta} + u_u \frac{dm_u}{d\theta} = \frac{\delta Q_u}{d\theta} + P\frac{dV_u}{d\theta} + h_u \frac{dm_u}{d\theta} \quad (6.7)$$

$$\frac{dU_b}{d\theta} = \frac{d}{d\theta}(m_b u_b) = m_b \frac{du_b}{d\theta} + u_b \frac{dm_b}{d\theta} = \frac{\delta Q_b}{d\theta} + P\frac{dV_b}{d\theta} + h_b \frac{dm_b}{d\theta}$$

$$m_b \frac{\delta u_b}{\delta T_b}\frac{dT_b}{d\theta} + u_b \frac{dm_b}{d\theta} = m_b C_{v,b}\frac{dT_b}{d\theta} + u_b \frac{dm_b}{d\theta} = \frac{\delta Q_b}{d\theta} + P\frac{dV_b}{d\theta} + h_b \frac{dm_b}{d\theta} \quad (6.8)$$

$$P\frac{dV_u}{d\theta} + V_u \frac{dP}{d\theta} = R_u m_u \frac{dT_u}{d\theta} + R_u T_u \frac{dm_u}{d\theta} \quad (6.9)$$

$$P\frac{dV_b}{d\theta} + V_b \frac{dP}{d\theta} = R_b m_b \frac{dT_b}{d\theta} + R_b T_b \frac{dm_b}{d\theta} \quad (6.10)$$

Based on mathematical rearrangement and combination of equations 6.7 through 6.10, equations describing the evolution of the thermodynamic state of burned and un-burned region (individually lumped consideration) are evolved. The set of equations describing the evolution of the thermodynamic conditions within the engine cylinder during the turbulent flame propagation phase for single zone lumped consideration and twin zone individually lumped consideration are presented as below;

1. Single zone lumped consideration

P In-cylinder pressure (Pa)

V In-cylinder volume (m^3)

T In-cylinder temperature (K)

δQ_{wht} Heat transfer between the working fluid and the cylinder wall (J)

δQ_{chr} Chemical heat release due to combustion of fuel air mixture (J)

R Gas constant $(J/kg-K)$

C_v Specific heat at constant volume $(J/kg-K)$

V_c Clearance volume (m^3)

CR Compression ratio

ξ Ratio of connecting rod to crank length

$$\frac{\delta T}{d\theta} = \frac{1}{mC_v}\left[\frac{\delta Q_{wht}}{d\theta} + \frac{\delta Q_{chr}}{d\theta} + P\frac{dV}{d\theta}\right] \tag{6.11}$$

$$\frac{dP}{d\theta} = \frac{P}{T}\frac{dT}{d\theta} + \frac{P}{R}\frac{dR}{d\theta} - \frac{P}{V}\frac{dV}{d\theta} \tag{6.12}$$

$$\frac{dV}{d\theta} = \frac{V_c}{2}(CR-1)\left[\sin\theta + \frac{\sin\theta\cos\theta}{\sqrt{\xi^2 - \sin^2\theta}}\right] \tag{6.13}$$

2. Twin zone individually lumped consideration

$$\frac{dT_u}{d\theta} = \frac{1}{m_u C_{p,u}}\left[\frac{\delta Q_u}{d\theta} + V_u\frac{dP}{d\theta}\right] \tag{6.14}$$

$$\frac{dT_b}{d\theta} = \frac{P}{m_b R_b}\left[\frac{dV}{d\theta} + \frac{V}{P}\frac{dP}{d\theta} + \left(\frac{V_u}{m_u} - \frac{V_b}{m_b}\right)\frac{dm}{d\theta} - \frac{V_u}{T_u}\frac{dT_u}{d\theta}\right] \tag{6.15}$$

$$\frac{dV}{d\theta} = \frac{V_c}{2}(CR-1)\left[\sin\theta + \frac{\sin\theta\cos\theta}{\sqrt{\xi^2 - \sin^2\theta}}\right] \tag{6.16}$$

$$\frac{dV_u}{d\theta} = \frac{1}{P}\left[R_u m_u \frac{dT_u}{d\theta} + R_u T_u \frac{dm}{d\theta} - V_u \frac{dP}{d\theta}\right] \tag{6.17}$$

$$\frac{dV_b}{d\theta} = \frac{1}{P}\left[R_b m_b \frac{dT_b}{d\theta} + R_b T_b \frac{dm}{d\theta} - V_b \frac{dP}{d\theta}\right] \tag{6.18}$$

$$\frac{dP}{d\theta} = \frac{A+B}{C} \tag{6.19}$$

$$A = \left[-\left(1 + \frac{C_{v,b}}{R_b}\right) P \frac{dV}{d\theta} - \frac{\delta Q}{d\theta}\right]$$

$$B = -\left[(U_b - U_u) - C_{v,b}\left(T_b - \frac{R_u}{R_b} T_u\right)\right] \frac{dm}{d\theta} + \left[\frac{C_{v,u}}{C_{p,u}} - \frac{C_{v,b}}{C_{p,u}} \frac{R_u}{R_b}\right] \frac{\delta Q_u}{d\theta}$$

$$C = \left[\frac{C_{v,u}}{C_{p,u}} - \frac{C_{v,b}}{C_{p,u}} \frac{R_u}{R_b} V_u + \frac{C_{v,b}}{R_b} V\right]$$

The following correlations corresponding to the relation between the total in-cylinder volume with the burned and un-burned volume and the rate of change burned and un-burned mass hold good for the above set of equations.

$$\frac{dm_u}{d\theta} = -\frac{dm_b}{d\theta} = -\frac{dm}{d\theta} \qquad ; \qquad \frac{dV}{d\theta} = \frac{dV_u}{d\theta} + \frac{dV_b}{d\theta}$$

Analyzing the heat release component of the described set of equations for the single and twin zone analysis, the following observations can be made;

1. For the single zone analysis (equations 6.11 to 6.13), the term $(\frac{\delta Q_{chr}}{d\theta})$ dictates the in-cylinder heat release which is related to the mass burn term by the correlation $\frac{dQ_{chr}}{d\theta} = LCV_{mix}\frac{dm}{d\theta}$.

2. For the twin zone analysis (equations 6.14 to 6.19), the un-burned to burned mass conversion rate $(\frac{dm}{d\theta})$ dictates the in-cylinder heat release.

It is evident from the above analysis that estimation of in-cylinder heat release essentially boils down to the estimation of the mass burn rate be it single zone analysis or twin zone analysis. In the current investigation, two different approaches, catering individually to the single zone and twin zone approach are adopted for the estimation of the mass burn rate. The formulations for are discussed in a subsequent section.

While the above discussion focused primarily on the in-cylinder heat release aspect, expressions for the estimation of other terms like heat and mass transfer that come into scope during different stages of the engine cycle (concurrently or otherwise) are also required. To provide for a closure to such terms, mathematical expressions based on appropriate governing principles need to be formulated. Subsequently, the system of coupled ordinary differential equations can be integrated based on appropriate initial conditions to evolve the thermodynamic state of the engine as a function of crank angle. This aspect of providing closure to the governing equations is described as below.

6.2.2 Sub-modules

Formulating expressions for the heat and mass transfer terms requires the analysis of complete engine cycle to identify the scope of the involved terms. Expressions providing closure to the governing equations can then be arrived at based on first principles and/or empirical analysis. The complete cycle of a four stroke SI engine can be segregated into a number of independent or partly / completely overlapping processes, each having well defined scope within the cycle. The key process and their scope in terms of starting crank angle and duration are identified in figure 6.2 and described as below.

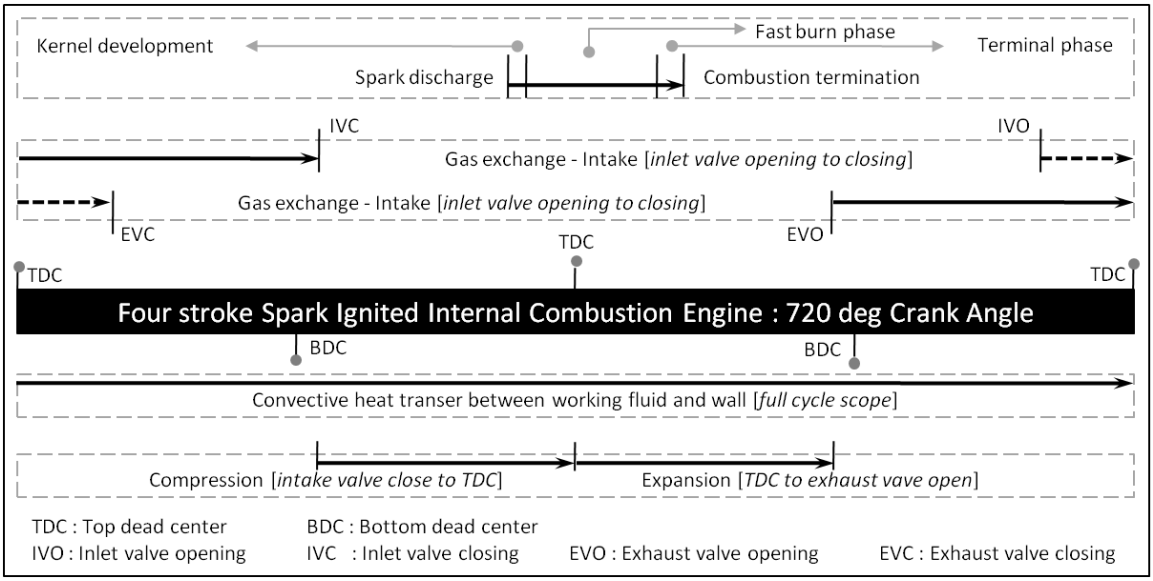

Figure 6.2: Sub modules of the thermodynamic model and their scope

The key processes required for providing a closure to the system of governing equations and the parameter(s) resolved are described as below.

1. **Gas exchange process**:- Involves the movement of mass across the engine valves covering the suction and exhaust stroke. The engine acts as an open system during this stage, exchanging both mass and energy with the surroundings. The gas exchange process primarily provides closure for the terms $\frac{dm_{iv}}{d\theta}$ and $\frac{dm_{ev}}{d\theta}$ in the set of governing equations.

2. **Heat transfer between the in-cylinder gases and the containing surfaces** :- Temperature difference between the in-cylinder gases and the containing surfaces causes heat exchange between the two. The heat transfer process provides closure for the term $\frac{\delta Q_{wht}}{d\theta}$ in the set of governing equations.

3. **Heat release in the cylinder due to controlled combustion** :- Discharge of a spark in the engine cylinder leads to controlled release of heat in due to the conversion of the un-burned mixture into burned gases. The heat release process provides a closure for the term $\frac{\delta Q_{chr}}{d\theta}$, $\frac{dm}{d\theta}$ in the set of governing equations.

The governing philosophy and the formulation of expression for the heat and mass transfer terms based on the identified modules is described in detail as below.

Gas exchange process

The gas exchange process, involving the exchange of mass between the engine cylinder and the intake / exhaust manifold, provides the mathematical formulation for the mass transfer terms as required by the governing equations. The gas exchange process is based on the analysis of one dimensional isentropic compressible fluid flow through a restriction (Anderson and Wendt 1995). The mass exchange is through the intake/exhaust poppet values with particular geometry and valve lift profile and is primarily driven by the pressure difference between the engine cylinder and the intake/exhaust manifold. The gas exchange process dictates the extent of scavenging of the products of combustion and induction of the fresh charge and hence dictates the quantity and quality of the mixture entrained in the engine cylinder in terms of energy content and the thermodynamic state. In line with the lumped approach, the gas exchange process is modeled along the filling and emptying technique (Heywood 1988) (Watson and Janota 1982). Suitability of the filling and emptying technique for modeling the gas exchange process has been well established, especially for compact manifolds (Janota, Hallam, Brock, and Dexter 1967). In the current case, the intake and exhaust manifold volume to swept volume ratio is 0.58 and 0.47 respectively, qualifying as compact manifold(s), justifying the use of filling and emptying technique. Along the philosophy of filling and emptying technique, the intake manifold, engine cylinder and exhaust manifold are considered as three finite volumes with respective spatially averaged thermo-physical properties. Further, towards simplifying the analysis, the gas in the intake and exhaust manifold is assumed to remain chemically inert, a reasonable assumption considering that for prevailing temperatures, even under turbocharged operation, all chemical reactions are virtually frozen (Heywood 1988). The expressions governing the mass flow across the poppet valve under free and choked flow conditions are as described in equations 6.20 and 6.21

1. Free flow

$$\frac{P_T}{P_o} > \left[\frac{2}{\gamma+1}\right]^{\frac{\gamma}{\gamma-1}}$$

$$\frac{dm}{dt} = C_d A_r \frac{P_o}{\sqrt{RT_o}} \left(\frac{P_T}{P_o}\right)^{\frac{1}{\gamma}} \left\{\frac{2\gamma}{\gamma-1}\left[1-\left(\frac{P_T}{P_o}\right)^{\frac{(\gamma-1)}{\gamma}}\right]\right\}^{\frac{1}{2}} \tag{6.20}$$

2. Choked flow

$$\frac{P_T}{P_o} \leq \left[\frac{2}{\gamma+1}\right]^{\frac{\gamma}{\gamma-1}}$$

$$\frac{dm}{dt} = C_d A_r \frac{P_o}{\sqrt{RT_o}} \gamma^{\frac{1}{2}} \left\{\frac{2}{\gamma+1}\right\}^{\frac{1}{2}\frac{(\gamma+1)}{(\gamma-1)}} \tag{6.21}$$

dm	Mass of fluid crossing the system boundary (kg)
P_o, T_o	Upstream stagnation pressure (Pa) and temperature (K)
P_T	Static pressure downstream of the flow restriction (Pa)
γ	Polytropic index of the fluid upstream of the restriction
A_r	Reference flow area - valve design dependent (m^2)
C_d	Discharge coefficient

The stagnation properties (P_o, T_o) refer to the upstream conditions while the static pressure (P_T) refers to the pressure downstream of valve. The polytropic index γ corresponds to the upstream fluid. For flow the cylinder to the manifold(s), the stagnation state corresponds to the condition within the cylinder and the static state corresponds to the manifold into which the gases are flowing. The reverse holds true for flow into the cylinder.

In equations 6.20 and 6.21, two parameters require special mention. The first one pertains to the reference flow area (A_r), an important parameter considering that the flow area changes continuously due to the valve motion. While literature suggests the use of a single common area like the valve head area / port area or lift dependent area

like the curtain area (Heywood 1988) (Taylor 1985) (Woods and Khan 1965), in the current analysis, the reference area is the instantaneous minimum area calculated based on the instantaneous valve lift and the valve geometry details. The valve lift based governing criteria and the corresponding reference area expressions are as described below.

For a typical poppet valve geometry, the instantaneous flow area estimation is based on segregation of the general flow into three distinct regimes depending on the valve lift. The three regimes designated as *low lift regime*, *medium lift regime* and *high lift regime*, correspond to three different stages of flow as the shape and dimension of the geometry available for flow evolves with valve lift.

- low lift regime

  Governing criterion; $$\frac{w}{\sin\beta\cos\beta} > L_v > 0$$

  Reference flow area; $$A_r = \pi L_v \cos\beta \left[D_v - 2w + \frac{L_v}{2}\sin 2\beta \right]$$

- medium lift regime

  Governing criterion; $$\left[\left(\frac{D_p^2 - D_s^2}{4D_m} \right)^2 - w^2 \right]^{\frac{1}{2}} + w\tan\beta \geq L_v > \frac{w}{\sin\beta\cos\beta}$$

  Reference flow area; $$A_r = \pi D_m \left[(L_v - w\tan\beta)^2 + w^2 \right]^{\frac{1}{2}}$$

- high lift regime

  Governing criterion; $$L_v > \left[\left(\frac{D_p^2 - D_s^2}{4D_m} \right)^2 - w^2 \right]^{\frac{1}{2}} + w\tan\beta$$

  Reference flow area; $$A_r = \frac{\pi}{4}\left(D_p^2 - D_s^2 \right)$$

The second parameter requiring consideration is the coefficient of discharge (C_d). The discharge coefficient, for the intake and exhaust valves is evaluated as a function of the valve lift (L_v) to valve diameter (D_v) ratio as discussed in (Heywood 1988) and (Ferguson and Kirkpatrick) and described in equation 6.22. The variation of discharge coefficient with valve lift, as indicated in figure 6.3, are consistent with values reported by Annand and Roe (Annand and Roe 1974) for valve geometry similar to that in the current investigation.

L_v Instantaneous valve lift (mm)

D_v Valve head diameter (mm)

D_s Valve stem diameter (mm)

D_p Port diameter (generally same as the inner seat diameter) (mm)

D_m Mean seat diameter (difference of valve head diameter and width (mm)

w Valve seat width (mm)

β Valve seat angle (deg)

$$C_d = 107.78\left[\frac{L_v}{D_v}\right]^4 - 77.21\left[\frac{L_v}{D_v}\right]^3 + 14.10\left[\frac{L_v}{D_v}\right]^2 - 1.01\left[\frac{L_v}{D_v}\right] + 0.669 \quad (6.22)$$

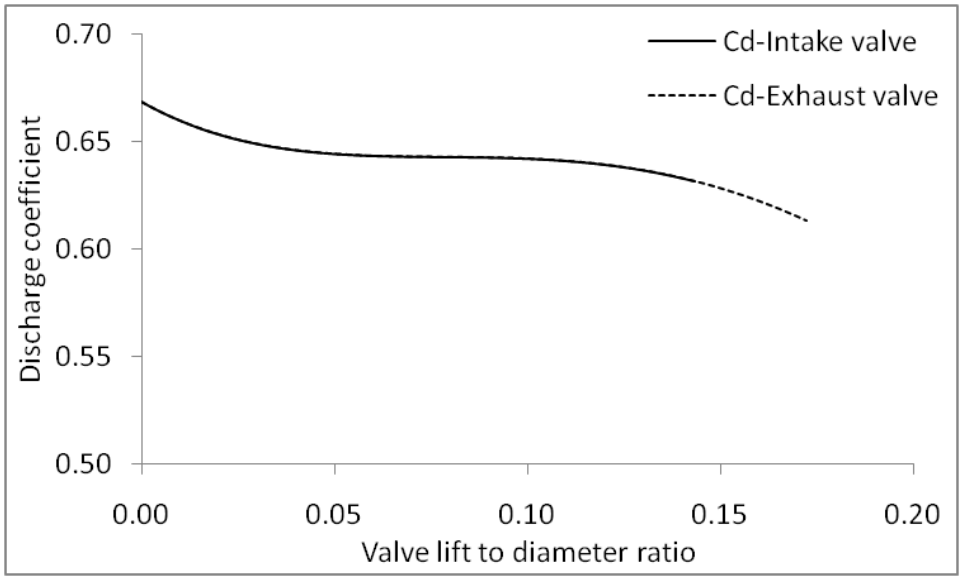

Figure 6.3: Variation of discharge coefficient with valve lift

Heat transfer between working fluid and containing surfaces

Heat transfer between the in-cylinder gases and the surroundings for a typical SI engine theoretically involves the three heat transfer modes of conduction, convection

and radiation. Generally, in an efforts towards simplification of the flux estimation process, conduction is eliminated by assigning a fixed temperature to the working fluid containing wall, a fairly reasonable approximation (Heywood 1988). Further, in case of SI engines, the contribution of radiative component is generally negligible (due to the absence of soot particles) and as such is generally neglected without any appreciable error (Woschni 1967) (Heywood 1988) (Finol and Robinson 2006). The modeling of heat transfer between the working fluid and the containing surfaces then boils down to effectively capturing the forced convective heat transfer.

The convective heat flux between the working fluid and the containing surface is modeled using the Newon's cooling law based on the consideration of the flux being proportional to temperature difference (Incropera 2011) as described in equation 6.23.

$$\dot{Q}''_{wht} = h_c \left(\overline{T}_f - T_w\right) \tag{6.23}$$

h_c Convective heat transfer coefficient $(W/m^2 - K)$
$\overline{T}_f$ Average temperature of the working fluid (K)
T_w Fixed wall temperature (K)

It is important to note that the expression for convective heat flux is valid exclusively for steady state conditions and as such monotonous extension to un-study conditions as in internal combustion engines is not thermodynamically feasible unless some simplifying assumptions are introduced. The fundamental simplifying assumption introduced is to treat the in-cylinder state change as quasi steady and evaluate instantaneous heat flux as a function of instantaneous temperature difference using *instantaneous convective heat transfer coefficient*. While experimental investigations indicate a well defined time lag between the temperature and heat flux (as a consequence, the instantaneous heat transfer coefficient approaches infinity as the average gas temperature approaches the wall temperature) (Overbye, Bennethum, Uyehara, and Myers 1961) (Alkidas 1980), measurements also suggest that the actual heat transfer in the immediate vicinity of zero temperature gradient is only a fraction

of the total heat transfer, permitting the adoption of the quasi steady assumption without any significant error.

The convective heat transfer coefficient (h_c) is derived based on the function relationship between the Nusselt (Nu), Reynolds (Re) and Prandtl (Pr) number for forced convective heat transfer in turbulent fluid flow over a flat plate / in a smooth circular tube as in equation 6.24. Considering that the Prandtl number for gases remains nearly invariant (Bernard and Wallace 2002), the same is clubbed with the coefficient a and the Nusselt number is expressed as a function of Reynolds number only.

$$Nu = aRe^b Pr^n = aRe^b \tag{6.24}$$

While almost all the heat transfer correlations rely unambiguously on the power law relation between Nusselt and Reynolds number (equation 6.24), the final form of the equation and the magnitude of various coefficients have been tuned based on experimental data for conventional hydrocarbon based high calorific value fuels. Some of the most frequently used correlations are listed in table 6.1.

In reviewing the listed correlations, it is observed that while Annand's formulation retains the basic nature of the Nusselt and Reynolds number, other formulations, in an effort to improve the predictions, incorporate multiple modifications and constants to accommodate in-cylinder phenomena, especially those associated with flow. A direct consequence is the percolation of multiple coefficients into the correlations. Further, transport properties like thermal conductivity and viscosity have been clubbed with the tunable coefficients. In clubbing the transport properties with the tunable coefficients, the possibility of parametric investigation involving varying the transport properties to assess the influence on the heat flux seems to have been discounted out. With the current investigation being strongly driven by the need to address the influence of producer gas thermophysical properties on the overall engine performance, Aannands correlation is used for estimating the convective heat transfer coefficient.

Table 6.1: Correlations for the estimation of instantaneous convective heat transfer coefficient

Author	Correlation
Annand	$h_c = \frac{k}{D} a Re^b$; a=0.35 for 4 stroke engines and b = 0.7
Annand and Ma	$h_c = \frac{k}{D} a Re^b$; a=0.12 and b=-0.20; $\frac{k}{D} a \frac{b}{\omega} \frac{d}{dt} T_f$ correction factor to account for the phase lag between the temperature and heat flux
Woschni	$h_c = 1.27 D^{-0.20} P^{0.80} T_f^{-0.53} \left[C_1 V_p + C_2 \frac{V_s T_r}{P_r V_r} (P - P_m) \right]^{0.80}$ $C_1 = 6.18, C_2 = 0$ for scavenging, $C_1 = 2.28, C_2 = 0$ for compression and $C_1 = 2.28, C_2 = 0.0034$ for combustion and expansion
Hohenberg	$h_c = C_1 V^{-0.06} P^{0.8} T_g^{-0.4} \left(V_p + C_2 \right)^{0.8}$

Heat release due to combustion

Normal combustion in-cylinder heat release in a typical spark ignition engine spans a period starting from the discharge of spark in the cylinder to the quenching of the flame at the walls. The complete in-cylinder heat release is segregated into three distinct phases of;

- Flame kernel development: Broadly corresponds to the period from spark discharge to the crank angle when the heat release becomes significant enough to introduce a discernible deviation between the motoring and firing curve.

- Fast burn/heat release : Corresponds to the propagation of a developed flame

front into the unburned mixture, the progression dictated predominantly by the in-cylinder turbulence and the mixture thermo-physical properties.

- Flame termination : Corresponds to the reduction of the rate of heat release, subsequently culminating in complete termination.

While the first law of thermodynamics theoretically requires the heat transfer to take place across the system boundary, virtually no restriction is placed on the mechanism and mathematical formulation adopted for quantifying the in-cylinder heat release. This provides the flexibility to model the in-cylinder heat release to confirm with the physical mechanism within the engine. In the modeling of in-cylinder heat release in the thermodynamic scope, two broad philosophies are generally adopted. The first philosophy involves experimental curve fit approach while the second philosophy involves geometrically evolving the in-cylinder flame propagation. The experimental curve fit approach corresponds to a pure *zero dimensional* model (catering to the single zone approach through the system of equations 6.11 to 6.13) since the in-cylinder heat release is evolved without accounting for any of the in-cylinder phenomena. On the other hand, the second approach involving evolving flame front in the engine cylinder is a *quasi dimensional* model (catering to the twin zone approach through the system of equations 6.14 to 6.19) considering that in-cylinder heat release is based on estimation of geometric parameters of a growing hypothetical flame front consuming the un-burned mixture. The model is termed quasi dimensional considering that, it is neither pure zero dimensional (certain flame related geometric features are invoked) nor does it have any dimensionality associated with it (since it does not evolve any spatially varying parameter within the cylinder). Considering that both zero and quasi dimensional models come within the purview of thermodynamic model formulation, and with each having specific advantages, limitations and utilities, in the current work, both the modules are individually considered in the full cycle thermodynamic engine simulation model. With the in-cylinder heat release forming a critical segment of engine cycle, the governing principle and mathematical formulation of the zero and quasi dimensional modules covering the three stages of combustion are accorded exhaustive treatment in the following sections.

6.3 Zero dimensional heat release module

The pressure crank angle trace of an SI engine can be used in a rearranged first law equation to quantify the heat exchange between the working fluid and the containing walls. Combining and rearranging equations 6.4 and 6.5, the following expression for the heat transfer can be arrived at.

$$\frac{\delta Q}{d\theta} = \frac{\delta Q_{app}}{d\theta} = \left[\frac{\delta Q_{wht}}{d\theta} + \frac{\delta Q_{chr}}{d\theta}\right] = \frac{1}{\gamma - 1} V \frac{dP}{d\theta} + \frac{\gamma}{\gamma - 1} P \frac{dV}{d\theta} \tag{6.25}$$

The right hand side of equation 6.25 represents the pressure change due to volume change and for adiabatic compression/expansion, the terms $\frac{1}{\gamma - 1} V \frac{dP}{d\theta}$ and $\frac{\gamma}{\gamma - 1} P \frac{dV}{d\theta}$ balance out each other. Any mismatch between the pressure change and the volume change leads to an imbalance on the right hand side leading to a non zero value. In the absence of mass transfer across the system boundary, imbalance (if any) in the pressure and volume change is attributed to the combined effect of heat transfer across the system boundary and heat release within the engine (if present), cumulatively known as the apparent heat release. This particular philosophy is used to estimate the apparent heat release (heat release due to combustion + wall heat transfer) in the engine based on the difference between the firing and motoring pressure traces. With the start of heat release, the pressure inside the engine cylinder will be substantially different as compared to a typical motoring cycle pressure (no heat release) as indicated in figure 6.4 (a). This difference reflects as differential heat release (based on equation 6.25) as indicated in figure 6.4 (b). One of the key requirements of accurate estimation of the heat release due to combustion is the appropriate choice of the polytropic index used in equation 6.25. The polytropic index is generally estimated rather accurately based on the slope of the logarithmic pressure volume trace as indicated in figure 6.4 (c). Having obtained the heat release pattern, the same needs to be mathematically modeled for subsequent use in engine simulation model. While the pointed asymmetric heat release curve with an elongated tail can be accurately captured in terms of some mathematical expression, any such expression will be of significantly higher order rendering the expression case

specific. Any generalization efforts could potentially influence various segments of the cycle and is as such not recommended.

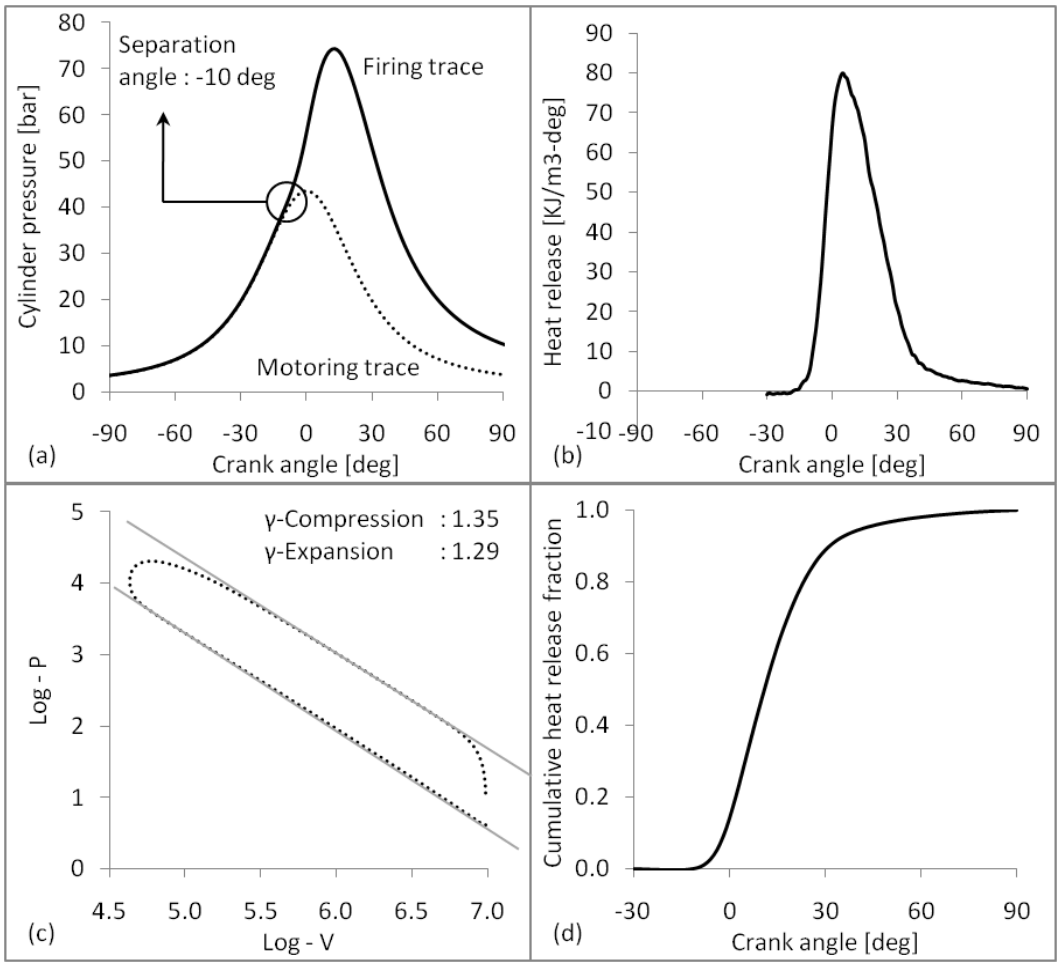

Figure 6.4: Pressure trace to heat release trace conversion methodology

This challenge is overcome by converting the generic heat release profile as in figure 6.4 (b) into cumulative heat release profile as in figure 6.4 (d). It can be observed that the S shaped profile is similar to a typical cumulative distribution function and arriving at generic curve fit expression is rather straight forward.

Correlation for cumulative heat release - Wiebe function

While arriving at a curve fit expression for the cumulative heat release profile appears more of a mathematical exercise, in a rather path breaking work, the Russian scientist Ivan Ivanovitch Wiebe (refer (Ghojel 2010)) provided a reaction chemistry basis for

the profile and proposed a correlation for the cumulative heat release profile. The correlation is named as the Wiebe function and the coefficients known as the Wiebe coefficients in honor of Ivan Ivanovitch Wiebe. The Wiebe function providing a curve fit for the cumulative heat release is of the form as in equation 6.26.

$$\frac{Q_{app}(\theta)}{Q_{app-total}} = 1 - exp\left[-a\left(\frac{\theta - \theta_{soc}}{(\theta_{eoc} - \theta_{soc})}\right)^{m+1}\right] \tag{6.26}$$

The Wiebe correlation is a function of three parameters a, m and θ, as described below.

- a : Finite rate combustion of fuel air mixture in an internal combustion engine generally leads to incomplete combustion with some reactant species moving out into the exhaust. The coefficient a represents the fuel conversion efficiency η_c and is estimated based on the analysis of the exhaust constituents for unburned reactants. The coefficient a is related to the fuel conversion efficiency by the following correlation;

$$\eta_c = \frac{Q_{released}}{Q_{supplied}} = 1 - e^{-a} \tag{6.27}$$

  Thus, the coefficient a is arrived at based on the knowledge of fuel calorific value and flow rate and the exhaust gas analysis. For typical hydrocarbon fuels, the efficiency factor is taken to be 5 amounting to fuel conversion efficiency of 99.3 % (Heywood 1988)(Oppenheim 2004) (Ghojel 2010).

- θ : The correlation is a function of the crank angle θ and permits evolution of cumulative heat release with crank angle. The correlation also requires the knowledge of the start of combustion angle (θ_{soc}) and end of combustion angle (θ_{eoc}), effectively the combustion duration. The estimation of start and end of combustion crank angles from experimental profiles is described briefly in a subsequent section and quantified in the discussions of the simulation results.

- m : While the efficiency factor and the combustion events are arrived at based

on experimental results, curve fit correlations require atleast one parameter that can be tuned to arrive at the best possible fit. The coefficient m represents the shape factor that permits tuning the S profile to minimize the difference with respect to the experimentally derived cumulative heat release profile. The shape factor for typical S profile of hydrocarbon fuels has been reported to be 2 (Heywood 1988)(Oppenheim 2004) (Ghojel 2010).

The nature of Wiebe function provides significant flexibility in terms of accommodating a variety of heat relesae profiles over a range of combustion duration by means of appropriate choice of the efficiency factor and tuning of the shape factor. Figure 6.5 indicates the nature of heat release profile for combustion duration of 40 and 80 deg crank angle (representative of fast and slow burn fuels) with three different shape factors of 1,2 and 3. It is evident that virtually any heat release profile can be conveniently accommodated by the Wiebe function with appropriate choice of coefficients.

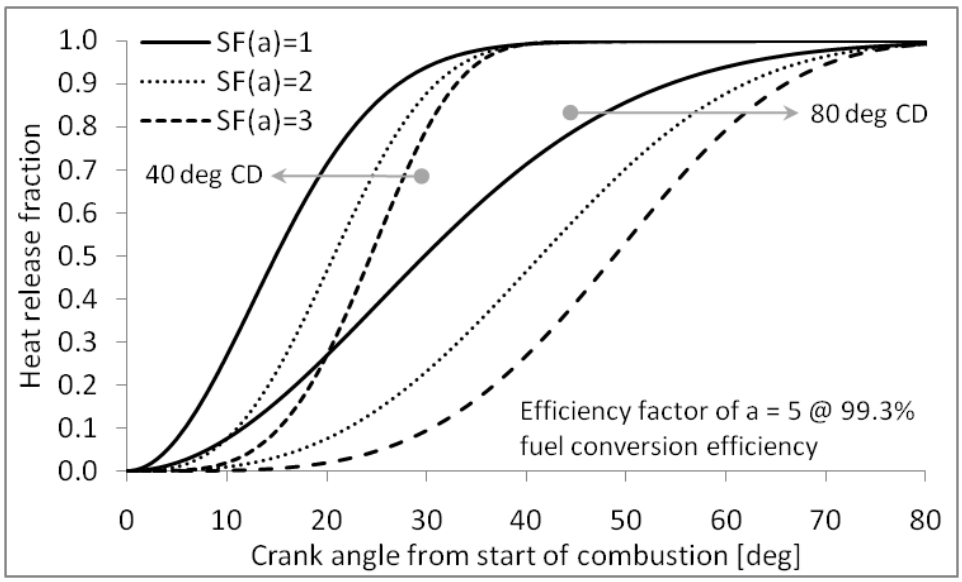

Figure 6.5: Influence of shape factor and combustion duration on the shape factor

Using the Wiebe function in simulation

The Wiebe function as in equation 6.26 on differentiation evaluates to equation 6.28 which can then on be used in the first law equation to evaluate the in-cylinder

pressure release.

$$\frac{1}{Q_{app-total}}\frac{d}{d\theta}Q_{app}(\theta) = a\frac{(m+1)}{(\theta_{eoc}-\theta_{soc})}\left[\frac{\theta-\theta_{soc}}{(\theta_{eoc}-\theta_{soc})}\right]^{m}. \\ exp\left[-a\left(\frac{\theta-\theta_{soc}}{(\theta_{eoc}-\theta_{soc})}\right)^{m+1}\right] \quad (6.28)$$

It may also be noted mass burn profiles extracted from pressure crank angle trace following the Rassweilier and Withrow (Heywood 1988) approach or the two zone approach (to be discussed subsequently) also have the typical S profile and the Wiebe function can be fit to the mass burn profile (x) also with the heat release being derived from the mass burn profile as in equation 6.29.

$$\frac{d}{d\theta}Q = m_{f_{cycle}} * LHV_f * \frac{dx}{d\theta} \quad (6.29)$$

Start and end of combustion crank angle

In the Wiebe analysis, the flame kernel development phase and the terminal combustion phase are not handled explicitly. All the three stages of combustion are handled by the Wiebe function itself within the span of start of combustion to end of combustion. Thus, the start of combustion and end of combustion crank angle form a critical input parameter pair towards evolving the in-cylinder heat release. The start and end of combustion crank angle are estimated based on the analysis of the cumulative mass burn profile. The start of combustion crank angle is the crank angle corresponding to the mass burn fraction reaching 1% (or any other fraction, generally under 10%, the choice being user specific). The end of combustion crank angle corresponds to the mass burn fraction reaching the burn fraction corresponding to the selected efficiency factor (dictated by the efficiency factor equation 6.27). A detailed case specific analysis quantifying the start and end of combustion is described in the next chapter dealing with the simulation results.

Important consideration

In the use of Wiebe function for modeling in-cylinder heat release, there are two key consideration that are important. The first one pertains to the choice of the efficiency factor a. The fact that the efficiency factor is not an arbitrary choice and must be selected based on the analysis of the exhaust gas is sought to be re-emphasized. This is critical because, a review of literature indicates that even the efficiency factor is being used as tuneable parameter without due diligence regarding the associated thermodynamic restriction. Efficiency factors as high as 6.9 (Borg and Alkidas 2009) and 10 (Shiao and Moskwa 1995) have been used in an effort to match the Wiebe heat release profile with the experimentally observed profiles. Choice of efficiency factor as high as 10 is rather surprising considering that the fuel conversion efficiency achieves a value of 99.32% at $a = 5$ and changes to 99.99% for $a = 10$. The fuel conversion efficiency in a typical SI engine seldom crosses 98% even under lean conditions (Heywood 1988). Thus, the selection of efficiency factor has to be under the ambit of thermodynamic considerations and tuning of a to match the heat release profile is unrealistic and thermodynamically untenable.

6.4 Quasi dimensional heat release module

Heat release in the quasi dimensional model is based on the evolution and propagation of a nearly spherical flame consuming the un-burned mixture. As such, accurate modeling of the flame propagation is critical to the success of the quasi dimensional model. Accurate modeling of flame propagation in the engine requires a preliminary analysis of the nature / characteristics of the premixed turbulent combustion regime prevalent within the engine. Such an analysis would permit selection of the appropriate model to numerically capture the physics governing the flame propagation. A brief overview of the premixed turbulent combustion regimes is presented in the following section.

Regimes of premixed turbulent combustion

In premixed turbulent combustion, the flow field turbulence influences / interferes with the laminar flame structure and different turbulent combustion regimes evolve

depending on the extent of influence / interference turbulence exerts on the laminar flame structure (Turns) (Lipatnikov 2012) (Heywood 1988). The extent of influence exerted by the turbulent flow field on the laminar flame structure and the nature of the evolving premixed turbulent combustion regime is dictated largely by the relative size of the turbulent length scales with respect to the laminar flame thickness. Depending on the comparison of the turbulent length scales (integral length scale l_i, Taylor micro-scale l_t and Kolmogorov micro-scale l_k) with the laminar flame thickness δ_l and/or the characteristics flow time τ_f with the chemical reaction times (the reaction rates) τ_c, premixed turbulent combustion is classified into three well defined regimes as described below.

- Wrinkled laminar flame regime: When the laminar flame thickness is smaller than or at the most equal to the smallest of the turbulence length scales (Kolomogrov scale) i.e., $\delta_l \leq l_k$, then the sole effect of turbulence is to wrinkle the flame surface without affecting the laminar flame structure itself. Perturbations to temperature and concentration profile of the laminar flame can be conveniently disregarded. For this criterion to be satisfied, the chemical times scales must be substantially faster than characteristics flow times i.e., $\tau_c > \tau_f$. The criterion describing the existence of the wrinkled laminar flame regime is generally referred to as the Williams-Klimov criterion (Williams 1986) and is represented in figure 6.6.

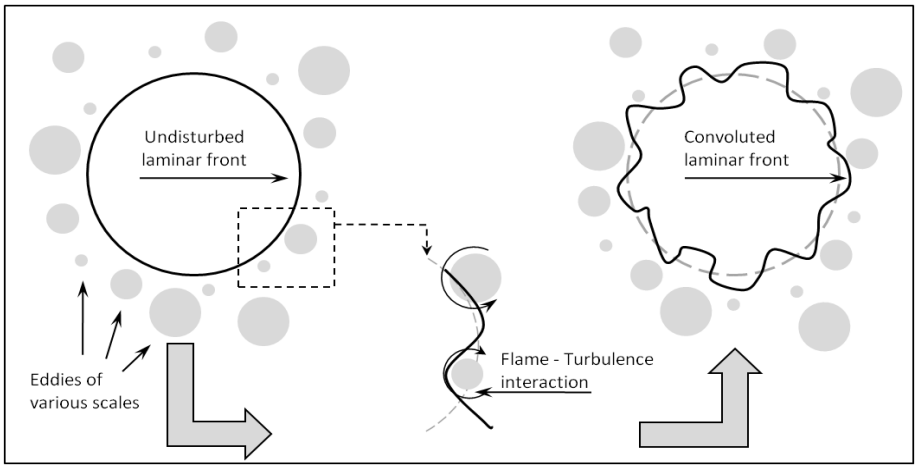

Figure 6.6: Wrinkling of the laminar flame by turbulent eddies in SI engines

- Distributed reaction regime : The distributed reaction regime corresponds to the other extreme of premixed turbulent combustion regime wherein the laminar flame thickness is bigger than the largest turbulence scale (Integral scale) i.e., $\delta_l > l_i$. Eddies from smallest to the largest length scale are present within the thickness of the flame and as a consequences, the temperature and concentration profile gets completely distorted as the specie transport is overbearingly influenced by convective transport due to the presence of the eddies. The criterion describing the existence of the distributed reaction regime is generally referred to as the Damkohler criterion (Damköhler 1947).

- Flamelets in eddies regime : If the relative scale of fluid turbulence with respect to laminar flame thickness is such that the laminar flame has a thickness smaller than the integral length scale but larger than the Kolmogorov scale i.e., $l_k < \delta_l < l_i$ then the combustion regime will be between wrinkled laminar and distributed reaction regime. In this regime, turbulent combustion has characteristics of both wrinkled laminar and distributed reaction flame. While the eddies of integral scale distort the flame surface, the smaller scale eddies (containing un-burned mixture) locally strain the flame to such an extent that they break off as pockets of un-burned mixture, also known as flamelets, moving downstream of the mean convoluted flame front. These flamelets could break down further but ultimately get converted to burned products of combustion at rates dictated by the local laminar flame speed. Due to such repeated stretching and subsequent segregation, the flame surface area keeps fluctuating between a low and a high value.

Having briefly reviewed the general premixed turbulent regimes, it is necessary to identify the nature of combustion in a typical spark ignition engine and the regime into which it fits in. Analysis of premixed turbulent combustion regimes in practical combustion devices is generally realized by the use of *regime plots* wherein the flame structure is mapped onto a two dimensional plot with the ratio of turbulent to laminar length scales (l_i/δ_l) and turbulent to laminar velocity scales (v'_{rms}/S_l) respectively. Such plots are commonly known as Borghi diagrams, named after the author who first proposed them (Kuo and Acharya 2012) (Warnatz, Maas, and Dibble). Another

common representation of the turbulent regime is through the variation of turbulent Reynolds number against the Damkohler number as represented in figure 6.7.

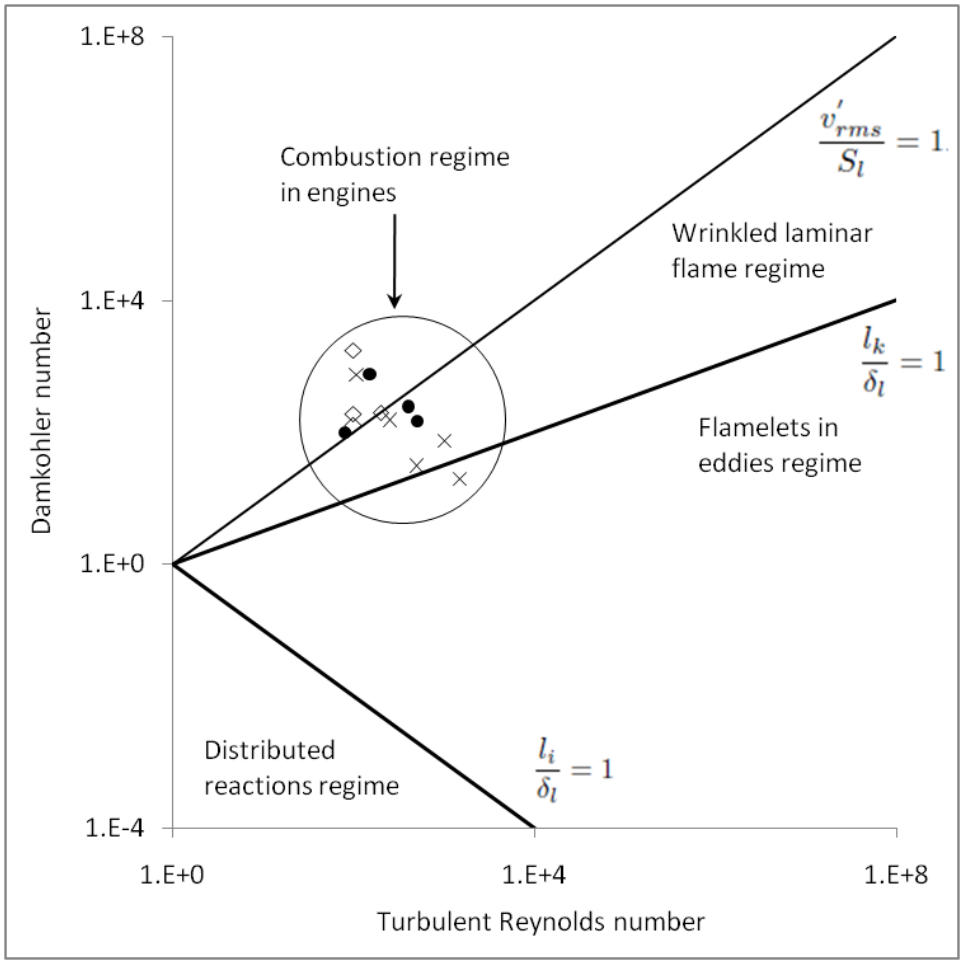

Figure 6.7: Regimes of premixed turbulent combustion with emphasis on engine like conditions

The region corresponding to turbulent combustion under engine like conditions is identified in the marked region based on exhaustive experimental data. It is evident from figure 6.7 that combustion under typical engine like conditions is predominantly in the wrinkled laminar flame regime with some extreme cases (high turbulence engines) bordering the flamelets in eddies regime.

With Borghi like diagrams clearly identifying the regime of combustion under engine like conditions, any mathematical model seeking to broadly capture the combustion phenomena within the engine to arrive at the mass burn rate as required for the evolution of cylinder average pressure and burned gas temperature will have to

broadly be along the lines of the flame being extremely thin with the sole effect of turbulence being to wrinkle the flame. The model adopted in the current analysis which follows the broad structure of wrinkled laminar flame regime is discussed in the next section.

Eddy entrainment and laminar burn up model

Based on the identified regime of turbulent combustion and laser diagnostics based observations, a rather broad consensus has evolved towards modeling of combustion in SI engines, especially in the quasi dimensional space (Keck 1982) (Beretta, Rashidi, and Keck 1983) (Tabaczynski 1976) (Tabaczynski, Trinker, and Shannon 1980). The combustion phenomena is sought to be captured by identifying a mean spherical (or part of a sphere) flame surface (hypothetical), an approximate silhouette of the turbulent flame, which segregates the in-cylinder domain into a burned and an un-burned region. The hypothetical flame progresses at laminar flame speed corresponding to the prevailing thermodynamic conditions consuming the un-burned mixture. The enhanced burn rate due to turbulence is accounted for by introducing eddies of characteristic length scale L_T that get convected across the hypothetical flame at characteristic velocity U_T from the un-burned side to the burned side. The eddies convected upstream of the hypothetical flame burn in a characteristic time T_B which is related to the characteristic eddy length L_T through the laminar flame speed S_L as $S_L = \frac{L_T}{T_B}$. The overall burn rate of the mixture is thus dictated by;

1. Growth rate of the near spherical flame
2. Entrainment rate of eddies
3. Burn rate of the entrained eddies.

The described philosophy of modeling the turbulent flame as a spherical front with convective transfer of un-burned mixture eddies upstream of the flame is described in figure 6.8.

Based on the broad philosophy described, the combustion phenomenon to evolve the mixture burn rate during the quasi steady phase is described by the following two equations;

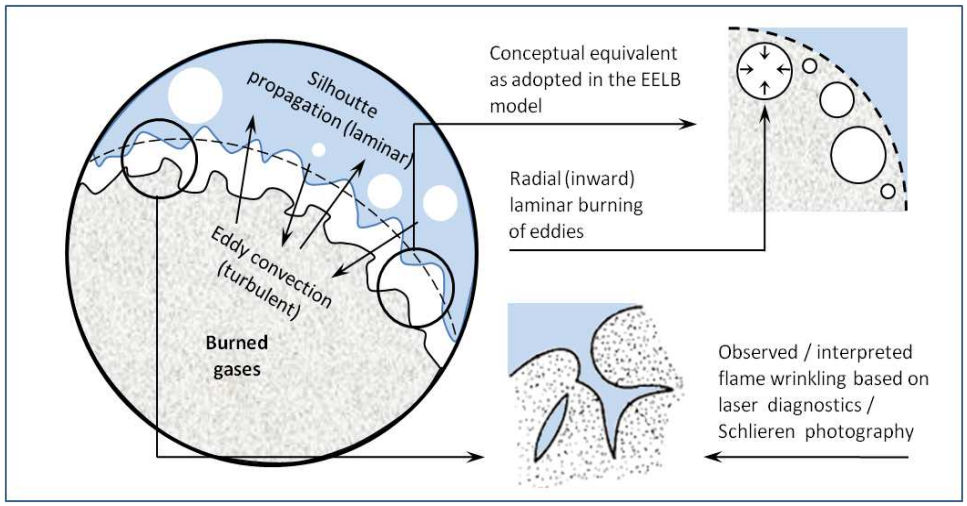

Figure 6.8: Wrinkling of the laminar flame by turbulent eddies in SI engines

$$\frac{dm_e}{d\theta} = \rho_u A_f \left(U_T + S_L\right) \tag{6.30}$$

$$\frac{dm_b}{d\theta} = \rho_u A_f S_L + \frac{m_e - m_b}{T_B} \tag{6.31}$$

In equations 6.30 and 6.31, m_e and m_b correspond to the entrained mass and burned mass respectively. The entrained mass is the total mass contained within the hypothetical flame front of area A_f and contains both the burned mass and the unburned eddies convected across the flame front. As evident from equation 6.30, the entrainment rate is dictated by laminar burn speed as well as the turbulent intensity. The burn rate as in equation 6.31 is dictated by the laminar propagation of the hypothetical flame front ($\rho_u A_f S_L$) and the laminar burning of the eddies entrapped behind the hypothetical flame $\left(\frac{m_e - m_b}{T_B}\right)$.

Towards evolving the mass burn rate based on equations 6.30 and 6.31 for use with the equation set 6.14 to 6.19 towards evolving the thermodynamic conditions within the engine during the flame propagation phase, the following input parameters are required;

1. Laminar flame speed corresponding to local prevailing thermodynamic condi-

tions

2. The area of the hypothetical propagating flame front at any crank angle

3. Spatially averaged turbulent parameters (turbulent intensity U_T and length scale L_T)

The formulations used for the evolution of the laminar flame speed, flame geometric information and the turbulent parameters are as described in the following sections.

Laminar flame speed correlations

The laminar flame speed of a fuel air mixture is a function of the mixture composition and the prevailing thermodynamic conditions. In respect of the quasi dimensional simulation, the laminar flame speed has to be estimated over the entire duration of combustion at steps of 0.5 deg crank angle (the integration time step). Broadly, covering various operating conditions and mixture quality, the laminar flame speed has to be estimated for 120 ± 30 times over one complete engine cycle. One of the fundamental challenges of numerical estimation of the laminar flame speed is that the estimation is not possible in zero dimensional space and the simplest method pertains to the solution of relevant governing equations in one dimensional space at the minimum in a double infinity domain considering full chemistry (Turns) (Kuo and Acharya 2012) (Warnatz, Maas, and Dibble). The 1D approach is dependent on full chemistry (limited availability of reduced mechanisms for mixture of gases) and is iterative in nature starting off as a transient problem and solved (iteratively) till the steady state is realized (Smooke, Miller, and Kee 1983). The 1D approach of numerically estimating the laminar flame speed is seldom adopted considering that, apart from being out of scope (the emphasis in the current investigation is on quasi dimensional approach while flame speed estimation would be one dimensional) the iterative nature of the process coupled with full chemistry render the process computationally expensive. The other option pertains to using a lookup table, generated from experimental data. The most fundamental challenge pertaining to the generation of a look up table relevant for SI engines arises from the substantially limited initial thermodynamic state (temperature and pressure) for which the laminar flame

speed data is available / can be generated, especially in the constant volume bomb apparatus, which has been identified as the most accurate and versatile of all the laminar flame speed estimation methods (Rallis and Garforth 1980). Generally, the initial thermodynamic state of the fuel-air mixture that can be ignited is limited to 25 bar pressure and 700 K temperature (Jerzembeck, Peters, Pepiot-Desjardins, and Pitsch 2009) (Gu, Haq, Lawes, and Woolley 2000) (Bradley, Hicks, Lawes, Sheppard, and Woolley 1998). It is also important to note that the indicated pressure temperature are the independent upper bounds and simultaneous measurement of flame speeds at both higher temperature and pressure is extremely limited.

Considering the computationally expensive nature of the 1D approach and non availability The most frequently used approach towards estimating the laminar flame speed in respect of use in simulation of premixed combustion in practical combustion devices in general and SI engines in particular is the use of curve fit correlations of various forms based on estimated data (Keck, Heywood, and Noske 1987) (Stone, Clarke, and Beckwith 1998) (Gülder 1984) (Rao 2003) (Syed, Yeliana, Mukherjee, Naber, and Michalek 2010). Keck et al (Metghalchi and Keck 1980), based on spherical combustion bomb experiments, have proposed a correlation of the form as in equation 6.32 in terms of dimensionless pressure $\left(\frac{P}{P_o}\right)$ and temperature $\left(\frac{T_u}{P_o}\right)$ the unburned mixture thermodynamic conditions, and a reference laminar flame speed ($S_{L,o}$) the flame speed corresponding to thermodynamic state of P_o, T_o. The coefficients α and β are the curve fit coefficients tuned based on experimentally estimated laminar flame speed data.

$$S_L = S_{L,o}\left(\frac{T_u}{T_o}\right)^{\alpha}\left(\frac{P}{P_o}\right)^{\beta} \tag{6.32}$$

The correlation has further been generalized by Keck et al to account for the variations in the air fuel ratio by expressing the reference laminar flame speed in terms of the mixture equivalence ratio (ϕ) in polynomial form as in equation 6.33 below. The approach is extended to the coefficients α and β to accommodate the variations in equivalence ratio.

$$S_{L,o} = S_1 + S_2(\phi - \phi_m)^2 \tag{6.33}$$

The initial thermodynamic state and the correlations for the coefficients α and β for typical conventional fuels are listed as below.

1. Propane; Metghalchi et al (Metghalchi and Keck 1980)

   $P_{max} = 2.0bar$; $T_{max} = 500K$
   α, β values provided for individual ϕ
   $S_{L,o} = 38.31 + 24.84(\phi - 1) - 153(\phi - 1)^2$

2. Gasoline; Rhodes et al (Rhodes and Keck 1985)

   $P_{max} = 8.1bar$; $T_{max} = 700K$
   $\alpha = 2.4 - 0.271\phi^3.51$; $\beta = -0.357 + 0.14\phi^2.77$
   $S_{L,o} = 30.5 - 54.9(\phi - 1.21)^2$

3. Natural gas; Liao et al (Liao, Jiang, and Cheng 2004)

   $P_{max} = 1.5bar$; $T_{max} = 400K$
   $\alpha = 5.75\phi^2 - 12.15\phi + 7.98$; $\beta = -0.925\phi^2 + 2\phi - 1.473$
   $S_{L,o} = -177.43\phi^3 + 340.77\phi^2 - 123.66\phi - 0.2297$

4. Liquified Petroleum Gas; Huzayyin et al (Huzayyin, Moneib, Shehatta, and Attia 2008)

   $P_{max} = 4.0bar$; $T_{max} = 400K$
   $\alpha = 2 + 2.75\phi - 2.13\phi^2$; $\beta = -0.137 + 0.029\phi - 0.026\phi^2$
   $S_{L,o} = -492.8 + 1209.1\phi - 935.5\phi^2 + 708.1\phi^3 - 229\phi^4$

Considering that the above methodology is used exhaustively for the estimation of laminar flame speed of conventional fuels under engine like conditions, the current work extends the described methodology for the estimation of laminar flame speed of producer gas under engine like conditions. A review of literature addressing the use of empirical correlation for estimation of laminar flame speed under engine like conditions indicates very limited availability. Hernandez et al (Hernandez, Lapuerta, Serrano, and Melgar 2005) and Ouimette et al (Ouimette and Seers 2009) have arrived at the reference laminar speed correlation and correlations for α and β for producer gas based on curve fit analysis for laminar flame speed data estimated from PREMIX module of CHEMKIN using the GRIMech 3.0 mechanism. While

Hernandez et al have reported the correlations for the upper bound thermodynamic conditions of 500 K and 10 bar, the Ouimette et al correlations have an upper bound thermodynamic conditions of 850 K and 15 bar. Tinaut et al (Tinaut, Melgar, Horrillo, and De La Rosa 2006) have proposed a correlation for the reference laminar flame speed based on computational laminar flame speed estimation by Mishra et al (D P Mishra and Mukunda 1994). The values of α and β are however maintained fixed. Sridhar et al (Rao 2003) based on laminar flame speed data estimated from an *in house* 1D code have proposed a temperature independent correlation for a limited data set containing pressure temperature pair (relevant for prevailing unburned gas pressure and temperature) but have included the recycled gas mass fraction ψ as a parameter. The correlations and the corresponding upper bound of the thermodynamic conditions for producer gas are consolidated as below.

1. Hernandez et al (Hernandez, Lapuerta, Serrano, and Melgar 2005)

   $P_{max} = 10.0bar$; $T_{max} = 500K$
   $\alpha = 0.68\phi^2 - 1.70\phi + 3.18$; $\beta = -0.52\phi^2 + 1.18\phi - 1.08$
   $S_{L,o} = -0.59\phi^2 + 1.64\phi - 0.65$

2. Ouimette et al (Ouimette and Seers 2009)

   $P_{max} = 15.0bar$; $T_{max} = 850K$
   $\alpha = 3.2\phi^2 - 6.9\phi + 6.1$; $\beta = -0.7\phi + 1.5\phi - 1.2$
   $S_{L,o} = -40.2\phi^3 + 63.1\phi^2 + 7.1\phi - 9.7$

3. Tinaut et al (Tinaut, Melgar, Horrillo, and De La Rosa 2006)

   $P_{max} = 15.0bar$; $T_{max} = 850K$
   $\alpha = 2.0$; $\beta = -0.4$
   $S_{L,o} = 0.506 - 0.827(\phi - 1.186)$

4. Sridhar et al (Sridhar, Paul, and Mukunda 2005)

   $$S_L = 94.35 \left(\frac{P}{P_o}\right)^{0.2744} [0.96 + 1.2(\phi - 1)] (1 - 2.4\psi)$$

While various correlations as listed above are readily available for the estimation of laminar flame speed, certain specific details, primarily corresponding to each of the above described correlations renders their direct use slightly questionable. While

the fuel composition used by Ouimette contains substantially less combustibles as compared to typical producer gas composition, the gas used by Mishra et al contains significantly higher levels of hydrogen. As such the correlations proposed by Ouimette and Tinaut cannot be directly used in the current analysis. The use of correlation proposed by Hernandez is not considered due to the fact that GRIMech 3.0 mechanism has been used which under predicts the laminar flame speed (refer section 2.3.2) while the correlation by Sridhar et al is based on a very narrow data set relevant for the particular engine frame. Considering that the available correlations are not really generic, at least as applicable for the producer gas composition of interest, fresh correlations for reference laminar flame speed, α and β as required in equation 6.32 are proposed in the current work.

Towards establishing the correlations, laminar flame speed for the temperature range of 600 to 1000 K in steps of 25 K and pressure range of 15 to 30 bar in steps of 1 bar is arrived at using the PREMIX module of CHEMKIN (Kee, Rupley, Miller, Coltrin, Grcar, Meeks, Moffat, Lutz, Dixon-Lewis, Smooke, et al. 2006). Considering that engine operation in the vicinity of stoichiometry is of primary interest, equivalence ratio variation is considered within ± 0.25 of stoichiometry. Residual gas fraction variation (ψ) from 0 to 10% has been considered. It is important to note that, following the conventional approach, when the reference pressure and temperature were set at 1 bar and 300 K with the laminar flame speed estimated at the corresponding and curve fit attempted over the pressure range of 1 bar to 30 bar and temperature range of 300 to 1000 K, the maximum laminar flame speed estimation error in the range of curve fit was recorded at 9.3 %. In an attempt to reduce this error, the range of curve fit was reduced to lower bound of 15 bar and 600 K which is logical considering that even with low compression ratio and intake pressures, these are the conditions in which the flame is initiated and the reference conditions changed from 1 bar and 300 K to 15 bar and 600 K. Based on the curtailed range and modified reference conditions, the error in the estimated laminar flame speed reduced to 3.2 %. The correlations arrived at for producer gas in the current investigation are as below;

$$S_L = S_{L,o}\left(\frac{T_u}{600}\right)^{\alpha}\left(\frac{P}{15}\right)^{\beta}$$

$$S_{L,o} = (-120.9\phi^2 + 312.7\phi - 125.9) * (1.02 - 0.036\psi) \tag{6.34}$$

$$\alpha = 2.9\phi^2 - 7.2\phi + 6.1 \qquad ; \qquad \beta = -0.8\phi^2 + 1.6\phi - 1.2 \tag{6.35}$$

Flame geometric parameters

The flame geometric characteristics are another set of parameters required in the quasi dimensional analysis. Towards arriving at the flame geometric parameters, a spherical flame front is assumed even though the actual front is significantly distorted due to the turbulence. The spherical flame front intersects the containing surfaces i.e, the piston, the chamber and the cylinder head and as such even for some simple geometries, direct analytical relationships do not exist to estimate the enflamed volume, the flame surface area (part of a sphere) and the wall area wetted by the enflamed volume. In the current investigation, the required geometric parameters are estimated based on numerical integration approach. In this approach, the flame sphere (or part of sphere) is sliced into a finite number of (near cylindrical) entities by planar segmenting in spatial steps of dy (the cylinder axis is designated the y axis). The area (flame surface area and the burned gas wetted area) is estimated by the summation of the product of the individual plane perimeter and the corrected spatial distance ($dy^{'} = dy\frac{R_f}{R_p}$) for all the hypothetical planes defined. Similarly the enflamed volume is estimated by the sum of the individual plane cylindrical volumes. The schematic representation of the most generic case of a radially and horizontally displaced flame intersecting the cylinder and piston bowl wall along with the critical geometric parameters is described in figure 6.9 as below. The symbols describing various parameters pertaining to the flame geometry are described subsequently. For a given flame radius R_f and distance of the piston crown from the cylinder head H_{ch}, the required geometric parameters are estimated as below;

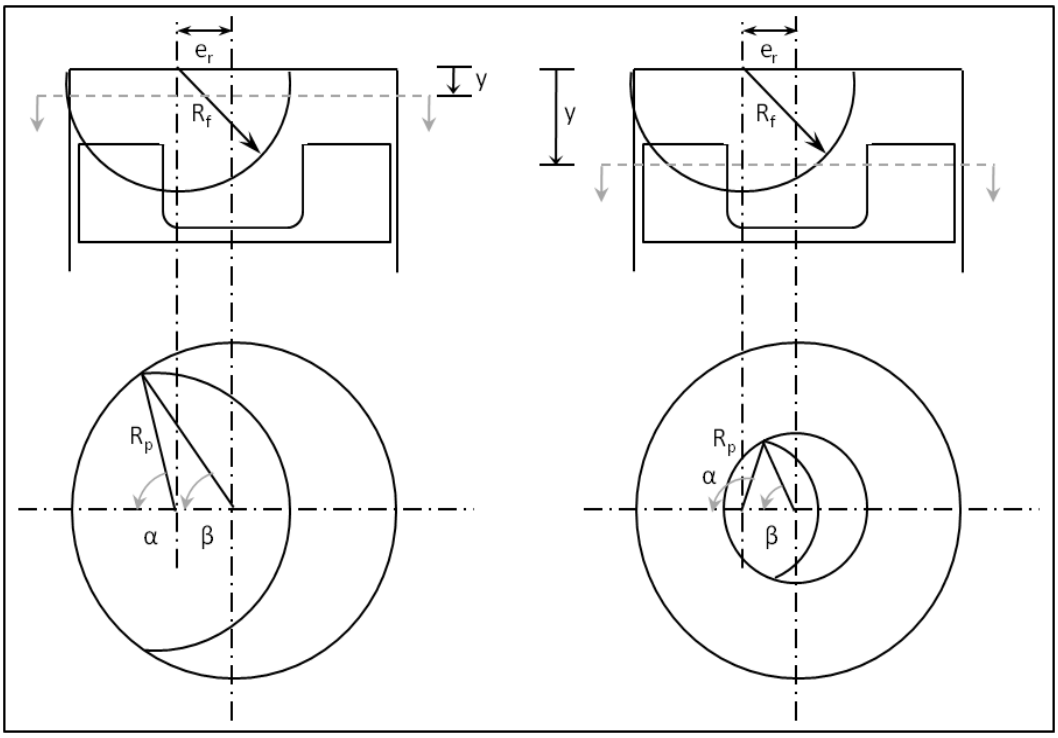

Figure 6.9: Geometric representation of the flame intersecting various segments of the containing surfaces

$$V_f = \int_0^x A_s dy = \int_0^x \left[\left(\pi - \alpha + \frac{1}{2}\sin(2\alpha) \right) R_p^2 + \left[2\beta - \sin(2\beta) \right] \frac{D^2}{8} \right] dy$$

A_s: Burned gas sector cross sectional area on the plane

$$A_f = \int_0^x P_f dy = \int_0^x 2R_p \left(\pi - \alpha \right) \frac{R_f}{R_p} dy$$

P_g: Flame sector free perimeter

$$A_{ww} = \int_0^x P_w dy = \int_0^x D\beta dy$$

P_w: Wetted wall segment perimeter

The angle $\pi - \alpha$ and β (refer figure 6.9) correspond to the free perimeter half angle (about the flame center projection on the plane) and the wetted wall perimeter half angle (about the cylinder axis on the flame) respectively. The limits for integration

R_f	Radius of the spherical flame
A_f	Flame surface area
V_f	Volume enflamed by the burned gases
e_r	Radial displacement of flame center from the spark point
e_y	Vertical displacement of flame center from the spark point
y	Vertical distance of the hypothetical plane from flame center
R_p	Radius of the flame segment in the hypothetical flame
D_c	Cylinder bore diameter
D_b	Cylinder bowl diameter
H_b	Cylinder bowl depth
A_{ww}	Area of contact of enflamed gases with cylindrical sections
A_{pc}	Area of contact of enflamed gases with the piston crown
A_{bw}	Area of contact of enflamed gases with the piston bowl wall
A_{bb}	Area of contact of enflamed gases with the piston bowl base
H_{ch}	Distance of the piston crown from the cylinder head

and the scope of the half angles are as indicated below;

Limits of integration

$R_f \leq H_{ch} + H_b - e_y \quad x = R_f$

$R_f > H_{ch} + H_b - e_y \quad x = H_{ch} + H_b - e_y$

The described formulation is used towards the estimating the variation of flame surface and the enflamed volume as a function of flame radius for different piston positions involving central and eccentric ignition for a flame piston and a bowl in piston geometry. The results of the flame area and enflamed volume estimation are represented as dimensionless parameters as in figure 6.10. The flame radius to the bore diameter ratio is used as the independent parameter while the flame surface to the piston cross sectional area and enflamed volume to the in-cylinder volume are considered as the dependent parameters.

Figure 6.10 (a) and (c) present the dimensionless plots for a flat piston configuration while figures 6.10 (b) and (d) present the dimensionless plots for a cylindrical bowl in piston configuration. The trends reported in figure 6.10 (a) and (c) ex-

Half angle definitions

If $y \leq H_{ch}$ and $R_p \leq \frac{D_c}{2} - e_r$	$\alpha = 0; \beta = 0$
If $y > H_{ch}$ and $R_p \leq \frac{D_b}{2} - e_r$	$\alpha = 0; \beta = 0$

Following condition applicable strictly only if $e_r \neq 0$

If $y \leq H_{ch}$ and $\frac{D_c}{2} - e_r < R_p < \frac{D_c}{2} + e_r$	$\cos\alpha = \dfrac{\left(\frac{\xi}{D_c}\right) - \left(\frac{\xi}{D_c}\right)^2 - \left(\frac{R_p}{D_c}\right)^2}{\left(1 - 2\frac{\xi}{D_c}\right)\frac{R_p}{D_c}}$
	$\cos\beta = 1 + \dfrac{\left(\frac{\xi}{D_c}\right)^2 - \left(\frac{R_p}{D_c}\right)^2}{\left(\frac{1}{2} - \frac{\xi}{D_c}\right)}$
	$\xi = \dfrac{D_c}{2} - e_r$

Following condition applicable strictly only if $e_r \neq 0$

If $y > H_{ch}$ and $\frac{D_b}{2} - e_r < R_p < \frac{D_b}{2} + e_r$	$\cos\alpha = \dfrac{\left(\frac{\xi}{D_b}\right) - \left(\frac{\xi}{D_b}\right)^2 - \left(\frac{R_p}{D_b}\right)^2}{\left(1 - 2\frac{\xi}{D_b}\right)\frac{R_p}{D_b}}$
	$\cos\beta = 1 + \dfrac{\left(\frac{\xi}{D_b}\right)^2 - \left(\frac{R_p}{D_b}\right)^2}{\left(\frac{1}{2} - \frac{\xi}{D_b}\right)}$
	$\xi = \dfrac{D_b}{2} - e_r$

If $y \leq H_{ch}$ and $R_p > \frac{D_c}{2} + e_r$	$\alpha = 180; \beta = 180$
If $y > H_{ch}$ and $R_p > \frac{D_b}{2} + e_r$	$\alpha = 180; \beta = 180$

actly follow the reported data by Annand (Annand 1970) for a flat piston geometry, validating the developed formulation.

Turbulence parameters

The eddy entrainment and laminar burn-up model as presented in the foregone discussion has two parameters, the characteristics length L_T and flow velocity U_T that needs to be quantified. From the discussions in the eddy entrainment and laminar burn up model, it is evident that both these parameters are primarily related to

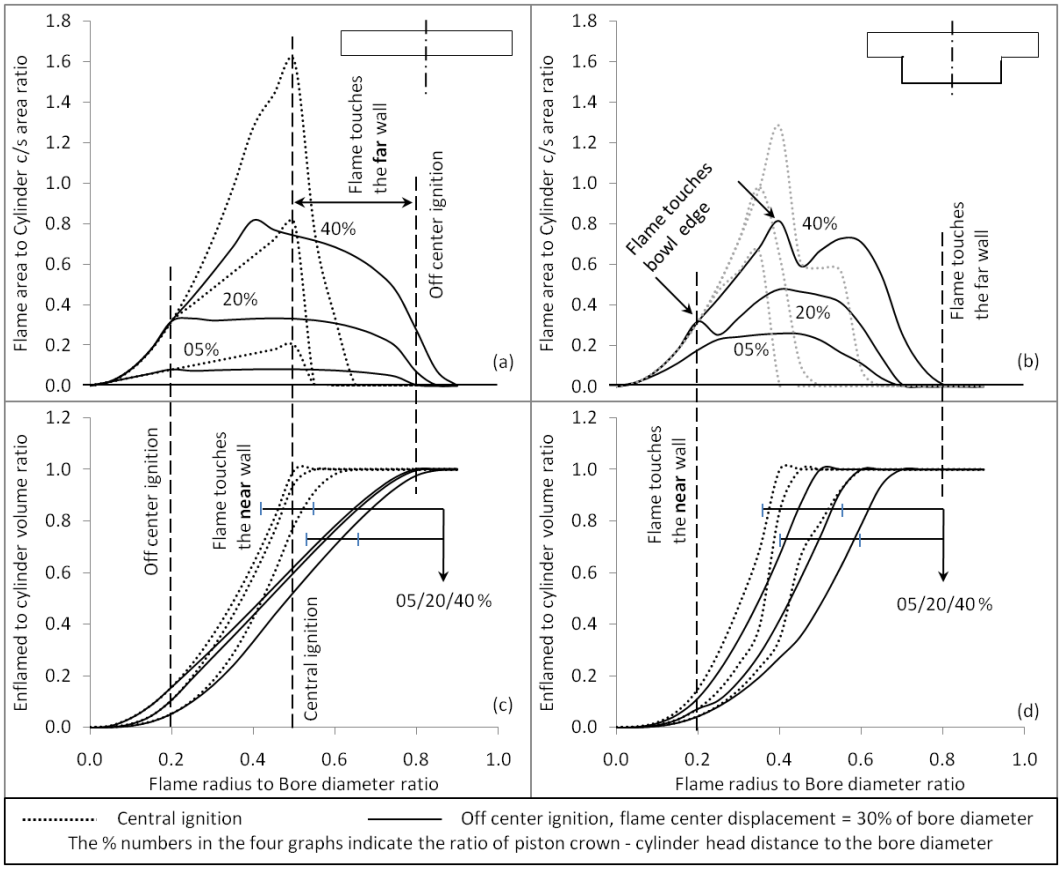

Figure 6.10: Analysis of flame surface area and enflamed volume for various configurations

in-cylinder turbulence and can be quantified based on the analysis of in-cylinder turbulence. Literature suggests different approaches towards quantifying U_T and L_T and some of the key reviews are described as below;

1. Keck et al have proposed a correlation for u_T and l_T in terms of density of the unburned mixture, a reference density, the mean intake flow velocity during the intake process $\overline{u}_m$ and the maximum inlet valve lift L_{iv}. Based on exhaustive experimental investigations, Keck et al have proposed correlations for the characteristic speed and length in terms of the intake conditions as below;

$$u_T = 0.08\overline{u}_m \left(\frac{\rho_u}{\rho_i}\right)^{\frac{1}{2}} \qquad l_T = 0.8L_{iv} \left(\frac{\rho_i}{\rho_u}\right)^{\frac{3}{4}}$$

2. Tabaczynski et al within the broad ambit of the eddy entrainment and laminar

burn up propose the characteristics velocity to be of the order of the local turbulence intensity and the characteristics length to be of the order of the Taylor microscale as indicated below.

$$U_T \approx u^{'} \qquad L_T \approx l_t = l_i \left(\frac{15}{A}\right)^{1/2} Re_t^{-1/2}$$

Effectively, the characteristic length and speed are represented in terms of the the local turbulence intensity and the integral length scale. While the approach proposed by Keck et al considered a constant values for U_T and L_T through out the combustion process, Tabaczynski et al accounted for potential variations in the characteristics parameters by linking them to the unburned gas density as indicated below;

$$u^{'} = \overline{u}_m \left(\frac{\rho}{\rho_o}\right)^{1/3} \qquad l_i = l_{i,o} \left(\frac{\rho_o}{\rho}\right)^{1/3}$$

The parameters with subscript o correspond to the start of combustion condition with ρ_o estimated from the thermodynamic conditions and $l_{i,o}$ being considered proportional to the clearance height. The above correlations suggest an increase in the turbulence intensity and hence the characteristic velocity and a decrease in the integral length scale, hence the characteristic length.

As is evident, the above correlation evaluate the characteristics length and velocity in terms of primarily inlet conditions and the density variation. While the above assessment may be valid for simple engine geometries, for engines with squish area, the turbulence parameters may be significantly influenced in the vicinity of the top dead center which is not captured in the above correlations. To accommodate for potential squish effects, the current work adopts computational fluid dynamic simulations for estimating the in-cylinder turbulence parameters. The variation of relevant turbulence parameters with crank angle for different engine operating conditions is described in a subsequent section.

Kernel initialization, flame out and terminal phase combustion

The foregone discussion primarily described the estimation of parameters as required for the quasi steady state combustion, initiated post the kernel development period and terminated when the flame in the engine cylinder dies out making way for the terminal stage of combustion. The strategy adopted for handling the flame kernel development phase and the terminal phase combustion is discussed in the current section.

Combustion of premixed mixture in a SI engine is initiated by localized electric spark discharge across a pair of electrodes. The spark discharge is designed to establish a *flame kernel*, the smallest possible (near spherical) volume with self sustaining chemical reactions on the surface (Pischinger and Heywood 1991) with close to adiabatic flame temperature. The establishment of a mature kernel from the time of initiation of spark discharge is a finite time process and is generally characterized by extremely small amount of heat release in the engine, not discernible by means of cylinder average pressure trace i.e., there will be no significant difference between the firing and motoring pressure trace till about the time of establishment of a mature flame kernel (Beretta, Rashidi, and Keck 1983) (Tabaczynski, Trinker, and Shannon 1980) (Keck, Heywood, and Noske 1987).

In the numerical simulation of a spark ignition engine, if the analysis of cycle to cycle variations is not of primary interest and if the engine operating conditions are close to stoichiometric and not lean (lean mixture combustion is particularly sensitive to the initial flame kernel development), the flame kernel development phase itself is foregone in favour of initializing a well defined spherical (or segment of sphere) flame kernel at the end of the hypothetical kernel development period (Verhelst and Sheppard 2009). The numerical simulation then on progresses in a two zone frame as the established kernel propagates into the unburned mixture at rate dictated by the mixture laminar flame speed and turbulence parameters. The current investigation also does not model the flame kernel development and a well defined, mature kernel is implanted into the chamber at the appropriate time. Initialization of the flame kernel within the engine cylinder requires the knowledge of;

- mass / volume of the flame kernel.

- thermodynamic state of the flame kernel.
- the time after the actual sparking when the flame kernel has to be introduced in the cylinder and
- the position of flame kernel with respect to some reference (generally spark plug)

Review of literature indicates the use of number of criteria towards evaluating the volume of the flame kernel that can be instantiated in the engine cylinder. Some of the key criteria are as listed below;

- Mass fraction based : The mass of the mature flame kernel is evaluated as as a fraction the total in-cylinder mass. $m_{kernel} = 1\% m_{total}$ (Wu, Roberts, Matthews, and Hall 1993) or $m_{kernel} = 2\% m_{total}$ (Bianco, Cheng, and Heywood 1991).
- Volume fraction based : The kernel volume is considered as a fraction of the total cylinder volume. $V_{kernel} = 0.1\% V_{total}$ (Benson, Annand, and Baruah 1975)
- Assumed kernel radius : The radius of the flame kernel is fixed at some number; $r_f = 0.5mm$ (Brehob and Newman 1992) (Verhelst and Sierens 2007) or is taken as half the electrode gap; $2r_f =$ electrode gap (Matthews and Chin 1991).

In the current investigation, the fraction of mass burn approach is adopted with the two zones considered to come into existence when the mass burn fraction approaches 1%. At the crank angle corresponding to 1% of the mass burn, the volume of the sphere is analytically estimated based on the equation of state with local pressure and adiabatic flame temperature (corresponding to the local thermodynamic conditions).

As the flame propagates in the in-cylinder region consuming the un-burned mixture, at a particular crank angle, the radius of the hypothetical flame equals the largest distance between the flame center and the containing surface. At this crank angle, it is obvious that the flame no longer exists i.e., $A_f = 0$. The crank angle at which this happens is dictated by the quasi dimensional burn rate and the descent

rate of the piston. While the flame dies out, the eddies trapped behind the hypothetical flame continue to burn. The crank angle range corresponding to the complete burning of the eddies persisting upstream of the flame at the flame out crank angle forms the terminal stage of combustion. The terminal stage combustion is modeled considering an exponential burn rate with the burn time being estimated from the experimental results.

The case specific implementation of flame kernel initialization and terminal stage combustion formulation and time estimation is described in the results section.

6.4.1 End gas reaction kinetics

With continuously changing temperature and pressure, the un-burned mixture downstream of the propagating flame experiences reactions between species. Generally these reactions are extremely slow permitting consideration of frozen composition for the entire duration of their existence within the engine. However, under certain thermodynamic conditions, the rates of some exothermic reactions become significant enough to cause rapid conversion of fuel air mixture to products before controlled conversion by the flame. Under such conditions, the break down is nearly uniform through out the entire end mixture and the energy released is proportional to mass of the mixture downstream of the flame and causes spikes in the in-cylinder pressure and temperature and such combustion is designated as abnormal combustion. While there could be various factors that cause the thermodynamic conditions to attain the threshold limit, causing rapid breakdown, the breakdown (verified by spike in some radicals) throughout the unburned domain leading to abormal combustion is a phenomena well established.

In the current work, abnormal combustion in the engine cylinder is sought to be captured by evolving the reaction kinetics driven temperature and pressure change in the unburned region. Due to the significant difference in the physical and chemical time scales, the approach adopted is to evolve the pressure and temperature change of the unburned mixture at under conditions of constant volume over one physical time step (details presented in the solution scheme). Any spike in temperature and pressure indicates end gas auto-ignition and the simulation is terminated. If there are no spikes in the pressure and temperature then at the end of the physical time step,

the in-cylinder thermodynamic conditions are evolved based on piston motion and normal flame propagation. The formulation, based on first law of thermodynamics is as described below;

The first law of thermodynamics for a fixed mass constant volume system can be represented as;

$$\frac{dU}{dt} = m\frac{du}{dt} = \dot{Q}$$

The specific internal energy can be expressed and expanded in terms of molar specific internal energy as;

$$u = \frac{U}{m} = \frac{\sum_{i=1}^{i=n} N_i \overline{u}_i}{m} \quad \text{and} \quad \frac{du}{dt} = \frac{1}{m}\left\{\sum_{i=1}^{i=n} N_i \frac{dU_i}{dt} + \sum_{i=1}^{i=n} U_i \frac{dN_i}{dt}\right\}$$

Replacing the following terms in the specific internal energy change rate term,

$$\frac{dU_i}{dt} = \frac{\delta U_i}{\delta T}\frac{\delta T}{dt} = C_{v,i}\frac{\delta T}{dt} \;\; ; \;\; \frac{dN_i}{dt} = V\frac{[X_i]}{dt} = V\dot{\omega}_i \;\; \text{where}$$

$$\dot{\omega}_i = \sum_{j=1}^{j=n} \upsilon_{ij} q_j \;\; ; \;\; \upsilon_{ij} = \left(\upsilon_{ij}^{''} - \upsilon_{ij}^{'}\right) \;\; ; \;\; q_j = K_{f,j}\prod_{i=1}^{i=n}[X_i]^{\upsilon_{ij}^{'}} - K_{r,j}\prod_{i=1}^{i=n}[X_i]^{\upsilon_{ij}^{''}}$$

$$\frac{du}{dt} = \frac{1}{m}\left\{\sum_{i=1}^{i=n} V[X_i]C_{v,i}\frac{dT}{dt} + \sum_{i=1}^{i=n} U_i V\dot{\omega}_i\right\}$$

Substituting in the first law equation as described previously and using the first law of thermodynamics in rate form and based on some rearrangement, the expression for the rate of change of temperature and pressure in terms of the specie concentration

change takes the form as below;

$$\frac{dT}{dt} = \frac{\frac{\dot{Q}}{V} - \sum_{i=1}^{i=n} U_i \dot{\omega}_i}{\sum_{i=1}^{i=n} [X_i] C_{v,i}} \qquad \frac{dP}{dt} = R_u T \sum_{i=1}^{i=n} \dot{\omega}_i + R_u \sum_{i=1}^{i=n} [X_i] \frac{dT}{dt}$$

A rapid change in the pressure and temperature due to a change in the concentration alone is designated as end gas auto ignition or knock.

6.5 Solution scheme

In the mathematical formulation presented in the foregone discussions, all the thermodynamic parameters are expressed as ordinary first order differential equations. Collectively, the set of governing equations represent a system of ordinary differential equations. The coupled set of ordinary differential equations with the corresponding initial conditions can be represented in general form as below;

$$\frac{d\mathbf{y}}{dt} = \mathbf{f}(t, \mathbf{y}) \qquad \mathbf{y}(t_o) = \mathbf{y}_o$$

The coupled set of equations is solved using the ODE45 solver or function of the MATLAB package which implements the Runge Kutta method with variable time step. The complete cycle is solved in 720 time steps with each time step representing a degree of progress.

For simulating end gas auto-ignition, as has been indicated in the foregone discussion, end gas reaction kinetics is introduced. The set of equations representing the rate of change of specie concentration essentially represent a stiff set of equations and the solver ODE cannot handle such a system of equations. Towards enabling the system to handle such a stiff set, the solver ODE23s is used which solves the stiff set of equations with a Resenbrock method.

Chapter 7

Numerical simulation - Results

The simulation results of the zero dimensional and quasi dimensional model described in chapter 6 are presented and compared with the experimental results in this chapter. The results are discussed in four broad segments as described below.

1. Validation of gas exchange and convective heat transfer process.
2. Zero dimensional results
3. Quasi dimensional results
4. End gas auto-ignition and fuel knock rating analysis

The validation of gas exchange and convective heat transfer processes is presented prior to the discussion of the full cycle simulation results considering that these two sub modules are common to both the models. Subsequently, zero and quasi dimensional model results for normal combustion are presented with independent treatment for the kernel initialization and flame termination with respect to both the models. The discussion on normal combustion is followed by the evaluation of quasi dimensional model for its ability to predict end gas auto-ignition and establish knock rating of a fuel.

7.1 Gas exchange and convective heat transfer

7.1.1 Gas exchange process

The gas exchange process is simulated as per the description presented in section 6.2.2 of chapter 6. Considering that the gas exchange process dictates the in-cylinder mixture quality and its thermodynamic state (for the subsequent compression process) validation of the process is critical. The tuning and validation of the gas exchange process is addressed in the current section. In the simulation of the gas exchange process, one of the key boundary conditions pertains to the manifold pressure, especially the intake manifold pressure. Specifying appropriate manifold pressure/pressure profile is absolutely critical considering the influence it has on the general thermodynamic state of system and the quantity of fresh and residual gas trapped in the engine. One of the simplest approaches adopted in the literature has been to specify an average manifold pressure for the entire duration of the gas exchange process (Rao 2003). In the current investigation, on adopting a constant manifold pressure boundary condition, it is observed that the experimental and simulation pressures traces deviate non-trivially at and beyond the inlet valve closure crank angle (refer figure 7.1 (a)).

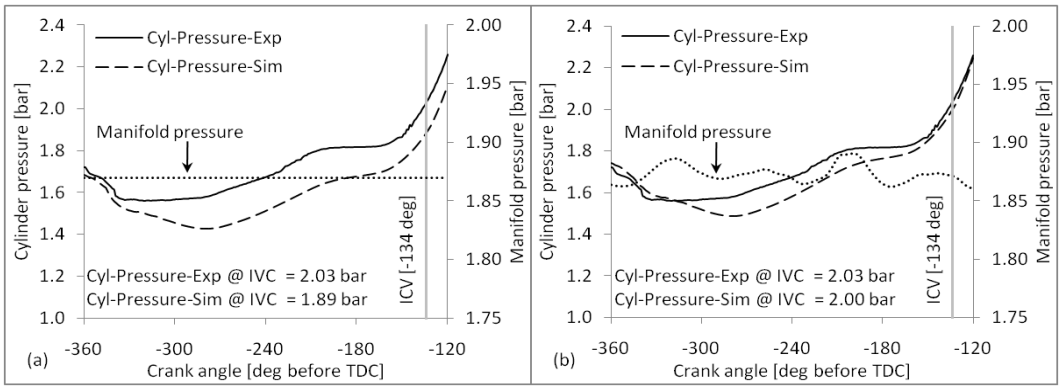

Figure 7.1: Turbocharged operation gas exchange process validation (a) Fixed manifold pressure and (b) Varying manifold pressure

To address this issue, the constant manifold pressure is replaced by the measured manifold pressure and subsequently, the gas exchange pressure trace indicated significant improvement as evident in figure 7.1 (b). Adopting this approach has enabled

maintaining the difference between the experimental and simulation traces within 5% of the experimental trace over the entire duration of the gas exchange process. For the 50 deg crank angle span leading upto the valve events, the difference is less than 1%. The other attribute contributing to the high degree of accuracy pertains to the use of valve lift dependent coefficient of discharge (refer section 6.2.2) as against the commonly adopted approach of using a fixed value . The above approach has been tested for a variety of operating conditions on the three engine frames and is found to be satisfactory.

The significance of validation of the gas exchange process rests in the fact that, with the simulated thermodynamic conditions at the inlet valve closure (-134 deg before the top dead center) matching closely with the experimental conditions, the error carried forward from the gas exchange process to the downstream processes would be minimal.

7.1.2 Convective heat transfer process

The current investigation adopts the Aanand's correlation as in equation 7.1 (refer section 6.2.2) for the estimation of the convective heat transfer coefficient. Analyzing the various parameters that constitute the correlation, $\overline{V}_c$ is the characteristic velocity and L_c is the characteristic length. In the current investigation, the mean piston speed and bore diameter are used for the characteristic velocity and characteristic length respectively. A review of literature suggests the choice to be acceptable, providing the desired levels of accuracy under engine like conditions (Annand et al. 1963) (Annand and Pinfold 1980) (Borman and Nishiwaki 1987). The thermal conductivity (k), dynamic viscosity (μ) and density (ρ) are estimated based on the in-cylinder composition and thermodynamic conditions adopting the curve fit estimation as described in Appendix A.

$$h_c = \frac{k}{L_c} a \left(\frac{\rho \overline{V}_c L_c}{\mu} \right)^b \tag{7.1}$$

Beyond the engine geometry and thermo-physical properties, two other coefficients a and b are also required to be estimated. Annand has suggested a value of 0.7

for b while the the choice of a is flexible within the range of 0.35 to 0.8; increasing with increasing intensity of charge motion within the cylinder. It is suggested that b be set close to 0.35 for spark ignition engines and close to 0.8 for diesel engine considering the difference in the turbulence intensities between the two engine types (Heywood 1988) (Han and Reitz 1995). In the current work, in line with the general recommendations, the value of b is maintained within 0.7 ± 0.02 while providing greater flexibility to the coefficient a in the 0.35 to 0.8 regime.

The choice of coefficients is based on comparing the simulation traces with experimental pressure traces. The first stage basically involves establishing the coefficients for the motoring cycle of the engine at various loads with specific emphasis on the peak load under both naturally aspirated and turbocharged after cooled mode of operation. The coefficients are tuned based on the criterion of the difference between the experimental and simulation in-cylinder pressure traces being less than 0.5% at any crank angle between the inlet valve closure and exhaust valve opening (closed segment of the cycle) regime.

In the current investigation, the motoring pressure traces at various loads are acquired by mechanically cutting off power supply to the instrumented cylinder and acquiring the pressure trace once stable conditions are attained (Heywood 1988). It is important to note that this approach could be adopted maximum upto 70 % of the peak load and beyond that no load recovery was possible due to saturation of supported cycle mass (for N-1 cylinders). This challenge was overcome by extracting the motoring pressure trace from the peak load firing pressure trace. In this approach, the compression process (beyond the inlet valve closure) is considered adiabatic and the polytropic index in the first law expression is set to obtain a near perfect overlap with the firing pressure trace upto 35 deg before the top dead center crank angle (the analysis is terminated about 10 deg before the physical spark discharge). Using the estimated polytropic index and considering a corresponding compression / expansion process, the complete motoring pressure trace is subsequently generated. Comparing the motoring trace so generated with the experimentally obtained motoring traces at part load suggest a very close match, validating the approach for generating the motoring pressure trace for peak load. Figure 7.2 (a) compares the simulation pressure trace with the experimental motoring pressure trace for 50 kWe load under

turbocharged operation of engine E6. A near complete overlap is evident. Figure 7.2 (b) presents the turbocharged peak firing and extracted compression pressure trace.

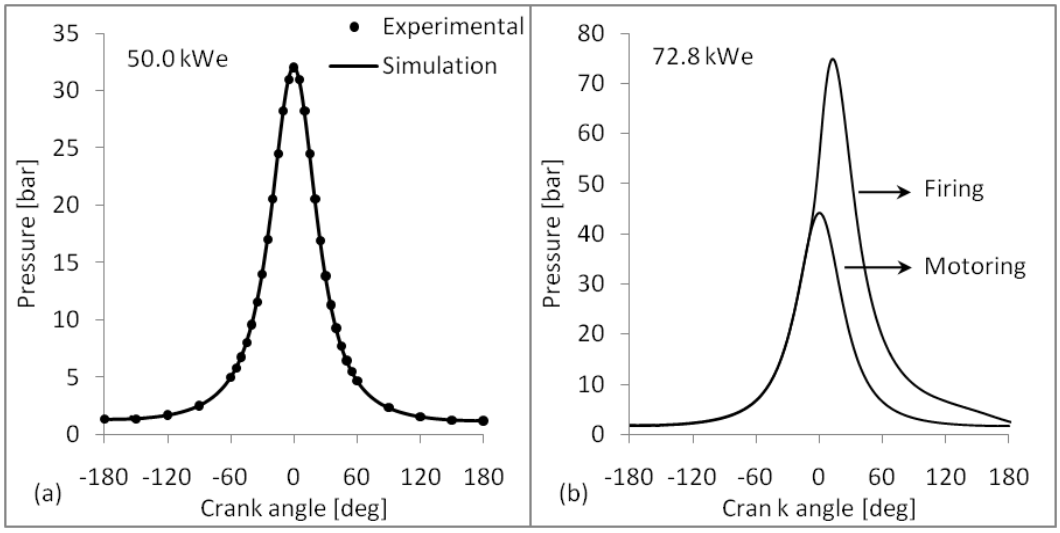

Figure 7.2: Extraction of motoring pressure trace from the firing pressure trace

Using the motoring traces, the coefficients a and b are tuned following the above described approach. Figure 7.3 presents the comparison of motored simulation pressure traces for the peak load turbocharged operation with the corresponding experimental pressure trace. Simulation pressure traces for conventional (relevant for spark ignited engine operation) and tuned coefficient pair $[a, b]$ along with the pair recommended by Sridhar (Rao 2003) are also presented for reference.

As visually evident, tuning the coefficients to $a = 0.76$ and $b = 0.71$ has provided a near exact match with the experimental trace. The peak pressure difference between the experimental and simulation trace is 0.3 bar (less than 0.7%). Analyzing figure 7.3 further, it can be observed that the peak pressure is over predicted (by 2 bar amounting to 4.5 %) on using the conventional coefficients while the peak pressure is under predicted by 11.6 bar amounting to 27 % when the coefficients adopted by Sridhar (Rao 2003) are used. The slight over prediction for conventional coefficients is justified considering that the value of a at 0.35 is almost half that of the tuned coefficient and the heat transfer coefficient responds linearly to the changes in coefficient a. The reduction in the heat transfer coefficient and hence the flux leads to a commensurate increase in the in-cylinder temperature and pressure. Addressing

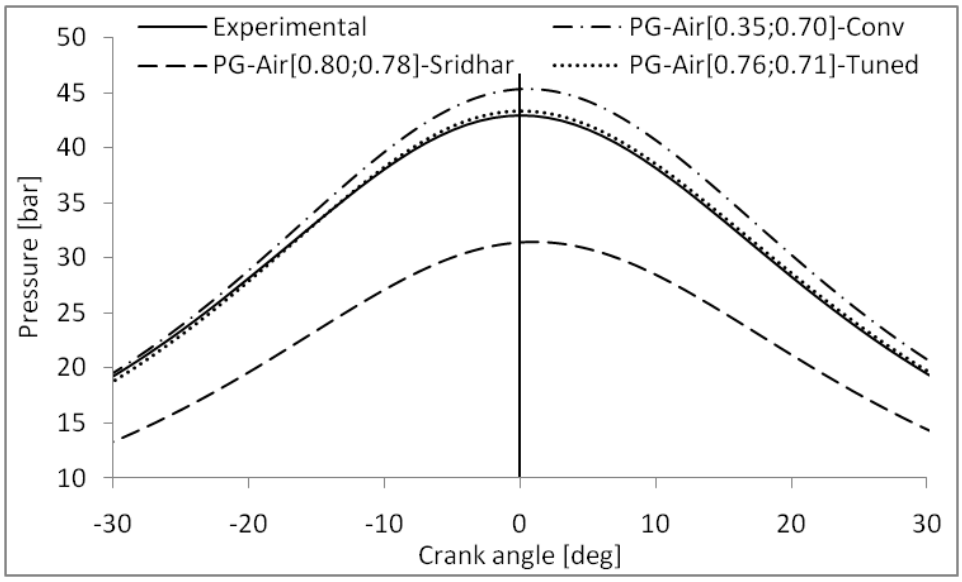

Figure 7.3: Comparison of experimental and simulation motoring pressure traces for different coefficient pairs

the pressure trace generated using the coefficients proposed by Sridhar, the under prediction of pressure to the tune of 27% is substantial considering that the basic geometry and speed of the engine used by Sridhar is similar to frames used in the current investigation.

A detailed analysis of the approach adopted by Sridhar towards handling the convective heat transfer indicates the use of a temperature dependent curve fit polynomial for the estimation of thermal conductivity and dynamic viscosity. The correlations used are of the form as below;

$$\mu = 0.033T^{0.6976}10^{-5}$$

$$k = T^{0.908}10^{-4} \qquad \text{if } T \leq 550 \text{ else} \qquad k = 0.0336 + 2T10^{-5} + T^{2}10^{-8}$$

The shortfall of the above correlations in that the estimated thermal conductivity and viscosity will be representative of values for air rather than the in-cylinder mixture. While such correlations are useful for conventional fuels wherein air dominates the mixture, extension of the same to low air to fuel ratio fuels like PG and

syngas introduces deviations as observed. Towards addressing the deviation, the thermal conductivity, viscosity and convective heat transfer coefficient for stoichiometric PG air mixture (composition: $CO-0.0\%$, $H_2-0.0$, $CH_4-0.0\%$, $CO_2-0.0\%$, $O_2-0.0\%$, $N_2-0.0\%$) are estimated using (a) the above correlations and (b) kinetic theory based approach. The variation of the three parameters as a function of crank angle following the two approaches is presented in figure 7.4.

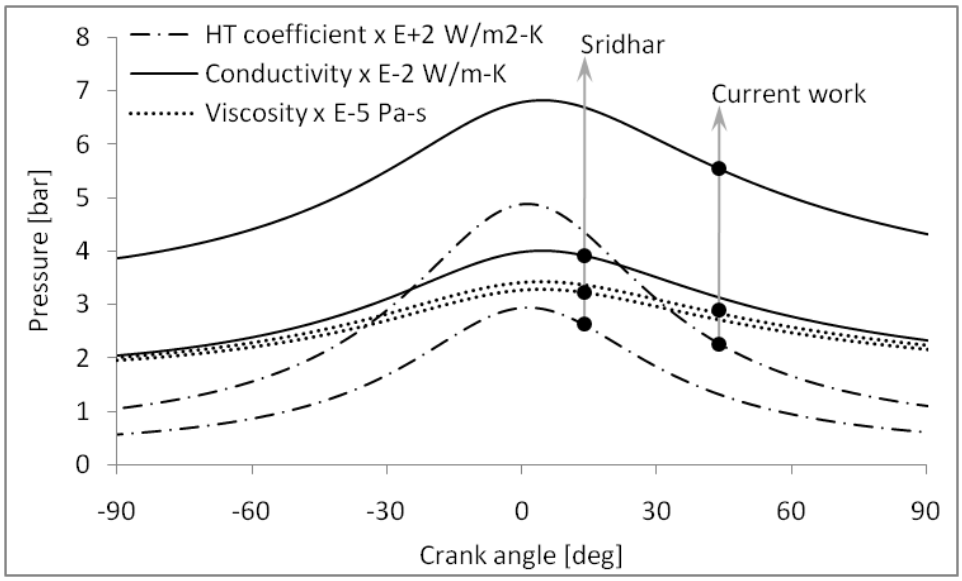

Figure 7.4: Comparison of thermal conductivity, dynamic viscosity and heat transfer coefficients for two different methods

It is interesting to note that, the correlation used by Sridhar estimates the thermal conductivity close to 50% lower as compared to the kinetic theory based analysis adopted in the current investigation. Similarly, the dynamic viscosity is also lower (albeit not as significant as thermal conductivity) than the estimation based on kinetic theory. With the convective heat transfer coefficient begin linearly dependent on the thermal conductivity (refer equation 7.1), a commensurate reduction in the convective heat transfer coefficient and hence the heat flux is observed (refer figure 7.4). It is evident from the above analysis that, to compensate for the reduction in the heat transfer coefficient due to under prediction of the thermal conductivity and viscosity, Shridhar restored to increasing the magnitude of the coefficients a and b to values as high as 0.80 and 0.78 respectively. Towards a comparative analysis, when these coefficients were used in the current investigation, the thermal conductivity and

diffusivity values estimated (using kinetic theory) coupled with the (high) values of 0.80 and 0.78 for a and b lead to substantially higher convective heat transfer coefficient and heat flux (loss). The nearly 27% under prediction of the peak pressure is thus attributed to the substantially enhanced heat loss from the engine. It may thus be argued that, from the perspective of a complete engine cycle, accurate quantification of the convective heat transfer coefficient is more critical and flexibility may be extended in the choice of coefficients and thermo-physical parameters in the tuning of the simulated pressure trace to match with the experimental pressure trace.

Extending the analysis, it can be observed from figure 7.5 that for a gaseous fuel like PG, the convective heat transfer coefficient and heat flux is significantly higher than that for air. The increase is attributed primarily to the presence of H_2.

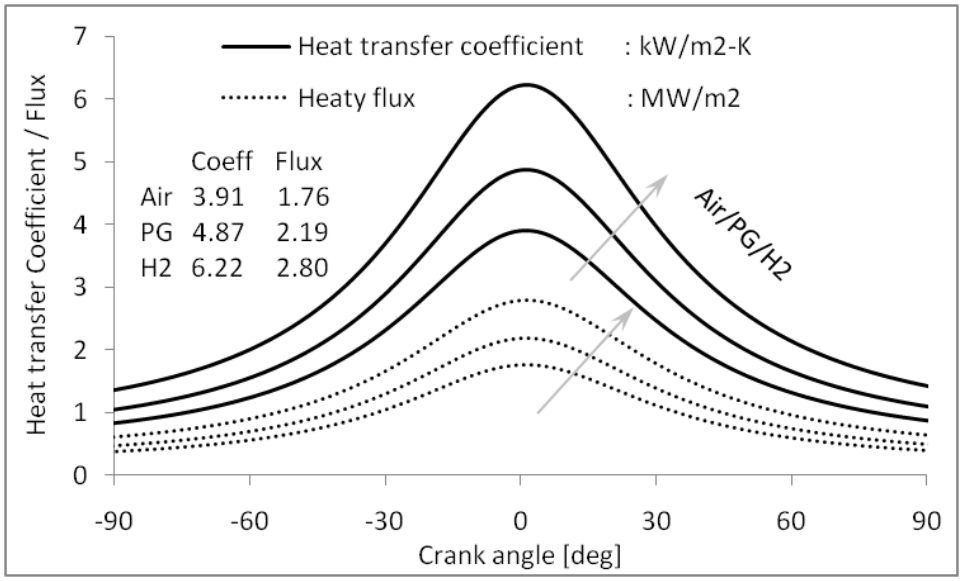

Figure 7.5: Variation of convective heat transfer coefficient with crank angle for air, PG and H_2

The above analysis explicitly establishes the criticality of accurate estimation of the fluid state thermo-physical properties and heat transfer analysis for gaseous fuels especially those with low air-fuel ratio wherein the combustible components constitute a significant fraction of the mixture.

7.2 Zero-dimensional model

The results from zero dimensional model simulation are presented in the current section. As a validation exercise, the simulation results for NG fuelled operation are presented prior to the discussion of PG results. The simulation results are compared with the available experimental results and extended to results sourced from literature wherever necessary. Appropriate inferences are drawn based on the quality of the simulation results and the capabilities / limitations of the zero dimensional model. The methodology adopted towards handling initiation and termination of combustion in the current investigation is discussed prior to the full simulation results.

7.2.1 Combustion initiation and termination

Discharge of a spark in the cylinder of an SI engine effectively initiates the mixture combustion process. The heat release in the initial few degrees after the spark discharge will be very nominal and will be insufficient to cause a perceivable pressure rise (due to heat release) (Kalghatgi 1987) (Herweg and Maly 1992) (Kravchik, Sher, and Heywood 1995) (Keck 1982) (Keck, Heywood, and Noske 1987). From the perspective of apparent heat release, there is no net heat transfer to the engine cylinder until the heat release due to combustion is significant enough to overcome the convective (and other, if any) heat losses and cause a perceivable deviation of the firing pressure trace from the hypothetical motoring curve. A common crank angle reference base comparison of the firing and and motoring trace with the mass burn trace indicates that a perceivable deviation of the motoring trace from the firing trace sets in only beyond a mass burn fraction of 1 %. This behavior is common across the board irrespective of the fuel or the operating condition.

In the zero dimensional heat release model, the Wiebe function is invoked (evolves a non zero positive value less than unity) at 1% or 2% of mass burn fraction. The crank angle for start of combustion is fixed based on the analysis of the experimental mass burn fraction trace. It is important to note that 1% to 2% is the generally acceptable limit as various uncertainties creep in below these levels (Heywood 1988) (Shiao and Moskwa 1995) (Tazerout, Le Corre, and Ramesh 2010). The heat release

through the Wiebe function is terminated when the mass burn fraction reaches a value corresponding to the fuel conversion efficiency (for example if the efficiency of conversion is 95%, the choice of a will lead to differential heat release evaluating to zero beyond the mass burn fraction of 95%). The discussed methodology of initiation and termination of combustion is represented in figure 7.6 wherein the Wiebe function with 1% and 98 % scope is superimposed over the experimental mass burn fraction trace.

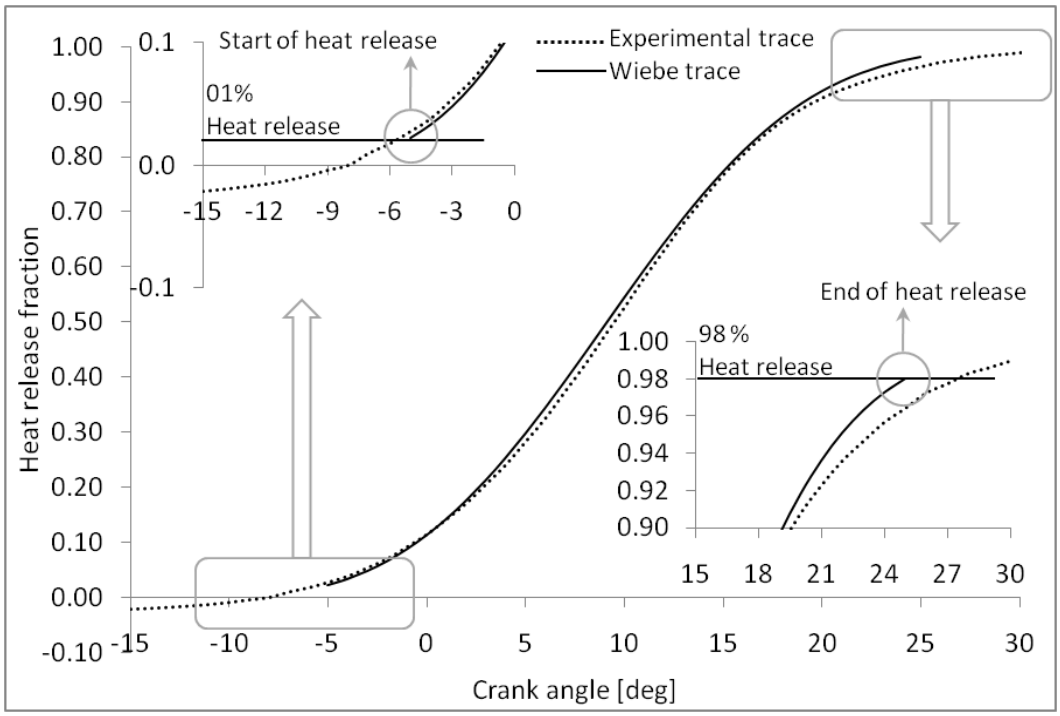

Figure 7.6: Ignition delay and heat release termination on the Wiebe function

7.2.2 Natural gas operation

Simulation for NG fuelled operation is using literature reported Wiebe coefficients of $m = 2$ and $a = 5$ for conventional high calorific value fuels (Heywood 1988) (Ghojel 2010) (Alla 2002) (Arsie, Pianese, and Rizzo 1998) (Lounici, Loubar, Balistrou, and Tazerout 2011).

The simulation is primarily an attempt at validation of the developed models. The simulation results for NG fuelled operation of the engine $E4$ at two loads of

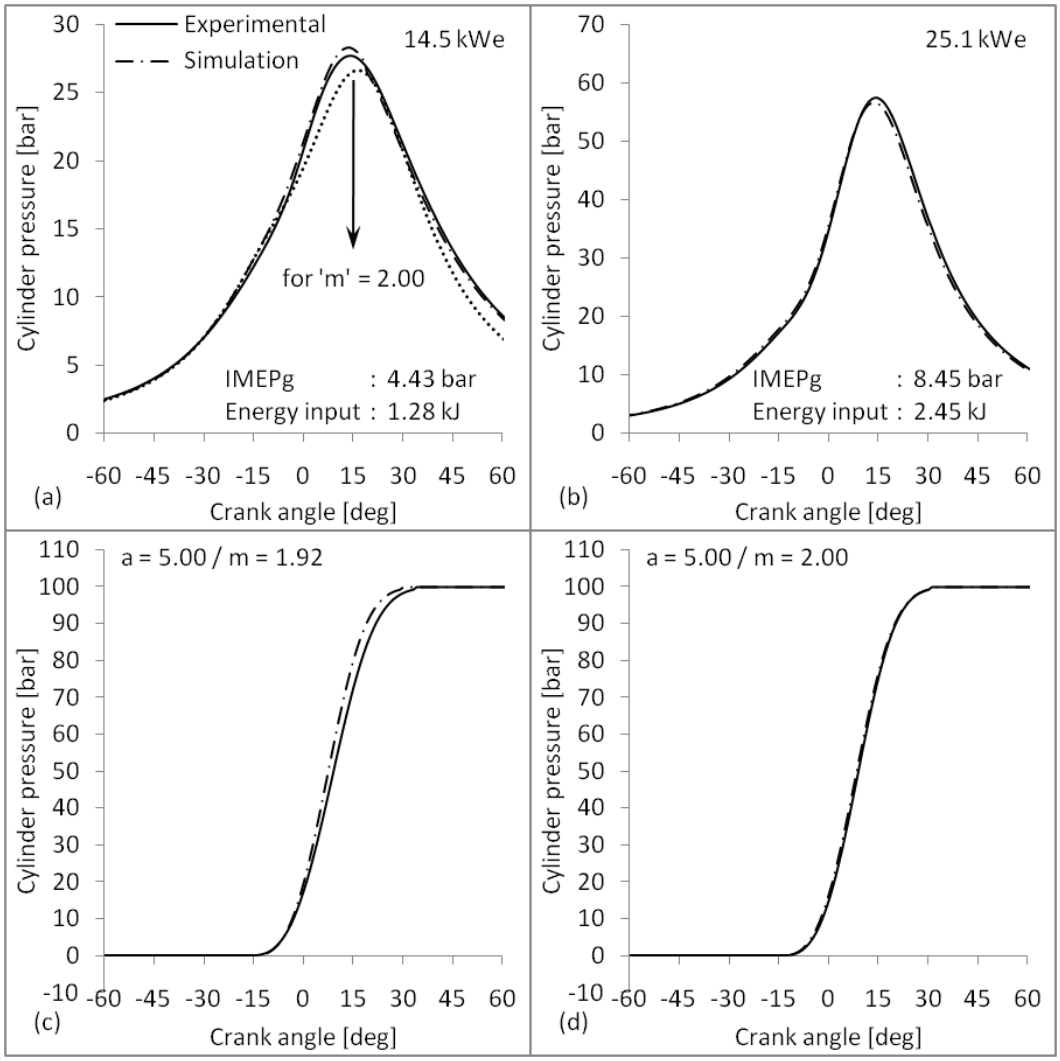

Figure 7.7: Zero dimensional simulations for compressed natural gas fuelled operation of engine E4

25.1 kWe (peak load) and 14.5 kWe (50% of the peak load) are compared with experimental results in figure 7.7. While figure 7.7 (a) and (c) present the pressure crank angle and heat release crank angle traces for the peak load operation, figure 7.7 (b) and (d) present the same for part load operation. In the simulation of the two operating conditions, the energy corresponding to gross indicated mean effective pressure estimated from the pressure trace is used as the input energy per cycle.

It is evident from figure 7.7 that the conventional Wiebe coefficients provide a near complete match for the heat release trace for compressed natural gas, especially for the full load operation. Minor tuning of the shape factor (from $m = 2.0$ to

$m = 1.92$) is however required at part load operation. It is important to note that the experimental data presented for the peak and part load operation corresponds to 1.1 $\pm$ 0.2 % oxygen in the exhaust. This is done to ensure that near complete combustion of the fuel takes place within the engine permitting the use of efficiency factor of 5.

The data presented for NG operation sufficiently validates the zero dimensional model and accordingly, the same is extended for PG fuelled operation.

7.2.3 Producer gas fuelled operation

The zero dimensional simulation using conventional Wiebe coefficients of $m = 2$ and $a = 5$ (Heywood 1988)(Ferguson and Kirkpatrick) is extended for PG fuelled peak load operation of engine E6 under both naturally aspirated and turbocharged after cooled mode of operation. The comparison of the pressure and heat release traces are presented in figure 7.8 (a) and (b) respectively with the inset data quantifying the differences. It is evident from the comparison that the results of Wiebe simulation differ substantially as compared to the experimental results. For the turbocharged after cooled mode of operation, the peak pressure is under predicted by over 15% and the position of peak pressure is displaced by 10 deg crank angle away from the top dead center. Similarly, for naturally aspirated mode of operation, the peak pressure is under predicted by about 45 %. This analysis clearly establishes the fact that the Wiebe coefficients for conventional fossil fuels are a clear misfit for PG fuelled operation.

A diagnostic analysis towards identifying the causative factors for such deviations between experimental and simulation results leads to the nature of the apparent heat release. Comparing the apparent heat release profile for PG under both naturally aspirated and turbocharged after-cooled mode of operation with the heat release profile generated using the conventional coefficients as in figure 7.8 (b), it can be observed that the heat release profiles for conventional fuel differs substantially for the PG profiles. The deviation is particularly severe beyond the 50% heat release region. As discussed previously (refer section 5.5), the deviation in the PG heat release profiles from the typical S shaped profile of conventional fuels is attributed to the presence of hydrogen in PG. The conventional fuel Wiebe coefficients proving

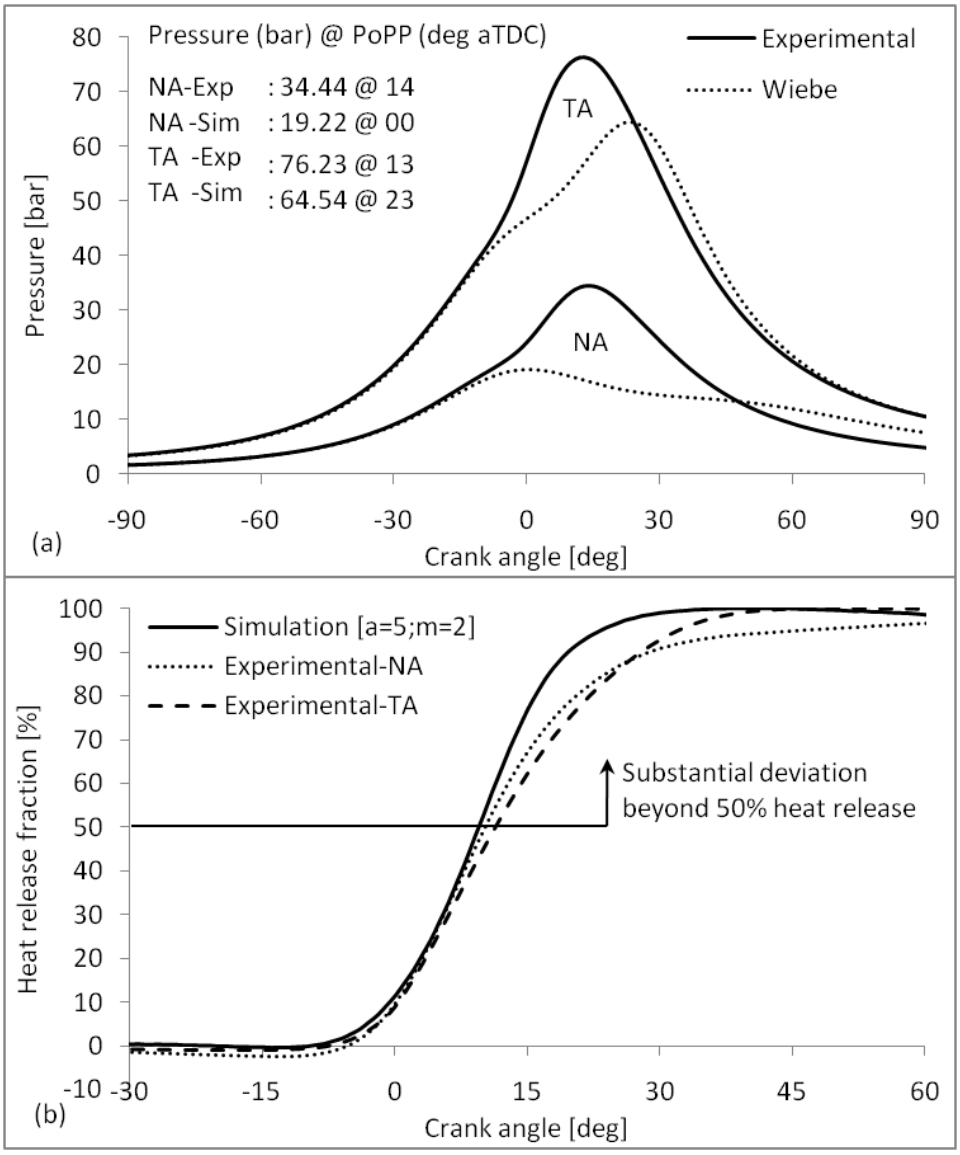

Figure 7.8: Use of conventional Wiebe coefficients for simulation of producer gas fuelled engine operation

to be misfit for PG fuelled operation calls for fuel specific Wiebe coefficients. The estimation of fuel specific Wiebe coefficients is described as below.

Towards estimating the Wiebe efficiency factor a, detailed measurements on the engine exhaust composition and temperature are used. Analysis of dry exhaust composition at higher loads has shown the presence of CO in the range of 0.75 to 1.3% on mass basis and the exhaust gas temperature in the range of 830 ± 10 K. This data is used in equation 7.2 (Heywood 1988) for estimating the combustion

inefficiencies.

$$1 - \eta_c = \frac{\sum_i X_i Q_{HV_i}}{\frac{F}{A} Q_{HV_f}} \tag{7.2}$$

Measurements on PG composition and subsequent analysis indicate the stoichiometric fuel air ratio (F/A) to be 0.75 ± 0.02 and the lower calorific value (Q_{HV_f}) to be 4.1 ± 0.05 MJ/kg. Considering LCV Q_{HV_i} and mass fraction X_i for CO as 10.01 MJ/kg and 0.013 respectively, the conversion inefficiency amounts to about 5%. The high exhaust gas temperatures for PG operation (by 70 - 80 K) could be related to the in-cylinder combustion process and indicate late burning with reduced contribution to the work transfer. The sensible heat corresponding to 75 K evaluates to another 5% of the input energy. The above two factors amount to about 10% compared to a typical fossil fuel combustion where the inefficiencies are in the range of 1 - 2% of the input fuel energy (Heywood 1988). On the basis of 90% fuel conversion efficiency, the value of efficiency factor is found to be 2.3 from equation 7.2. It is important to note that literature indicates choice of efficiency factors as high as 6.9 (Borg and Alkidas 2009) and 10 (Shiao and Moskwa 1995) in an effort to match the Wiebe heat release profile with the experimentally observed profiles. Choice of efficiency factor as high as 10 is rather surprising considering that the fuel conversion efficiency achieves a value of 99.32% at $a = 5$ and changes to 99.99% for $a = 10$. The fuel conversion efficiency in a typical spark ignition engine seldom crosses 98% even under lean conditions (Heywood 1988). Tuning of a to match the heat release profile thereby seems unrealistic and is thermodynamically untenable. Having estimated the efficiency factor, the shape factor is determined from the least square method.

Based on the above methodology, the Wiebe coefficients are estimated for PG fuelled stoichiometric operation on the three engine frames at various loads and are consolidated in table 7.1 as below.

Analysis of the data consolidated in table 7.1 indicates that for load above 40% of the peak supported load, the shape factor variation is nominal. Similarly, while the efficiency factor increases with load, the difference in efficiency factor between the peak and the part load remains well under 15 %. Based on the above consideration,

Table 7.1: Tuned Wiebe coefficients for produce gas fuelled operation at various loads

Engine	Load (kWe)					
*E*6 (TA)	72.8	60.5	51.0	39.8	30.5	20.4
a/m	2.30/0.70	2.23/0.69	2.17/0.72	2.04/0.71	1.87/0.68	1.45/0.76
*E*6 (NA)	27.3	24.2	20.3	15.2	10.2	–
a/m	2.32/0.71	2.25/0.71	2.23/0.72	2.09/0.73	1.51/0.77	
*E*4	14.5	10.3	7.55	5.30	3.50	–
a/m	2.46/0.72	2.54/0.73	2.16/0.72	2.13/0.75	1.92/0.78	
*E*2	7.0	4.2	2.0	–	–	–
a/m	2.44/0.71	2.21/0.72	1.73/0.78			

it can be concluded that for loads above 40% of the peak load a common shape factor and an efficiency factor can be arrived at based on averaging. The shape and efficiency factor based on the above approach for stoichiometric, producer gas fuelled operation are 0.71 and 2.23 respectively.

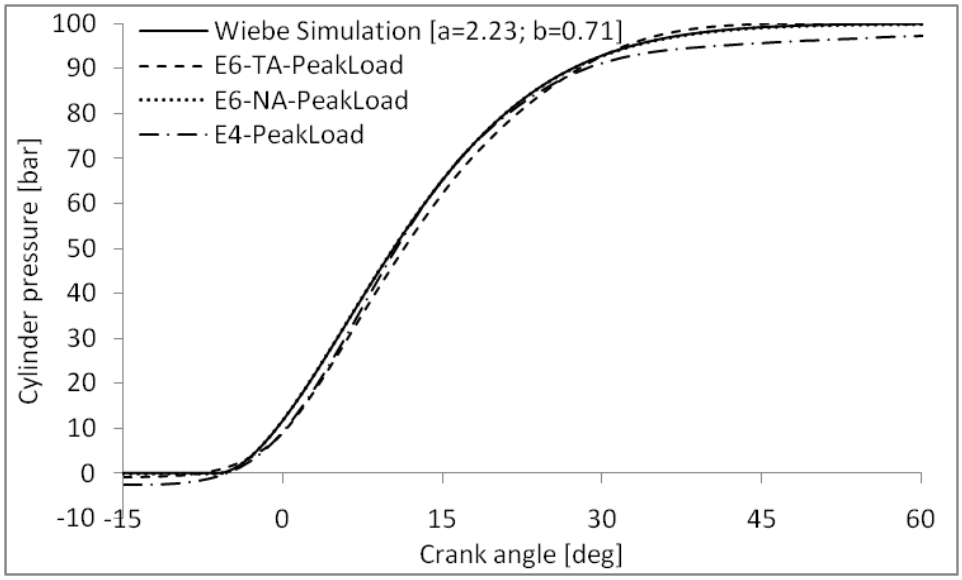

Figure 7.9: Comparison of experimental and Wiebe simulation results

The heat release profile based on the estimated Wiebe coefficients is compared

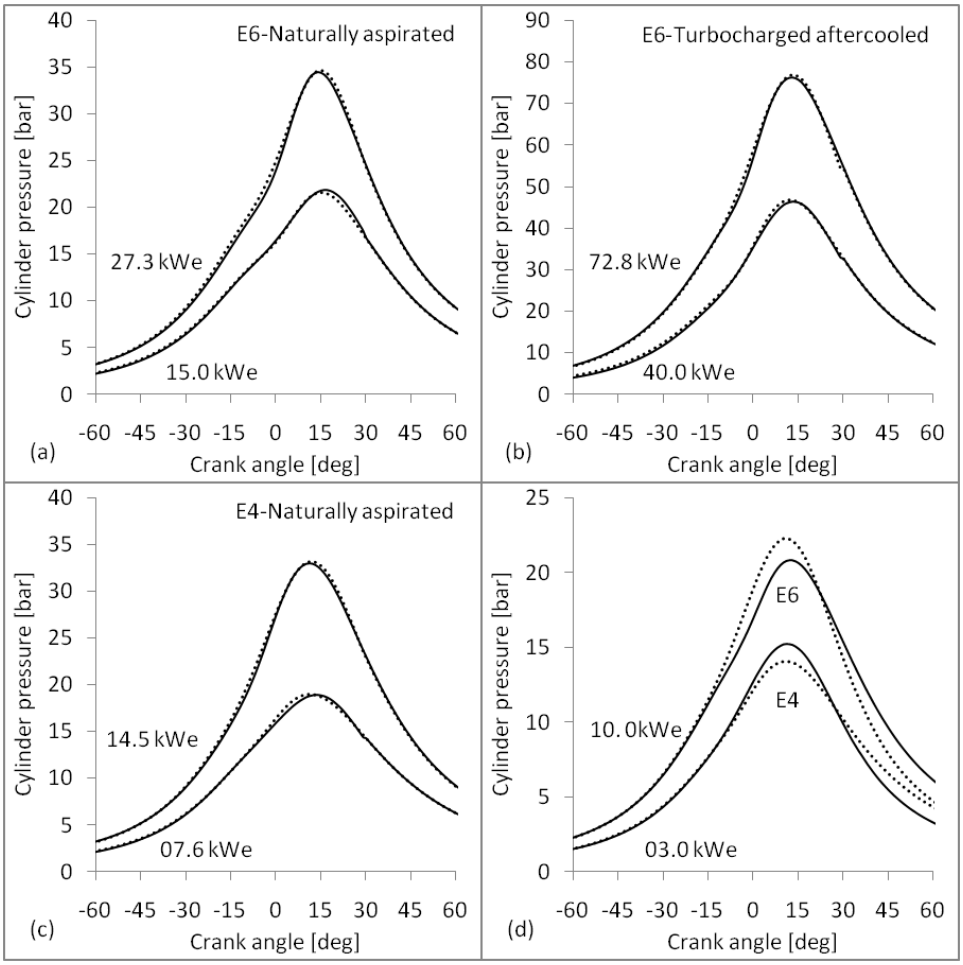

Figure 7.10: Zero dimensional simulation using tuned Wiebe coefficients (continuous lines represent experimental results and dotted lines represent simulation traces)

with the experimental traces for the peak load operation of the engine $E6$ under both naturally aspirated and turbocharged mode of operation and engine $E4$ as in figure 7.9. A very close match for the heat release trace is evident. Similar behavior is also observed for part load operation. The data for part load operation is however not indicated in the figure for the sake of brevity considering that the profiles are positioned within a very narrow band. The tuned Wiebe coefficients are used in the engine zero dimensional model to simulate various operating conditions. Some of the key results of the simulation are consolidated in figure 7.10 (a) through (d). Figure 7.10 (a) and (b) compare the pressure traces for the peak and part load operation of engines $E6$ under naturally aspirated and turbocharged after cooled mode respectively while figure 7.10 (c) presents the pressure trace for the engine

$E4$. It is interesting to note that for the indicated engine frames and operational loads (above 40% of respective peak load) a very close match is obtained. Both the magnitude and position of peak pressure match very closely. For load less than 40 % of the peak load, deviation, primarily in the magnitude of the peak pressure is observed.

The foregone discussion clearly establishes the versatility of producer gas specific Wiebe parameters (for stoichiometric operation) in terms of load independence, atleast for the regime of operational relevance (over 50% of peak load).

The analysis is extended to parametric variation involving ignition angle, the air to fuel ratio and CR. In so far as the the ignition angle and the air to fuel ratio parametric variation is concerned, it is important to note with change in ignition angle the combustion phasing is explicitly altered while with a change in mixture quality, the thermo-physical properties of the fuel air mixture are altered with an overall consequence of altered heat release pattern. Addressing the effect of CR, considering that the influence on the heat release pattern is only through the burn rate, a comparative analysis is presented based on literature reported results for a different engine geometry operating at a different CR.

Towards addressing the effect of a CR, simulations are carried out for a three cylinder naturally aspirated engine at two different CR of 11.5 and 13.5 and are compared with experimental results as in figure 7.11. A very close match is obtained for CR 11.5 with the peak pressure matching to the first decimal while the position of peak pressure differs only by a degree. However, in the case of CR 13.5, the magnitude of peak pressure is slightly low and the position gets advanced from the top dead center. It is assessed that high CR would entail higher in-cylinder temperatures (about 50 K higher for CR 13.5 than for CR 11.5 for motoring conditions based on polytropic assessment) and correspondingly influence the flame speed, resulting in reduced combustion duration and altered combustion phasing. From the figure it can be concluded that advancing the end of combustion angle would shift the pressure profile to match the experimental trace and accordingly, the end of combustion angle is reduced by about 6 degrees. Using the advanced condition of combustion angle results in near complete reproduction of the experimental pressure trace implying higher burn rates at higher CR.

The above results address the generality of the fuel specific Wiebe coefficients wherein the same coefficients could be used for a different geometry and CR while requiring the tuning of combustion duration. Tuning of the combustion duration is not only desirable but is consistent with the in-cylinder thermodynamic condition. The ignition timing is retarded with increasing CR (shorter combustion duration) and advanced with reducing CR (longer combustion duration) to phase the combustion to deliver maximum torque.

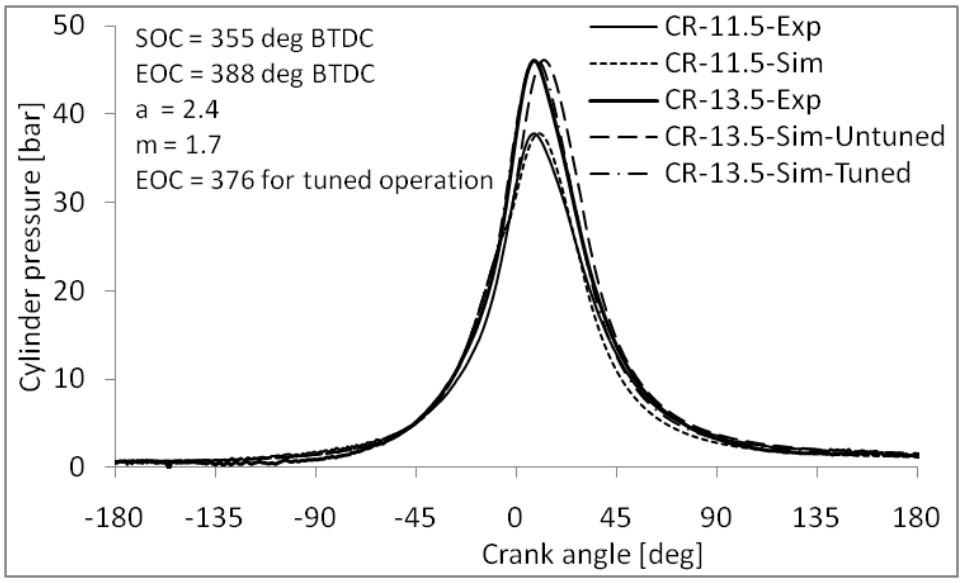

Figure 7.11: Comparison of experimental and simulated traces for $E2$ under WOT - MBT operation

Summarizing the zero dimensional results;

1. Literature reported Wiebe coefficients for conventional fuels (a=5 and m=2) provide excellent simulation results for natural gas fuelled operation.

2. The conventional coefficients prove to be misfit for PG simulation, establishing the need for fuel specific coefficients.

3. Conventional coefficients are rendered unsuitable due to significant differences in the heat release profile between conventional fuels and PG (influencing the shape factor) and relatively higher combustion inefficiencies for PG as compared to conventional fuels (influencing the efficiency factor)

4. Load independent (in the 40% to 100% regime) Wiebe coefficients have been established with efficiency factor of 2.23 (based on exhaust analysis) and shape factor of 0.71 (based on subsequent curve fit analysis)

5. The fuel specific coefficients have been validated for generality by extending the comparative analysis to a range of compression ratios and different engine geometry.

7.3 Quasi-dimensional model

The results of the quasi dimensional model simulation are presented in the current section. The emphasis of simulation is primarily on producer gas fuelled operation of engine $E6$ under both naturally aspirated and turbocharged after cooled mode of operation. Parametric sensitivity analysis is also reported for engine $E6$. The possibility of extending the turbulence parameters of engine $E6$ to $E4$ for similar operating conditions is also evaluated considering that the engine geometries are not too dissimilar.

Prior to the discussion of the full simulation results, aspects related to initial and termination of combustion and the computational fluid dynamics analysis towards the estimation of turbulence parameters are discussed. Subsequent to the discussion of the simulation results for normal combustion, the analysis is extended to abnormal combustion, the focus being on the prediction of occurrence and angle of end gas auto-ignition. The results of quasi dimensional model with knock prediction ability are presented in a separate section.

7.3.1 Combustion initiation and termination

In case of the zero dimensional model, while the initiation and termination of combustion was based on the analysis of the mass burn fraction / heat release fraction traces, the quasi dimensional model requires the knowledge of both the mass burn fraction / heat release fraction trace as well as the pressure crank angle trace. The knowledge of mass burn fraction trace is essential to identify the crank angle for the initialization of the twin zones in the engine cylinder while the pressure trace is required to establish the thermodynamic state of the flame kernel. It is however important to note that a complete firing pressure trace itself is not necessary and even a validated simulation pressure trace would suffice. The information required for the initialization of twin zones within the engine cylinder are consolidated as below;

- mass / volume of the flame kernel.
- thermodynamic state of the flame kernel.

- the time after the actual sparking when the flame kernel has to be introduced in the cylinder and
- the position of flame kernel with respect to some reference (generally spark plug)

As discussed previously in the model formulation section (refer section 6.4), in the current investigation, the fraction of mass burn approach is adopted with the flame kernel initialized when the mass burn fraction reaches 1% leading to establishment of two distinct zones, one burned and the other un-burned. This method is adopted since this is the only approach that permits establishing the appropriate thermodynamic and geometric condition for the two zones which serves as the initial condition for the subsequent turbulent combustion process. The thermodynamic state of the flame kernel at the time of initialization is estimated as per the procedure described by Benson et al (Benson, Annand, and Baruah 1975) as below. In this approach, as the mass burned reaches 1% of the total, a flame kernel instantly appears with equilibrium temperature corresponding to the prevailing initial conditions. Corresponding to the temperature rise, an hypothetical pressure rise of the kernel is also considered which subsequently equilibrates with the unburned mixture pressure. The appearance of the flame kernel at equilibrium temperature and the equilibration of the the kernel and mixture pressure are both adiabatic and constant volume processes with the internal energy conserved. The relevant sequences as invoked in the discussion along with the corresponding thermodynamic states are identified in figure 7.12 (a), (b) and (c).

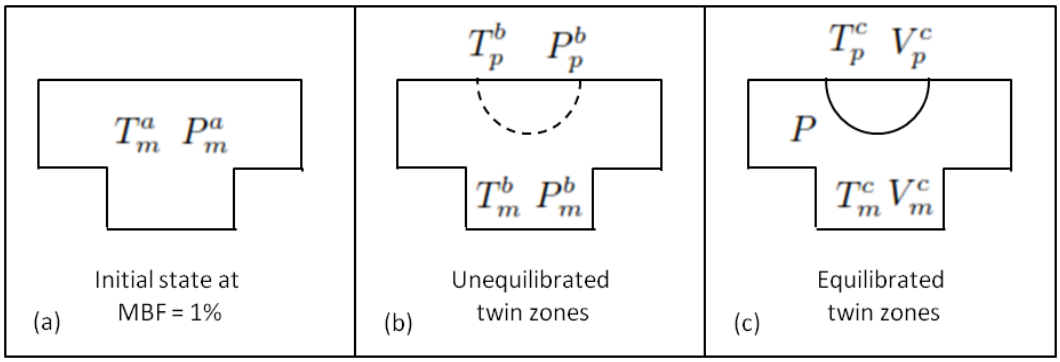

Figure 7.12: Stages of flame kernal initialization in the engine cylinder

1. Identify the crank angle corresponding to 1% of the mass burn fraction based on the experimental mass burn fraction trace as described in the zero dimensional model formulation (refer section 7.2.1).

2. **Mixture base state estimation** : Estimate the thermodynamic state corresponding to the crank angle of initiation based on the solution of the single zone first law equations (refer section 6.2) and the final mass trapped in the engine cylinder from the gas exchange process (refer section 6.2.2).The thermodynamic state of the system is identified by T_m^a P_m^a and marks the end of stage A.

3. **Flame kernel initiation** : Estimate the temperature of the flame kernel T_p^b based on equilibrium analysis with internal energy conserved. An hypothetical pressure rise for the flame kernel is assumed and is estimated based on the equilibrium temperature of the kernel using the expression as below;

$$P_p^b = P_m^b \frac{T_p^b}{T_m^b} \frac{MW_m}{MW_p} \qquad\qquad T_m^b = T_m^a \text{ and } P_m^b = P_m^a$$

   Thus, now there are two distinct states within the engine cylinder with P_m^b, T_m^b describing the mixture and P_p^b, T_p^b describing the flame kernel. This marks the end of state B.

4. **Kernel-Mixture pressure equilibration** : As mentioned, the equilibration is based on the conservation of internal energy as described below;

$$U_b = U_c$$

$$m_m^b u_m^b + m_p^b u_p^b = m_m^c u_m^c + m_p^c u_p^c$$

$$\underbrace{m_m u_m^b + m_p u_p^b}_{\text{before eqilibration}} = \underbrace{m_m u_m^c + m_p u_p^c}_{\text{after eqilibration}}$$

$$m_m C_{v,m}(T_m^b - T_m^c) = m_p C_{v,p}(T_p^c - T_p^b)$$

$$m_m C_{v,m} T_m^b \left[1 - \frac{T_m^c}{T_m^b}\right] = m_p C_{v,p} T_p^b \left[\frac{T_p^c}{T_p^b} - 1\right]$$

$$\frac{T_m^c}{T_m^b} = \left[\frac{P}{P_m^b}\right]^{(\gamma_m - 1)/\gamma_m} \qquad \frac{T_p^c}{T_p^b} = \left[\frac{P}{P_p^b}\right]^{(\gamma_p - 1)/\gamma_p}$$

$$\frac{P}{P_b^b} = \frac{P}{P_m^b}\frac{P_m^b}{P_b^b} = \frac{P}{P_m^b}\frac{R_m T_m^b}{R_p T_p^b}$$

Rearranging using the final three equations, the internal energy conservation can be expressed as;

$$\delta - 1 = A(1 - B\delta^{\alpha}) \tag{7.3}$$

$$\delta = \frac{T_m^c}{T_m^b}; \qquad \alpha = \frac{\gamma_m}{\gamma_m - 1}\frac{\gamma_p - 1}{\gamma_p}$$

$$A = \frac{m_p C_{v,p} T_p^b}{m_m C_{v,m} T_m^b}; \qquad B = \left(\frac{R_m T_m^b}{R_p T_p^b}\right)^{(\gamma_p - 1)/\gamma_p}$$

Equation 7.3 is solved iteratively for known values of A, B and α to arrive at δ. Arriving at δ, first the final state mixture temperature (T_m^c) is arrived at which subsequently permits estimating the uniform in-cylinder pressure (P) after the establishment of the flame kernel. The knowledge of the kernel pressure, temperature and mass permits estimating the volume of the kernel.

The estimated kernel and mixture thermodynamic state and the kernel volume/radius following the above approach are as listed in table 7.2. The consolidated data forms the initial condition for the subsequent turbulent combustion phase. The kernel radius based on the assumed kernel volume is also (0.1 % of the total cylin-

der volume) which has no thermodynamic basis is also indicated for representative purpose. The radius based on assumed volume is 25% smaller than the mass burn fraction based radius.

Table 7.2: Flame kernel volume estimation for naturally aspirated and turbocharged operation.

Kernel radius based on 1% of mass burn analysis (current analysis)				
	Naturally aspirated		Turbocharged	
Parameter	Pre-Equ	Post-Equ	Pre-Equ	Post-Equ
Mixture temperature (K)	723.1	729.4	747.6	753.9
Mixture pressure (bar)	21.2	21.9	45.7	47.2
Kernel temperature (K)	2522.8	2018.2	2555.4	2052.6
Kernel pressure (bar)	64.1	21.9	135.4	47.2
In-cylinder mass (kg)	$9.87E^{-4}$		$2.10E^{-3}$	
Kernel volume (m^3)	$2.5125E^{-6}$		$2.5265E^{-6}$	
Kernel radius (m)	0.00848		0.00850	
Kernel radius (mm)	8.48		8.50	
Kernel radius based on 0.1% of total cylinder volume (comparative assessment)				
Total cylinder volume(m^3)	$1.084E^{-3}$			
Kernel volume (m^3)	$1.084E^{-6}$			
Kernel radius (m)	0.006406			
Kernel radius (mm)	6.41			

In the zero dimensional model, the terminal phase of heat release was handled by terminating the scope of the Wiebe function at the crank angle corresponding to mass burn fraction reaching the fraction dictated by the choice of efficiency factor a. Effectively, the mass corresponding to energy equivalent of the inefficiencies remains un-burned. The quasi dimensional model adopts an altogether different approach towards handling the terminal phase of combustion and is described as below.

Following the eddy entrainment philosophy, in the quasi dimensional model it is assumed that when the entire mixture is en-flamed ($A_f = 0$ and $V_f = C_{cyl}$), un-burned eddies of characteristic size l_T persist in the burned mixture. These un-burned

eddies burn with an exponential burn rate (an approximate sphere burning peripherally radially inwards) captured through an exponential correlation as in equation 7.4;

$$\frac{1}{m_f}\frac{dm_b}{dt} = \frac{\dot{m}_b}{m_f} = e^{-\frac{t-t_f}{\tau_b}} \tag{7.4}$$

m_f	Trapped in-cylinder mass (kg)
$\dot{m}_b$	Mass burn rate (kg/s)
t_f	Time at which the complete in-cylinder gases are enflamed, $A_f = 0$ (sec)
τ_b	Characteristic burn time when the eddies burn out (sec)
t	Some time in the cycle such that $t_f \geq t \leq t_f + \tau_b$ (sec)

Effectively, in the quasi dimensional model, the flame completely engulfing the entire contents of the cylinder ($A_f = 0$) initiates the start of the terminal phase of the combustion which remains in scope for the duration τ_b. As evident from equation 7.4, the terminal burn rate is independent of all thermo-physical properties and depends only on the characteristic burn time τ_b. It is important to note that while τ_b can be estimated based on the knowledge of the laminar flame speed and the characteristic turbulent length scale (further details presented in the next section) an alternative and more accurate approach has been to use the experimental mass burn fraction traces as suggested by the authors of the quasi dimensional model (Keck 1982) (Heywood 1988). The suggested approach is described based on figure 7.13.

The mass burn fraction (kg/kg) and the mass burn fraction change rate (1/sec) for two cases at the same load of 14 kWe are depicted in figure 7.13. One case (dotted lines) represents operation of $E4$ with natural gas while the other represents operation of $E4$ with producer gas. The near asymptotic approach of the cumulative mass burn fraction trace suggests exponential burn time during the terminal phase of combustion which is also verified by plotting the mass burn rate profile on a log scale. As evident from figure 7.13 (a), the terminal phase of combustion (identified by the oval region) presents a near liner trend for both the cases on a log plot.

The characteristic burn time as required in equation 7.4 is extracted from the log plot mass burn rate profile as shown in figure 7.13 (b) and (c). Superimposing a

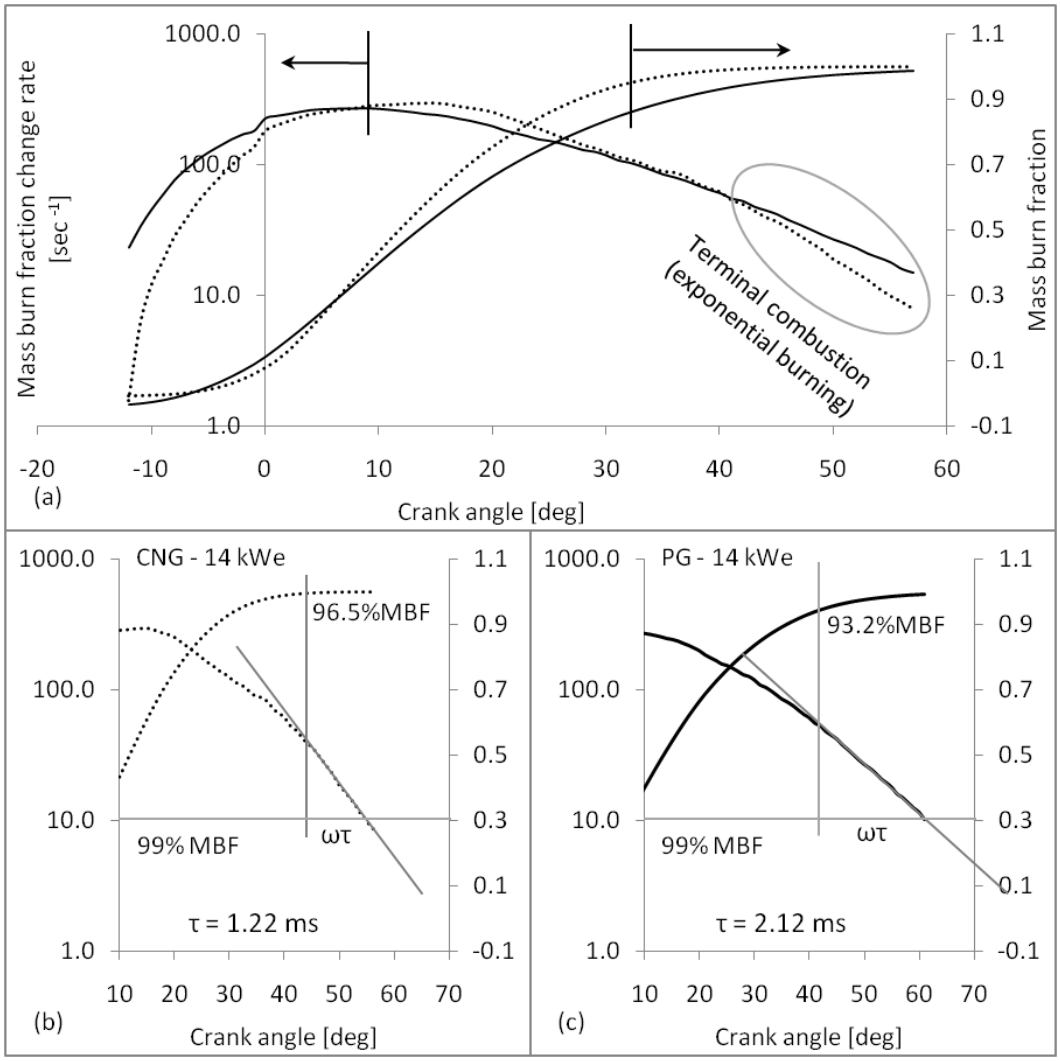

Figure 7.13: Terminal phase burn time estimation based on in-cylinder data

straight line (with slope as close as possible to the terminal stage linear regime) on the terminal stage (near) linear profile permits identifying the start of terminal phase of combustion. The point of deviation of the burn rate profile from the superimposed straight line fixes the crank angle corresponding to the start of terminal phase of combustion (refer figure 7.13 (b) and (c)). For the ensemble average mass burn rate profile, the start of terminal combustion stage for natural gas corresponds to 96.5 % mass burn fraction at a crank angle of 43.5 deg after the top dead center while it is 93.2 % for producer gas at a crank angle of 41 deg after the top dead center. The end of the terminal phase is fixed arbitrarily by considering a mass burn fraction beyond 98 %. In the current investigation, the crank angle corresponding to 99 % of mass

burn fraction is considered to identify the termination crank angle. The crank angle in absolute degrees corresponding to the start and end of combustion constitute the terminal stage combustion duration. The characteristic burn time is subsequently measured from the following correlation;

$$\tau_b = \frac{\text{Terminal combustion duration (deg)}}{\text{Angular velocity (deg/sec)}}$$

For the two cases considered, the terminal combustion duration evolves to 1.22 ms for natural gas and 2.12 ms for producer gas. The timing of 1.22 ms for natural gas is comparable with literature reported values (Keck 1982) (Heywood 1988).

7.3.2 Turbulence parameters

The turbulent parameters as required by the eddy entrainment and laminar burn-up model are estimated from the cold flow computational fluid dynamic studies using the ANSYS-FLUENT solver. Engine simulation being an unsteady / transient problem, the predictor-corrector PISO (Pressure implicit with splitting of operator) algorithm is used for pressure - velocity coupling. The default scheme(s) recommended by ANSYS FLUENT are adopted for the discretization of the convective terms of the governing equations (first order upwind for turbulence quantities and second order upwind for flow and scalar quantities). The details pertaining to the flow domain and the grid independence studies are described in detail in appendix D. The initial and boundary conditions for producer gas fuelled naturally aspirated and turbocharged peak load operation of engine E6 are described as below;

Initial conditions

The initial domain pressure was set at 67370 Pa and 154000 Pa for the naturally aspirated and turbocharged operation respectively. Similarly, for the corresponding operations, the domain temperature was set at 300 and 320 K respectively.

Boundary conditions

The following boundary conditions have been used for the simulation;

1. Intake and exhaust port : Pressure inlet and outlet boundary type with 300 K total temperature.

2. Cylinder wall : Treated as a stationary wall with 450 K constant temperature.

The full three dimensional computational fluid dynamic simulation evolves the relevant governing parameters over the entire domain at the individual cell level. Substantial variations in the parameters could persist from region to region depending on the local flow conditions. Using such three dimensional results in quasi dimensional simulations requires averaging of the relevant properties since the input to quasi dimensional model is restricted to temporal variation only. While in the strict quasi dimensional sense, spatial averaging has to be based on the complete in-cylinder domain (under the assumption that the flame sheet does not alter the in-cylinder turbulence), the fact that turbulence levels in the bowl and the clearance region could be substantially different calls for a judicious choice of the regime of averaging. In the current investigation, three regions within the engine cylinder are considered for averaging (the clearance region, bowl region and the complete domain) and the final choice is based on the best solution approach described in a subsequent section.

Prior to the extraction of the turbulence parameters, the motoring pressure traces for the operating conditions of interest are to be validated. The experimental and computational fluid dynamics simulation motoring pressure traces for peak load naturally aspirated and turbocharged after-cooled mode of operation are compared in figure 7.14. Figure 7.14 (a) and (b) compare the pressure traces for the suction stroke while figure 7.14 (c) and (d) compare the traces 90 deg on either side of the top dead center.

The variation of mass average turbulent intensity and the integral length scale (derived from the turbulent kinetic energy and dissipation rate) for the turbocharged after cooled peak load operation of engine $E6$ is as indicated in figure 7.15. Figure 7.15 (a) and (b) presents the variation of the integral length scale and the turbulent intensity respectively for the three domains considered. The turbulent intensity and length scale are tabulated for every 0.5 deg crank angle from 30 deg before the top dead center to 90 deg after the top dead center and are used during the simulation.

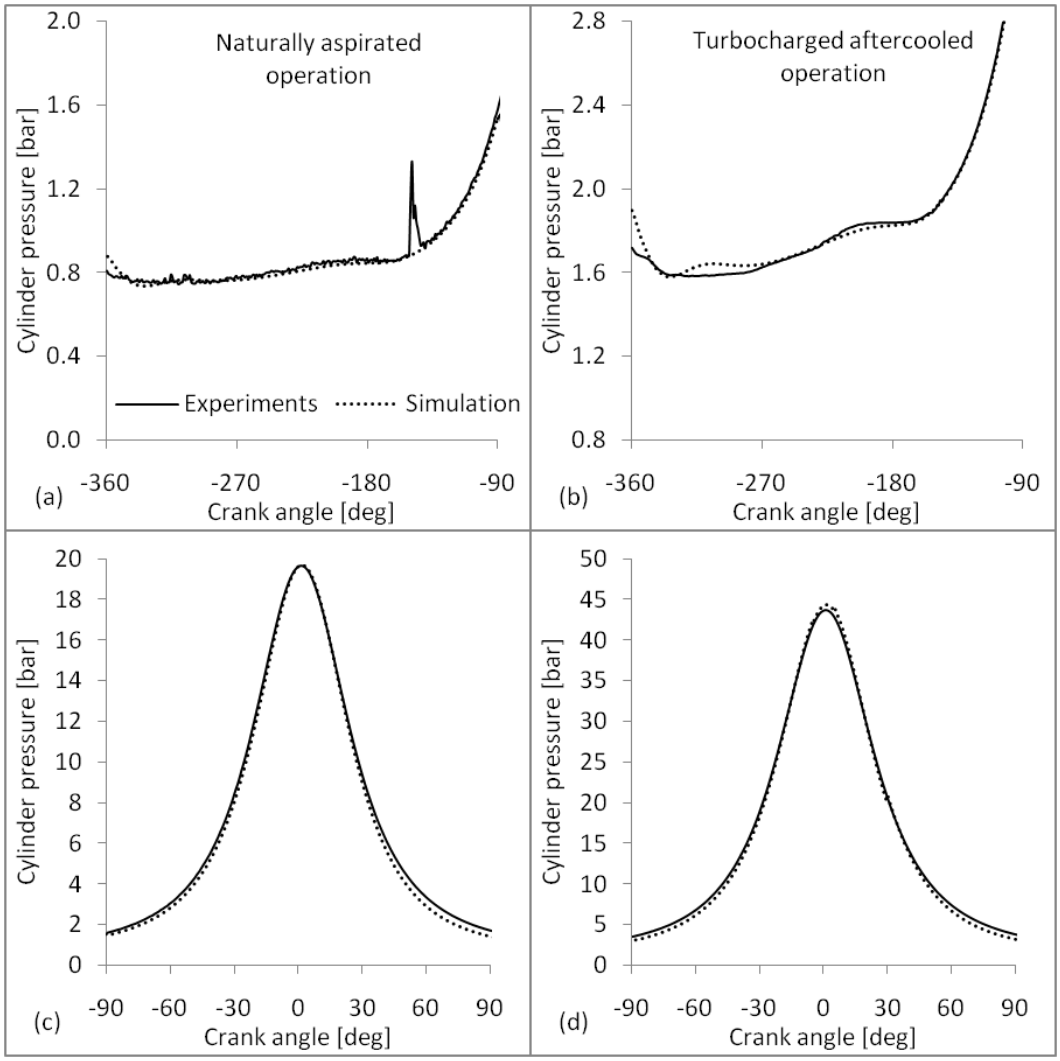

Figure 7.14: Comparison of experimental and simulation motoring pressure traces

7.3.3 Analysis of flame speed ratio

The flame speed ratio corresponding to an SI engine is defined as the ratio of the turbulent flame speed (S_T) to the laminar flame speed (S_L). Under quasi steady conditions, the turbulent flame speed being the simple addition of laminar flame speed and turbulent intensity, the flame speed ratio represents the relative significance of turbulence over the laminar flame speed in altering the un-burned mixture burning rate. The flame speed ratio is compared with the ratio of the turbulence intensity to the laminar flame speed as in figure 7.16 for naturally aspirated and turbocharged after cooled mode of operation of engine $E6$.

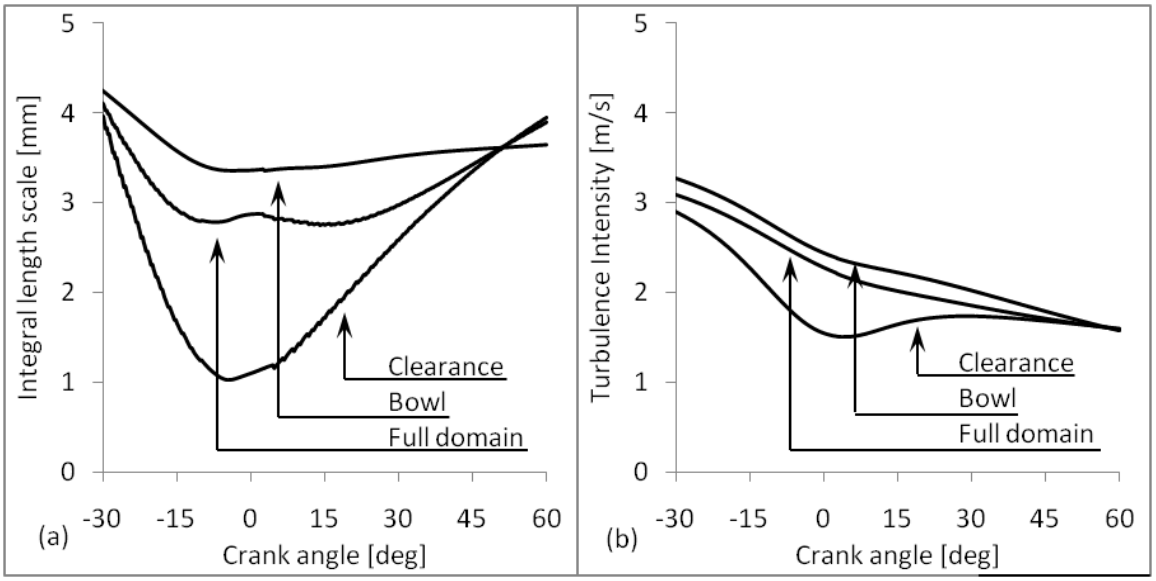

Figure 7.15: Turbocharged operation peak load integral length scale and turbulent intensity

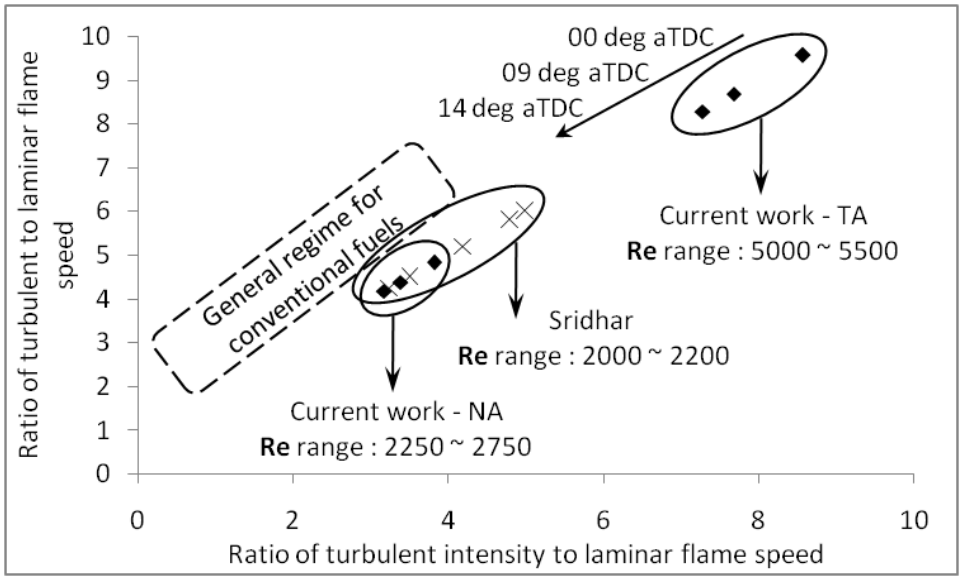

Figure 7.16: Variation of the flame speed ratio with the ratio of turbulence intensity to the laminar flame speed

The comparison is presented at three piston positions of top dead center, 9 deg after the top dead center (corresponds to 50% mass burn fraction) and 14 deg after the top dead center (corresponds to the position of peak pressure, refer section 5.5.3). The data reported by Sridhar et al (Rao 2003) for PG fuelled operation and the

general regime for conventional fuels as reported in literature (Ballal and Lefebvre 1974) (Tabaczynski 1976) (Abdel-Gayed and Bradley 1977) (Clavin and Williams 1979) (Groff 1987) (Gillespie, Lawes, Sheppard, and Woolley 2000) is also presented. It is evident from figure 7.16 that the data from the current work matches well with the literature, especially for the turbulent intensity to laminar flame speed ratio of under 5. The reported numbers are comparable with the data reported by Sridhar for naturally aspirated operation with CR under 13.5. Further, for a given intensity to laminar flame speed ratio, it can be observed that the flame speed ratio for conventional fuels is higher than that for PG. This is primarily attributed to the higher laminar flame speed for PG as compared to other typical conventional fuels like gasoline, propane etc.

Based on the relative comparison of the laminar flame speed and turbulent intensity data used in the current work with the literature reported values for both conventional fuels and PG, the choice of these two most critical parameters (laminar flame speed and turbulent intensity) is broadly validated.

7.3.4 Simulation results for engine $E6$

Quasi dimensional simulation results for PG fuelled operation of engine $E6$ under both naturally aspirated and turbocharged after cooled mode of are presented in this section. The analysis itself is presented in two broad sections. The first section primarily addresses the selection of turbulent parameters, establishing the necessary input parameters and the regime of validity while the second section deals with actual simulations addressing case specific simulations and parametric sensitivity analysis. The specifics corresponding to the two sections are listed as below.

1. Turbulent parameter selections
    - Selection of in-cylinder domain for estimating turbulent parameters
    - Selection of load range for averaging turbulence parameters
2. General simulations and sensitivity analysis
    - Sensitivity to initial and terminal combustion parameters

- Stoichiometric operation naturally aspirated and turbocharged after-cooled mode simulation
- Sensitivity analysis - Mixture quality
- Sensitivity analysis - Ignition angle

Selection of in-cylinder domain for estimating turbulent parameters

In line with the lumped approach of the quasi dimensional model, the turbulent parameters as required by the eddy entrainment laminar burn up model are estimated based on mass averaging over relevant in-cylinder domain. Towards estimation of the turbulent parameters as a function of crank angle only, three in-cylinder regions, the clearance, the bowl and the full in-cylinder domain are considered. Simulation results using turbulent parameters from the three domains are compared with the experimental pressure and heat release traces as in figure 7.17 [a-p;a-m] , [b-p;b-m] and [c-p;c-m] respectively. Some of the key features relevant for comparison are quantified and included as inset data.

Analyzing the data presented in figure 7.17 the following key features are evident.

1. Using clearance region based turbulent parameters leads to under prediction of the in-cylinder pressure by over 10 % (refer figure 7.17 a-p). The under prediction is attributed to the sluggishness in mass burn as evident from the mass burn profile (refer figure 7.17 a-m) which is in turn attributed to low turbulent intensity for the clearance region (refer figure 7.15).

2. Simulations considering turbulence from the bowl region and full domain (figure 7.17 b-p and c-p respectively) follow the experimental result very closely with the maximum difference in the pressure being under 3 %. With all other conditions being the same, the improvement is solely attributed to higher turbulent intensity for the bowl and full domain regions (refer figure 7.15).

Considering that both the bowl region and full domain based turbulence parameters evolve provide satisfactory results, in the current investigation, the full in-cylinder domain covering the clearance and the bowl region is considered for estimating the mass averaged turbulence parameters. The consideration of full domain

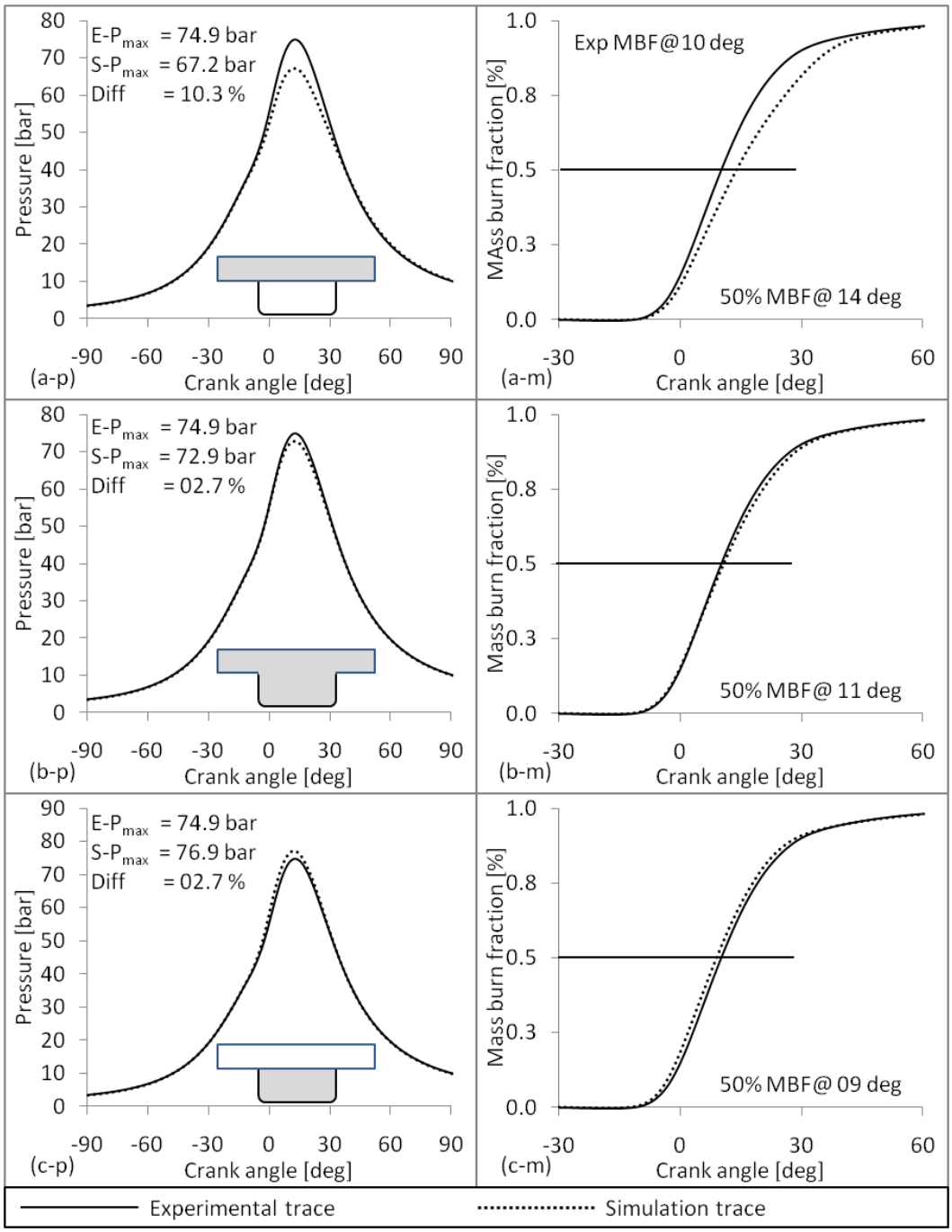

Figure 7.17: Influence of choice of domain for turbulence parameters averaging on mass burn rate and in-cylinder pressure

gels well with the general philosophy of thermodynamic simulation where no spatial discretization whatsoever is considered, hence the choice.

Selection of load range for averaging turbulence parameters

Addressing the load dependence of the turbulence parameters and hence the quasi dimensional simulation, towards simultaneously retaining sufficient generality as well as accuracy, the turbulence parameter for the full cylinder domain are averaged over various load ranges and used in the quasi dimensional model to assess the influence on the simulation results. The primary objective is to identify the range of load for averaging while maintaining the error between the experimental and simulation pressure traces being within the permissible limit. Representative results of the load range analysis for three load ranges are presented in figure 7.18.

It is evident from figure 7.18 that with a reduction in the load range, the deviation of the simulation pressure trace from the experimental pressure trace also decreases. For the case of 50 kWe to 72.8 kWe regime averaging, the maximum difference in the pressure is 3.1 % and when the range is extended to 40 kWe to 72.8 kWe load regime, the difference in the pressure is 5.2 %. While the 40 kWe to 72.8 kWe load regime just exceeds the maximum permissible limit of 5% by only 0.2 %, strictly adhering to the set limit, in the current analysis a load regime of 30% of the peak load is considered for averaging the turbulence parameters and is also extended to naturally aspirated mode of operation.

Sensitivity to initial and terminal combustion parameters

The sensitivity of quasi dimensional simulation to the flame initiation and termination parameters is addressed in the present section.

The influence of flame kernel initialization crank angle (in the engine cylinder) on the quasi dimensional simulation is presented in figure 7.19. Considering -4 deg initiation as the reference, while retarding the initialization leads to a small displacement of the pressure trace (peak pressure decreases by under 2.5 %), advancing the initialization leads to significant displacement (peak pressure increasing by over 10 %), making it evident that simulation remains significantly sensitive to the initialization crank angle. It is thus recommended to adopt operating condition specific kernel initialization crank angle (and thermo-physical conditions) rather than a operating condition regime averaged value.

Extending the analysis to the terminal stage combustion, sensitivity is addressed

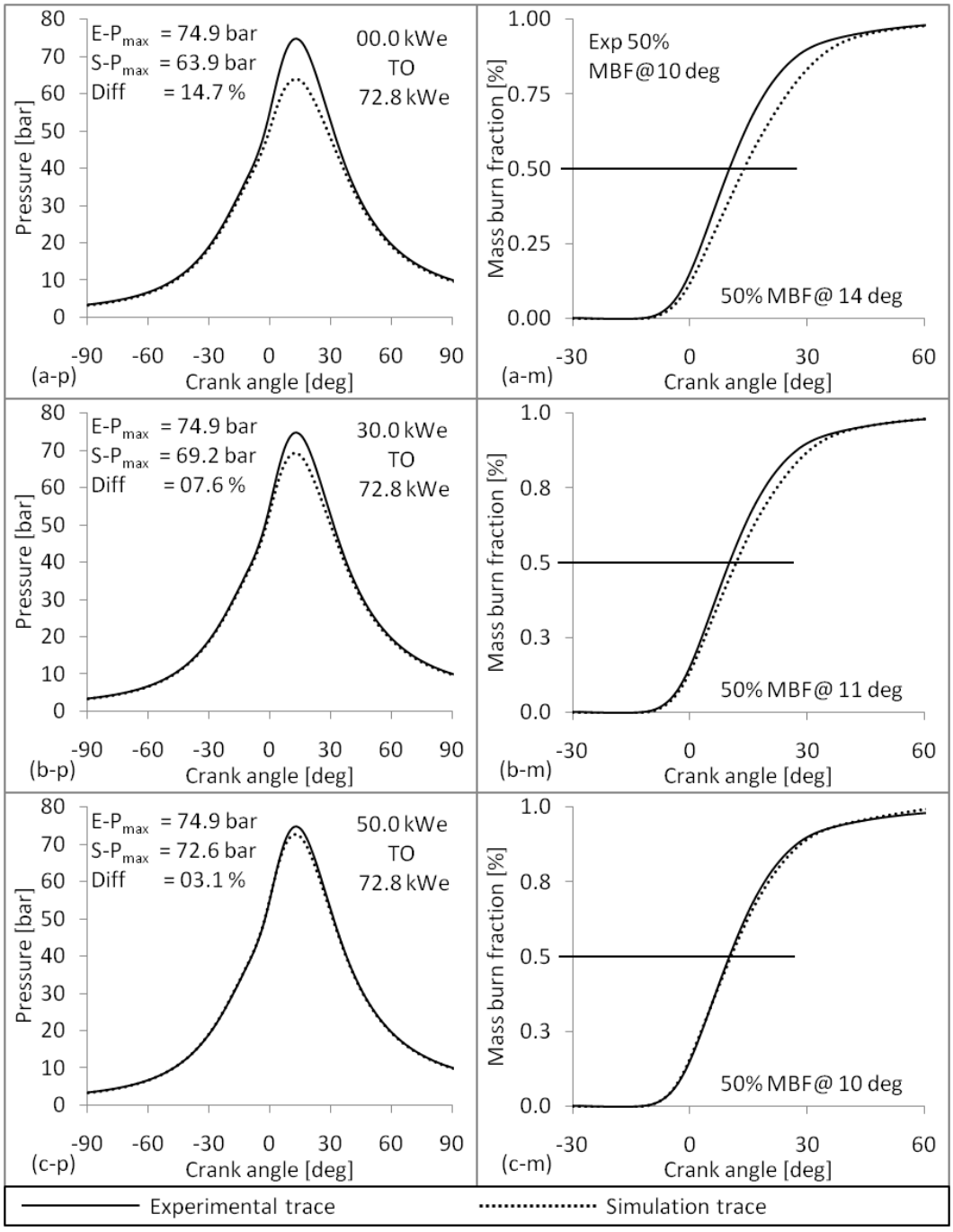

Figure 7.18: Influence of load range for turbulent intensity averaging on mass burn rate and in-cylinder pressure

by terminating the flame propagation based heat release at a crank angle of 30 deg after the top dead center (some hypothetical crank angle considered for the analysis) and considering three different duration of 10, 30 and 50 deg crank angle absolute

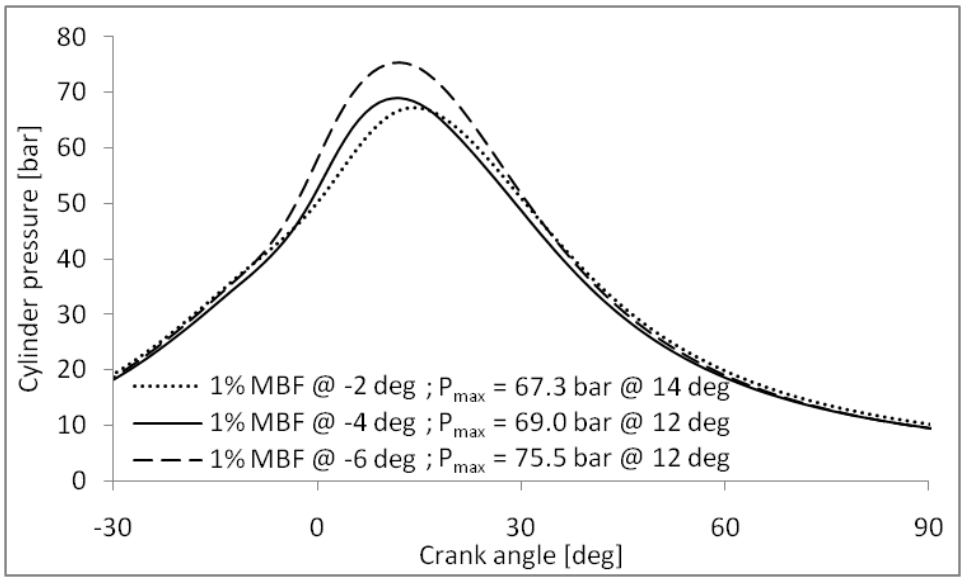

Figure 7.19: Influence of kernel initiation angle on the simulation results

(1.11, 3.33 and 5.55 milli seconds respectively at the rate of 9000 deg per minute) for the terminal stage (exponentially) burning. The differential heat release and pressure traces for the three combustion duration are indicated in figure 7.20.

As evident from figure 7.20 (a), the influence of terminal stage combustion duration are only post the flame out period and hence the in-cylinder pressure traces and the key combustion descriptors remain completely unaffected. The pressure trace is nominally altered only beyond the burn out period as evident from figure 7.20 (b) with minimal influence on the indicated mean effective pressure (refer inset data in figure 7.20 (b)). Thus, it can safely be concluded that the terminal stage combustion remains insensitive to the choice of terminal stage combustion timing.

Stoichiometric operation naturally aspirated and turbocharged after-cooled mode simulation

Having established the necessary conditions for the quasi dimensional simulation, the simulation results of stoichiometric operation of engine $E6$ under both naturally aspirated and turbocharged after-cooled mode of operation are reported in the current section. The initial / boundary conditions corresponding to peak load operation of engine $E6$ are consolidated in table 7.3 and the corresponding simulation

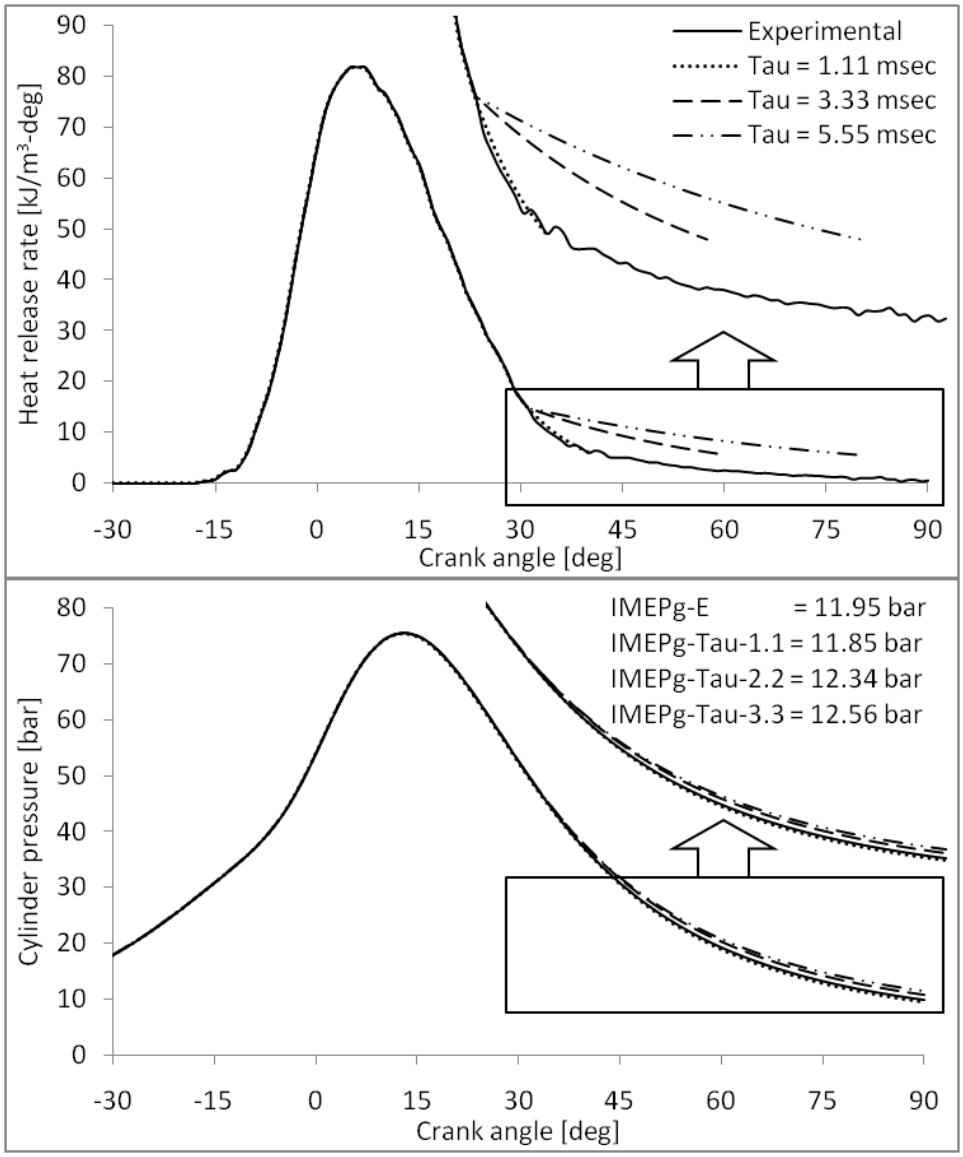

Figure 7.20: Influence of exponential burn time on the simulation results

results are presented in figure 7.21 and 7.22 for naturally aspirated and turbocharged after-cooled operation respectively.

Referring to figure 7.21 and 7.22, it can in general be observed that the simulation pressure and mass burn traces for both naturally aspirated and turbocharged operation closely follow the corresponding experimental traces. Some key observations are consolidated as below;

1. For naturally aspirated operation, the peak pressure is over predicted to the tune of 5% while for turbocharged after-cooled operation, the peak pressure is

Table 7.3: Initial and boundary conditions for naturally aspirated and turbocharged peak load operation quasi dimensional simulation

Parameter	Natural aspiration	Charged aspiration
Load (kWe)	27.3	72.8
Physical ignition timing (deg)	-24	-22
Kernel initialization angle (deg)	-6	-9
Kernel radius at initialization (mm)	8.48	8.50
Terminal burn time (ms)	1.55	2.00
Cycle energy input (kJ)	1.98	4.22

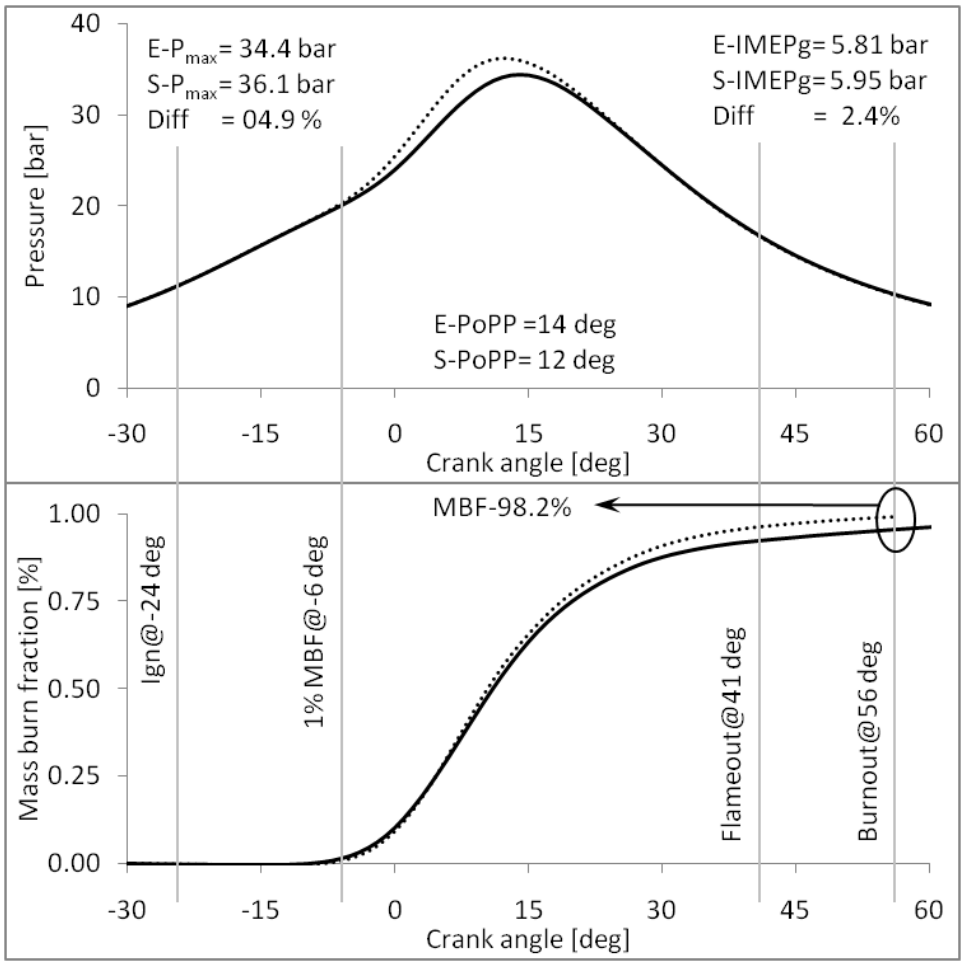

Figure 7.21: Pressure and mass burn fraction against crank angle traces for engine *E*6 under stoichoimetric naturally aspirated operation

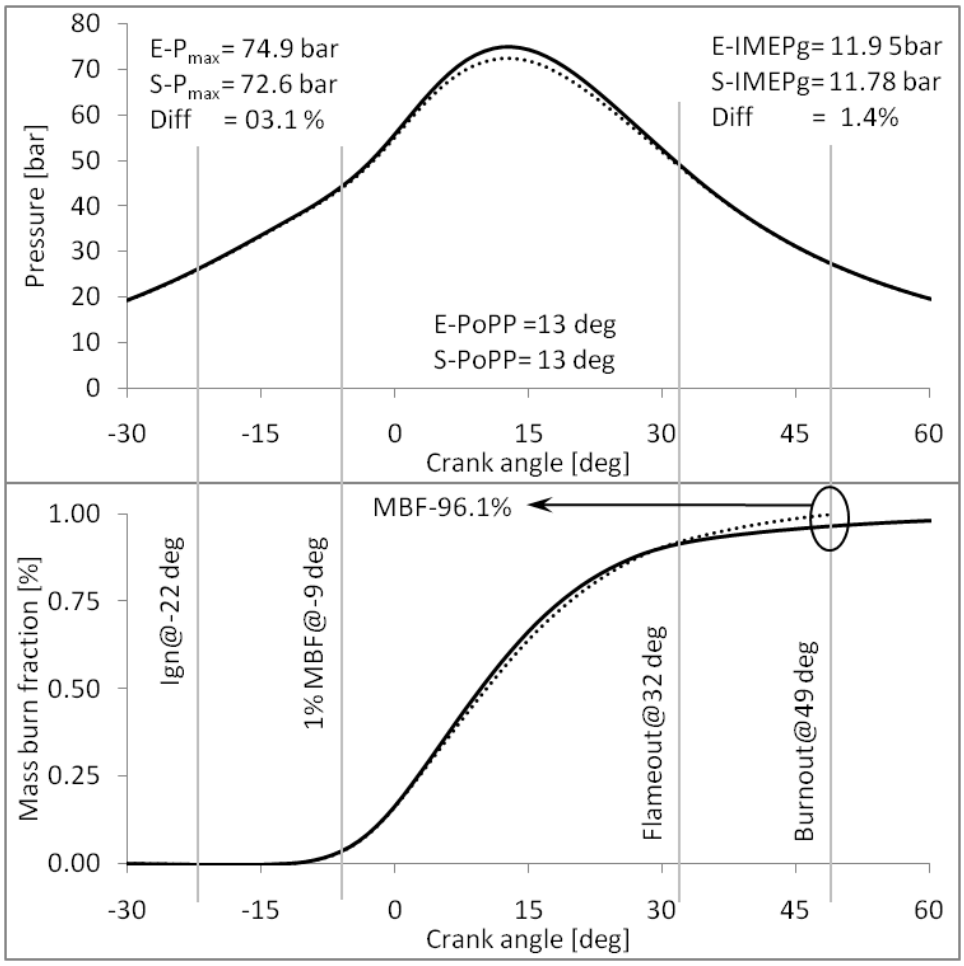

Figure 7.22: Pressure and mass burn fraction against crank angle traces for engine $E6$ under stoichoimetric turbocharged after-cooled operation

under predicted by just over 3% as compared to the corresponding experimental data. The over prediction and under prediction correlates well with the mass burn fraction trace with the naturally aspirated and turbocharged after cooled mass burn fraction trace being positioned slightly advanced and retarded as compared to the corresponding experimental traces respectively. It is important to note that in both the cases, the deviation in the mass burn fraction traces from the experimental traces emerge beyond the 25% mass burn fraction and persist over the quasi steady combustion stage. The fact that the differences are primarily restricted to the quasi steady stage suggest that the differences in the rate of combustion primarily arise due to either the laminar flame speed or turbulent intensity or both.

2. Analyzing the indicated mean effective pressure (included as inset data), it can be observed that the deviation from the experimental data is nominal and is less than half the deviation of the peak cylinder pressure. One of the key contributing factors to the superior indicated mean effective pressure data corresponds to the fact that there is literally no deviation upto the kernel initialization in the engine cylinder and beyond the flame out stage ($A_f = 0$, the deviation is nominal because of the fact that the terminal stage exponential burn time is a measured parameter) and the deviation is restricted primarily to the quasi steady burn stage. In the vicinity of the top dead center, with the change in the cylinder volume per degree crank angle being minimum the contribution to the deviation in the indicated mean effective pressure significantly reduces, hence the close match.

3. Analyzing the flame termination stage, it can be observed that flame out (when $A_f = 0$) for turbocharged operation occurs at 32 deg after the top dead center while it occurs at 41 deg after the top dead center, a full 9 degree advance. This is along expected lines considering the higher turbulent intensity for turbocharged operation as compared to naturally aspirated operation leading to faster flame propagation. Beyond flame out, the measured burn out times for naturally aspirated and turbocharged operation corresponds to 1.55 and 2 milli seconds (14 and 18 deg crank angle absolute) respectively. It is interesting to note that the terminal stage for turbocharged operation is sluggish as compared to naturally aspirated operation. For the considered terminal burn time, the mixture burn out for quasi dimensional simulation corresponds to 98.2 % and 96.1% for naturally aspirated and turbocharged operation respectively.

Sensitivity analysis - Mixture quality

Addressing the sensitivity to mixture quality, simulation results for two mixture qualities of $\phi = 1.3$ (rich operation) and $\phi = 0.9$ (lean operation) are compared with corresponding experimental results as in figure 7.23 (a-p, a-m) and (b-p,b-m) respectively.

It can be observed from figure 7.23 that for the simulation corresponding to $\phi = 1.3$, the difference between the experimental and simulation trace is close to

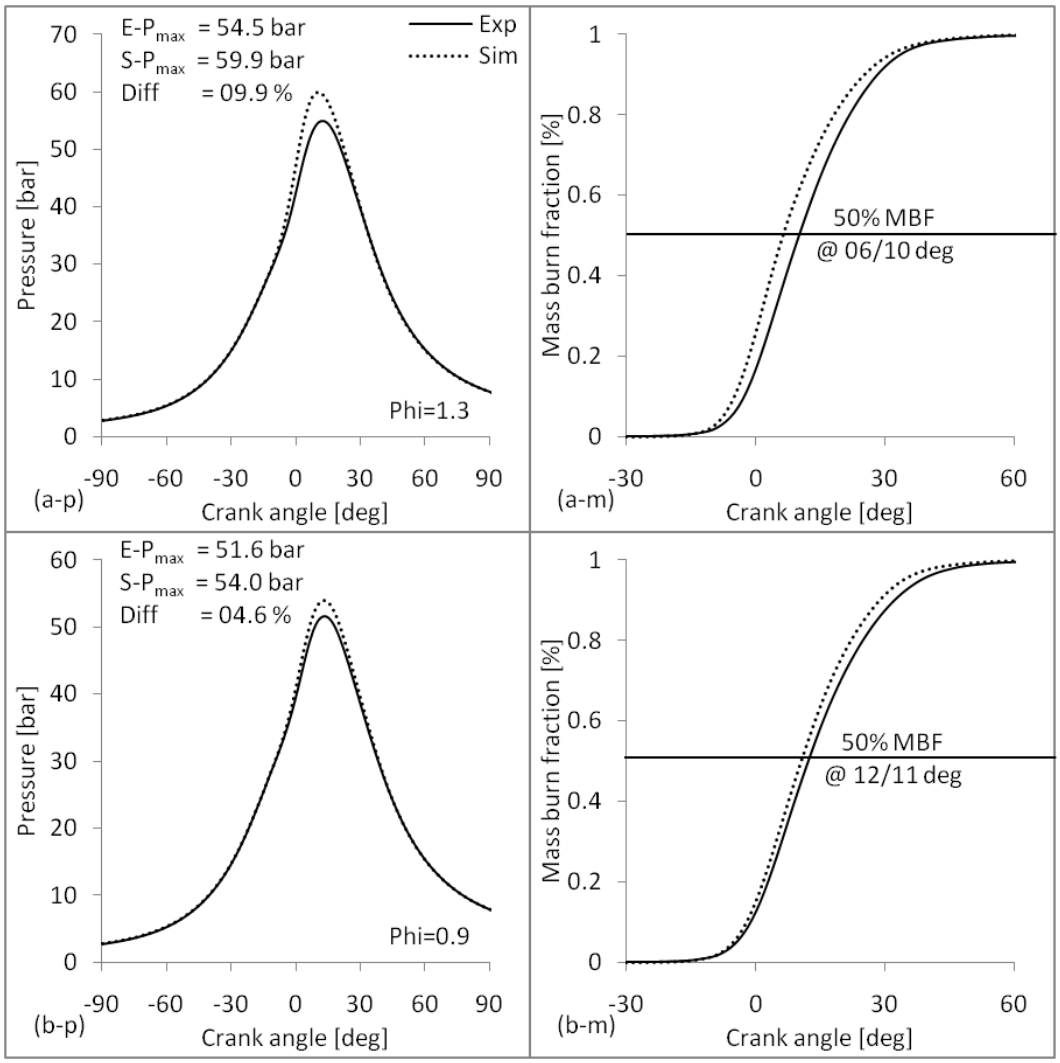

Figure 7.23: Sensitivity of engine simulation to mixture quality

10% while it is less than 5% for the case of $\phi = 0.9$. The differential response is primarily attributed to the laminar flame speed considering that turbulent intensity used is unchanged. A detailed analysis indicates that in the tuning of the laminar flame speed correlation (refer section 6.4) using the CHEMKIN results, the focus has primarily been in the $\phi = 1 \pm 0.1$ regime. In this regime, the difference between the laminar flame speed as estimated by the flame speed correlation and the CHEMKIN data is less than 3%. Beyond this regime, the deviation increases significantly, especially so on the rich side leading to over prediction of the laminar flame speed. With significant increase in the laminar flame speed, the simulation combustion is much faster (4 deg advanced) than the corresponding experimental burn rate (refer figure

7.23 (a-m))

Sensitivity analysis - Ignition angle

Addressing the sensitivity to ignition angle, three cases, two corresponding to retarded ignition (4 and 6 deg from maximum brake torque timing) and one corresponding to advanced ignition (4 deg from maximum brake torque timings) are considered. The results of the ignition timing parametric analysis are consolidated in figure 7.24 (for retarded ignition simulation) and figure 7.25 (for advanced ignition simulation).

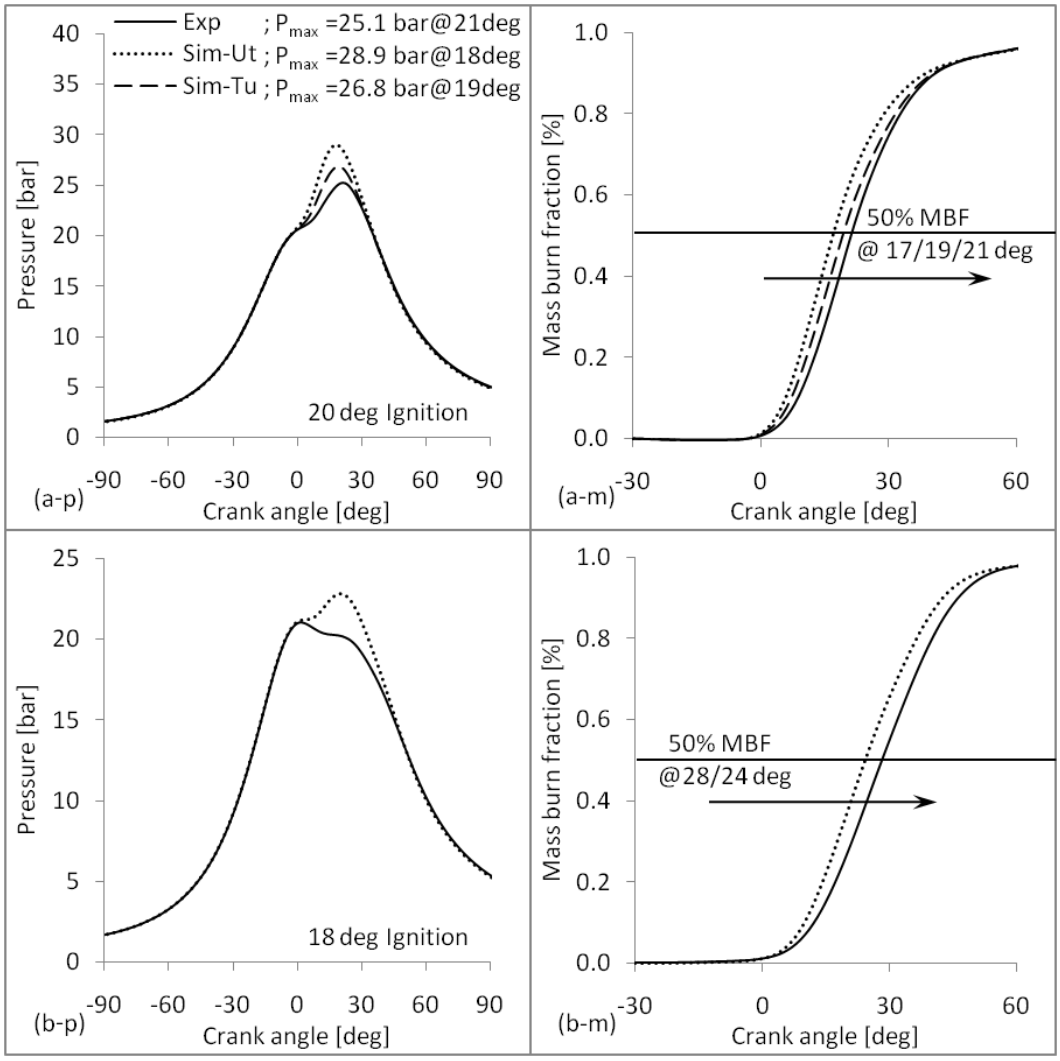

Figure 7.24: Sensitivity of engine simulation to retarded ignition engine operation

Analyzing the results for 4 deg retarded ignition simulation, the pressure trace in the quasi steady region differs significantly from the experimental trace both in terms of the magnitude and position of the peak pressure. While the peak pressure is higher by over 15 %, the position of peak pressure is advanced by 3 deg crank angle. Reviewing the experimental mass burn profile, it is observed that the ignition angle corresponding to 1% mass burn is retarded between 6 and 7 deg. Thus the ignition retard by 4 deg corresponds to advanced combustion, verified by the placement of the mass burn profile, and consequently higher in-cylinder pressure. Tuning the initialization crank angle to the actual crank angle when the 1% mass burn is realized leads to some improvement in the predictions. In the case of 18 deg ignition, even with the flame kernel initialization based on experimental data, the simulation trace difference substantially from the experimental trace as evident from figure 7.24 (b-p) and (b-m). It is important to note that while the experimental trace represents a classic case of partial burning, the simulation fails to capture the same. This is attributed to the absence of any additional governing physics that can terminate the flame propagation depending on the prevailing conditions. In the current simulation model, flame propagation will continue so long as there are no discontinuities in either the laminar flame speed estimation or the turbulent intensity. The only means by which partial burning can occur in the current model is if for the piston to outrun the propagating flame. If that happens then theoretically, the flame surface will continue to have a finite non zero value over the entire expansion stroke. This is an extremely unlikely even considering that during the initial stages of the expansion stroke the turbulent flame speed far outruns the instantaneous piston speed and within few tens of crank angle, the entire mixture is engulfed. Thus, effectively, abnormal combustion in terms of partial burning cannot be handled by the current model.

Analyzing the advanced ignition, it is again observed that advancing the ignition timing by the same magnitude as the physical ignition timing leads to substantial deviation in the pressure trace. Tuning the ignition timing to initialize the flame in the engine cylinder based on experimental traces leads to some improvement but the difference between the experimental and simulation remains higher than 10%. The simulation response for both advanced and retarded ignition is in line with the observations of the sensitivity analysis of the initial and terminal stage parameters

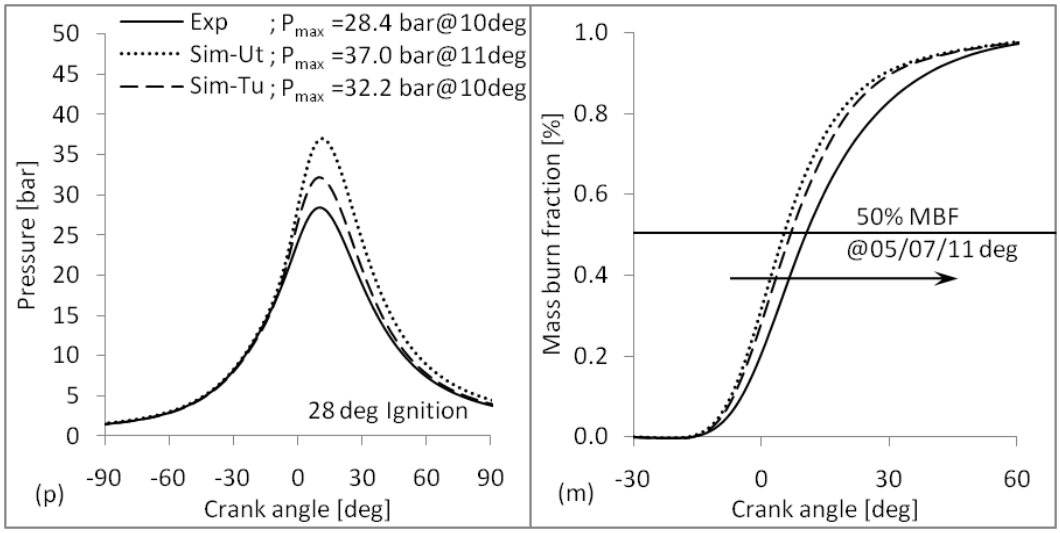

Figure 7.25: Sensitivity of engine simulation to advanced ignition engine operation

(refer section 7.3.4). A simple analysis involving simulation with 2 deg sweep on either side of the maximum brake torque operation indicates the simulation results to be well within the 5% deviation limit if the flame kernel initialization is based on the experimental mass burn fraction analysis. The deviation in excess of 10% when the ignition advance / retard is greater than 4 deg crank angle points to potential influence of the flame propagation on the in-cylinder turbulence, un-burned mixture thermodynamic conditions not accounted for in the simulation tool.

The analysis summarily establishes the need for experimentally measured mass burn fraction traces towards appropriate initialization of the flame kernel.

7.3.5 Simulation results for engine $E4$

The quasi dimensional simulation results addressing two cases corresponding to 25.1 kWe (peak load) and 14.5 kWe (part load) for NG fuelled operation and once case corresponding to 14.5 kWe (peak load) for PG fuelled operation of the engine $E4$ are presented in this section. While the overall approach is similar to that adopted for the simulation of engine $E6$, the correlations for the estimation of laminar flame speed of compressed natural gas and the turbulence parameters are adopted from Ma et al (Ma, Wang, Wang, Liu, Wang, Ding, and Zhao 2008) and Ali et al (Pourkhesalian, Shamekhi, and Salimi 2010). The laminar flame speed and turbulent intensity

correlation are of the form as in equation 7.5 and 7.6 presented below. In equation 7.6 the term ξ has been used as a parameter to be tuned during calibration and has been used so in the current investigation.

$$S_L = 0.36 \left(\frac{T_u}{T_o}\right)^{1.162} \left(\frac{P}{P_o}\right)^{-0.374} \tag{7.5}$$

$$U_T = \xi \left(\frac{2LN}{60}\right) \left(\frac{\rho_u}{\rho_{in}}\right)^{\frac{1}{3}} \tag{7.6}$$

Natural gas fuelled operation

Natural gas fuelled simulation pressure crank angle and mass burn fraction crank angle traces for peak load (25.1 kWe) are consolidated in figure 7.26 a-p and a-m while those for part load (14.5 kWe) operation are consolidated in figure 7.26 b-p and b-m respectively.

In figure 7.26 a-p and a-m, two simulation traces are indicated. One of the traces corresponds to un-tuned turbulence intensity while the other corresponds to tuned turbulence intensity. The simulation trace for part load operation corresponds to tuned turbulence intensity. It is important to note that for under 10% tuning of the turbulence intensity, the simulation pressure trace could be matched with the experimental pressure trace within an error of 3%.

Producer gas fuelled operation

The simulation trace for peak load PG fuelled operation of engine $E4$ is presented in figure 7.27. For this particular simulation, the same value of turbulence intensity tuning parameter as used for NG part load operation is adopted. It can be observed that the the simulation result matches with the experimental trace within an error of 3%.

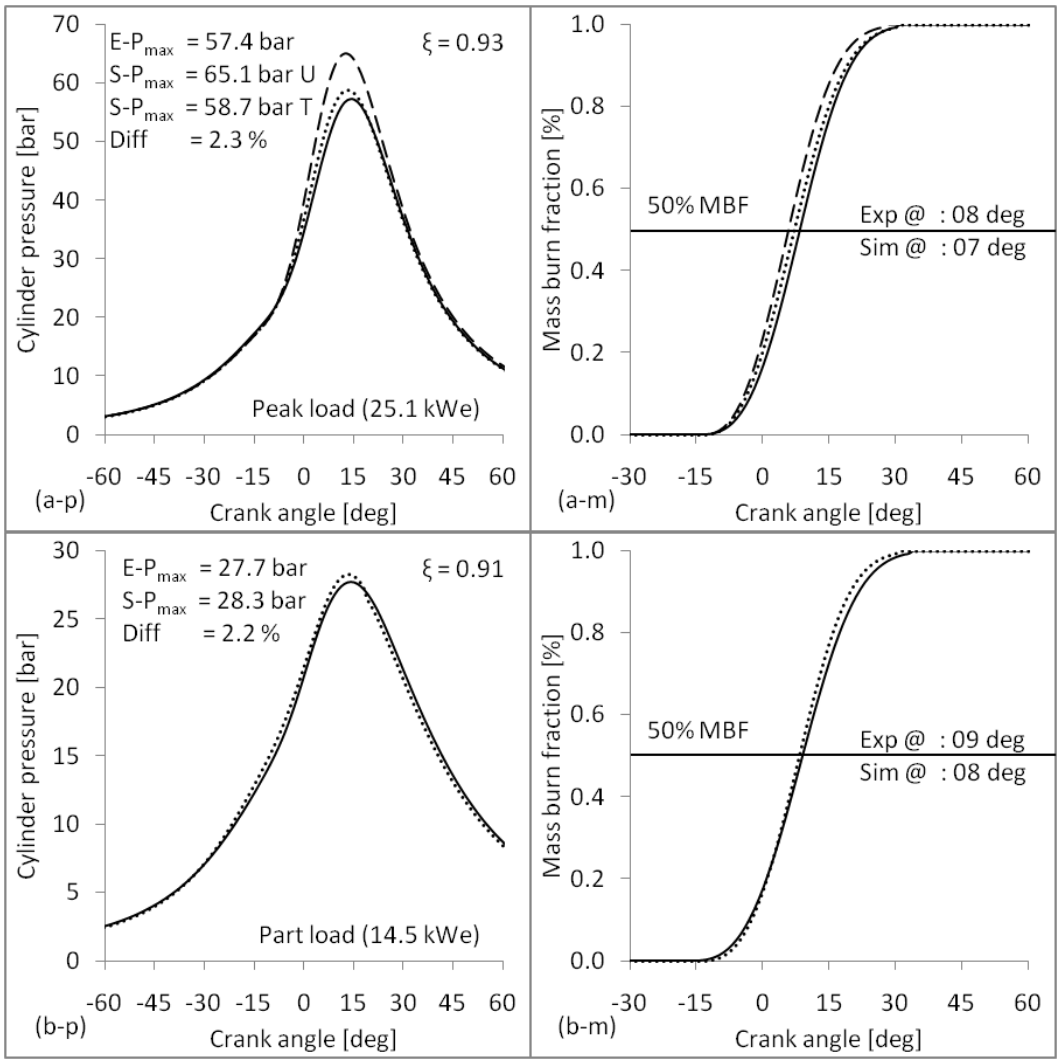

Figure 7.26: Natural gas fuelled quasi dimensional simulation of engine $E4$

Summarizing quasi dimensional simulation for engine $E4$

The quasi dimensional simulation of engine $E4$ operated with both NG and PG has provided results well within the maximum permissible deviation of 5% for key parameters. One of the primary outcome of the quasi dimensional simulation of engine $E4$ pertains to the establishment of the suitability of simple mean piston speed and un-burned density based correlation for estimating the turbulence intensity even for a bowl in piston geometry, albeit with minor tuning of under 10%.

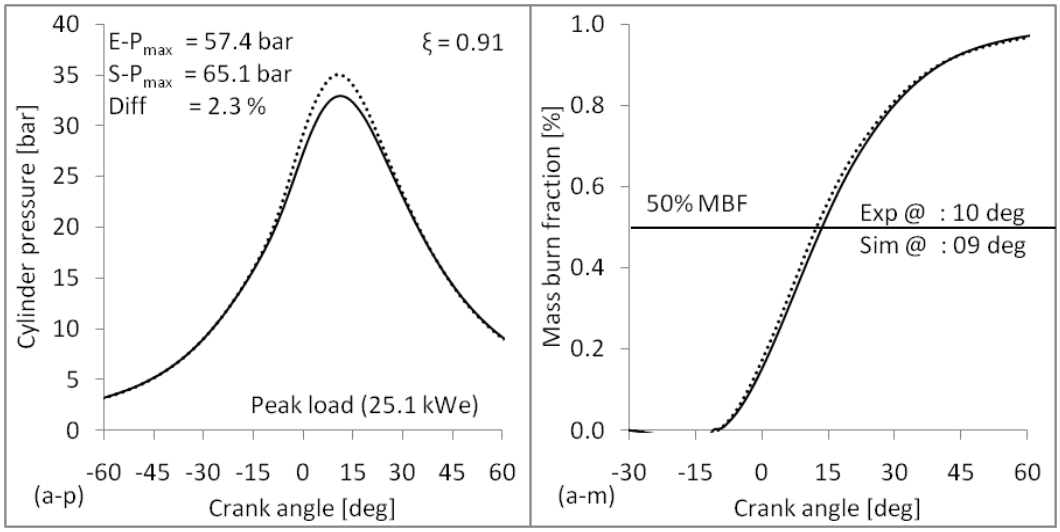

Figure 7.27: Producer gas fuelled quasi dimensional simulation of engine $E4$

7.4 End gas auto-ignition and producer gas knock rating

7.4.1 Analysis and validation of the chemical kinetics module

The basic quasi dimensional model with frozen chemistry for un-burned mixture and equilibrium chemistry for burned gases is limited to handling normal combustion as the un-burned mixture will not auto ignite. Towards enabling auto-ignition of the un-burned mixture, chemical reaction kinetics is invoked in the un-burned mixture as described in section 6.4.1. Incorporation of chemical reaction kinetics ensures sudden release of all the energy associated with the un-burned mixture, representing knock, if the mixture thermodynamic conditions are such that the induction time (time for auto-ignition) at any particular time is lower than the corresponding burnout time.

Prior to the incorporation of the chemical reaction kinetics sub module into the quasi dimensional model, the chemical reaction kinetics formulation and the solution scheme described in section 6.4.1 are to be validated and towards the same, two cases are considered. The first involves the simulation of a constant density isobaric system for temporally evolving the specie concentration and comparing with the profiles generated by CHEMKIN for the same system. The second involves simulation of a homogeneous charge compression ignition (HCCI) engine and comparing the evolution of in-cylinder pressure with literature reported simulation results.

The temporal specie evolution for the constant density isobaric system with initial temperature and pressure of 1200 K and 1.013 bar for a stoichiometric methane air mixture is presented in figure 7.28. In the figure, the continuous lines represent the specie evolution from the model developed in the current study while the dots represent the CHEMKIN results. It can be observed that the specie evolution and the time of fuel structure breakdown from the current model matches very closely with the CHEMKIN results.

Towards validating the chemical kinetics module in an HCCI engine, the results reported by Komninos et al (Komninos, Hountalas, and Rakopoulos 2007) involving numerical simulation of hydrogen fuelled HCCI engine are used as reference. The engine configuration as used by Komninos (bore- 120.65 mm; Stroke- 140 mm; Con-

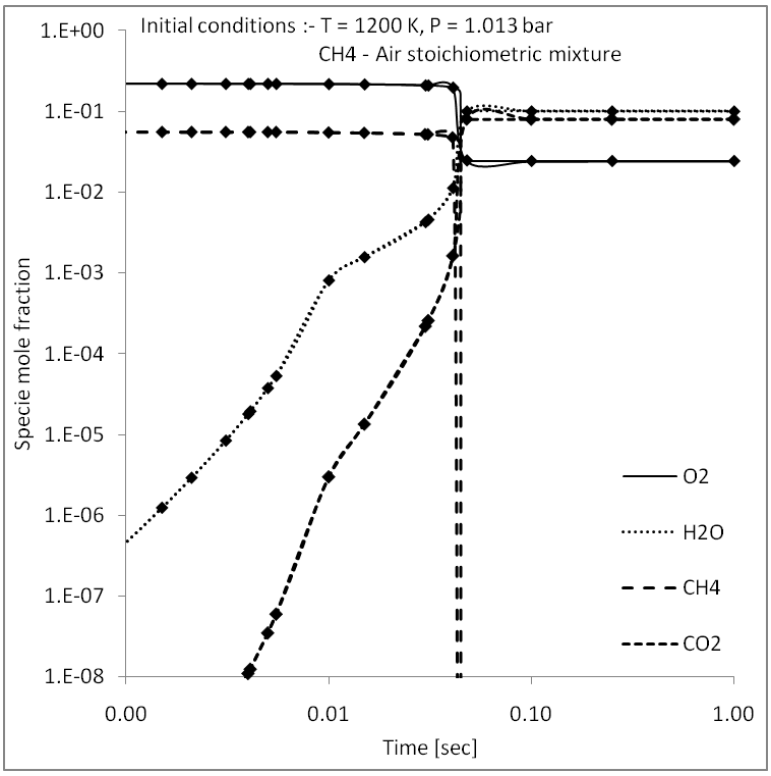

Figure 7.28: Validation of iso-choric system specie concentration evolution

necting rod- 260 mm; Speed- 2000 rpm) are used in the simulation. The simulation results for parametric variation of operating equivalence ratio and compression ratio are compared with literature reported values as in figure 7.29 (a) and (b) respectively. In the figure, the continuous lines represent the results from the developed HCCI engine model while the dots represent the results from the literature. For brevity, the reference results are reported for a single compression ratio and a single equivalence ratio respectively. The results as in figure 7.29 explicitly validate the chemical kinetics module coupled with the engine simulation sub modules.

7.4.2 Chemical kinetics module integration and auto-ignition prediction

Having validated the chemical kinetics sub-module for a constant density isobaric model and a homogeneous charge compression ignition engine case, chemical kinetics is invoked in the un-burned region of the quasi dimensional model for the engine

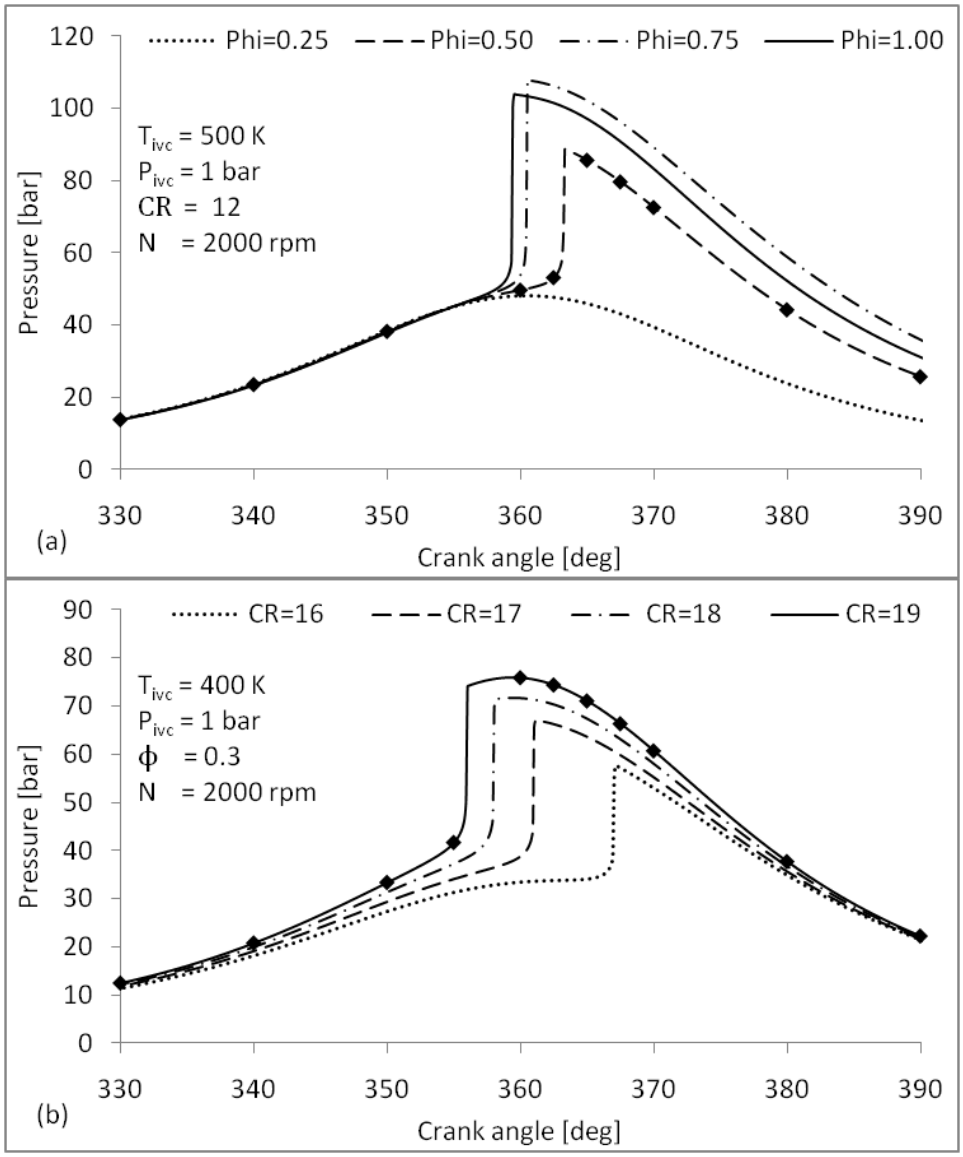

Figure 7.29: Hydrogen fuelled HCCI engine simulation

E6 while retaining equilibrium chemistry in the burned region. Coupling the chemical kinetics module with the quasi dimensional model enables identifying the limiting intake manifold conditions (in terms of temperature, pressure, mixture quality etc) under which the engine could knock. The upgraded quasi dimensional model is tested for its ability to predict end gas auto-ignition by means of parametric variation of manifold mixture temperature. Precise control over the temperature is exercised by forcing the desired temperature for the intake manifold throughout the suction segment of the gas exchange process. The baseline data for validating knock simula-

tion through parametric variation of temperature in the upgraded quasi dimensional model is generated through explicit control of the intake manifold mixture temperature in the turbocharged mode operation of engine $E6$ during experimental investigations. The manifold mixture temperature is controlled by controlling the cooling water flow rate through the after cooler. The after-cooler is required for cooling the mixture issuing out of the compressor which is at significantly higher temperature (at peak load, compressor exit temperature is 140 ^0C corresponding to pressure ratio of 2.30).

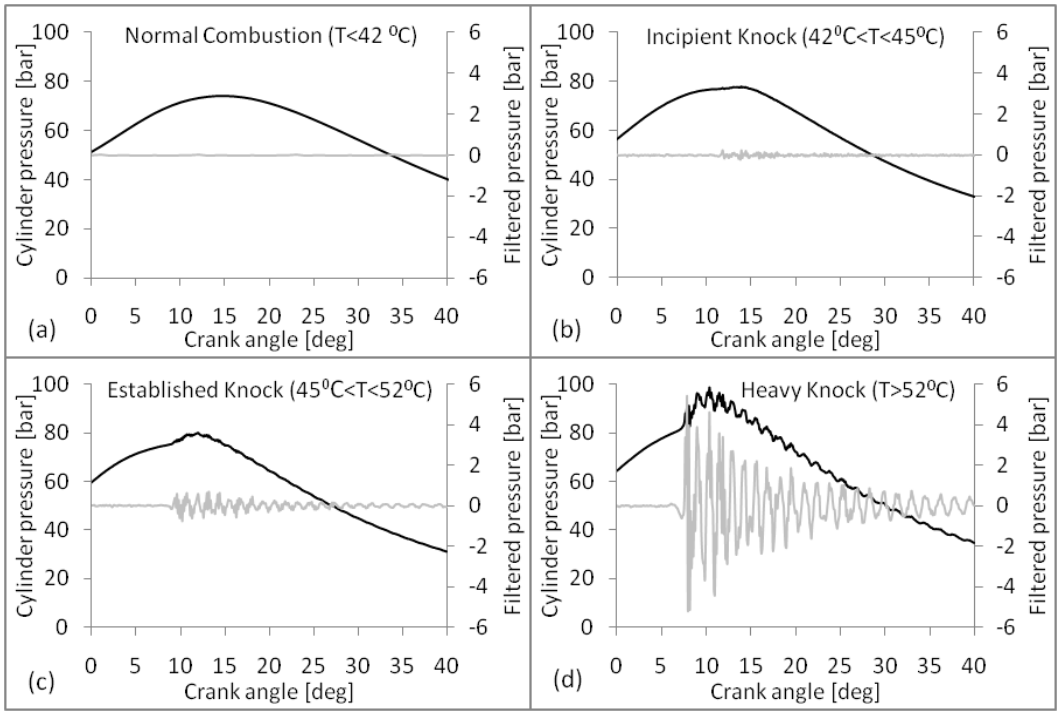

Figure 7.30: Nature of combustion at various mixture inlet temperatures

The nature of combustion in the cylinder in terms of the absolute cylinder pressure trace and the low frequency filtered pressure trace, at peak load of 72.8 kWe at different mixture inlet temperatures is shown in figure 7.30. The mixture temperature at peak load under normal operating conditions is at 41 $\pm$ 1 ^0C. As the mixture temperature in the inlet manifold is increased beyond 42 ^0C upto about 45 ^0C, some small pressure disturbances occurring only intermittently are evident on the pressure trace as indicated in figure 7.30 b. Between 45 ^0C and 52 ^0C well established knock

can be observed as indicated in figure 7.30 c and the frequency of occurring is more than 50 % in acquisition of 250 consecutive cycles. At mixture temperatures beyond 52 ^0C, heavy knocking is observed as indicated in figure 7.30 d and the distinct ringing noise indicative of heavy knock is also audible.

While the foregone discussion established the possibility of initiating knock in the engine through explicit control of mixture temperature, of utility for the current investigation is the temperature at which incipient knock is observed at different loads considering that the model is essentially limited to prediction of end gas auto-ignition occurrence but not the intensity. Towards the same, auto-ignition in the engine is initiated by controlling the temperature at three loads of 50 kWe, 60 kWe and 70 kWe. The manifold thermodynamic conditions and the crank angle band within which knock is observed for the three loads is indicated in table 7.4 below.

Table 7.4: Thermodynamic conditions and knocking crank angle band at various loads

	Manifold conditions		
Load	Pressure (bar)	Temperature (K)	Knock angle (deg aTDC)
50 kWe	1.47	331 ± 2	13 ± 5
60 kWe	1.71	324 ± 2	12 ± 3
70 kWe	1.80	317 ± 2	10 ± 5

It is important to note that end gas auto-ignition is a highly random phenomenon and the crank angle at which the mixture auto-ignited and intensity vary significantly for the same manifold conditions. The variation of angle at auto-ignition for two consecutive cycles for the same operating condition is indicated in figure 7.31. As such, in experimental analysis of end gas auto-ignition, for a particular manifold thermodynamic condition, a range of crank angle within which the end gas can auto-ignite must be specified (as in table 7.4) rather than a single knock occurring crank angle.

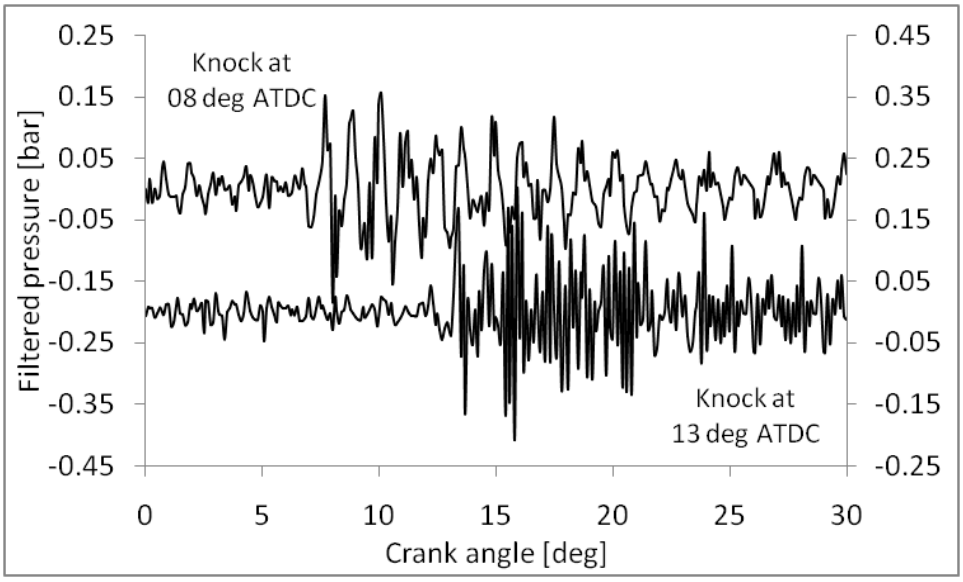

Figure 7.31: Consecutive auto-ignition pressure traces at same manifold conditions

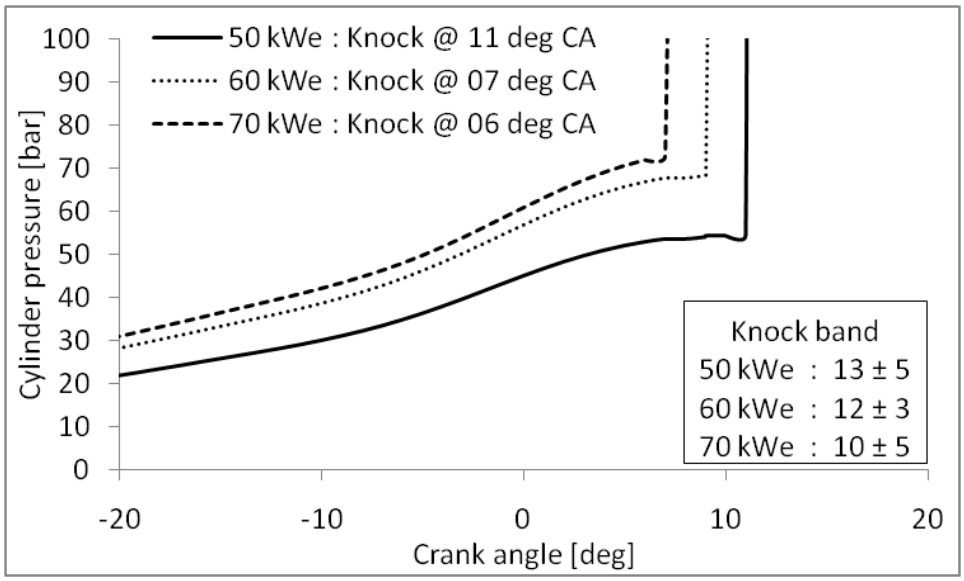

Figure 7.32: Auto ignition pressure traces from the upgraded quasi dimensional knock simulation model

Based on the manifold conditions corresponding to the data consolidated in table 7.4 in the upgraded quasi dimensional model, while knock has been observed for all the three cases, the crank angle at which knock occurs is advanced (positioned

closer to the top dead center) by varying degrees. The pressure crank angle traces corresponding to simulations with the upgraded quasi dimensional model for the three operating conditions consolidated in table 7.4 are presented in figure 7.32.

Advanced phasing of knocking crank angle essentially means a greater mass of the mixture is auto-igniting as compared to the experimental knock condition. In a broader sense, based on the above results it could be interpreted that the experimental thermal limiting conditions represented in table 7.4 need not necessarily be the limiting conditions for the simulation cycles. Towards evaluating the same, the manifold temperature in the upgraded quasi dimensional model is reduced below the experimental limiting conditions till the numerical limiting conditions are reached (below which no end gas auto ignition is observed). The results of thermal limiting analysis is as presented in table below.

Table 7.5: Numerical and experimental thermal limiting conditions for end gas auto ignition at various loads

Load	Pressure	Temperature-K		Knock angle-deg		MBF
kWe	bar	Exp	Sim	Exp	Sim	(%)
50	1.47	331 ± 2	320	13 ± 5	32	92
60	1.71	324 ± 2	317	12 ± 3	31	92
70	1.80	317 ± 2	312	10 ± 5	27	89

One of the key features of the above analysis pertains to the difference in the limiting manifold temperature between the experimental and simulation results and the knock occurring crank angle. While the difference in the limiting manifold temperature is between 5 to 10 K, the difference in crank angle at which incipient knock is observed (about 18 deg crank angle) is much more severe. The observed differences are primarily attributed to the limitation of using single point acquisition based pressure traces as used in the current investigation (centrally mounted spark plug adapted pressure sensor). The sensor can detect the high frequency components (due to knock) provided the pressure fluctuations percolate to the vicinity of the spark plug. With a reduction in the total mass of the un-burned mixture participating in the end gas auto-ignition (delayed auto-ignition) the pressure fluctuations may not

be intense enough for the pressure sensor to pick up the high frequency components. As such, a knocking cycle may pass off as normal combustion. With the philosophy of knock detection being entirely different for the quasi dimensional model, any auto-ignition before the burnout (volume of un-burned mixture reaching zero) gets recorded, hence the observed result of lower thermal limit with a consequential effect of retarded knocking crank angle for quasi dimensional simulations.

Having validated the knock prediction ability of the upgraded model based on load and manifold temperature parametric variation, the upgraded quasi dimensional analysis is extended to evaluate a particular case reported in literature where high pressure rise rates (first derivative of the cylinder pressure trace) without any high frequency pressure fluctuations were reported terming the operation knock free. The details are as described below.

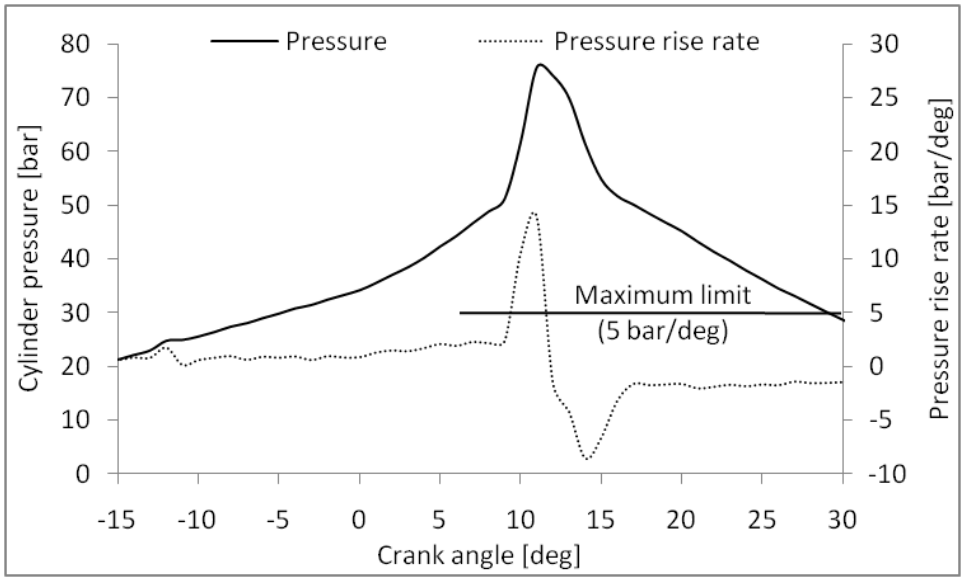

Figure 7.33: Pressure and pressure rise rate variation for RB33 at compression ratio of 17

In the operation of a three cylinder diesel engine converted for PG fuelled operation, Sridhar (Rao 2003) has reported the pressure crank angle trace at compression ratio 17.0 as in figure 7.33. Reviewing the data in figure 7.33, it can be observed that the pressure crank angle trace does not indicate any knock like characteristics (high frequency fluctuations as in figure 7.30) but the pressure rise rate exceeds 10

bar/deg. A review of literature suggests the permissible peak pressure rise rate to be limited to 5 bar/deg (Taylor 1985). In general it has been observed that such high pressure rise rates are realized only when the end gas auto-ignites.

Considering that the pressure rise rate suggests potential end gas auto-ignition, the validated quasi dimensional model is used for the three cylinder engine geometry. The estimation and validation of the turbulence parameters is along the approach adopted in the simulation of engine $E4$ (refer section 7.3.5). Some of the model input parameters suggested by Sridhar (Rao 2003) (wherever applicable) are used for the simulation (Compressoin ratio of 17, residual gas fraction of 6.5%, ignition angle 12 deg before the top dead center, ignition delay - kernel initialization angle for thw current work 6 deg crank angle from the physical ignition). The result of the upgraded quasi dimensional simulation is compared with the experimental trace as in figure 7.34.

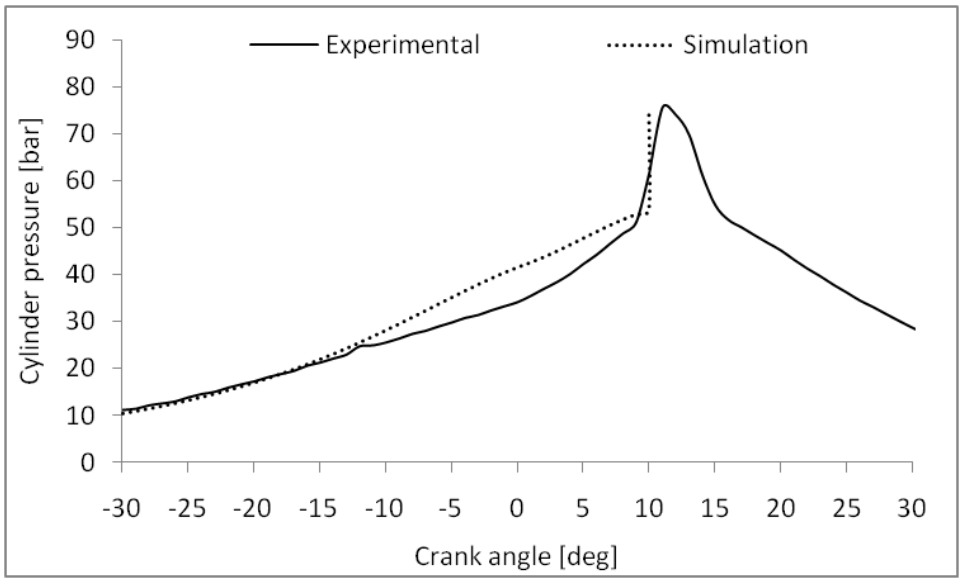

Figure 7.34: Quasi dimensional simulation for the RB33 engine

It can be observed that, along the lines indicated by the pressure rise rates, the quasi dimensional model indeed indicates end gas auto-ignition for the considered operating conditions while Sridhar (Rao 2003) has claimed the operation to be normal. Further, Sridhar (Rao 2003) also reports normal combustion in a quasi dimensional simulation model for the same operating conditions. It is important to note that,

the interpretation of knock free operation based on the experimental pressure trace could be primarily attributed to the limitation of the on the instrumentation resolution which has failed to pick up the high frequency components. In so far as the quasi dimensional model reported by Sridhar is concerned, with frozen chemistry consideration for the un-burned mixture the model is limited to prediction of normal combustion.

7.4.3 Knock rating estimation for producer gas

Having validated the upgraded quasi dimensional model for abnormal combustion, the auto-ignition capability of the model is used towards estimating the knock rating of PG (standard composition). The knock rating of PG is sought to be quantified in terms of motoring Methane number, the de facto standard for gaseous fuels (LEIKER, K, W, Pfeifer, and Rankl 1972) (Ryan, Callahan, and King 1993) (Callahan, Ryan III, Buckingham, Kakockzi, and Sorge 1996) along the lines of Octane number for liquid fuels (Heywood 1988) (Douaud and Eyzat 1978). The motoring methane number so estimated for PG is verified against experimental data reported by Olsen et al (Malenshek and Olsen 2009) (Arunachalam and Olsen 2012) (Wise, Olsen, and Kim 2013). Towards estimating the Methane number for PG, the validated quasi dimensional model is adopted for a Waukesha cooperative fuels research (CFR) engine of specifications (Company 2015) as mentioned in table 7.6.

The general procedure adopted for estimation of motoring Methane number using CFR engines with specifics reported by Olsen et al (Malenshek and Olsen 2009) is briefly discussed and is adopted for the numerical studies.

Experimental estimation of motoring Methane number basically involves operating a CFR engine at the prescribed operating conditions (refer (Company 2015) for Waukesha specifications). Fuelling the CFR engine with the test fuel, the engine operation is initiated with a low CR and keeping all other conditions same, the CR is gradually increased till (incipient) knock is detected on the engine. The CR at which the engine knocks is described as the *critical* CR and the corresponding knock intensity (in terms of suitable number) is recorded as a reference. Continuing with the engine operation at the critical CR, the test fuel is replaced with pure methane. If no knock is detected then pure methane is replaced with a mixture of methane

Table 7.6: Specifications of Waukesha CFR (F2) engine

Geometric specifications	
Bore	82.55 mm
Stroke	114.3 mm
Con rod length	112.7 mm
CR Range	4:1 - 18:1
Chamber	Flat piston and head
MON operational specifications	
Speed	900 rpm
Intake temperature	310.9 K
Ignition angle	15 deg bTDC

and hydrogen, the latter being used as a knock inducer. The fraction of hydrogen is increased in the mixture to reproduce knock of the same intensity as observed with the test fuel. The hydrogen volume fraction in methane - hydrogen mixture at which knock similar to the test fuel is replicated is the methane number for the test fuel. In the event that the engine knocks for pure methane, then methane is replaced with a mixture of methane and carbon dioxide, the latter being used as knock inhibitor. The fraction of carbon dioxide is increased in the mixture to reproduce knock of the same intensity as observed with the test fuel. The volume fraction of carbon dioxide in the mixture + 100 is then the methane number for the test fuel. If the methane number is greater than 100 then the test fuel has anti knock characteristics superior to methane else the knock resistance is poor.

The above procedure is used towards establishing the critical compression ratio and knock rating of producer gas using the validated quasi dimensional model. Prior to the discussion of knock rating analysis results, some aspects related to the laminar flame speed and turbulent parameters as required by the EELB model relevant for simulating the CFR engine are discussed as below;

1. Geometric / Kinematic parameters : The parameters described in table 7.6 form the basic geometric / kinematic input to the engine model.

2. Laminar flame speed : While the laminar flame speed correlations for PG (fuel specific coefficients) are established (equations 6.34 and 6.35), since the CFR analysis requires fuelling the engine with different composition mixtures involving methane-hydrogen-carbon dioxide, coefficients for the laminar flame speed correlation coefficients (simple correlation without dependencies on equivalence ratio and residual gas fraction) are estimated for 16 different gas compositions starting with the most reactive mixture of $75\%CH_4$ - $25\%H_2$ to least reactive mixture of $50\%CH_4$ - $50\%CO_2$ with the specie volume fraction changing by 5%. The estimation is again based on the tabulated laminar flame speed data using the PREMIX module of CHEMKIN. For all the cases, a residual gas fraction of 5% has been considered.

3. The turbulent parameter are estimated using the density ratio based correlations proposed by Keck and are scaled to ensure a close match with literature reported mass burn fraction. The parameter being density based are responsive to the change in compression ratio.

4. The terminal stage burn time is estimated to get the best fit with the literature reported mass burn fraction.

Having established the necessary parameters, as described, the turbulence intensity is scaled to ensure the evolution of appropriate mass burn profile for the engine geometry considered (similar to the approach adopted for simulation of engine $E4$; refer section 7.3.5). The mass burn profile reported by Bayraktar (Bayraktar 2003) for the Waukesha CFR engine is used as the reference and the turbulent intensity scaled to evolve a close match with the mass burn profile. Along with the scaling of the turbulent intensity, the terminal stage combustion duration is also tuned to evolve a best fit profile. The literature reported mass burn profile is compared with the tuned simulation result as in figure 7.35 (a) while the corresponding simulation pressure profile is indicated in figure 7.35 (b) (no pressure profile was available in the literature). The operating conditions and tuning parameters are indicated as inset data.

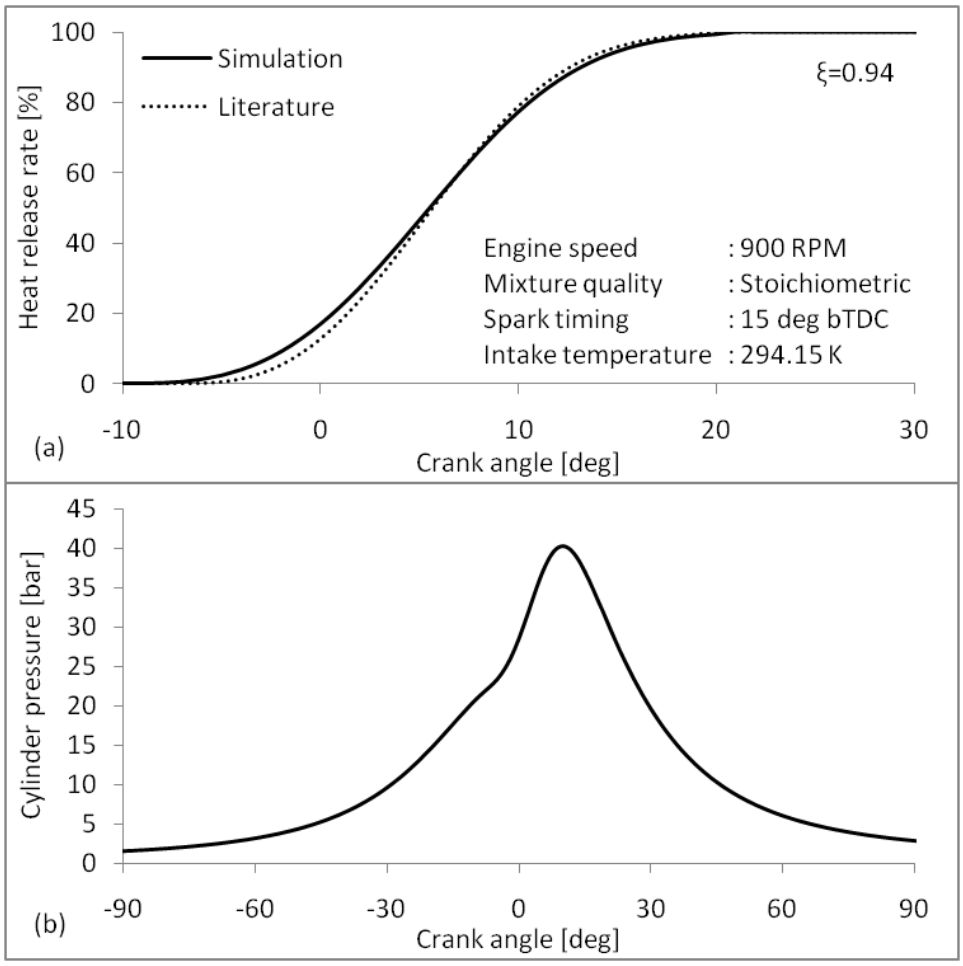

Figure 7.35: Mass burn and pressure crank angle profiles for Waukesha CFR engine

The turbulent intensity scaling factor and the terminal stage combustion duration tuned for the particular operating condition as indicated in figure 7.35 are used for all other operating conditions. In so far as the turbulent intensity is concerned, the validity of such a consideration has already been established in the simulation of engine $E4$ (section 7.3.5 and image 7.26) wherein the change in the scaling factor for a change in load of over 40% was nominal. On the terminal stage combustion duration, while the choice of duration is flexible for normal combustion (refer section 7.3.4) the same argument cannot be carried forward to the simulation of abnormal combustion considering that occurrence of a specific event is being evaluated. To avoid the uncertainty associated with the assessment of knock occurrence due to consideration of a single terminal stage combustion duration, knock is considered

only if it occurs before the flame out crank angle ($A_f < 0$). If the flame out occurs before the knock event the combustion is qualified as normal and the process is terminated (as the normal operation is of no interest in the current analysis). This consideration ensures that knock assessment does not spill over into the burn out zone and the terminal stage combustion duration is only of nominal interest towards validating the complete burn profile. It is important to note that such a strategy is also adopted in experimental investigations albeit in a different sense to render the results neutral of parameters of interest. Olsen et al (Malenshek and Olsen 2009) in the knock rating analysis for syngas adjust the mixture quality to realize a predefined knock intensity across all tests, be it with test fuel or the reference mixtures, thereby rendering the results mixture quality neutral.

Based on the discussed methodology, the validated quasi dimensional model is used in CR parametric analysis and as a test case, methane is used as the fuel. The analysis indicates 13.5 as the critical CR for methane. Reviewing the literature, experimental critical CR has been reported at 14.4 (Ryan, Callahan, and King 1993) (Malenshek and Olsen 2009). It is important to note the since noise based methods and even average cylinder pressure based methods cannot detect knock below a particular threshold, it is obvious that end gas auto-ignition would have occurred at a much lower compression. Thus, a difference of unit compression ratio between the experimentally reported and simulation compression ratio is well within acceptable limits. Extending the analysis to PG fuelled operation, the critical CR is at 15. The critical CR being higher than that for methane is consistent with the thermo-physical properties of PG, especially the higher laminar flame speed. The literature reported critical CR is however reported at 13.2, close to 2 units lower than simulation critical CR. Assessing the motoring methane number through composition parametric variation of methane-hydrogen-carbon dioxide mixture, the mixture corresponding to 90% methane and 10% carbon dioxide knocks just ahead of the flame out crank angle. The motoring methane number for producer gas is thus assigned the value of 110 as against the literature reported motoring methane number of 125.7.

It is important to note that, while the simulation based knock rating results indicate some deviation with the experimental results, not entirely unexpected considering the impracticality of accounting and accommodating all the experimental

operating conditions and influence of turbulence, the simulation results in themselves are consistent with the fuel thermo-chemistry. As such, considering the uncertainties associated with the numerical simulation tool, the utility of the validated quasi dimensional simulation tool for the estimation of fuel knock rating is well established.

Chapter 8

Conclusions and future Work

8.1 Conclusions

The current research has addressed the influence of variations in the thermo-physical properties of bio-derived gaseous fuel, producer gas, on the performance of a natural gas spark ignited engine. The investigation has focused both on experiments involving response characterization (through energy balance studies and thermo-kinematic response analysis) and numerical studies involving zero and quasi dimensional models. The key findings of the current work are summarized in this chapter with highlights of outcome from each chapter followed by an overall summary of the key contributions.

The first chapter has introduced the reader to the broad objective of the reported work by addressing the three fundamental questions of *WHAT*, *WHY* and *HOW* pertaining to the current work. Experimental and numerical investigations to holistically quantify the operational performance of conventional fuel gas engine (natural gas) with producer gas, a bio-derived alternative fuel and diagnostic interventions (if required and feasible) has been identified as the core theme of the current work. The need for such an intervention has been established based on the (a) assessment of the prevailing energy and environmental scenario which dictates a transition from fossilized to bio-derived alternative fuels and (b) review of literature which indicates limited exploration of producer gas fuelled engine operation. The near total absence of literature along the **evaluate-diagnose-optimize** ap-

proach in addressing operation of conventional fuel engines with alternative fuels in general and producer gas in particular is the underlying motivation for the current work. Based on a broad review of literature covering a range of engines and fuels, in-cylinder thermo-kinematic response characterization and engine energy balance assessment have been identified as the key experimental investigation strategies and zero and quasi dimensional analysis (under the broad ambit of thermodynamic simulation) have been identified as the key numerical investigation strategies towards the indicated performance analysis.

The second chapter has reported on the quantification of producer gas/syngas and corresponding stoichiometric mixture thermo-physical properties and the potential influence on engine operational performance. Comparing the thermo-physical properties of stoichiometric fuel air mixture for producer gas with those of natural gas/gasoline, it is reported that while the calorific value is lower by 21%, the thermal conductivity and diffusivity are higher by 160%. The reduced lower calorific value of the fuel is shown to have an explicit influence while higher thermal conductivity and diffusivity are reported to implicitly influence the peak supported load through enhanced cooling of the unburned mixture. Similarly, the adiabatic flame temperature has been reported to be lower by about 300 K. Extending the analysis to flame speed related properties, the inability of the one dimensional double infinity domain flame speed codes to accurately estimate the laminar flame speed of producer gas has been established based on comparison of experimental and numerical results. The quantification of fuel thermo-physical properties and assessment of the potential influence on the engine performance is the contribution of this chapter.

Apparatus, equipment used and procedure adopted in the experimental investigations have been presented in Chapter three. The general technical specifications along with details corresponding to adoption of the baseline natural gas engine(s) for producer gas/syngas operation has been described. Three multi-cylinder baseline diesel engines available as adopted natural gas engines (a six cylinder engine – E6, a four cylinder engine – E4 and a two cylinder engine – E2) have been used for the investigation. While producer gas fuelled performance characterization remains the core theme, four different syngas compositions with varying hydrogen fraction have been used to explicitly address the stated influence of hydrogen. The specifications

and operating principle of various instruments used in the investigation have also been described with special emphasis on the in-cylinder data acquisition system covering the spark-plug adapted pressure sensor and the crank angle encoder along with the support infrastructure. Finally, the general procedure adopted for evaluating each of the three engines considered has been described.

In Chapter four, the qualitative analysis of the influence of fuel thermo-physical properties on the engine operational performance, particularly the peak supported load, has been formally quantified through energy conservation based thermodynamic expressions for naturally aspirated and turbocharged after cooled modes. Towards validating the developed expression(s), baseline diesel and natural gas power rating of the engines considered for experimental investigation have been evaluated and compared with standard specification. The estimated power rating has been reported to be within 6% of the specifications, validating the developed expression. Based on the developed expressions and the correction factors, power de-rating in the range of 45 ± 5 % for producer gas operation over the corresponding natural gas rating has been reported. The magnitudes of the constituent parameters of the power rating expression provide the benchmark data towards comparative analysis of the operational performance of the engines, permitting diagnostic intervention (if required) and is the key contribution of the chapter.

Chapter five presents the results of the experimental investigation. The engine E6 supports a peak load of 35.6 kWe under turbocharged mode of operation as against the estimated load of 69.4 kWe at the maximum brake torque timing of 22 deg before the top dead centre. Based on turbocharger matching analysis, adoption of a smaller turbine has enabled realization of peak supported load of 72.8 kWe, surpassing the estimated load of 69.4 kWe by 3.4 kWe. Peak load performance analysis indicates a gas to electricity efficiency of 29 % and biomass to electricity efficiency of 23 % corresponding to specific biomass consumption of 1.00 ± 0.05 kg/kWh and specific energy consumption of 12.4 ± 0.6 MJ/kWh. Analysing the energy balance, cooling load of 33 %, higher by 6% to 8% as compared to typical conventional fuel operational cooling loads has been observed and has been attributed to the presence of hydrogen as argued in the assessment of the thermo-physical properties. Thermodynamic analysis of the turbocharger indicates compressor efficiency of 73% as against 74%

estimated from the compressor maps while 88% turbocharger mechanical efficiency is realized.

Comparative analysis of in-cylinder apparent heat release profiles has indicated significant deviations between the profiles for producer gas and conventional high calorific fuels. Quantifying and comparing the combustion duration(s) indicates shorter flame kernel development and fast burn phases but close to double terminal stage duration for producer gas as compared to conventional fuels. The observed behaviour is attributed to the presence of hydrogen. This aspect has been explicitly verified based on syngas hydrogen fraction parametric variation wherein for gas (mixture) hydrogen volumetric fraction increase from 12.8% (7.1%) to 37.2% (14.2%), while the initial and fast burn durations reduce from 14.9% and 59.6% to 8.5% and 42.6% respectively, the terminal stage duration increases from 25.5% to 48.9%. Independent analysis to address the response on the three regimes has been reported. The reduction in initial stage combustion duration has been attributed to the significantly excess ignition energy being dumped by the spark plug (designed for natural gas) while the threshold requirement reduces with the addition of hydrogen leading strengthening of the flame kernel and enabling faster growth. The reduced duration for the quasi steady stage has been attributed to hydrogen enhancing the laminar burning velocity, a fundamental dictating property in the turbulent burning of the in-cylinder mixture. The sluggishness of the terminal stage has been primarily attributed to the enhanced cooling of the end mixture (corresponding to mass burn fraction greater than 90%) mostly concentrated near the walls within the thermal boundary layers due to the enhanced thermal conductivity / diffusivity. Extending the analysis to combustion descriptors, significant influence on pressure based descriptors and relatively mild influence on the cumulative heat release and mass burn based profiles has been observed. The combustion descriptors based analysis has been extended to abnormal combustion to assess the behaviour of the thermo-kinematic response under incipient, established and heavy knock operating conditions. Extending the investigations to transient response characterization, superior response quality for producer gas over natural gas has been observed.

Comprehensive experimental performance analysis of producer gas fuelled operation, quantification of the influence of fuel thermo-physical properties on in-cylinder

response and off cylinder components and explicit verification of the role of hydrogen in unfavourably altering the engine energy balance are the key contributions of the current chapter.

The sixth and seventh chapters primarily address the rationale behind the choice of the thermodynamic models for numerical simulation, aspects related to model formulation and the results of numerical simulations. The numerical models have been based on the principle of conservation of energy in the rate form of first law of thermodynamics with one complete cycle segregated partially as an open system and as a closed system. In-cylinder heat release has been modelled along the empirical, cumulative distribution type Wiebe function for zero dimensional modelling and along the Eddy Entrainment and Laminar Burn-up concept for quasi dimensional modelling. Preliminary zero dimensional numerical simulation while establishing the suitability of conventional Wiebe coefficients of shape factor 2 and efficiency factor 5 have explicitly established the need for producer gas specific coefficients. The superiority of fuel specific coefficients (shape factor of 0.71 and efficiency factor of 2.23), arrived at based on curve fit and exhaust analysis, has also been established based on load sensitivity analysis and by validating the in-cylinder geometry independent nature. Extending the analysis to quasi dimensional models, simulations have been reported for flame speed ratio value ranges of 4 to 5 for naturally aspirated mode of operation with turbulent Reynolds number of 2500 ± 250 and 8 to 10 for turbocharged after-cooled mode of operation with turbulent Reynolds number of 5250 ± 250 which completely encompass the fluid and thermodynamic effects. Quasi dimensional model prediction for naturally aspirated and turbocharged mode of operation including parametric variation for a range of loads, ignition timing, operating equivalence ratio have been found in agreement with the experimental results within the required level of accuracy. Comparative analysis based on the mass burn/heat release profiles and the gross indicated mean effective pressure has established the robustness of the developed model. The developed quasi dimensional model has been extended to predict end gas auto-ignition by invoking reaction kinetics in the unburned mixture region and a specific cooperative fuels research engine model has been implemented. The cooperative fuels research engine model has been used to estimate the motoring methane number for producer gas which at 110 indicates slight

superiority over methane permitting increasing the compression ratio from 11.5 to 13 with potential for improvement in both power rating and fuel conversion efficiency.

In summary, following are the key outcome of the current investigation;

1. Producer gas as an energy carrier differs significantly from the conventional fuels in terms of the thermo-physical properties and influences in-cylinder thermo-kinematic response. The need for optimization of turbocharger for alternate fuel has been established and realizing BMEP comparable to fossil fuel operation is possible. The possibility of load recovery up to the thermodynamic limit based on turbocharger optimization has also been established. The approach of the analysis and optimization strategy is sufficiently generic and can be extended to any conventional / alternative fuel.

2. The influence of hydrogen on the engine performance through its influence on the transport properties, basically the thermal conductivity has been explicitly established. It is important to note that, while conventionally hydrogen has been associated with improved engine efficiency, attributed to the higher laminar flame speed, the current work has explicitly established the holistic influence of hydrogen through the influence on transport properties, not commonly addressed in the literature.

3. For the first time, combustion descriptors are used towards addressing the in-cylinder performance for an alternate fuel. The deviations in combustion descriptors sensitivity with potential influence on ignition timing control and the use of combustion descriptors for knock occurrence and regime detection has been established.

4. In addressing numerical simulation, the need for fuel specific Wiebe coefficients towards zero dimensional simulation established and a full chemistry based knock prediction model has been developed and utility of the same to establish knock rating of gaseous fuels in general and producer gas in particular has been established. Superiority of producer gas in terms of knock rating has been established permitting potential increase in the engine compression ratio towards realizing higher load and fuel conversion efficiency.

8.2 Scope for future work

The experimental and numerical investigations carried out in this research activity have provided a basis to address the fuel dependence of gas engine performance and a generic methodology to address alternate fuels in a systematic manner. Future work based on the generic scenario of producer gas fuelled operation of an adapted natural gas engine with emphasis on improving the peak supported load/fuel conversion efficiency and improving the versatility of the developed models can lead to new areas of research as described below.

1. With no scope for altering the fuel composition, one of the potential options towards improving the engine energy balance (in terms of enhancing the brake output by reducing the cooling / exhaust load) corresponds to enhancing the wall temperature by increasing the cooling jacket temperature. Such an intervention is expected to reduce the convective cooling load by reducing the temperature gradient between the in-cylinder gases and the cylinder wall. Thus, the potential to counter the influence of the thermo-physical properties (at least partially) needs to be explored. As such, cooling jacket temperature as a parametric investigation forms an important feature that can be exploited towards improving the engine energy balance. However caution has to be exercised considering that increasing the cooling jacket temperature could enhance the knock potential. Thus, a balance between the allowable cooling jacket temperature and knock could be an important area of future work, involving predominantly experimental and supporting numerical investigations.

2. Numerical simulation based knock rating analysis evolves greater than 100 Methane number for producer gas, suggesting the possibility of increasing the compression ratio for a given natural gas engine. With close to 3% influence on the engine power rating per unit change in the compression ratio, any practically realizable compression ratio increase would improve the producer gas fuelled engine power rating and the fuel conversion efficiency. As such, engine operating compression ratio parametric variation forms an important investigation that can be initiated towards improving the engine power rating and fuel conversion efficiency.

3. In the analysis of the laminar flame speed estimation for producer gas, the difference between the flame speed estimated by the planar laminar flame speed model in the double infinity domain and the experimentally reported numbers (significant under prediction by the former) is attributed to the onset of cellularity and subsequent acceleration of the flame due to the presence of hydrogen. While the argument is in-line with the observations made for spherically expanding pure hydrogen flames, investigation may be extended towards in-cylinder optical investigations of producer gas flames to explicitly compare with the observations available in the literature.

4. The current Quasi Dimensional model based on Eddy Entrainment Laminar Burn-up concept adopts a two zone concept, segregating the in-cylinder domain into a burned and an unburned zone. The model can be made multi-zone to enable analysis of the combustion in the near wall region which has been argued to have substantial influence on the terminal combustion duration. A multi-zone model with specific emphasis on the near wall region possibly provides better understanding towards addressing the observed behaviour of sluggish terminal stage combustion duration.

5. The cooperative fuels research engine model for the estimation of the motoring methane number is currently tuned only for producer gas. The limitation primarily arises from the laminar flame speed correlation which is currently a function of temperature and pressure only and the coefficients are tuned for producer gas. The model can be made generic for syngas by evolving a fuel composition dependent laminar flame speed correlation.

The need for future work, especially in the scope of experimental investigations, have not been addressed in the current work primarily due to certain infrastructure limitations (like the non-availability of test bed) and it is accordingly recommended that the same may be accounted for in the course of addressing the aforementioned aspects.

References

Abdel-Gayed, R. G. and D. Bradley (1977). Dependence of turbulent burning velocity on turbulent reynolds number and ratio of flaminar burning velocity to rms turbulent velocity. In *Symposium (International) on Combustion*, Volume 16, pp. 1725–1735. Elsevier.

Abraham, J., F. A. Williams, and F. V. Bracco (1985). A discussion of turbulent flame structure in premixed charges. Technical report, SAE Technical Paper No 850345.

Agency, E. P. (2014 (accessed January 30, 2015)a). *Nonroad Large Spark-Ignition Engines – Exhaust and Evaporative Emission Standards*.

Agency, E. P. (2014 (accessed January 30, 2015)b). *Nonroad Spark-Ignition Engines 19 Kilowatts and Below – Exhaust Emission Standards*.

Ajav, E., B. Singh, and T. Bhattacharya (2000). Thermal balance of a single cylinder diesel engine operating on alternative fuels. *Energy conversion and management 41*(14), 1533–1541.

Alkidas, A. (1980). Heat transfer characteristics of a spark-ignition engine. *Journal of Heat Transfer 102*(2), 189–193.

Alla, G. A. (2002). Computer simulation of a four stroke spark ignition engine. *Energy conversion and Management 43*(8), 1043–1061.

Allen, M. R., D. J. Frame, C. Huntingford, C. D. Jones, J. A. Lowe, M. Meinshausen, and N. Meinshausen (2009). Warming caused by cumulative carbon emissions towards the trillionth tonne. *Nature 458*(7242), 1163–1166.

Anderson, J. D. and J. Wendt (1995). *Computational fluid dynamics*, Volume 206. Springer.

Ando, Y., K. Yoshikawa, M. Beck, and H. Endo (2005). Research and development of a low-btu gas-driven engine for waste gasification and power generation. *Energy 30*(11), 2206–2218.

Annand, W. (1970). Geometry of spherical flame propagation in a disc-shaped combustion chamber. *Journal of mechanical engineering science 12*(2), 146–149.

Annand, W. et al. (1963). Heat transfer in the cylinders of reciprocating internal combustion engines. *Proceedings of the Institution of Mechanical Engineers 177*(1), 973–996.

Annand, W. and D. Pinfold (1980). Heat transfer in the cylinder of a motored reciprocating engine. Technical report, SAE Technical Paper No. 800457.

Annand, W. and G. Roe (1974). *Gas Flow in the Internal Combustion Engine: Power, Performance, Emission Control, and Silencing*. GT Foulis.

Arroyo, J., F. Moreno, M. Muñoz, C. Monné, and N. Bernal (2014). Combustion behavior of a spark ignition engine fueled with synthetic gases derived from biogas. *Fuel 117*, 50–58.

Arsie, I., C. Pianese, and G. Rizzo (1998). Models for the prediction of performance and emissions in a spark ignition engine-a sequentially structured approach. Technical report, SAE Technical Paper No. 980779.

Arunachalam, A. and D. B. Olsen (2012). Experimental evaluation of knock characteristics of producer gas. *biomass and bioenergy 37*, 169–176.

Babajimopoulos, A., D. Assanis, D. Flowers, S. Aceves, and R. Hessel (2005). A fully coupled computational fluid dynamics and multi-zone model with detailed chemical kinetics for the simulation of premixed charge compression ignition engines. *International journal of engine research 6*(5), 497–512.

Baines, N., K. D. Wygant, and A. Dris (2010). The analysis of heat transfer in automotive turbochargers. *Journal of Engineering for Gas Turbines and Power 132*(4), 042301.

Ballal, D. R. and A. H. Lefebvre (1974). Turbulence effects on enclosed flames. *Acta Astronautica 1*(3), 471–483.

Baratta, M., S. dAmbrosio, E. Spessa, and A. Vassallo (2006). Cycle-resolved detection of combustion start in si engines by means of different in-cylinder pressure data reduction techniques. In *ASME 2006 Internal Combustion Engine Division Spring Technical Conference*, pp. 303–316. American Society of Mechanical Engineers.

Bargende, M. (1995). Most optimal location of 50% mass fraction burned and automatic knock detection. components for automatic optimization of si-engine calibrations. *M T Z 56*(10), 632–638.

Bayraktar, H. (2003). Mathematical modeling of spark-ignition engine cycles. *Energy sources 25*(5), 439–455.

Beccari, A., S. Beccari, and E. Pipitone (2010). An analytical approach for the evaluation of the optimal combustion phase in spark ignition engines. *Journal of Engineering for Gas Turbines & Power 22*(3), 032802.

Beccari, A. and E. Pipitone (2004). Proportional integral spark timing control by means of in-cylinder pressure analysis. FISITA 2004 World Automotive Congress.

Benson, R. S., W. Annand, and P. Baruah (1975). A simulation model including intake and exhaust systems for a single cylinder four-stroke cycle spark ignition engine. *International Journal of Mechanical Sciences 17*(2), 97–124.

Beretta, G., M. Rashidi, and J. Keck (1983). Turbulent flame propagation and combustion in spark ignition engines. *Combustion and Flame 52*, 217–245.

Bergman, T. L., F. P. Incropera, and A. S. Lavine (2011). *Fundamentals of heat and mass transfer*. John Wiley & Sons.

Bernard, P. S. and J. M. Wallace (2002). *Turbulent flow: analysis, measurement, and prediction*. John Wiley & Sons.

Bianco, Y., W. K. Cheng, and J. B. Heywood (1991). The effects of initial flame kernel conditions on flame development in si engine. Technical report, SAE Technical Paper No. 912402.

Blizard, N. C. and J. C. Keck (1974). Experimental and theoretical investigation of turbulent burning model for internal combustion engines. Technical report, SAE Technical Paper No. 740191.

Blumberg, P. N., G. A. Lavoie, and R. J. Tabaczynski (1979). Phenomenological models for reciprocating internal combustion engines. *Progress in Energy and Combustion Science 5*(2), 123–167.

Borg, J. and A. Alkidas (2009). On the application of wiebe functions to simulate normal and knocking spark-ignition combustion. *International Journal of Vehicle Design 49*(1), 52–69.

Borghi, R. (1985). On the structure and morphology of turbulent premixed flames. In *Recent advances in the Aerospace Sciences*, pp. 117–138. Springer.

Borman, G. and K. Nishiwaki (1987). Internal-combustion engine heat transfer. *Progress in energy and combustion science 13*(1), 1–46.

Bozza, F., G. Fontana, E. Galloni, and E. Torella (2007). 3d-1d analyses of the turbulent flow field, burning speed and knock occurrence in a turbocharged si engine. Technical report, SAE Technical Paper No. 2007-24-0029.

Bozza, F., A. Gimelli, L. Strazzullo, E. Torella, and C. Cascone (2007). Steady-state and transient operation simulation of a downsized turbocharged si engine. Technical report, SAE Technical Paper No. 2007-01-0381.

Bradley, D., R. Hicks, M. Lawes, C. Sheppard, and R. Woolley (1998). The measurement of laminar burning velocities and markstein numbers for iso-octane–air and iso-octane–n-heptane–air mixtures at elevated temperatures and pressures in an explosion bomb. *Combustion and flame 115*(1), 126–144.

Bradley, D., C. Sheppart, R. Woolley, D. Greenhalgh, and R. Lockett (2000). The development and structure of flame instabilities and cellularity at low markstein numbers in explosions. *Combustion and Flame 122*(1), 195–209.

Brehob, D. D. and C. E. Newman (1992). Monte carlo simulation of cycle by cycle variability. Technical report, SAE Technical Paper No. 922165.

Brunt, M. F. and A. L. Emtage (1997). Evaluation of burn rate routines and analysis errors. Technical report, SAE Technical Paper No. 970037.

Brunt, M. F., C. R. Pond, and J. Biundo (1998). Gasoline engine knock analysis using cylinder pressure data. Technical report, SAE Technical Paper No. 980896.

Brunt, M. F., H. Rai, and A. L. Emtage (1998). The calculation of heat release energy from engine cylinder pressure data. Technical report, SAE Technical Paper No. 981052.

By, A., B. Kempinski, and J. Rife (1981). Knock in spark ignition engines. Technical report, SAE Technical Paper No. 810147.

C, D. J. (1997). The spatial and temporal variation of engine cylinder pressure - origins and consequences. In *Proceedings of the XV national conference on I.C. Engines and Combustion*, pp. 3–29. Allied Publishers Limited.

Callahan, T. J., T. Ryan III, J. P. Buckingham, R. J. Kakockzi, and G. Sorge (1996). Engine knock rating of natural gases–expanding the methane number database. Technical report, American Society of Mechanical Engineers, New York, NY (United States).

Caris, D. and E. Nelson (1959). A new look at high compression engines. Technical report, SAE Technical Paper No. 590015.

Caton, J. A. (2000). Operating characteristics of a spark-ignition engine using the second law of thermodynamics: effects of speed and load. Technical report, SAE Technical Paper No. 2000-01-0952.

Centeno, F., K. Mahkamov, E. E. S. Lora, and R. V. Andrade (2012). Theoretical and experimental investigations of a downdraft biomass gasifier-spark ignition engine power system. *Renewable Energy 37*(1), 97–108.

Chakravarthy, P., D. Mishra, P. Paul, and H. Mukunda (1993). The theoretical calculations of the limits of flame propagation for producer gas mixture. *Proceedings, 4th National meet on biomass gasification and combustion*, 28–37.

Chen, J.-Y., J. Lumley, and F. Gouldin (1988). Modeling of wrinkled laminar flames with intermittency and conditional statistics. In *Symposium (International) on Combustion*, Volume 21, pp. 1483–1491. Elsevier.

Chiodi, M. and M. Bargende (2001). Improvement of engine heat-transfer calculation in the three-dimensional simulation using a phenomenological heat-transfer model. Technical report, SAE Technical Paper No. 2001-01-3601.

Cho, H. M. and B.-Q. He (2007). Spark ignition natural gas engines—a review. *Energy Conversion and Management 48*(2), 608–618.

Chun, K. M. and J. B. Heywood (1989). Characterization of knock in a spark-ignition engine. Technical report, SAE Technical Paper No. 890156.

Chung, T. (2010). *Computational fluid dynamics*. Cambridge university press.

Clavin, P. and F. Williams (1979). Theory of premixed-flame propagation in large-scale turbulence. *Journal of fluid mechanics 90*(03), 589–604.

Cohen, E. R. (1998). An introduction to error analysis: The study of uncertainties in physical measurements. *Measurement Science and Technology 9*(6).

Coleman, H. W. and W. G. Steele (2009). *Experimentation, validation, and uncertainty analysis for engineers*. John Wiley & Sons.

Commission, C. E. R. et al. (2010). *Government of India 'Indian Electricity Grid Code (IEGC)-2010'*.

Company, G. E. (2013 (accessed January 30, 2015)). *Wakuesha CFR - Combination research and motor method octane rating unit*.

Cook, H. A., O. H. Heinicke, and W. H. Haynie (1947). Spark-timing control based on correlation of maximum-economy spark timing, flame-front travel and cylinder-pressure rise. Technical report, DTIC Document.

Cormerais, M., P. Chesse, and J.-F. Hetet (2009). Turbocharger heat transfer modeling under steady and transient conditions. *International Journal of Thermodynamics 12*(4), 193–202.

D P Mishra, P. J. P. and H. S. Mukunda (1994). Computational prediction of flame speed of producer gas and comparison with experiments. *Proceedings of 13th National Conference on I.C. Engines and Combustion*, 256–262.

Damköhler, G. (1947). The effect of turbulence on the flame velocity in gas mixtures.

D'Andrea, T., P. Henshaw, and D. Ting (2004). The addition of hydrogen to a gasoline-fuelled si engine. *International Journal of Hydrogen Energy 29*(14), 1541–1552.

Das, A. and H. Watson (1997). Development of a natural gas spark ignition engine for optimum performance. *Proceedings of the Institution of Mechanical Engineers, Part D: Journal of Automobile Engineering 211*(5), 361–378.

Das, L., R. Gulati, and P. K. Gupta (2000). A comparative evaluation of the performance characteristics of a spark ignition engine using hydrogen and compressed natural gas as alternative fuels. *International Journal of Hydrogen Energy 25*(8), 783–793.

Dasappa, S. (2001). On the estimation of power from a diesel engine converted for gas operation : a simple analysis. In *Proceedings of the seventeenth national conference on I.C. Engines and Combustion*, pp. 167–174.

Dasappa, S., S. D. Krishna, B. Bose, and H. Tauri (2015). Adaptation of MW level natural gas lean burn engine for producer gas operation - a grid connected power plant. In *22nd European International Biomass Conference - Setting the Course for a Bio-based Economy*, pp. 554–557. ETA-FLORENCE.

Dasappa, S., P. Paul, H. Mukunda, N. Rajan, G. Sridhar, and H. Sridhar (2004). Biomass gasification technology-a route to meet energy needs. *Current Science 87*(7), 908–916.

Dasappa, S., G. Sridhar, and P. Paul (2011). Adaptation of small capacity natural gas engine for producer gas operation. *Proceedings of the Institution of Mechanical Engineers, Part C: Journal of Mechanical Engineering Science*, 0954406211424678.

Dasappa, S., G. Sridhar, and P. Paul (2012). Adaptation of small capacity natural gas engine for producer gas operation. *Proceedings of the Institution of Mechanical Engineers, Part C: Journal of Mechanical Engineering Science 226*(6), 1568–1578.

Dasappa, S., H. Sridhar, and M. Indrajit (2011). Experiments on and thermodynamic analysis of a turbocharged engine with producer gas as fuel. *Proceedings of the Institution of Mechanical Engineers, Part C: Journal of Mechanical Engineering Science*, 0954406211419063.

Dasappa, S., D. Subbukrishna, K. Suresh, P. Paul, and G. Prabhu (2011). Operational experience on a grid connected 100kwe biomass gasification power plant in karnataka, india. *Energy for Sustainable Development 15*(3), 231–239.

Davis, S. G., A. V. Joshi, H. Wang, and F. Egolfopoulos (2005). An optimized kinetic model of h 2/co combustion. *Proceedings of the Combustion Institute 30*(1), 1283–1292.

De Nicolao, G., R. Scattolini, and C. Siviero (1996). Modelling the volumetric efficiency of ic engines: parametric, non-parametric and neural techniques. *Control Engineering Practice 4*(10), 1405–1415.

de Rocquigny, E., N. Devictor, and S. Tarantola (2008). *Uncertainty in industrial practice: a guide to quantitative uncertainty management*. John Wiley & Sons.

Demirbas, A. (2008). Biofuels sources, biofuel policy, biofuel economy and global biofuel projections. *Energy conversion and management 49*(8), 2106–2116.

Demirbas, A. (2009a). Biofuels securing the planet's future energy needs. *Energy Conversion and Management 50*(9), 2239–2249.

Demirbas, A. (2009b). Political, economic and environmental impacts of biofuels: A review. *Applied Energy 86*, S108–S117.

Douaud, A. and P. Eyzat (1978). Four-octane-number method for predicting the anti-knock behavior of fuels and engines. Technical report, SAE Technical Paper No. 780080.

Eisazadeh-Far, K., F. Parsinejad, H. Metghalchi, and J. C. Keck (2010). On flame kernel formation and propagation in premixed gases. *Combustion and Flame 157*(12), 2211–2221.

Fathi, M., A. Holland, F. Ansari, and C. Weber (2011). *Integrated Systems, Design and Technology 2010: Knowledge Transfer in New Technologies*. Springer.

Ferguson, C. and A. Kirkpatrick. *Internal combustion engines: applied thermosciences". 2nd*. John Wiley & Sons, Inc, ISBN 0-471-35617-4.

Ferguson, C. R. and A. T. Kirkpatrick (2001). *Internal Combustion Engines: Applied Thermosciences*. John Wiley & Sons.

Fernald, R. H. (1909). *Recent development of the producer-gas power plant in the United States*, Volume 416. Govt. Print. Off.

Finol, C. and K. Robinson (2006). Thermal modelling of modern engines: a review of empirical correlations to estimate the in-cylinder heat transfer coefficient. *Proceedings of the Institution of Mechanical Engineers, Part D: Journal of Automobile Engineering 220*(12), 1765–1781.

Gallo, W. L. R. and L. F. Milanez (1992). Exergetic analysis of ethanol and gasoline fueled engines. Technical report, SAE Technical Paper No. 920809.

Gatowski, J. A., J. B. Heywood, and C. Deleplace (1984). Flame photographs in a spark-ignition engine. *Combustion and Flame 56*(1), 71–81.

Gharehghani, A., M. Koochak, M. Mirsalim, and T. Yusaf (2013). Experimental investigation of thermal balance of a turbocharged si engine operating on natural gas. *Applied Thermal Engineering 60*(1), 200–207.

Ghojel, J. (2010). Review of the development and applications of the wiebe function: a tribute to the contribution of ivan wiebe to engine research. *International Journal of Engine Research 11*(4), 297–312.

Gillespie, L., M. Lawes, C. Sheppard, and R. Woolley (2000). Aspects of laminar and turbulent burning velocity relevant to si engines. Technical report, SAE Technical Paper No. 2000-01-0192.

Gosman, A. (1999). State of the art of multi-dimensional modeling of engine reacting flows. *Oil & Gas Science and Technology 54*(2), 149–159.

Gouldin, F. (1987). An application of fractals to modeling premixed turbulent flames. *Combustion and Flame 68*(3), 249–266.

Grill, M., T. Billinger, and M. Bargende (2006). Quasi-dimensional modeling of spark ignition engine combustion with variable valve train. Technical report, SAE Technical Paper.

Groff, E. (1987). An experimental evaluation of an entrainment flame-propagation model. *Combustion and flame 67*(2), 153–162.

Gu, X., M. Haq, M. Lawes, and R. Woolley (2000). Laminar burning velocity and markstein lengths of methane–air mixtures. *Combustion and flame 121*(1), 41–58.

Gülder, Ö. L. (1984). Correlations of laminar combustion data for alternative si engine fuels. Technical report, SAE Technical Paper No. 841000.

Halter, F., C. Chauveau, N. Djebaili-Chaumeix, and I. Gökalp (2005). Characterization of the effects of pressure and hydrogen concentration on laminar burning velocities of methane–hydrogen–air mixtures. *Proceedings of the Combustion Institute 30*(1), 201–208.

Han, Z. and R. D. Reitz (1995). Turbulence modeling of internal combustion engines using rng κ-ε models. *Combustion science and technology 106*(4-6), 267–295.

Han, Z. and R. D. Reitz (1997). A temperature wall function formulation for variable-density turbulent flows with application to engine convective heat transfer modeling. *International journal of heat and mass transfer 40*(3), 613–625.

Hartman, J. (2007). *Turbocharging Performance Handbook*. MotorBooks International.

Hasler, P. and T. Nussbaumer (1999). Gas cleaning for ic engine applications from fixed bed biomass gasification. *Biomass and Bioenergy 16*(6), 385–395.

Hayes, T., L. Savage, and S. Sorenson (1986). Cylinder pressure data acquisition and heat release analysis on a personal computer. Technical report, SAE Technical Paper No. 860029.

Heinberg, R. (2010). *Peak everything: waking up to the century of declines*. New Society Publishers.

Henriksen, U., J. Ahrenfeldt, T. K. Jensen, B. Gøbel, J. D. Bentzen, C. Hindsgaul, and L. H. Sørensen (2006). The design, construction and operation of a 75kw two-stage gasifier. *Energy 31*(10), 1542–1553.

Hernandez, J. J., M. Lapuerta, C. Serrano, and A. Melgar (2005). Estimation of the laminar flame speed of producer gas from biomass gasification. *Energy & fuels 19*(5), 2172–2178.

Herweg, R. and R. Maly (1992). A fundamental model for flame kernel formation in si engines. Technical report, SAE Technical Paper No. 922243.

Heywood, H. (1943). Tests on transport producer-gas units. *Proceedings of the Institution of Mechanical Engineers 149*(1), 34–47.

Heywood, J. B. (1988). Fundamentals of internal combustion engines. *NY: McGraw Hill*, 619.

Hiroyasu, H. and T. Kadota (1975). Computer simulation for combustion and exhaust emissions in spark ignition engine. In *Symposium (International) on Combustion*, Volume 15, pp. 1213–1223. Elsevier.

Hirschfelder, J. O., C. F. Curtiss, R. B. Bird, and M. G. Mayer (1954). *Molecular theory of gases and liquids*, Volume 26. Wiley New York.

Hoel, M. and S. Kverndokk (1996). Depletion of fossil fuels and the impacts of global warming. *Resource and energy economics 18*(2), 115–136.

Höök, M. and X. Tang (2013). Depletion of fossil fuels and anthropogenic climate change—a review. *Energy Policy 52*, 797–809.

Howarth, M. H. (1966). *The design of the high speed diesel engines.* American Elsevier Pub. Co.

Hrovat, D. and J. Sun (1997). Models and control methodologies for ic engine idle speed control design. *Control Engineering Practice 5*(8), 1093–1100.

Hu, E., Z. Huang, J. He, C. Jin, and J. Zheng (2009). Experimental and numerical study on laminar burning characteristics of premixed methane–hydrogen–air flames. *international journal of hydrogen energy 34*(11), 4876–4888.

Huang, Y., C. Sung, and J. Eng (2004). Laminar flame speeds of primary reference fuels and reformer gas mixtures. *Combustion and Flame 139*(3), 239–251.

Huang, Z., B. Liu, K. Zeng, Y. Huang, D. Jiang, X. Wang, and H. Miao (2007). Combustion characteristics and heat release analysis of a spark-ignited engine fueled with natural gas-hydrogen blends. *Energy & Fuels 21*(5), 2594–2599.

Hubbard, M., P. Dobson, and J. Powell (1976). Closed loop control of spark advance using a cylinder pressure sensor. *Journal of Dynamic Systems, Measurement, and Control 98*, 414.

Hurley, T. and A. Fitton (1949). Producer gas for road transport. *Proceedings of the Institution of Mechanical Engineers 161*(1), 81–97.

Huzayyin, A., H. Moneib, M. Shehatta, and A. Attia (2008). Laminar burning velocity and explosion index of lpg–air and propane–air mixtures. *Fuel 87*(1), 39–57.

IHS-Engineering-360 (2015 (accessed December 25, 2015)). *Rotary Encoders.*

Incropera, F. P. (2011). *Fundamentals of heat and mass transfer.* John Wiley & Sons.

Janota, M., A. Hallam, E. Brock, and S. Dexter (1967). Paper 7: The prediction of diesel engine performance and combustion chamber component temperatures

using digital computers. In *Proceedings of the Institution of Mechanical Engineers, Conference Proceedings*, Volume 182, pp. 58–70. SAGE Publications.

Jeans, J. (1982). *An introduction to the kinetic theory of gases*. CUP Archive.

Jerzembeck, S., N. Peters, P. Pepiot-Desjardins, and H. Pitsch (2009). Laminar burning velocities at high pressure for primary reference fuels and gasoline: Experimental and numerical investigation. *Combustion and Flame 156*(2), 292–301.

Ji, C. and S. Wang (2009). Effect of hydrogen addition on the idle performance of a spark ignited gasoline engine at stoichiometric condition. *International Journal of Hydrogen Energy 34*(8), 3546–3556.

Johansson, B. (1996). Cycle to cycle variations in si engines-the effects of fluid flow and gas composition in the vicinity of the spark plug on early combustion. Technical report, SAE Technical Paper No. 962084.

Johansson, B. and K. Olsson (1995). Combustion chambers for natural gas si engines part i: Fluid flow and combustion. Technical report, SAE Technical Paper No. 950469.

Jomaas, G., C. Law, and J. Bechtold (2007). On transition to cellularity in expanding spherical flames. *Journal of fluid mechanics 583*, 1–26.

Kalam, M. and H. Masjuki (2011). An experimental investigation of high performance natural gas engine with direct injection. *Energy 36*(5), 3563–3571.

Kalghatgi, G. T. (1987). Spark ignition, early flame development and cyclic variation in ic engines. Technical report, SAE Technical Paper No. 870163.

Kanitkar, S., P. Chakravarty, P. Paul, and H. Mukunda (1993). The flame speeds, temperature and limits of flame propagation for producer gas-air mixtures–experimental results. *Proceedings of Fourth National Meet on Biomass Gasification and Combustion, Mysore, India 4*, 50–62.

Kawamura, Y., M. Shinshi, H. Sato, N. Takahashi, and M. Iriyama (1989). Mbt control through individual cylinder pressure detection. *SAE transactions 97*, 1724–1730.

Keck, J. C. (1982). Turbulent flame structure and speed in spark-ignition engines. In *Symposium (International) on Combustion*, Volume 19, pp. 1451–1466. Elsevier.

Keck, J. C., J. B. Heywood, and G. Noske (1987). Early flame development and burning rates in spark ignition engines and their cyclic variability. Technical report, SAE Technical Paper No. 870164.

Kee, R., F. Rupley, J. Miller, M. Coltrin, J. Grcar, E. Meeks, H. Moffat, A. Lutz, G. Dixon-Lewis, M. Smooke, et al. (2006). Chemkin release 4.1. *Reaction Design, San Diego, CA*.

Kee, R. J., F. M. Rupley, E. Meeks, J. A. Miller, and A. Chemkin-III (1996). A fortran chemical kinetics package for the analysis of gas phase chemical and plasma kinetics. *Sandia National Laboratories*.

Klose, W., P. Parikh, et al. (1994). Development of a 15 kwe spark ignition producer gas engine and some investigations of its in-cylinder processes. *Renewable energy 5*(5), 835–837.

Komninos, N., D. Hountalas, and C. Rakopoulos (2007). A parametric investigation of hydrogen hcci combustion using a multi-zone model approach. *Energy conversion and management 48*(11), 2934–2941.

Korakianitis, T., A. Namasivayam, and R. Crookes (2011). Natural-gas fueled spark-ignition (si) and compression-ignition (ci) engine performance and emissions. *Progress in Energy and Combustion Science 37*(1), 89–112.

Kravchik, T., E. Sher, and J. Heywood (1995). From spark ignition to flame initiation. *Combustion science and technology 108*(1-3), 1–30.

Kuo, K. K.-y. and R. Acharya (2012). *Fundamentals of Turbulent and Multi-Phase Combustion*. John Wiley & Sons.

Kurdyumov, V., J. Blasco, A. Sánchez, and A. Linan (2004). On the calculation of the minimum ignition energy. *Combustion and flame 136*(3), 394–397.

Kwon, O., G. Rozenchan, and C. Law (2002). Cellular instabilities and self-acceleration of outwardly propagating spherical flames. *Proceedings of the combustion Institute 29*(2), 1775–1783.

Lamarque, J.-F., T. C. Bond, V. Eyring, C. Granier, A. Heil, Z. Klimont, D. Lee, C. Liousse, A. Mieville, B. Owen, et al. (2010). Historical (1850–2000) gridded anthropogenic and biomass burning emissions of reactive gases and aerosols: methodology and application. *Atmospheric Chemistry and Physics 10*(15), 7017–7039.

Lancaster, D. R., R. B. Krieger, and J. H. Lienesch (1975). Measurement and analysis of engine pressure data. Technical report, SAE Technical paper No No. 750026.

Laser-Components (2015 (accessed December 25, 2015)). *NDIR Gas Analysis*.

Law, C. (1989). Dynamics of stretched flames. In *Symposium (International) on Combustion*, Volume 22, pp. 1381–1402. Elsevier.

Lecointe, B. and G. Monnier (2003). Downsizing a gasoline engine using turbocharging with direct injection. Technical report, SAE Technical Paper No. 2003-01-0542.

LEIKER, M., C. K, C. W, U. Pfeifer, and M. Rankl (1972). Evaluation of anti-knocking property of gaseous fuels by means of methane number and its practical application to gas engines. In *MECHANICAL ENGINEERING*, Volume 94, pp. 55. ASME-AMER SOC MECHANICAL ENG 345 E 47TH ST, NEW YORK, NY 10017.

Leonhardt, S., N. Muller, and R. Isermann (1999). Methods for engine supervision and control based on cylinder pressure information. *Mechatronics, IEEE/ASME Transactions on 4*(3), 235–245.

Li, H.-M., G.-X. Li, Z.-Y. Sun, Y. Zhai, and Z.-H. Zhou (2014). Research on cellular instabilities of lean premixed syngas flames under various hydrogen fractions using a constant volume vessel. *Energies 7*(7), 4710–4726.

Liao, S., D. Jiang, and Q. Cheng (2004). Determination of laminar burning velocities for natural gas. *Fuel 83*(9), 1247–1250.

Lipatnikov, A. (2012). *Fundamentals of premixed turbulent combustion*. CRC Press.

Livengood, J. and P. Wu (1955). Correlation of autoignition phenomena in internal combustion engines and rapid compression machines. In *Symposium (International) on Combustion*, Volume 5, pp. 347–356. Elsevier.

Lounici, M. S., K. Loubar, M. Balistrou, and M. Tazerout (2011). Investigation on heat transfer evaluation for a more efficient two-zone combustion model in the case of natural gas si engines. *Applied Thermal Engineering 31*(2), 319–328.

Ltd, A. T. S. (2010 (accessed January 30, 2015)). *High pressure turbocharging on gas engines*.

Lüdtke, K. H. (2004). *Process centrifugal compressors: basics, function, operation, design, application*. Springer Science & Business Media.

Lyford-Pike, E. J. and J. B. Heywood (1984). Thermal boundary layer thickness in the cylinder of a spark-ignition engine. *International journal of heat and mass transfer 27*(10), 1873–1878.

Lyn, W. (1963). Study of burning rate and nature of combustion in diesel engines. In *Symposium (International) on Combustion*, Volume 9, pp. 1069–1082. Elsevier.

Ma, F. and Y. Wang (2008). Study on the extension of lean operation limit through hydrogen enrichment in a natural gas spark-ignition engine. *International Journal of Hydrogen Energy 33*(4), 1416–1424.

Ma, F., Y. Wang, H. Liu, Y. Li, J. Wang, and S. Zhao (2007). Experimental study on thermal efficiency and emission characteristics of a lean burn hydrogen enriched natural gas engine. *International Journal of Hydrogen Energy 32*(18), 5067–5075.

Ma, F., Y. Wang, M. Wang, H. Liu, J. Wang, S. Ding, and S. Zhao (2008). Development and validation of a quasi-dimensional combustion model for si engines fuelled by hcng with variable hydrogen fractions. *International journal of hydrogen energy 33*(18), 4863–4875.

Malenshek, M. and D. B. Olsen (2009). Methane number testing of alternative gaseous fuels. *Fuel 88*(4), 650–656.

Maly, R. (1984). Spark ignition: its physics and effect on the internal combustion engine. In *Fuel Economy*, pp. 91–148. Springer.

Mandilas, C., M. Ormsby, C. Sheppard, and R. Woolley (2007). Effects of hydrogen addition on laminar and turbulent premixed methane and iso-octane–air flames. *Proceedings of the combustion institute 31*(1), 1443–1450.

Matekunas, F. A. (1986, November 25). Engine combustion control with dilution flow by pressure ratio management. US Patent 4,624,229.

Mathur, S., P. Tondon, and S. Saxena (1967). Thermal conductivity of binary, ternary and quaternary mixtures of rare gases. *Molecular physics 12*(6), 569–579.

Matthews, R. D. and Y.-W. Chin (1991). A fractal-based si engine model: comparisons of predictions with experimental data. Technical report, SAE Technical Paper No. 910079.

Meinshausen, M., N. Meinshausen, W. Hare, S. C. Raper, K. Frieler, R. Knutti, D. J. Frame, and M. R. Allen (2009). Greenhouse-gas emission targets for limiting global warming to 2 c. *Nature 458*(7242), 1158–1162.

Merker, G., C. Schwarz, G. Stiesch, and F. Otto (2005). *Simulating combustion: simulation of combustion and pollutant formation for engine-development*. Springer Science & Business Media.

Metghalchi, M. and J. Keck (1980). Laminar burning velocity of propane-air mixtures at high temperature and pressure. *Combustion and flame 38*, 143–154.

Metghalchi, M. and J. C. Keck (1982). Burning velocities of mixtures of air with methanol, isooctane, and indolene at high pressure and temperature. *Combustion and flame 48*, 191–210.

Millo, F. and C. V. Ferraro (1998). Knock in si engines: a comparison between different techniques for detection and control. Technical report, SAE Technical Paper No. 982477.

Milne, T. A., N. Abatzoglou, and R. J. Evans (1998). *Biomass gasifier" tars": their nature, formation, and conversion*, Volume 570. National Renewable Energy Laboratory Golden, CO.

Mishra, D., P. Paul, and H. Mukunda (1994). Computational studies on the flame propagation in producer gas-air mixture and experimental comparisons. In *Proceedings, 13th National conference on IC engines and Combustion, Bangalore*, pp. 256–262.

Moccia, V. and J. D'Alessio (2013). Burning behaviour of high-pressure ch4-h2-air mixtures. *Energies 6*(1), 97–116.

Morse, P. and K. Ingard (1968). Theoretical acoustics, international series in pure and applied physics. *New York: McGraw Hill 603*, 604.

Mounaïm-Rousselle, C., L. Landry, F. Halter, and F. Foucher (2013). Experimental characteristics of turbulent premixed flame in a boosted spark-ignition engine. *Proceedings of the Combustion Institute 34*(2), 2941–2949.

Mueller, R., M. Hart, A. Truscott, A. Noble, G. Kroetz, M. Eickhoff, and C. Cavalloni (2000). Combustion-pressure-based engine management system.

Mukunda, H. (2011). *Understanding clean energy and fuels from biomass*. Wiley India.

Munoz, M., F. Moreno, J. Morea-Roy, J. Ruiz, and J. Arauzo (2000). Low heating value gas on spark ignition engines. *Biomass and Bioenergy 18*(5), 431–439.

Nano-Physics-KHT (2015 (accessed December 25, 2015)). *AFM and Piezoresponsive Materials*.

Natarajan, J., S. Nandula, T. Lieuwen, and J. Seitzman (2005). Laminar flame speeds of synthetic gas fuel mixtures. In *ASME Turbo Expo 2005: Power for Land, Sea, and Air*, pp. 677–686. American Society of Mechanical Engineers.

of Environment, M. (2013 (accessed January 30, 2015)). *Environment (Protection) (Second Amendment) Rules, 2013 - Ministry of Environment Notification*.

Oppenheim, A. (2004). *Combustion in piston engines: technology, evolution, diagnosis, and control*. Springer Verlag.

Ouimette, P. and P. Seers (2009). Numerical comparison of premixed laminar flame velocity of methane and wood syngas. *Fuel 88*(3), 528–533.

Overbye, V. D., J. E. Bennethum, O. Uyehara, and P. Myers (1961). Unsteady heat transfer in engines. Technical report, SAE Technical Paper No. 610041.

Ozdor, N., M. Dulger, and E. Sher (1994). Cyclic variability in spark ignition engines a literature survey. Technical report, SAE Technical Paper No. 940987.

Papagiannakis, R., C. Rakopoulos, D. Hountalas, and E. Giakoumis (2007). Study of the performance and exhaust emissions of a spark-ignited engine operating on syngas fuel. *International Journal of Alternative Propulsion 1*(2-3), 190–215.

PCB-Piezotronics (2015 (accessed December 25, 2015)). *Introduction to Dynamic Pressure Sensors*.

Peters, N. (1989). Length and time scales in turbulent combustion. In *Turbulent Reactive Flows*, pp. 242–256. Springer.

Peters, N. (1999). The turbulent burning velocity for large-scale and small-scale turbulence. *Journal of Fluid mechanics 384*, 107–132.

Peters, N. (2000). *Turbulent combustion*. Cambridge university press.

Pipitone, E. (2008). A comparison between combustion phase indicators for optimal spark timing. *Journal of engineering for gas turbines and power 130*(5).

Pischinger, S. and J. B. Heywood (1991). A model for flame kernel development in a spark-ignition engine. In *Symposium (International) on Combustion*, Volume 23, pp. 1033–1040. Elsevier.

Pletcher, R. H., J. C. Tannehill, and D. Anderson (2012). *Computational fluid mechanics and heat transfer*. CRC Press.

Poinsot, T., D. Veynante, and S. Candel (1991). Quenching processes and premixed turbulent combustion diagrams. *Journal of Fluid Mechanics 228*, 561–606.

Pope, S. (1987). Turbulent premixed flames. *Annual review of fluid mechanics 19*(1), 237–270.

Poulos, S. G. and J. B. Heywood (1983). The effect of chamber geometry on spark-ignition engine combustion. Technical report, SAE Technical Paper No. 830334.

Pourkhesalian, A. M., A. H. Shamekhi, and F. Salimi (2010). Alternative fuel and gasoline in an si engine: A comparative study of performance and emissions characteristics. *Fuel 89*(5), 1056–1063.

Rakopoulos, C., C. Michos, and E. Giakoumis (2008). Availability analysis of a syngas fueled spark ignition engine using a multi-zone combustion model. *Energy 33*(9), 1378–1398.

Rallis, C. J. and A. M. Garforth (1980). The determination of laminar burning velocity. *Progress in Energy and Combustion Science 6*(4), 303–329.

Ramachandra, A. (1993). Performance studies on a wood gas run ic engine. *Proceedings of Fourth National Meet on Biomass Gasification and Combustion, Mysore, India 4*, 213–218.

Ramos, J. (1986). Comparisons between thermodynamic and one-dimensional combustion models of spark-ignition engines. *Applied mathematical modelling 10*(6), 409–422.

Rao, S. G. (2003). *Experiments and modelling studies of producer gas based spark-ignited reciprocating engines*. Ph. D. thesis, Indian Institute of Science.

Rautenberg, M., M. Malobabic, and A. Mobarak (1984). Influence of heat transfer between turbine and compressor on the performance of small turbochargers. In *IN: 1983 Tokyo International Gas Turbine Congress, Tokyo, Japan, October 23-29, 1983, Proceedings. Volume 2 (A85-41776 20-07). Tokyo, Gas Turbine Society of Japan, 1984, p. 567-574.*, Volume 2, pp. 567–574.

Reed, T. B. (1981). Biomass gasification: principles and technology.[monograph].

Reitz, R. D. (2013). Directions in internal combustion engine research. *Combustion and Flame 160*(1), 1–8.

Rhodes, D. B. and J. C. Keck (1985). Laminar burning speed measurements of indolene-air-diluent mixtures at high pressures and temperatures. Technical report, SAE Technical Paper No. 850047.

Rice, O. (1955). Molecular theory of gases and liquids. *Journal of the American Chemical Society 77*(7), 2031–2032.

Richard, S., S. Bougrine, G. Font, F.-A. Lafossas, and F. Le Berr (2009). On the reduction of a 3D CFD combustion model to build a physical 0D model for simulating heat release, knock and pollutants in si engines. *Oil & Gas Science and Technology-Revue de l'IFP 64*(3), 223–242.

Roache, P. J. (1997). Quantification of uncertainty in computational fluid dynamics. *Annual Review of Fluid Mechanics 29*(1), 123–160.

Ross, S. M. (2009). *Introduction to probability and statistics for engineers and scientists*. Academic Press.

Ryan, T., T. Callahan, and S. R. King (1993). Engine knock rating of natural gases—methane number. *Journal of engineering for gas turbines and Power 115*(4), 769–776.

Sandeep, K. and S. Dasappa (2014a). First and second law thermodynamic analysis of air and oxy-steam biomass gasification. *International Journal of Hydrogen Energy 39*(34), 19474–19484.

Sandeep, K. and S. Dasappa (2014b). Oxy–steam gasification of biomass for hydrogen rich syngas production using downdraft reactor configuration. *International Journal of Energy Research 38*(2), 174–188.

Schmillen, K. P. and M. Rechs (1991). Different methods of knock detection and knock control. Technical report, SAE Technical Paper No. 910858.

Serrano, C., J. Hernandez, C. Mandilas, C. Sheppard, and R. Woolley (2008). Laminar burning behaviour of biomass gasification-derived producer gas. *International Journal of Hydrogen Energy 33*(2), 851–862.

Serrano, J., P. Olmeda, A. Paez, and F. Vidal (2010). An experimental procedure to determine heat transfer properties of turbochargers. *Measurement Science and Technology 21*(3), 035109.

Shaaban, S. (2004). *Experimental investigation and extended simulation of turbocharger non-adiabatic performance*. Ph. D. thesis, University of Hannover.

Shaaban, S. and J. Seume (2006). Analysis of turbocharger non-adiabatic performance. In *Institution of Mechanical Engineers: 8th International Conference on Turbochargers and Turbocharging, London, May*, pp. 17–18.

Shah, A., R. Srinivasan, S. D. F. To, and E. P. Columbus (2010). Performance and emissions of a spark-ignited engine driven generator on biomass based syngas. *Bioresource technology 101*(12), 4656–4661.

Shashikantha, Banerjee, P. and P. Parikh (1992). Producer gas operated si engine-development and analysis. In *Proceedings of the X national conference on I.C. Engines and Combustion*, pp. 100–108.

Shashikantha, Banerjee, P. and P. Parikh (1993). Development and performance analysis of a 15 kwe producer gas operated si engine. In *Proceedings of the Fourth National Meet on Biomass Gasification and Combustion, Mysore, India*, Volume 4, pp. 219–231.

Shashikantha, S. and P. Parikh (1999). Spark ignition producer gas engine and dedicated compressed natural gas engine-technology development and experimental performance optimisation. Technical report, SAE Technical Paper No. 1999-01-3515.

Shayler, P., M. Wiseman, and T. Ma (1990). Improving the determination of mass fraction burnt. Technical report, SAE Technical Paper No. 900351.

Shen, H., P. C. Hinze, and J. B. Heywood (1994). A model for flame initiation and early development in si engine and its application to cycle-to-cycle variations. Technical report, SAE Technical Paper No. 942049.

Shen, H., P. C. Hinze, and J. B. Heywood (1996). A study of cycle-to-cycle variations in si engines using a modified quasi-dimensional model. Technical report, SAE Technical Paper No. 961187.

Shiao, Y. and J. Moskwa (1995). Cylinder pressure and combustion heat release estimation for si engine diagnostics using nonlinear sliding observers. *Control Systems Technology, IEEE Transactions on 3*(1), 70–78.

Shivapuji, A. M. and S. Dasappa (2014). Selection and thermodynamic analysis of a turbocharger for a producer gas-fuelled multi-cylinder engine. *Proceedings of the Institution of Mechanical Engineers, Part A: Journal of Power and Energy 228*(3), 340–356.

Sinha, A. K. (2003). *Physical metallurgy handbook*. McGraw-Hill Professional Publishing.

Smith, G. P., D. M. Golden, M. Frenklach, N. W. Moriarty, B. Eiteneer, M. Goldenberg, C. T. Bowman, R. K. Hanson, S. Song, W. C. Gardiner Jr, et al. (1999). Gri-mech 3.0.

Smooke, D. M., J. A. Miller, and R. J. Kee (1983). Determination of adiabatic flame speeds by boundary value methods. *Combustion Science and Technology 34*(1-6), 79–90.

Som, S., A. Ramirez, J. Hagerdorn, A. Saveliev, and S. Aggarwal (2008). A numerical and experimental study of counterflow syngas flames at different pressures. *Fuel 87*(3), 319–334.

Son, Y.-I., S. J. Yoon, Y. K. Kim, and J.-G. Lee (2011). Gasification and power generation characteristics of woody biomass utilizing a downdraft gasifier. *biomass and bioenergy 35*(10), 4215–4220.

Soylu, S. (2002). Simple modeling of combustion for natural gas engines. Technical report, SAE Technical Paper No. 2002-01-2733.

Soylu, S. and J. Van Gerpen (2004). Development of empirically based burning rate sub-models for a natural gas engine. *Energy Conversion and Management 45*(4), 467–481.

Sridhar, G., P. Paul, and H. Mukunda (2001). Biomass derived producer gas as a reciprocating engine fuel—an experimental analysis. *Biomass and Bioenergy 21*(1), 61–72.

Sridhar, G., P. Paul, and H. Mukunda (2005). Computational studies of the laminar burning velocity of a producer gas and air mixture under typical engine conditions. *Proceedings of the Institution of Mechanical Engineers, Part A: Journal of Power and Energy 219*(3), 195–201.

Sridhar, G., H. Sridhar, S. Dasappa, P. Paul, N. Rajan, and H. Mukunda (2005). Development of producer gas engines. *Proceedings of the Institution of Mechanical Engineers, Part D: Journal of Automobile Engineering 219*(3), 423–438.

Stassen, H. (1993). Strategies for upgrading producer gas from fixed bed gasifier systems to internal combustion engine quality. *Biomass gasification: hot-gas clean-up. IEA Biomass Gasification Working Group*, 33–44.

Stephen, R. T. (2000). An introduction to combustion: concepts and applications. *McGrw-Hill Companies, Inc.*

Stocker, T., D. Qin, G.-K. Plattner, M. Tignor, S. K. Allen, J. Boschung, A. Nauels, Y. Xia, V. Bex, and P. M. Midgley (2014). *Climate change 2013: The physical science basis*. Cambridge University Press Cambridge, UK, and New York.

Stone, C. and D. Green-Armytage (1987). Comparison of methods for the calculation of mass fraction burnt from engine pressure—time diagrams. *Proceedings of the Institution of Mechanical Engineers, Part D: Journal of Automobile Engineering 201*(1), 61–67.

Stone, R. (2012). *Introduction to internal combustion engines*. Palgrave Macmillan.

Stone, R., A. Clarke, and P. Beckwith (1998). Correlations for the laminar-burning velocity of methane/diluent/air mixtures obtained in free-fall experiments. *Combustion and Flame 114*(3), 546–555.

Svehla, R. A. (1995). *Transport coefficients for the NASA Lewis chemical equilibrium program*, Volume 4647. National Aeronautics and Space Administration, Office of Management, Scientific and Technical Information Program.

Syed, I. Z., Y. Yeliana, A. Mukherjee, J. Naber, and D. Michalek (2010). Numerical investigation of laminar flame speed of gasoline-ethanol/air mixtures with varying pressure, temperature and dilution. Technical report, SAE Technical Paper No. 2010-01-0620.

Szwaja, S., K. Bhandary, and J. Naber (2007). Comparisons of hydrogen and gasoline combustion knock in a spark ignition engine. *International Journal of Hydrogen Energy 32*(18), 5076–5087.

Tabaczynski, R. J. (1976). Turbulence and turbulent combustion in spark-ignition engines. *Progress in energy and combustion science 2*(3), 143–165.

Tabaczynski, R. J., C. R. Ferguson, and K. Radhakrishnan (1977). A turbulent entrainment model for spark-ignition engine combustion. Technical report, SAE Technical Paper No. 770647.

Tabaczynski, R. J., F. H. Trinker, and B. A. Shannon (1980). Further refinement and validation of a turbulent flame propagation model for spark-ignition engines. *Combustion and Flame 39*(2), 111–121.

Tang, C., Z. Huang, J. Wang, and J. Zheng (2009). Effects of hydrogen addition on cellular instabilities of the spherically expanding propane flames. *international journal of hydrogen energy 34*(5), 2483–2487.

Taylor, C. F. (1985). *The Internal-combustion Engine in Theory and Practice: Combustion, fuels, materials, design*, Volume 2. MIT press.

Taylor, J. R. (1997). An introduction to error analysis: the study of uncertainties in physical measurements. univ. *Science, Sausalito, CA*, 45–92.

Taymaz, I. (2006). An experimental study of energy balance in low heat rejection diesel engine. *Energy 31*(2), 364–371.

Tazerout, M., O. Le Corre, and A. Ramesh (2010). A new method to determine the start and end of combustion in an internal combustion engine using entropy changes. *International Journal of Thermodynamics 3*(2), 49–55.

Tewari, P., J. Subrahmanyam, and M. G. Babu (2001). Experimental investigations on the performance characteristics of a producer gas fuelled spark ignition engine. Technical report, SAE Technical Paper No. 2001-01-1189.

Thurnheer, T., P. Soltic, and P. D. Eggenschwiler (2009). Si engine fuelled with gasoline, methane and methane/hydrogen blends: heat release and loss analysis. *International Journal of Hydrogen Energy 34*(5), 2494–2503.

Tinaut, F., A. Melgar, B. Giménez, and M. Reyes (2010). Characterization of the combustion of biomass producer gas in a constant volume combustion bomb. *Fuel 89*(3), 724–731.

Tinaut, F. V., A. Melgar, A. Horrillo, and A. D. De La Rosa (2006). Method for predicting the performance of an internal combustion engine fuelled by producer gas and other low heating value gases. *Fuel processing technology 87*(2), 135–142.

Turns, S. R. An introduction to combustion, 2000.

Verhelst, S. and C. Sheppard (2009). Multi-zone thermodynamic modelling of spark-ignition engine combustion–an overview. *Energy conversion and Management 50*(5), 1326–1335.

Verhelst, S. and R. Sierens (2007). A quasi-dimensional model for the power cycle of a hydrogen-fuelled ice. *International Journal of Hydrogen Energy 32*(15), 3545–3554.

Versteeg, H. K. and W. Malalasekera (2007). *An introduction to computational fluid dynamics: the finite volume method*. Pearson Education.

Veynante, D. and L. Vervisch (2002). Turbulent combustion modeling. *Progress in energy and combustion science 28*(3), 193–266.

Vu, T. M., J. Park, O. B. Kwon, and J. S. Kim (2009). Effects of hydrocarbon addition on cellular instabilities in expanding syngas–air spherical premixed flames. *international journal of hydrogen energy 34*(16), 6961–6969.

Warnatz, J., U. Maas, and R. Dibble. Combustion: physical and chemical fundamentals, modeling and simulation, experiments, pollutant formation. 2006.

Watson, N. and M. S. Janota (1982). *Turbocharging: The internal combustion engine*. MacMillan.

Westin, F., J. Rosenqvist, and H.-E. Ångström (2004). Heat losses from the turbine of a turbocharged si-engine-measurements and simulation. Technical report, SAE Technical Paper No. 2004-01-0996.

Wilke, C. (2004). A viscosity equation for gas mixtures. *The Journal of Chemical Physics 18*(4), 517–519.

Williams, F. (1986). Asymptotic methods in turbulent combustion. *AIAA Journal 24*(6), 867–875.

Wise, D. M., D. B. Olsen, and M. Kim (2013). Characterization of methane number for producer gas blends. In *ASME 2013 Internal Combustion Engine Division Fall Technical Conference*, pp. V002T02A015–V002T02A015. American Society of Mechanical Engineers.

Woods, W. and S. Khan (1965). Paper 3: An experimental study of flow through poppet valves. In *Proceedings of the Institution of Mechanical Engineers, Conference Proceedings*, Volume 180, pp. 32–41. SAGE Publications.

Woschni, G. (1967). A universally applicable equation for the instantaneous heat transfer coefficient in the internal combustion engine. Technical report, SAE Technical paper No. 2004-01-0996.

Wu, C., C. Roberts, R. D. Matthews, and M. Hall (1993). Effects of engine speed on combustion in si engines: comparisons of predictions of a fractal burning model with experimental data. Technical report, SAE Technical Paper No. 932714.

Yan, B., Y. Wu, C. Liu, J. Yu, B. Li, Z. Li, G. Chen, X. Bai, M. Aldén, and A. Konnov (2011). Experimental and modeling study of laminar burning velocity of biomass derived gases/air mixtures. *international journal of hydrogen energy 36*(5), 3769–3777.

Yan, H. and H. Guo (2012). Efficiency and its bounds for thermal engines at maximum power using newton's law of cooling. *Physical Review E 85*(1), 011146.

Yates, A. D., A. Swarts, and C. L. Viljoen (2005). Correlating auto-ignition delays and knock-limited spark-advance data for different types of fuel. Technical report, SAE Technical Paper No. 2005-01-2083.

Yüksel, F. and M. Ceviz (2003). Thermal balance of a four stroke si engine operating on hydrogen as a supplementary fuel. *Energy 28*(11), 1069–1080.

Yüksel, F. and B. Yüksel (2004). The use of ethanol–gasoline blend as a fuel in an si engine. *Renewable energy 29*(7), 1181–1191.

Zhen, X., Y. Wang, S. Xu, Y. Zhu, C. Tao, T. Xu, and M. Song (2012). The engine knock analysis–an overview. *Applied Energy 92*, 628–636.

Appendix A

Gaseous mixture thermo-physical properties

Thermal conductivity and viscosity

The transport properties k and μ can be calculated from the kinetic theory of gases based on the knowledge of parameters like the collision diameter, collision integral, dipole moment, self diffusion coefficient etc., (Hirschfelder, Curtiss, Bird, and Mayer 1954) (Rice 1955). However, to avoid the general complexity and estimation of a large number of intermediate coefficients, National Aeronautics and Space Administration (NASA) has made available curve fit coefficients as a function of temperature for the estimation of specie transport properties (Svehla 1995) in the temperature range between 300 K (200 K for few species) to 5000 K (6000 K for few species). The common expression for thermal conductivity and dynamic viscosity is of the form as in equation A.1 where, A_k, B_k, C_k, D_k and $A_\mu, B_\mu, C_\mu, D_\mu$ are the NASA curve fit coefficients for thermal conductivity and viscosity respectively. The current work uses equation A.1 for the estimation of specie transport properties.

$$ln(k) = A_k ln(T) + \frac{B_k}{T} + \frac{C_k}{T^2} + D_k \quad ln(\mu) = A_\mu ln(T) + \frac{B_\mu}{T} + \frac{C_\mu}{T^2} + D_\mu \quad \text{(A.1)}$$

The individual specie viscosity data is used in the formulation proposed by Wilke (Wilke 2004), as in equation A.2, for estimating the mixture viscosity (μ_{mix}), in

terms of the specie viscosity (μ_i), mole fraction (x_i) and molecular weight (M_i).

$$\mu_{mix} = \sum_{i=1}^{i=n} \frac{\mu_i}{\frac{1}{x_i}\sum_{j=1}^{j=n} x_j \phi_{ij}} \qquad \phi_{ij} = \frac{\left[1 + \left(\frac{\mu_i}{\mu_j}\right)^{1/2} \left(\frac{M_j}{M_i}\right)^{1/4}\right]^2}{\left(\frac{4}{\sqrt{2}}\right)\left[1 + \left(\frac{M_i}{M_j}\right)\right]^{1/2}} \tag{A.2}$$

The mixture thermal conductivity (λ_{mix}) is estimated using a combination averaging formula proposed by Mathur et al (Mathur, Tondon, and Saxena 1967) as in equation A.3.

$$\lambda_{mix} = \frac{1}{2}\left[\sum_{i=1}^{i=n} x_i \lambda_i + \frac{1}{\sum_{i=1}^{i=n} \frac{x_i}{\lambda_i}}\right] \tag{A.3}$$

Specific heat and Calorific value

Towards estimating the specie and mixture specific heats, while the ideal method would be to adopt the kinetic theory of gases (Rice 1955) (Jeans 1982), in light of the availability of curve fit coefficients (Kee, Rupley, Miller, Coltrin, Grcar, Meeks, Moffat, Lutz, Dixon-Lewis, Smooke, et al. 2006), the constant pressure specie specific heat ($\overline{C}_p$) and mixture specific heat ($\overline{C}_{p_{mix}}$) are evaluated from the expression as in equation A.4. The constant pressure specie specific heat ($\overline{C}_p$) and mixture specific heat ($\overline{C}_{p_{mix}}$) are evaluated from the expression as in equation A.4 which in turn permits estimating the specific heat at constant volume.

$$\begin{aligned}
&\frac{\overline{C}_{p_i}}{R_u} = a_1 + a_2 T + a_3 T^2 + a_4 T^3 + a_5 T^4; \\
&\overline{C}_{p_{mix}} = \sum_{i=1}^{i=n} x_i \overline{C}_{p_i}; \\
&\overline{C}_{p_{mix}} - \overline{C}_{p_{mix}} = R_u
\end{aligned} \tag{A.4}$$

Appendix B

Engine instrumentation operating principle

This section briefly discusses the fundamental principle(s) adopted by the measuring instruments used in the current investigation. While a range of instruments are used, the following paragraphs highlights the details pertaining to some of the special instruments used in the study. It may also be noted that only the broad principles are discussed and the exact implementation details being proprietary and not available in public domain have not been described.

In-cylinder instrumentation

The AVL make spark plug in-cylinder pressure sensor used in the present work is based on the piezoelectric principle. Piezoelectric effect is the appearance of an electrical potential (voltage) across the sides of special crystalline materials (designated piezoelectric crystals) when subject to mechanical stress. The electric potential developed across the surface of a piezoelectric material is proportional to the applied force and is a measure of the applied force. This basic pressure to charge conversion is as indicated in figure B.1 below.

The spark plug adapted pressure sensor model GU13Z with ZF43 adaptor uses Gallium Orthophosphate ($GaPO_4$), a piezo material specifically suitable for high temperature applications and is characterized by high temperature resistance of up

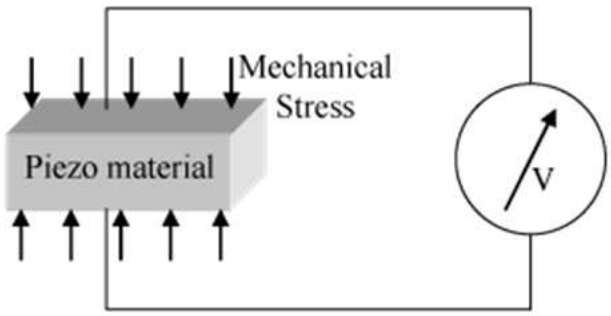

Figure B.1: Piezo electric principle - Force to charge (Nano-Physics-KHT 2015)

to 900 0^C. The pressure acts on the piezoelectric crystal through a pliable diaphragm and a short rigid pressure plate (used primarily to create even mechanical stress on the measuring element). The pressure transducer is housed in a capsule which is electrically connected to the positive electrode of the measurement element and represents the ground while the electric charge output is connected to a connector which is highly insulated against the housing. The charge output from the transducer generated on application of pressure is converted into a voltage signal through a charge amplifier required due to the extremely small magnitude of the generated charge on the piezoelectric material itself. The general arrangement of a piezoelectric pressure sensor used for cylinder pressure measurement is indicated in figure B.2 as below.

Crank angle encoder

The crank angle encoder is basically an optical sensor and is based on the principle of light ray interception. In this, an emitter – receiver pair is used along with a slotted disk mounted on the engine crank shaft. As the slotted disk rotates along with the engine shaft, the beam of light is interrupted and restored, generating a temporal pulse. The basic operating principle is as indicated in figure B.3 below. The crank angle encoder adopted in the current investigation has 720 slots and as such provides a physical crank angle resolution of 0.5 deg which can extended to 0.1 deg by means of internal multiplication.

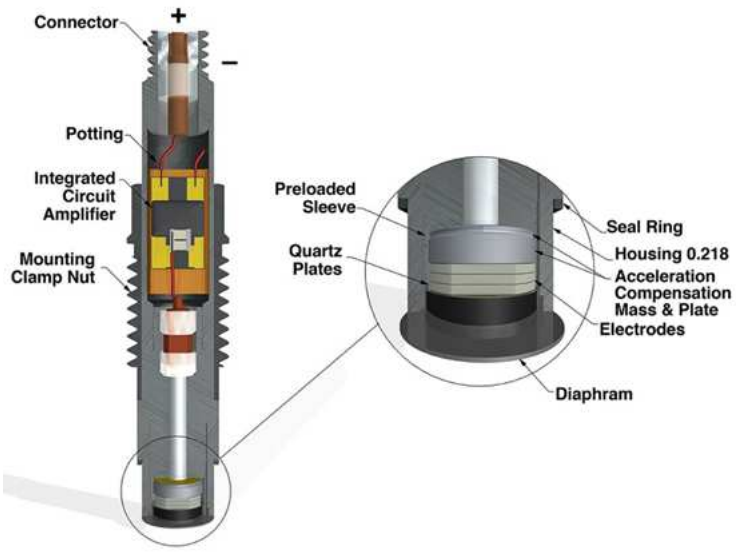

Figure B.2: Representative image of the in-cylinder pressure sensor (PCB-Piezotronics 2015)

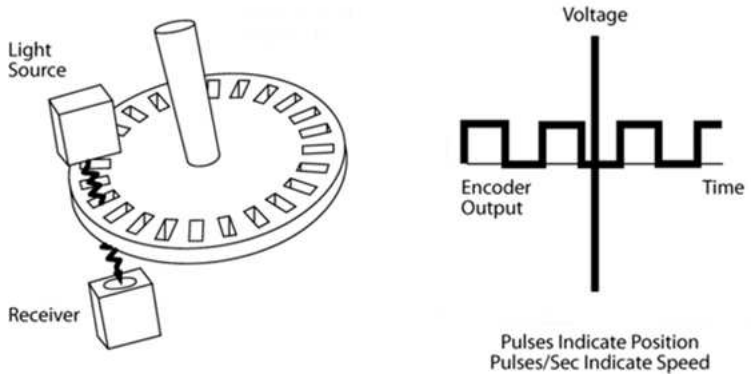

Figure B.3: Operating principle of a typical optical encoder (IHS-Engineering-360 2015)

Fuel gas analyser

The SICK MAIHAK S700 series gas analyser is a continuous type extractive gas analyser used for measuring the gas composition (volume basis) of CO, H_2, CH_4, O_2 and CO_2 with the balance being accounted for by N_2. Different principles used to quantify the indicated gaseous species are briefly described as below;

1. Quantifying CO,CO_2 and CH_4 : The analyser adopts the Non-Dispersive Infra-Red (NDIR) technique to quantify Carbon Monoxide, Carbon Dioxide and

Methane in the sample gas. The NDIR technique works on the principle that each of the indicated gases absorbs infra-red radiation at a particular frequency. The basic principle is described with respect to quantification of CO_2 which is replicated for CO and CH_4 in independent columns. An infra-red lamp directs waves of light through a tube filled with sample gas towards an infra-red light detector which can detect the amount of light received. Depending on the wavelength of the emitted light (which corresponds to absorption spectrum of one of the three gas components) some light is absorbed by CO_2 in the sample gas (proportional to the mole fraction). The balance gas is incident on the detector through a filter (which filters out all frequencies except that corresponding to CO_2). The difference between the quantity of light emitted by the lamp and the detector is taken as the measure of CO_2 present in the gas.

2. Quantifying O_2: The analyser adopts the paramagnetic principle for the quantification of Oxygen. The paramagnetic nature of Oxygen causes O_2 in the gas to selectively drift towards a strong magnetic field. This selective motion of O_2 is used to create a physical deflection (in the current set-up on a suspended dumbbell) and the extent of deflection is taken as a measure of O_2 content in the gas.

3. Quantifying H_2: The analyser adopts the thermal conductivity principle to quantify Hydrogen. Hydrogen has thermal conductivity significantly different form the other typical gas components and when passed over a balanced Wheatstone bridge, sets in imbalance due to enhanced heat transfer induced change in the resistance. The extent of bridge imbalance corrected to the presence of other gases is taken as a measure of the presence of H_2.

Flue gas analyser

The KANE QUNITOX (KM-9106) flue gas analyser makes use of electro-chemical sensors to monitor CO,NO, NO_2, SO_2, H_2S and O_2 and the NDIR method to monitor hydrocarbons. The general philosophy adopted for NDIR method is the same

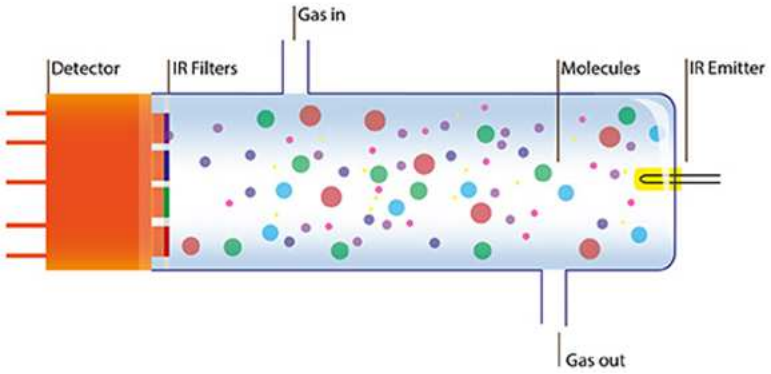

Figure B.4: Non-Dispersive Infra-Red operating principle (Laser-Components 2015)

as described in the foregone discussion on fuel gas analysis. The electro-chemical principle adopted of quantifying the balance gases is basically a typical fuel cell involving oxidation/reduction at the electrodes and transfer of electrons through an external circuit. The magnitude of the current through the external circuit is an indication of the mole fraction of the component of interest.

Appendix C

Turbocharger Matching and Selection

Turbocharging an engine basically entails a complex interaction between the compressor, engine and the turbine under the constraint of the turbine and compressor being mechanically coupled. For a particular engine frame and required power, turbocharger matching essentially involves the selection of appropriate turbine and compressor frames that can efficiently provide the necessary density boost to the mixture so as to enable the engine to deliver the required load. The turbocharger selection methodology adopted in the current investigation is briefly described as below;

1. Estimate the mixture mass flow rate to the engine based on the engine power rating, brake thermal efficiency (consider typical values from literature and experience) and mixture calorific value.

2. Based on the engine volumetric capacity, estimate the mixture density and pressure for threshold mixture temperature as indicated in equation C.1.

$$P_{man} = \frac{\dot{m}_{mix}}{\dot{V}_{swept}} R_{mix} T_{man} \tag{C.1}$$

3. Using the typical values from literature, based on experience and other possible sources, make an estimate of the pressure drop across the after-cooler and add it up to the manifold absolute pressure to get the compressor outlet pressure.

4. The ratio of the compressor outlet pressure to the compressor inlet pressure (should be considered close to but slightly lower than the prevailing ambient

pressure; again a mostly heuristic approach) gives the pressure ratio required for the designated load.

5. Use the compressor pressure ratio information along with the corresponding flow rate (in appropriate units as corrected mass flow, mass flow parameter etc, depending on the manufacturer) on the compressor map family to identify the suitable compressor frame (representing the complete compressor). A representative compressor family map is shown in the figure below. Considering that the compressor maps overlap, based on the identified operating point, a small group of compressors (usually not more than four) form the first choice. The operating point is then identified on the individual compressor maps and a final selection of one or two compressor frames is made based on efficiency and a minimum margin of around 25 % from the surge line.

6. Having identified the compressor frame, based on the pressure ratio, mass flow handled and the compressor efficiency η_{ic} (from the turbocharger map) the required compressor work input is estimated from equation C.2 as below. The compressor work sets the requirement for the turbine frame considering that the turbine drives the compressor.

$$W_{comp} = \frac{1}{\eta_{ic}} \dot{m}_{mix} C_{P_{mix}} T_{c_{in}} \left[Pr^{\frac{\gamma-1}{\gamma}} - 1 \right] \tag{C.2}$$

7. Identifying the turbine frame requires two key input parameters, the (turbine to compressor) mechanical efficiency η_{t-mech} and the turbine inlet thermodynamic conditions. While generally, these values are fixed based on literature or heuristically, the turbine inlet thermodynamic conditions can also be identified based on simple zero or one dimensional simulation tools. The turbine exhaust pressure is set slightly higher than the ambient for obvious reasons. With the knowledge of the mass flow rate (in the current case same as compressor mass flow rate) and the turbine expansion ratio ($\frac{P_{t-in}}{P_{t-out}}$), the information (mass flow rate may have to be represented in appropriate units as corrected mass flow, mass flow parameter etc, depending on the manufacturer) is mapped onto the turbine family map to get the turbine frame size, generally in terms of the turbine wheel diameter and housing A/R ratio. It is important to note that the

selection of turbine is technically more challenging as compared to the turbine selection considering that the choice of the turbine frame starts off with double end approximation of the turbine thermodynamic conditions. Thus, the choice can only be as good as the approximations (accounting for the fact that some simulation tools are available). As such, generally, while the (approximated) expansion ratio and the mass flow rate are used to get the preliminary regime, the final choice is essentially heuristic. Similar to the selection of the compressor, a range of turbines is selected in the immediate vicinity of the operating point.

8. Having zeroed in on the turbine frames, for the rotational speed corresponding to the compressor rotational speed, the efficiency for each of the turbines corresponding to the operating point is determined either directly from the map of the respective frames or by mapping the ratio of the mean tangential blade velocity to the nozzle exit velocity onto the turbine maps. With the efficiency available, the turbine work required at the shaft is estimate from equation C.3. The final selection of a couple of turbocharger frames is based on how close the turbine work matches the required work at the shaft (accounting for the mechanical efficiency).

$$W_{turb} = \eta_{ti}\dot{m}_{pro}C_{P_{pro}}T_{t_{in}}\left[1 - \frac{1}{Pr^{\frac{\gamma-1}{\gamma}}}\right] \tag{C.3}$$

9. The final selection of the compressor-turbine pair is mostly based on experimental investigations wherein the selected frames are paired and tested to evaluate the overall performance in respect of the engine load delivery target.

Appendix D

Grid Independence Studies

Discretization of the flow domain relevant for the analysis essentially involves breaking the domain into small chunks and solve the discretized version of the governing equations. One of the fundamental requirements in the discretization of the domain pertains to mesh density. It is imperative that the grid/mesh be fine enough for the solution to be independent of the grid/mesh size (Anderson and Wendt 1995) (Pletcher, Tannehill, and Anderson 2012). Grid independence is generally realized by starting off with a coarse mesh which is subsequently refined, either in specific regions or over the entire domain. Simulation with the same set of initial/boundary conditions are carried out using the two mesh sizes and key results relevant to the problem on hand are compared to quantify the difference. Mesh refinement and comparison is continued till the difference between two consecutive results are well within the acceptable limits.

In the current investigation, the mesh density of the starting coarse grid is dictated by the dynamic mesh error wherein for mesh density lower than a critical density, negative volumes are created within the domain during some dynamic mesh events (valve motion in the current case). The first coarse mesh that supported a full mesh preview without any (volume) error corresponds to a reference size of 3.69 with the corresponding maximum element size of 11.07 mm and minimum element size of 1.23 mm. Subsequent meshes were generated based on the approach suggested by Roache (Roache 1997) wherein the number of elements for two consecutive meshes are estimated based on the following correlation with the grid refinement ratio r (the ratio of the coarse element size to the fine element size) being in the range of

$1.15 \leq r \leq 2.0$.

$$\text{Grid refinement ratio} \quad r = \left(\frac{N_f}{N_c}\right)^{\frac{1}{D}}$$

D is the dimensionality, taking values of 1,2 or 3 depending on the flow domain considered being one, two or three dimensional and N_c, N_f are the number of elements in the coarse and fine grid respectively. In the current investigation, a grid refinement ratio of 1.15 has been considered. Towards comparing the solutions from two consecutive grids, the following parameters are used;

1. Average turbulent intensity along a 20 mm line coincident with the cylinder axis starting from the cylinder head.

2. Average turbulent intensity on a plane of 60 mm diameter normal to the cylinder axis 20 mm from the cylinder head.

3. Cylinder average temperature and

4. Cylinder average pressure

In the analysis of results towards establishing grid independence, the region in the vicinity of the cylinder head is of primary interest considering that this region experiences very high turbulence and severe parameter gradients could persist. Parametric invariance for two mesh densities in this region would guarantee mesh independence in the complete domain. Further, comparison is primarily based on line and area average parameters so as to avoid errors in comparative assessment associated with volume averaged parameters. The details of domain discretization for the considered mesh densities are consolidated in table D.1 below.

The four parameters identified for evaluating the grid independent solution are compared for the considered mesh densities as in figure D.1 (a) through (d). The line average (figure D.1 a) and area average (figure D.1 b) turbulent intensities are compared at two crank angles, one at 90 deg after the top dead center during the suction stroke and the other at the end of the compression stroke. The cylinder average temperature (figure D.1 c) and pressure (figure D.1 d) are compared 90 deg on either side of the top dead center. From figure D.1 it is evident that when

Table D.1: Correlations for the estimation of turbulent characteristic velocity and length

Name	$N1$	$N2$	$N3$	$N4$	$N5$
Number of nodes	2,71,847	4,23,065	6,40,582	9,73,632	14,84,698
Reference size	3.69	2.70	2.09	1.61	1.23
Maximum element size	11.07	8.10	6.27	4.83	3.69
Minimum element size	1.23	0.90	0.69	0.53	0.41

cylinder average parameters are considered, the second mesh $N2$ itself evolves a grid independent solution. However, when line and area average turbulent intensities are considered, the change in the parameters beyond mesh $N4$ are under 0.5 % and hence the solution adopting grid $N4$ can be considered to be grid independent. Apart from establishing the mesh density for the current investigation, the foregone discussion also highlights the criticality of appropriate choice of the parameters / averaging methodology towards establishing grid independence.

The details of the discretized domain at the top and bottom dead center for the selected mesh density (on a plain passing through the cylinder and valves axes) are shown in figure D.2 with the Tetrahedral and Hexahedral regions clearly identified. The number of nodes in the three core regions are indicated as inset data.

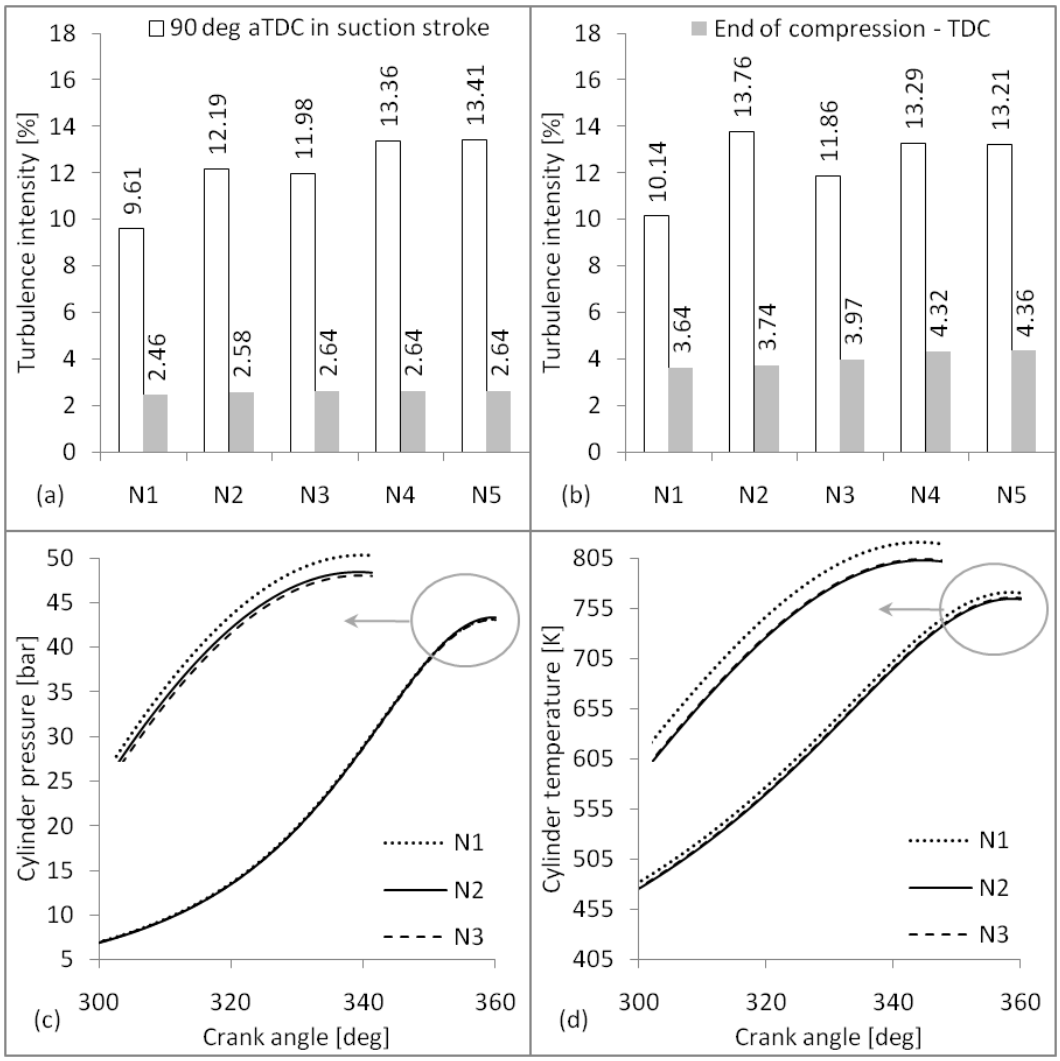

Figure D.1: Grid independence studies - Parametric comparison

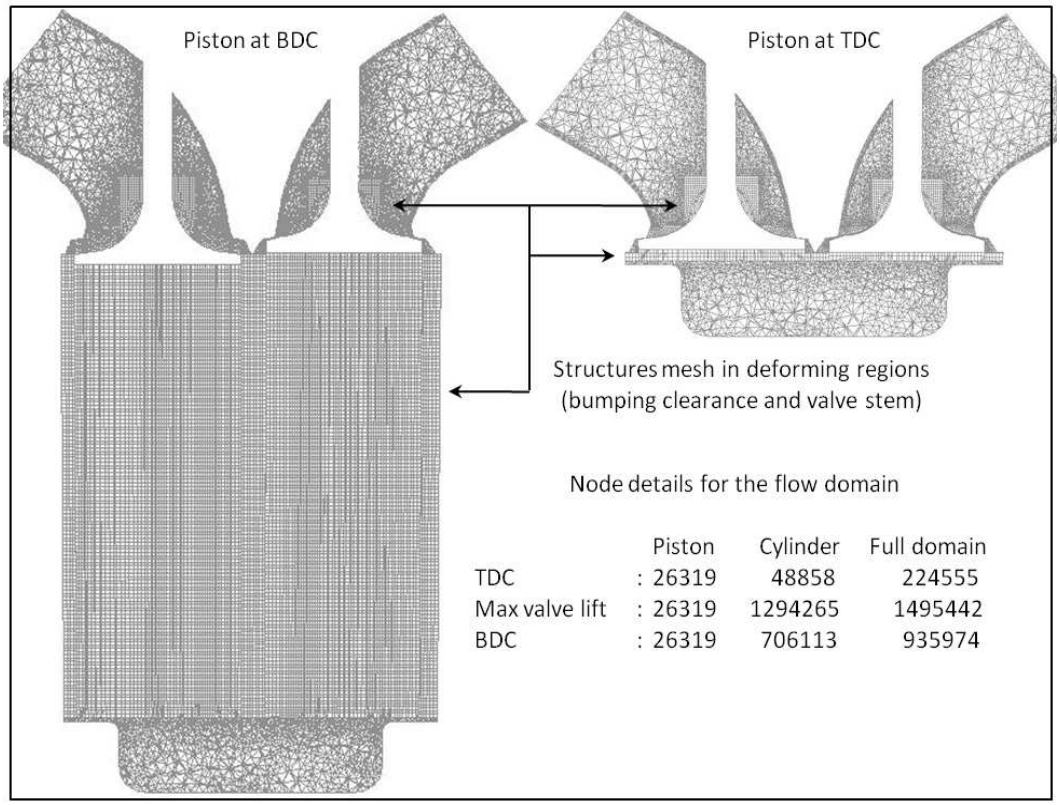

Figure D.2: Mesh structure and node details for engine $E6$ at TDC and BDC